Universidade Federal do Rio Grande do Sul
Escola de Engenharia
Programa de Pós-Graduação em Engenharia Civil

Eflorescência em geopolímeros à base de metacaulim: formação, efeitos e mitigação

Márlon Augusto Longhi

Porto Alegre
2019

MÁRLON AUGUSTO LONGHI

EFLORESCÊNCIA EM GEOPOLÍMEROS À BASE DE METACAULIM: FORMAÇÃO, EFEITOS E MITIGAÇÃO

Tese apresentada ao Programa de Pós-Graduação em Engenharia Civil: Construção e Infraestrutura da Universidade Federal do Rio Grande do Sul, como parte dos requisitos para obtenção do título de Doutor em Engenharia

Prof. Ana Paula Kirchheim
Dra. pela Universidade Federal do Rio Grande do Sul, Brasil

Prof. Erich D. Rodríguez
Dr. pela Universitat Politècnica de València, Espanha

Porto Alegre
2019

MÁRLON AUGUSTO LONGHI

EFLORESCÊNCIA EM GEOPOLÍMEROS À BASE DE METACAULIM: FORMAÇÃO, EFEITOS E MITIGAÇÃO

Esta tese de doutorado foi julgada para a obtenção do título de DOUTOR EM ENGENHARIA CIVIL, área de construção, e aprovada em sua forma final pelo Professor Orientador e pelo Programa de Pós-Graduação em Engenharia Civil: Construção e Infraestrutura da Universidade Federal do Rio Grande do Sul.

Porto Alegre, julho de 2019

Prof. Ana Paula Kirchheim
Dra. pela Universidade Federal do Rio Grande do Sul, Brasil
orientadora

Prof. Erich D. Rodríguez
Dr. Pela Universitat Politècnica de València, Espanha
co-orientador

Prof. Angela Borges Masuero
Coordenadora do PPGCI/UFRGS

BANCA EXAMINADORA

Prof. Angela Borges Masuero (UFRGS)
Dra. Pela Universidade Federal do Rio Grande do Sul

Prof. Robinson Carlos Dudley Cruz (UCS)
Dr. Pela Universita et Karlsruhe (Alemanha)

Prof. Zuhua Zhang (USQ)
Dr. Pela University of Southern Queensland (Austrália)

Prof. John L. Provis (University of Sheffield)
Dr. Pela University of Melboune (Austrália)

Dedico este trabalho a minha família e amigos, pelo suporte emocional durante mais esse período

AGRADECIMENTOS

Agradeço a CAPES pela bolsa de estudos durante parte do período no Brasil, e ao CNPq durante o período de doutorado sanduíche, o possibilitou a realização dessa pesquisa.

À toda minha família, pelo apoio e incentivo em todas as etapas e decisões, em especial meus pais Valnei e Jucilene e minhas irmãs Iane e Lorenza que mesmo fisicamente longe então sempre comigo. À minha "tipo irmã" Muriel, que chorou e pedalou junto durante esses 4 anos.

Aos meus amigos de Rondinha e Porto Alegre que escutaram alguns "não, tenho que escrever a tese".

A todo grupo de professores do NORIE/UFRGS pelos ensinamentos e suporte desde a graduação até o doutorado. Em especial à Prof. Angela que foi minha primeira referência na pesquisa e primeira orientadora.

Em especial aos meus orientadores. À Prof. Ana Paula Kirchheim, por sempre me incitar a dar um passo a mais e por me possibilitar oportunidades de crescer como pessoa e profissional. E ao Prof. Erich, por me ensinar a ajudar muito em todas as etapas desde o mestrado.

À University of Southearn Queensland e ao Centre for Future Material, que me acolheram durante 2018 e início de 2019. À todos os professores e funcionários que me ajudaram muito na adaptação e realização da pesquisa, em especial ao Prof. Hao Wang e principalmente ao Prof. Zuhua Zhang, que orientou durante o período na USQ e foi fundamental para o desenvolvimento e realização da tese. Aos demais alunos e pesquisadores do centro, que sempre foram muito prestativos e amigáveis, em especial aos amigos Yanru, Yubin, Yuwey and Lakshmikanth.

Aos demais professores, pesquisados e instituições que me auxiliaram durante o processo de doutorado. Entre eles os professores John Provis e Susan Bernal, que me auxiliaram no início do doutorado na escolha do tema. Ao Dr. Brant Walkley da University of Sheffiled, que me auxiliou na realização e interpretação de algumas análises químicas apresentadas no trabalho. Ao Prof. Sandro Marden da Universidade da Paraíba por me receber na UFPB durante um mês e me auxiliar na etapa inicial do doutorado no delineamento da pesquisa.

À UFRGS, for ser uma Universidade pública, resistente e forte, que preza pela qualidade da educação e desenvolvimento da ciência.

Um agradecimento muito especial à toda família NORIE/UFGRS, que tenho o prazer de fazer parte a 9 anos. Durante esses anos conheci muitas pessoas, fiz muitos e muitos amigos, alguns compadres e tive bons momentos. O paragrafo é pequeno pra citar todos, mas certamente o carinho não será. Ao longo de todos esses anos a instituição me proporcionou todo conhecimento científico que possuo até o momento e me direcionou para o mundo acadêmico como profissão, mas o mais importante são as pessoas que entraram e fazem parte da minha graças a oportunidade de fazer parte desse grupo.


QUEM FAZ CIÊNCIA DEVE SER CURIOSO, DUVIDAR, ESTUDAR, DESCOBRIR.
CIÊNCIA PRODUZ CONHECIMENTO...
...O CONHECIMENTO DESTRÓI MITOS.
Assembleia UFSC Alexandre Beck 29/01/18

RESUMO

LONGHI, M. A. **Eflorescência em geopolímeros à base de metacaulim: formação, efeitos e mitigação**. 2019. Tese (Doutorado em Engenharia Civil) – Programa de Pós-Graduação em engenharia civil: construção e infraestrutura (PPGCI), UFRGS, Porto Alegre.

Os geopolímeros são um tipo de ligantes produzidos a partir de uma mistura entre um mineral aluminossilicato (conhecido como precursor) e uma solução altamente alcalina (ativador). Esse tipo de cimento tem grandes vantagens relacionadas à sua reduzida emissão de CO_2 associada durante sua produção, assim como seu elevado desempenho quando é dosado e produzido corretamente. Apesar do atual desenvolvimento e interesse comercial nestes cimentos alternativos, tem-se ainda muitos questionamentos sobre sua de durabilidade em uso. Um desses fatores está relacionado a formação excessiva de eflorescência, decorrente do processo de lixiviação e carbonatação dos álcalis na superfície. Neste sentido, o objetivo desse trabalho é avaliar a susceptibilidade no desenvolvimento e/ou formação de eflorescências, seus efeitos mecânicos e microestruturais e meios de mitigar tal formação em geopolímeros produzidos com metacaulim como precursor. O metacaulim (MK) foi adotado como precursor por ser uma argila calcinada de elevada pureza (relação Si/Al $\approx$ 1 e baixo conteúdo de minerais contaminantes), elevada reatividade (alto conteúdo de fases amorfas) e homogeneidade comparada com outras adições minerais usados como precursores. Para isso, foram utilizados diferentes condições de ativação, tais como: tipo de íon alcalino (M^+= Na^+ ou K^+), concentração de ativação expressa como percentual em peso de M_2O (com valores entre 15 e 25%) e presença de silicato solúveis a partir da incorporação de silicato de sódio com diferentes módulos SiO_2/M_2O (MS entre 0 e 1,5). A susceptibilidade ao desenvolvimento de eflorescências foi avaliada e quantificada mediante análises físicas e químicas, alteração de aspecto visual e efeito nas propriedades microestruturais e mecânicas quando submetidos a diferentes condições de exposição. Também, a otimização dos critérios de dosagem, a utilização de reduzidos teores adições minerais, o uso de cimentos especiais e aditivos químicos foram avaliados como alternativa para redução de tal fenômeno. Os resultados demonstraram que a formação de eflorescência é dependente principalmente da estrutura porosa do geopolímero e da estabilidade dos álcalis na estrutura, os quais são determinados pelos teores de ativação. As amostras se mostraram susceptíveis aos efeitos associados a formação de eflorescência como carbonatação e lixiviação, o que causou uma redução no desempenho mecânico, decorrente da formação excessiva de cristais nos poros e superfície ou pelas mudanças microestruturais. Por fim, pode-se perceber que é possível reduzir e controlar a formação de eflorescência com a correta dosagem dos matérias e com o uso de outras adições minerais associadas ou aditivos.

Palavras-chave: Geopolímeros, metacaulim, eflorescência, lixiviação.

ABSTRACT

LONGHI, M. A. **Efflorescence formation in metakaolin-based geopolymers: formation, effects and mitigation.** 2019. Tese (Doutorado em Engenharia Civil) – Programa de Pós-Graduação em engenharia civil: construção e infraestrutura (PPGCI), UFRGS, Porto Alegre.

Geopolymers are a type of binder produced from a simple mixture of an aluminossilicate mineral (known as a solid precursor) and a highly alkaline (activator) solution. Despite the current development of these alternative cements, there are still many questions about its durability. This type of cement has great advantages related to its reduced associated CO_2 emission during its production and its high performance when it is designed and produced correctly. Despite the current development and commercial interest in these alternative cements, there are still a knowledge lack about its durability in use. One of these factors is related to excessive formation of efflorescence, due to the leaching and carbonation of alkalis on the surface. In this sense, the aim of this study is to evaluate the susceptibility in the development and/or formation of efflorescence, its mechanical and microstructural effects and alternatives to mitigate this formation in geopolymers produced with metacaulim as precursor. In MK geopolymers there is a more detailed understanding of the microstructural characteristics (reaction products) and prediction of the properties of durability because of its high purity and homogeneity. In this sense, the geopolymers were produced from different activation conditions, such as: alkaline ion type (M^+= Na^+ or K^+), activation concentration expressed as percentage by weight of M_2O (with values between 10 and 20%) and presence of silicate soluble from sodium silicate with different SiO_2/M_2O module (MS between 0 and 1.5). The susceptibility to the development of efflorescence was evaluated and quantified by the visual observation and the effect of microstructural and mechanical properties of the materials subjected to aggressive conditions as efflorescence, air carbonation and leaching. The optimization of the design parameters, the use of reduced mineral additions and chemical additives were evaluated as an alternative to reduce this phenomenon. The results demonstrated that the formation of efflorescence is mainly dependent on the porous structure of the geopolymer and the stability of the alkalis in the structure, which are determined by the activation levels. The samples showed to be susceptible to the effects associated to the formation of efflorescence such as carbonation and leaching, which caused a reduction in the mechanical performance, due to the excessive formation of crystals in the pores and surface or by the microstructural changes. Finally, it is observed that it is possible to reduce and control the formation of efflorescence with the correct dosage of the materials and with the use of other associated mineral additives or additives.

Key-words: Geopolymer, durability, efflorescence, metakaolin, calcined kaolin sludge.

LISTA DE FIGURAS

LISTA DE TABELAS

SUMÁRIO

1 INTRODUÇÃO

1.1 IMPORTÂNCIA DO TEMA

No contexto atual, principalmente países em desenvolvimento como o BRICS (Brasil, Rússia,
No contexto atual, principalmente países em desenvolvimento como o BRICS (Brasil, Rússia,
Índia, China e África do Sul) necessitam e utilizam uma grande quantidade de concreto para construção de edificações e obras de grande porte para suprir o déficit habitacional e de infraestrutura. Esta demanda elevada, torna o concreto, o segundo material mais consumido no mundo (VAN DEVENTER; PROVIS; DUXSON, 2012). O cimento, por sua vez, é um dos principais constituintes do concreto e o responsável pelas propriedades de resistência e durabilidade do concreto. Dados de 2018 (USGS, 2019) indicam uma produção mundial de cimento de aproximadamente 4.1 bilhões de toneladas, o que corresponde ao consumo aproximado de 530 kg por habitante por ano.

Mundialmente, o tipo de cimento mais utilizado é o Portland, material com amplo conhecimento na comunidade científica (DUXSON et al., 2007b; SCRIVENER; NONAT, 2011; SHI; JIMÉNEZ; PALOMO, 2011), um material versátil e com propriedades adequadas para a maioria das aplicações requeridas. No entanto, apesar das inegáveis qualidades desse tipo de cimento, o mesmo apresenta uma elevada emissão de CO_2 decorrente da decomposição da calcita e demais processos necessários para a produção do mesmo, podendo emitir um quantidade de aproximadamente 0,8 kg de dióxido de carbono para cada kg de cimento produzido (DAMTOFT et al., 2008; MÜLLER; HARNISCH, 2008; SCRIVENER; KIRKPATRICK, 2008). Segundo dados do IPCC (2014), a produção do cimento Portland representa aproximadamente 13% das emissões mundiais de dióxido de carbono (CO_2) relacionadas aos processos industriais. Já de acordo com Provis e Bernal (2014b), considerando todos setores, a produção de cimento representa 8% da emissões totais de CO_2 do mundo. Desse modo, se a previsão de aumento de consumo se confirmar para os próximos anos, principalmente para países emergentes, os níveis de emissão de CO_2 se tornarão alarmantes e ambientalmente perigosos.

Com o aumento de consumo de cimento, algumas estratégias são necessárias para garantir o desenvolvimento de uma forma ambientalmente mais amigável, estando ligado diretamente às reduções das emissões de CO_2. Uma dessas estratégias está relacionada à utilização de ligantes alternativos que tenham uma emissão de CO_2 inferior ao cimento Portland, com maior quantidade de materiais provenientes de resíduos ou de baixo impacto ambiental para sua produção. Entre eles é possível destacar os cimentos de aluminato de cálcio, sulfoaluminatos, supersulfatados (JUENGER et al., 2011), os quais são baseados na produção de um clínquer no sistema forno, em um processo similar ao convencional, no entanto com melhorias no processo ou na utilização de materiais ou dosagens diferentes, o que reduz o impacto ambiental dos mesmos. Além desses, existem também cimentos livres de clínquer, como são os cimentos tipo álcali-ativados (DAVIDOVITS, 1991; DUXSON et al., 2006; PROVIS; BERNAL, 2014).

Os álcali-ativados, são provenientes da reação entre um mineral de aluminossilicato (precursor), com uma solução alcalina (ativador) a partir de uma mistura em ótimas proporções (PROVIS; BERNAL, 2014). Conforme nomenclatura utilizada na literatura, no grande grupo denominado álcali-ativados, estão os sistemas produzidos com materiais com a presença de Al_2O_3, SiO_2 e um elevado conteúdo de CaO (~40% em massa). Dentro deste, tem-se um grupo específico denominado geopolímeros, o quais são caracterizados por utilizar precursores com reduzido teor de CaO, apresentando assim um elevado teor de SiO_2 e Al_2O_3 em sua composição. Esses materiais aluminossilicatos não reagem com água, por isso, sua reatividade se dá a partir da reação com soluções aquosas de elevado pH, identificado como precursor e usualmente produzido com a mistura entre hidróxidos, silicatos e água. Segundo Gartner e Macphee, (2011), a principal fase dos ligantes álcali-ativados com baixo teor de Ca^{2+} é o gel de aluminossilicato alcalino hidratado, (N, K)-A-S-H, mal ordenado, mas composto por ligações tridimensionais. O produto gerado dessa reação pode apresentar propriedades mecânicas e de durabilidade similares ou superiores aos cimentos tradicionais produzidos com cimento Portland (PROVIS; BERNAL, 2014), além da possibilidade de uso dos mesmos para aplicações específicas. Os materiais utilizados como precursores nessa pesquisa apresentam uma composição de óxidos predominante de SiO_2 e Al_2O_3, por isso, o termo geopolímero será utilizado ao longo de todo o trabalho.

Os geopolímeros são mundialmente conhecidos como uma opção ambientalmente amigável para uso como ligantes. Esses materiais estão sendo aplicados em grande escala, em obras de

edificações e infraestrutura[a] (Figura 1), com empresas consolidadas no setor[bc] e possuem diversas pesquisas em desenvolvimento (BUCHWALD et al., 2013; VAN DEVENTER; PROVIS; DUXSON, 2012), o que os torna uma possibilidade real de uso. No entanto, é necessário um maior conhecimento principalmente em situações de uso. Entre elas, como é o seu comportamento ao longo do tempo quando exposto aos diferentes ambientes agressivos, sua relação com agregados e demais características de conhecimento comum para o cimento Portland, fatores que são ainda lacunas de conhecimento na área de geopolímeros.

(a) (b)

Figura 1 - Obras realizadas na Austrália (a) aeroporto de Queenlaand (b) Global Change Institute na Universidade de Queersland

Mesmo com exemplos bem-sucedidos de aplicação, o desenvolvimento e utilização dos geopolímeros encontra algumas barreiras perante sua utilização em larga escala. Uma delas está relacionada justamente ao precursor e sua disponibilidade. Os precursores mais tradicionais e já utilizados são proveniente de argilas calcinadas e resíduos e/ou subprodutos industriais. O metacaulim é um dos precursores mais utilizados sendo este produzido a partir da calcinação do caulim de elevada pureza, não sendo considerado um resíduo (GAO et al., 2014; GRANIZO; PALOMO; FERNANDEZ-JIMENEZ, 2014; ZHANG et al., 2012, 2013). Já os materiais proveniente de resíduo usualmente utilizados são a escória de alto forno (DUXSON; PROVIS, 2008; SHI; KRIVENKO; ROY, 2006) e a cinza volante (CRIADO; FERNÁNDEZ-JIMÉNEZ; PALOMO, 2007; CRIADO; PALOMO; FERNANDEZ-JIMENEZ, 2005; MOLIN et al., 2007). Estes materiais são utilizados na produção de cimentos Portland compostos (CP III e CP

[a] http://www.wagner.com.au/main/what-we-do/earth-friendly-concrete/efc-home

[b] http://www.zeobond.com/products-e-crete.html

[c] http://www.wagner.com.au/media/36773/Geopolymer-concrete_Saudi-Conference_2015.pdf

IV, segundo NBR 5735/1991 e 5736/1991) e na produção de concretos, além disso, não são disponíveis em todas localidades.

Segundo Scrivener, John e Gartner (2017), a busca por precursores para geopolímeros deve ser por materiais ou coprodutos não utilizados na indústria do cimento, uma vez que os materiais tradicionais já são utilizados na indústria de cimento Portland em quase sua totalidade. Com isso, novos precursores derivados de resíduos industriais estão sendo pesquisados como possibilidade, entre eles a cinza pesada (FROENER, 2016; LONGHI et al., 2014; LONGHI, 2015), resíduos da indústria de petróleo (BERNAL et al., 2016b), argilas naturais (CRISTIANE et al., 2007, 2012) e resíduos de beneficiamento de argilas de elevada pureza (BARATA; ANGÉLICA, 2012; LONGHI et al., 2016).

Em um planejamento a longo prazo, onde supõe-se a utilização de geopolímeros em maior escala e em qualquer local, é necessária a busca por materiais disponíveis localmente e em abundância. Neste sentido, Scrivener, John e Gartner (2017) destacam que a principal fonte de material com potencial de utilização como adição mineral para a indústria do cimento Portland, podendo ser estendido este entendimento para o uso como precursores para geopolímeros, é baseada em argilas calcinadas. Os autores ainda apontam que devido a disponibilidade desse material em abundância, a quantidade estimada de material disponível é muitas vezes superior ao somatório de todos materiais atualmente utilizados. Os diversos tipos de argilas disponíveis, e até mesmo os resíduos provenientes do seu beneficiamento apresentam características diferentes, que podem ser beneficiadas de modo a proporcionar um material adequado para o uso como precursor. Desse modo, as argilas calcinadas se tornam a classe de precursores com maior potencial para utilização em geopolímero.

A partir da disponibilidade e utilização desse material em larga escala, a análise da durabilidade dos geopolímeros produzidos com este precursor se torna um fator determinante e deve ser compreendida perante as diferentes condições de exposição e uso. A avaliação de durabilidade de novos materiais é ampla e muitas vezes necessita de um extenso período de estudos, tornando importante a avaliação de efeitos ou manifestações patológicas isoladas. Diversos fatores compõem a durabilidade em geopolímeros e muitos deles ainda carece de entendimento.

Um desses fenômenos está relacionada à formação de eflorescência, a qual é constantemente observada durante o desenvolvimento de pesquisas, no entanto pouco reportada e compreendida. Segundo Arbi et al. (2016), eflorescência é uma formação superficial decorrente

de deposição de sal, proveniente da carbonatação dos álcalis lixiviados. Essa formação já foi avaliada em cimento Portland por Dow e Glasser (2003) e sistematizada em seis passos, que envolvem a dissolução de CO_2, conversão do CO_2 em fases aquosas, lixiviação dos álcalis, dissolução do hidróxido de cálcio, difusão dos reagentes na solução e precipitação do carbonato. Essa formação pode ser considerada como uma manifestação patológica, que gera efeitos visuais e possivelmente mecânicos e de durabilidade, no entanto, pouco se sabe sobre os efeitos causados.

Apesar da similaridade com o produto formado, onde predominantemente se observa a presença de carbonatos, devido a diferença entre os materiais utilizados na produção bem como pelos produtos de geopolimerização ou hidratação formados, os efeitos da eflorescência são diferentes. Em geopolímeros, reduzida quantidade de pesquisas foram realizadas, e, devido à complexidade do fenômeno, muitos fatores ainda não são plenamente compreendidos. Na Figura 2 é apresentado o aspecto das amostras de geopolímeros com a formação de eflorescência.

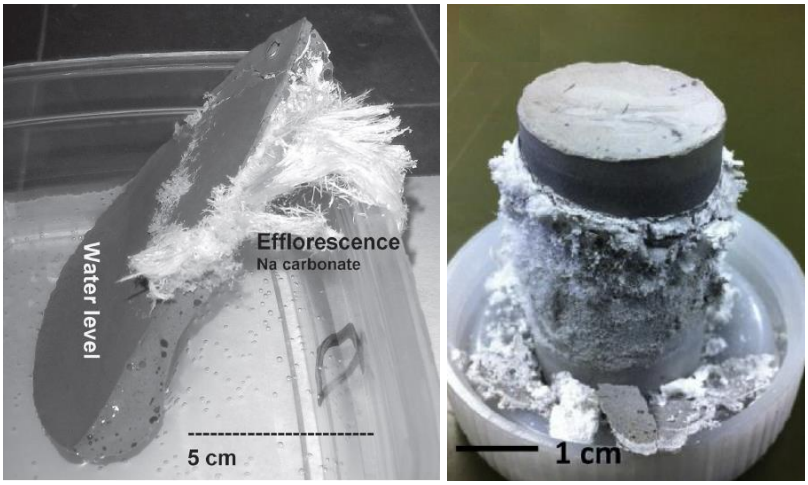

(a) (b)

Figura 2 - geopolímeros com formação de eflorescência (a) cristais de carbonato em geopolímero produzidos baseado em cinza volante (Škvára et al. 2009) (b) deterioração superficial causada pela excessiva formação de eflorescência em geopolímero baseado em cinza volante (Zhang et al. 2018).

1.2 PROBLEMA E JUSTIFICATIVA DA PESQUISA

Apesar de ser um fenômeno recorrente em situações de laboratório, a formação de eflorescência não é amplamente pesquisada e reportada na comunidade científica. Acredita-se que uma pesquisa específica relacionada à compreensão do processo de formação de eflorescência em

geopolímeros pode contribuir cientificamente para entendimento do fenômeno, bem como possibilitar o uso de geopolímeros em larga escala.

Atualmente, na área de geopolímeros, tem-se uma grande quantidade de trabalhos publicados e avaliando o metacaulim como precursor. No entanto, a questão relacionada à eflorescência é abordada em poucos trabalhos, na maioria dos casos estudos avaliam geopolímeros com cinza volante e escória de alto forno como precursores (BERNAL, 2016; NAJAFI; ALLAHVERDI; PROVIS, 2012; ŠKVÁRA et al., 2009, 2012; ZHANG et al., 2018).

De acordo com Škvára et al. (2009, 2012), a formação de eflorescência em geopolímeros com cinza volante é dependente da lixiviação de álcalis. Segundo os autores, na estrutura geopolimérica, o álcali, representado na pesquisa pelo cátion Na^+, está presente na forma de $Na(H_2O)_n^+$ ou em uma ligação fraca com o gel N-A-S-H. Desse modo, os autores observaram a partir de análises que o álcali pode ser lixiviado em quase sua totalidade. Complementar ao estudo de eflorescência em geopolímeros a base de cinza volante, Zhang et al. (2014) indica uma forte dependência da eflorescência com o tipo de ativador, temperatura de cura e teor de adição de escória de alto forno. Os autores também observaram uma lixiviação de álcalis em uma proporção entre 12 e 16%, muito inferior aos valores observados por Škvára et al. (2012). Além disso, na pesquisa de Zhang et al. (2014), o potencial de formação de eflorescência foi também atribuído ao grau de porosidade do material, onde tal propriedade está relacionada a difusão tanto dos álcalis como do CO_2 atmosférico na estrutura porosa. A partir desses trabalhos, os dois principais fatores associados à formação de eflorescência estão associados ao potencial de lixiviação de álcalis e à mobilidade dos mesmos, sendo estes dependentes da porosidade da estrutura. No entanto, há uma incompatibilidade nos resultados frente a compreensão da estabilidade dos álcalis na estrutura geopolimérica. Do mesmo modo, a relação entre os fatores de ativação com o grau de geopolimerização do precursor, associados com as propriedades físico-químicas não foi investigado. O que potencializou o interesse deste trabalho em entender a relação entre fatores de ativação, propriedades físico-químicas e como se dá a formação de eflorescência.

Quanto aos efeitos desta propriedade deletéria, Škvára et al. (2012) avaliaram geopolímeros com cinza volante mediante a resistência à compressão e observaram que a mesma não sofreu efeitos negativos perante a remoção dos álcalis. Já Yao et al. (2009), em misturas com o uso de cinza volante e diferentes teores de escória de alto forno, observaram a redução da resistência à compressão quando estas eram expostas a condição de lixiviação, bem como perante formação

de eflorescência. No entanto, os autores reportam um efeito reduzido para sistemas com elevados teores de escória de alto forno. Esse comportamento está associado à diferença de porosidade e à maior estabilidade do álcali no gel C-A-S-H, fruto da reação entre o ativador e o precursor (escória, rica em CaO) em relação ao gel N-A-S-H, formado na reação com o ativador e cinza volante. Por sua vez, Zhang et al. (2018) também observaram uma expressiva redução da resistência à compressão de geopolímeros a base de cinza volante expostos a lixiviação e à formação de eflorescência. De acordo com os autores, não é observada mudança estrutural do geopolímero perante formação de eflorescência, no entanto, o efeito físico decorrente da formação de cristais nos poros e tensões internas reduz o desempenho do material. Os diferentes resultados observados nas pesquisas citadas indicam a complexidade da avaliação de tais propriedades. A única propriedade mecânica avaliada geralmente em pesquisas é a resistência à compressão, no entanto, a resistência à tração e/ou flexão também são propriedades importantes e que podem sofrer um efeito diferente devido ao seu mecanismo. Além disso, os trabalhos avaliados comumente identificam a manifestação patológica como eflorescência, porém, entende-se que a formação dessa eflorescência seja decorrente de diferentes fenômenos associados.

A disponibilidade de álcali se dá a partir da remoção dos mesmos da estrutura ou da porosidade, por isso, o primeiro fenômeno que pode ser identificado é a lixiviação. Associado a isso, em condições de umidade adequada, o CO_2 dissolvido e absorvido na porosidade no material e em contato com os álcalis disponíveis pode proporcionar um segundo fenômeno, identificado como carbonatação interna. Da mesma forma, em sistemas onde há uma maior movimentação dos álcalis, de modo a possibilitar a presença de grande parcela de álcalis livres na superfície, ocorre a cristalização de carbonatos. Segundo Zhang et al. (2018), essa formação se apresenta externamente (eflorescência) ou na primeira camada externado material (subflorescência). Por isso, a formação de eflorescência é o resultado final de diferentes fenômenos envolvidos, no entanto, ainda existem diversas lacunas sobre o entendimento de como cada etapa está associada a tal formação e seus efeitos. Sendo este mais um motivador deste trabalho.

Após a compreensão do mecanismo de formação de eflorescência, bem como identificação dos efeitos causados, é necessário controlar ou inibir esse fenômeno. Najafi et al. (2012) avaliaram o uso de pozolana natural como precursor e observaram que o uso de cura hidrotérmica e a adição do cimentos de elevado teor de alumina auxiliam na redução de eflorescência. O efeito benéfico da cura hidrotérmica é decorrente do acréscimo de reatividade do precursor a partir da

introdução de uma fonte adicional de temperatura. Já a adição de uma fonte suplementar de alumínio aumentou a extensão de ligações moleculares no ligante e reduziu a mobilidade dos álcalis. Como já observado por Zhang et al. (2014), a formação de eflorescência está também relacionada com a estrutura porosa do geopolímero. Desse modo, a mitigação da eflorescência pode ser obtida a partir da redução da quantidade de álcalis livres na estrutura a partir da redução de mobilidade dos mesmos. Para isso, primeiramente é necessário compreender como a dosagem dos materiais altera a porosidade e a estabilidade dos álcalis do geopolímero. Além disso, também é necessário compreender como adições binárias entre precursores, ou uso de aditivos químicos pode inibir o processo de movimentação ou lixiviação destes álcalis.

Apesar da valiosa contribuição dos trabalhos citados, muitos fatores necessitam de uma maior compreensão, podendo-se citar que o uso de metacaulim como precursor não foi avaliado perante sua susceptibilidade a formação de eflorescência. Logo, esse trabalho busca agregar contribuições a essa lacuna de conhecimento relacionada à durabilidade perante a formação de eflorescência em geopolímeros a base argila calcinada, nesse caso o metacaulim.

Segundo Zhang et al. (2014), em sistemas que o precursor é a base de aluminossilicato com reduzida parcela de cálcio, como é o caso das argilas calcinadas, observa-se a maior lixiviação de álcalis e isso se deve inicialmente ao tipo de estrutura formada, onde a porosidade será maior que em sistemas com Ca^{+} como precursor. Destaca-se por fim a importância deste estudo, visto a crescente demanda da utilização de argilas calcinadas como precursores para geopolímeros.

1.3 ORIGINALIDADE

A originalidade deste trabalho está em analisar a formação de eflorescência em geopolímeros com o uso de metacaulim de elevada pureza como precursor. Do mesmo modo, será uma pesquisa que avalia a eflorescência desde os mecanismos básicos de formação, efeitos associados a tal formação, até a identificação de meios para mitigar tal formação. Trabalhos anteriores avaliam fatores isolados e com uso de precursores distintos, de modo que a utilização de um material de elevada pureza ao longo de todas as fases do trabalho possibilita a compreensão mais ampla do fenômeno. Além disso, a avaliação da influência de cada um dos critérios de dosagem perante diferentes propriedades mecânicas e microestruturais quando expostos a diferentes condições de exposição, gera informações importantes para a compreensão do fenômeno de formação de eflorescência.

1.4 OBJETIVOS

O objetivo geral da pesquisa é avaliar os fatores que favorecem a formação de eflorescências, seus mecanismos, efeitos e modos de mitigar essa manifestação patológicas em geopolímeros a base de metacaulim como precursor.

Os objetivos secundários são:

a) avaliar o efeito das condições de ativação, principalmente concentração de ativação (teores de Na_2O), assim como características do ativador alcalino (mediante a presença de silicatos solúveis a partir do módulo de solução MS, que expressa a relação molar SiO_2/Na_2O exclusiva do ativador);

b) avaliar o efeito do incremento de temperatura durante a etapa de cura na formação da estrutura do geopolímero e como a matriz se comporta frente a formação de eflorescências;

c) avaliar o efeito do tipo e natureza do ativador a partir da incorporação de potássio (K) em substituição parcial ao sódio (Na) na solução alcalina;

d) avaliar a relação entre resistência mecânica, porosidade das misturas frente a lixiviação e a formação de eflorescência;

e) avaliar a influência do teor de gel formado diferentes graus de reatividade a partir de diferentes teores de ativação, perante o teor de gel formado e relacionar com a formação de eflorescência;

f) otimizar o procedimento de ensaio acelerado para identificar a formação de eflorescências;

g) avaliar o efeito da lixiviação de álcalis na estrutura molecular dos geopolímeros e relacionar com o comportamento mecânico;

h) verificar a ocorrência de formação de cristais de carbonato nos poros e seu efeito associado a geração de tensões internas;

i) avaliar o efeito da formação de eflorescência em escala nano/microestrutural;

j) relacionar os mecanismos isolados de lixiviação, carbonatação interna e cristalização externa com o mecanismo identificado como formação de eflorescência;

k) propor, a partir das dosagens utilizadas e de combinações binárias, maneiras de minimizar a formação de eflorescência.

1.5 DELIMITAÇÕES

A partir dos materiais produzidos e utilizados, algumas delimitações são impostas, a fim de direcionar o estudo aos objetivos propostos e possibilitar uma análise mais efetiva.

a) o metacaulim será utilizado como precursor;

b) hidróxidos de sódio e potássio (PA) e silicato de sódio comercial serão utilizados como ativadores;

c) os teores relacionados à ativação foram definidos tendo como base trabalhos anteriormente realizados (LONGHI, 2015) e a partir de dados de revisão bibliográfica.

1.6 PREMISSA

Tem-se como premissa que todos os materiais utilizados, sejam eles produzidos em laboratório ou comerciais, apresentam as mesmas características e propriedades ao longo do desenvolvimento de todo o trabalho.

REFERÊNCIAS

ARBI, Kamel et al. A Review on the Durability of Alkali-Activated Fly Ash / Slag Systems : Advances , Issues , and Perspectives. **Ind. Eng. Chem. Res.**, v. 55, p. 5439–5453, 2016.

BARATA, M. S.; ANGÉLICA, R. S. Caracterização dos resíduos cauliníticos das indústrias de mineração de caulim da amazônia como matéria-prima para produção de pozolanas de alta reatividade (Characterization of kaolin wastes from kaolin mining industry. **Cerâmica**, v. 58, p. 36–42, 2012.

BERNAL, Susan A. et al. Management and valorisation of wastes through use in producing alkali-activated cement materials. **Journal of Chemical Technology and Biotechnology**, 2016.

BERNAL, Susan A. Microstructural Changes Induced by CO2 Exposure in Alkali-Activated Slag/Metakaolin Pastes. **Frontiers in Materials**, [s. l.], v. 3, n. September, p. 1–10, 2016.

BUCHWALD, Anja et al. Purdocement: application of alkali-activated slag cement in Belgium in the 1950s. **Materials and Structures**, 2013.

CRIADO, M.; FERNÁNDEZ-JIMÉNEZ, A.; PALOMO, A. Alkali activation of fly ash: Effect of the SiO2/Na2O ratio. **Microporous and Mesoporous Materials**, v. 106, n. 1–3, p. 180–191, 2007.

CRIADO, M.; PALOMO, A.; FERNANDEZ-JIMENEZ, A. Alkali activation of fly ashes . Part 1 : Effect of curing conditions on the carbonation of the reaction products. v. 84, p. 2048–2054, 2005.

CRISTIANE, Kelly et al. Activation Alkaline Waste Kaolin for Fabrication of Building Blocks. n. June, 2012.

DAMTOFT, J. S. et al. Sustainable development and climate change initiatives. **Cement and Concrete Research**, v. 38, n. 2, p. 115–127, 2008.

DAVIDOVITS, Joseph. Geopolymers: Inorganic polymeric new materials. **Journal of thermal analysis**, v. 37, n. 8, p. 1633–1656, 1991.

DOW, C.; GLASSER, F. P. Calcium carbonate efflorescence on Portland cement and building materials. **Cement and Concrete Research**, v. 33, n. 1, p. 147–154, 2003.

DUXSON, P. et al. Geopolymer technology: the current state of the art. **Journal of Materials Science**, v. 42, n. 9, p. 2917–2933, 2006.

DUXSON, Peter et al. The role of inorganic polymer technology in the development of ‘green concrete’. **Cement and Concrete Research**, v. 37, n. 12, p. 1590–1597, 2007.

DUXSON, Peter; PROVIS, JL Jhon L. Designing precursors for geopolymer cements. **Journal of the American Ceramic Society**, v. 91, n. 12, p. 3864–3869, 2008.

FROENER, Muriel. **Valorização de Cinza de Fundo por meio da sintese de ligantes geopoliméricos: Otimiação de traços em pastas e avaliação dos sistemas em argamassa**. 2016. 2016.

GAO, Kang et al. Effects SiO2/Na2O molar ratio on mechanical properties and the microstructure of nano-SiO2 metakaolin-based geopolymers. **Construction and Building Materials**, v. 53, p. 503–510, 2014.

GARTNER, Ellis M.; MACPHEE, Donald E. A physico-chemical basis for novel cementitious binders. **Cement and Concrete Research**, v. 41, n. 7, p. 736–749, 2011.

GRANIZO, N.; PALOMO, A.; FERNANDEZ-JIMENEZ, A. Effect of temperature and alkaline concentration on metakaolin leaching kinetics. **Ceramics International**, v. 40, n. 7, p. 8975–8985, 2014.

IEA; WORLD BUSINESS COUNCIL FOR SUSTAINABLE DEVELOPMENT (WBCSD).; INTENATIONAL_ENERGY_AGENCY_(IEA). Cement Technology Roadmap 2009 Carbon emissions reductions up to 2050. . 2009, p. 26.

IPCC. **Chapter 10 Industry, In "Intergovernamental panel on climate change)**Berlin, 2014.

JUENGER, M. C. G. et al. Advances in alternative cementitious binders. **Cement and Concrete Research**, v. 41, n. 12, p. 1232–1243, 2011.

LONGHI, Márlon et al. Geopolymers based on calcined kaolin sludge/ bottom ash blendsandan alternative sodium silicate activator. In: 34TH CEMENT AND CONCRETE SCIENCE CONFERENCE 2014, Sheffield. United Kingdom. **Anais**. Sheffield. United Kingdom

LONGHI, Márlon A. Málon A. M. A. et al. Valorisation of a kaolin mining waste for the production of geopolymers. **Journal of Cleaner Production**, v. 115, 2016.

LONGHI, Marlon Augusto Márlon Augusto. **Álcali-ativação de lodo de caulim calcinado e cinza pesada com ativadores convencionais e silicato de sódio alternativo**. 2015. Universidade Federal do Rio Grande do Sul, Porto Alegre, 2015.

MOLIN, Dal et al. Cinzas volantes álcali-ativadas com solução combinada de NaOH e Ca (OH)2. p. 462–469, 2007.

MÜLLER, N.; HARNISCH, J. A blueprint for a climate friendly cement industry. **Report for the WWF–Lafarge Conservation Partnership.**, 2008.

NAJAFI, Ebrahim; ALLAHVERDI, Ali; PROVIS, John L. Efflorescence control in geopolymer binders based on natural pozzolan.pdf. v. 34, p. 25–33, 2012.

PROVIS, John L.; BERNAL, Susan a. Geopolymers and Related Alkali-Activated Materials. **Annual Review of Materials Research**, v. 44, n. 1, p. 140205180727009, 2014.

SCRIVENER, Karen L.; JOHN, Vanderley M.; GARTNER, Ellis M. **Eco-efficient cements: Potential economically viable solutions for a low-CO 2 cement-based materials industryUnited Nations Environment Programme**. Paris.

SCRIVENER, Karen L.; KIRKPATRICK, R. James. Innovation in use and research on cementitious material. **Cement and Concrete Research**, v. 38, n. 2, p. 128–136, 2008.

SCRIVENER, Karen L.; NONAT, André. Hydration of cementitious materials, present and future. **Cement and Concrete Research**, v. 41, n. 7, p. 651–665, 2011.

SHI, Caijun; JIMÉNEZ, A. Fernández; PALOMO, Angel. New cements for the 21st century: The pursuit of an alternative to Portland cement. **Cement and Concrete Research**, v. 41, n. 7, p. 750–763, 2011.

SHI, Caijun; KRIVENKO, Pavel; ROY, Della. **Alkali-activated Cement and concretes**. 1. ed. New York: Taylor & Francis, 2006.

ŠKVÁRA, František et al. Aluminosilicate polymers - Influence of elevated temperatures, efflorescence. **Ceramics - Silikaty**, v. 53, n. 4, p. 276–282, 2009.

ŠKVÁRA, František et al. A weak alkali bond in (N, K)-A-S-H gels: Evidence from leaching and modeling. **Ceramics - Silikaty**, v. 56, n. 4, p. 374–382, 2012.

VAN DEVENTER, Jannie S. J.; PROVIS, John L.; DUXSON, Peter. Technical and commercial progress in the adoption of geopolymer cement. **Minerals Engineering**, v. 29, p. 89–104, 2012.

YAO, Xiao et al. Geopolymerization process of alkali-metakaolinite characterized by isothermal calorimetry. **Thermochimica Acta**, v. 493, p. 49–54, 2009.

ZHANG, Zuhua et al. Quantitative kinetic and structural analysis of geopolymers. Part 1. The activation of metakaolin with sodium hydroxide. **Thermochimica Acta**, v. 539, p. 23–33, 2012.

ZHANG, Zuhua et al. Quantitative kinetic and structural analysis of geopolymers. Part 2. Thermodynamics of sodium silicate activation of metakaolin. **Thermochimica Acta**, v. 565, p. 163–171, 2013.

ZHANG, Zuhua et al. Fly ash-based geopolymers: The relationship between composition, pore structure and efflorescence. **Cement and Concrete Research**, v. 64, p. 30–41, 2014.

ZHANG, Zuhua et al. Efflorescence and subflorescence induced microstructural and mechanical evolution in fly ash-based geopolymers. **Cement and Concrete Composites**, v. 92, n. March, p. 165–177, 2018.

2 ESTRUTURA DA PESQUISA

O trabalho foi organizado em capítulos, onde cada um deles é composto por um artigo publicado ou submetido em periódicos internacionais. No capítulo antecedente (capítulo 1) foi apresentada uma breve introdução à tecnologia dos geopolímeros, com contextualização da pesquisa em relação ao fenômeno de eflorescência e uma análise dos trabalhos anteriores realizados para situar a pesquisa nas lacunas de conhecimentos. Além disso, os objetivos, delimitações e limitações foram apresentados a fim de direcionar o desenvolvimento da pesquisa. Já a estrutura da pesquisa é apresentada nesse capítulo para facilitar o entendimento do desenvolvimento da pesquisa.

Após os dois capítulos iniciais, são apresentados os capítulos específicos. De modo geral, o desenvolvimento da tese foi dividido em 5 tópicos de pesquisa. O primeiro é decorrente da revisão do estado da arte sobre o assunto, com apresentação de hipótese/teoria sobre o processo de formação de eflorescência. O segundo e o terceiro sobre os mecanismos de formação da eflorescência, o quarto sobre efeitos da eflorescência em diversas situações e o quinto sobre formas de mitigar a eflorescência. A Figura 3 apresenta a estrutura organizacional da pesquisa, onde é exposto o título de cada artigo/capítulo, e na sequência é descrito o seu conteúdo.

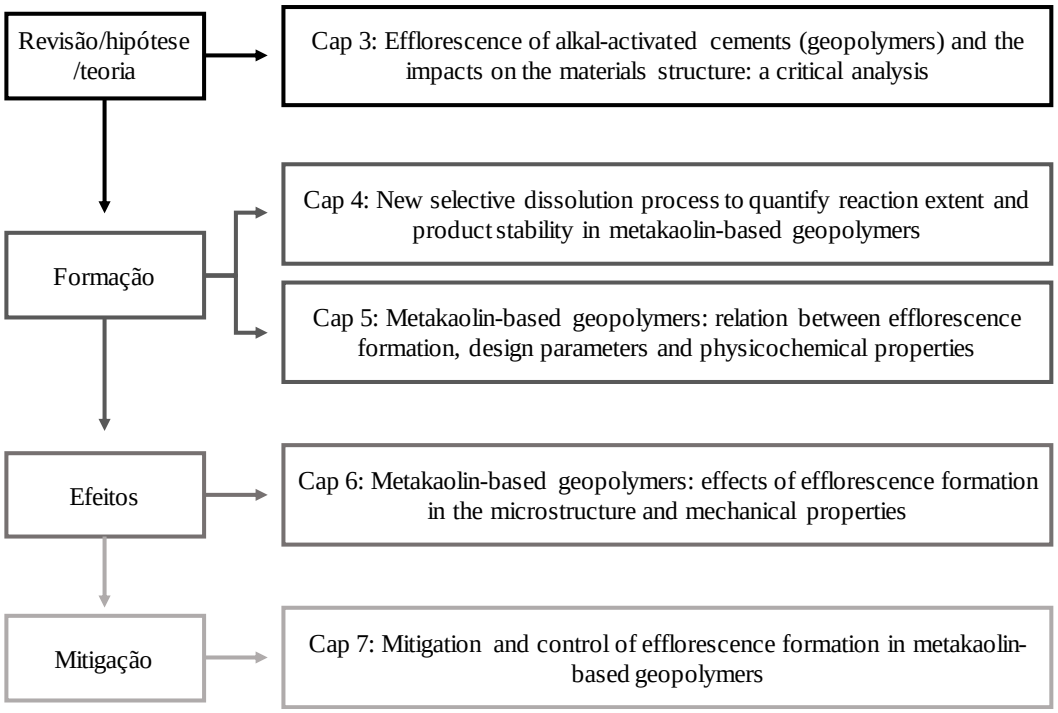

Figura 3 - estrutura organizacional dos capítulos do trabalho

O capítulo 3 apresenta uma extensa revisão do estado arte sobre a formação da eflorescência em geopolímeros e os mecanismos que compõem este fenômeno que são de conhecimento até o momento. Devido a reduzida quantidade de trabalhos divulgados nesta área específica e considerando a elevada produção de pesquisas dos grupos da Universidade Federal do Rio Grande do Sul (UFRGS) e da University of Southearn Queenland (USQ), estes foram apresentados juntamente com dados de revisão bibliográfica. Com isso, a partir das proposições feitas durante a etapa de estudo da bibliografia, associada a fenômenos e mecanismos já observados. O capítulo foi organizado em formato de artigo de revisão com hipótese e teoria, e foi publicado no periódico Frontiers in Materials.

No capítulo 4, é avaliado o processo de formação da eflorescência frente aos parâmetros de dosagem e cura, identificando a parcela de gel produzido e a estabilidade dos materiais. Estas características foram correlacionadas com as propriedades microestruturais e mecânicas dos geopolímeros analisados. Foram produzidas 15 misturas com propriedades diferentes, obtidas a partir de diferentes parâmetros de dosagem. Além disso, foi desenvolvido um novo método de dissolução seletiva que viabilizou a quantificação e identificação das parcelas de precursor não reagido, do gel formado e de materiais solúveis. A partir da dissolução dos elementos durante o processo de dissolução seletiva, foi identificada a predominância de álcalis solúveis, os quais são um dos responsáveis pelo processo de formação de eflorescência. Análises químicas e microestruturais como difração de raios X (DRX/XRD), fluorescência de raios X (FRX/XRF), ressonância nuclear magnética (RNM/MAS NMR), espectroscopia de infravermelho com transformada de Fourier (FTIR) e microscopia eletrônica de varredura (MEV/SEM) foram utilizadas para avaliar aspectos microestruturais dos materiais. Além da quantificação das diferentes fases presentes nos geopolímeros, essa etapa da pesquisa buscou um maior entendimento sobre a estabilidade dos álcalis e a microestrutura do gel. A Figura 4 ilustra as combinações e análises que foram realizadas. O objetivo desse capítulo foi determinar o teor de precursor não reagido, gel formado e materiais solúveis, relacionar essas proporções com a propriedades mecânicas e microestruturais e entender a estabilidade do sódio na estrutura do gel. O artigo resultante desse capítulo foi publicado o periódico Composites Part B e se encontra disponível online.

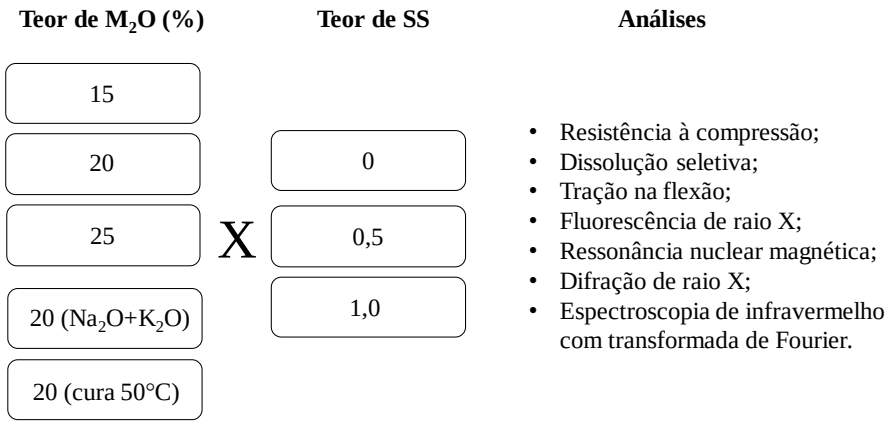

Figura 4 - organograma das combinações e análises realizadas no capítulo 4

A identificação do teor de materiais solúveis em geopolímeros, principalmente álcalis, indica o potencial de eflorescência. Por isso, no capítulo 5, a partir das informações sobre a solubilidade dos materiais, a formação da eflorescência foi avaliada e relacionada com propriedades mecânicas e físicas, as quais são dependentes dos parâmetros de ativação. O objetivo dessa etapa foi compreender a relação entre a dosagem dos materiais com as propriedades físico-mecânicas e como isso altera o processo de formação de eflorescência e produtos formados durante tal processo. O método experimental foi composto por uma análise visual ao longo do tempo, pela DRX dos produtos formados, pela mensuração de álcalis lixiviados a partir do pH e por análises de espectroscopia de absorção atômica (AAS), absorção de água, porosimetria por intrusão de mercúrio, densidade e por análises químicas do gel formado como DRX, FTIR e SEM. A Figura 5 ilustra as combinações e análises que foram realizadas. O artigo resultante desse capítulo foi publicado o periódico Composites Part B e se encontra disponível online.

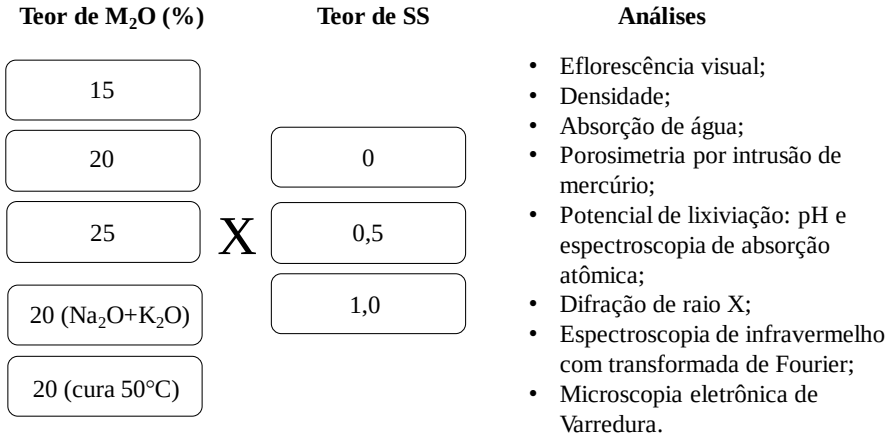

Figura 5 - organograma das combinações e análises realizadas no capítulo 5

A partir dos estudos citados anteriormente, foi observado que a formação excessiva de eflorescência bem como o processo de lixiviação pode gerar a degradação superficial e

possivelmente a redução do desempenho em geopolímeros. No entanto, para uma compreensão mais ampla sobre o fenômeno, foi necessário compreender como as propriedades físico-mecânicas, associadas ao grau de formação de eflorescência e as diferentes condições de exposição podem influenciar as propriedades mecânicas e microestruturais. Por isso, esses fatores foram avaliadas no capítulo 6. Entende-se que a formação de eflorescência é decorrente dos processos de lixiviação, carbonatação interna e carbonatação externa (subflorescência e eflorescência). Para isso, cinco geopolímeros com composições diferentes foram submetidos a quatro meios de exposição, sendo um deles de controle (sem contato com o ar) e outros três para favorecer a formação de diferentes fenômenos, entre eles a exposição à água na base, para formação de eflorescência, em contato com o ar para carbonatação e submerso em água para favorecer o processo de lixiviação do álcalis. Cada uma das exposições associadas causa efeitos diferentes nos geopolímeros. Foram avaliadas propriedades mecânicas como resistência à compressão, tração diametral, tração na flexão e deformação linear. Propriedades microestruturais e nanoestruturais como DRX, NMR, MEV e microtomografia também foram avaliadas para auxiliar na compreensão dos fenômenos observados. A Figura 6 ilustra as combinações e análises que foram realizadas. O objetivo desse capítulo foi compreender como os diferentes meios de exposição podem influenciar na formação de eflorescência, na propriedade mecânica e microestrutural do geopolímero exposto.

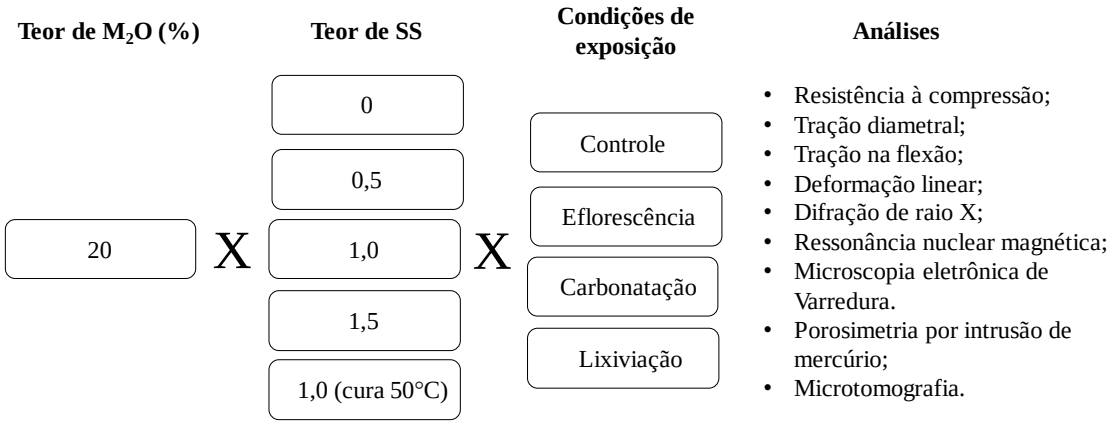

Figura 6 - organograma das combinações e análises realizadas no capítulo 6

Com o entendimento do processo de formação de eflorescência bem como seus efeitos e mecanismos de deterioração, buscou-se modos de minimizar a ocorrência de tais fenômenos. No capítulo 7, diferentes materiais, associados à melhoria de algumas propriedades foram avaliados com o objetivo de otimizar a estrutura porosa dos geopolímeros e reduzir a lixiviação dos álcalis a fim de proporcionar a redução da formação de eflorescência. Nas etapas anteriores,

observou-se que a adição de silicato solúvel no ativador proporcionou a redução na porosidade dos geopolímeros, bem como uma menor lixiviação dos álcalis, desse modo, a adição de elevados teores de silicato de sódio no ativador ou sílica ativa e cinza volante como parcela do ativador foram avaliadas. Do mesmo modo, a adição de uma fonte de óxido de cálcio ou alumínio pode alterar o gel formado e influenciar na estabilidade dos álcalis. Desta forma, foi avaliada a adição de pequenos teores de escória de alto forno e cimento aluminato de cálcio. Além disso, conforme identificando nos capítulos iniciais, materiais mais densos e menos permeáveis são menos suscetíveis à formação de eflorescência, por isso, buscou-se otimizar essa a estrutura porosa a partir do uso de um aditivo cristalizante e do uso de óleo silicoso em baixos teores de adição. A avaliação da efetividade dos diferentes métodos propostos para a mitigação da eflorescência foi realizada de modo visual sendo estas relacionadas com propriedades físicas como resistência à compressão e absorção de água. Análises químicas como lixiviação dos álcalis por absorção atômica (AAS), XRD e NMR também foram realizadas para correlacionar os resultados físico-mecânico com a microestrutura e produtos formados. A Figura 7 ilustra as combinações e análises que foram realizadas. O objetivo desse capítulo foi identificar de mitigar a formação de eflorescência.

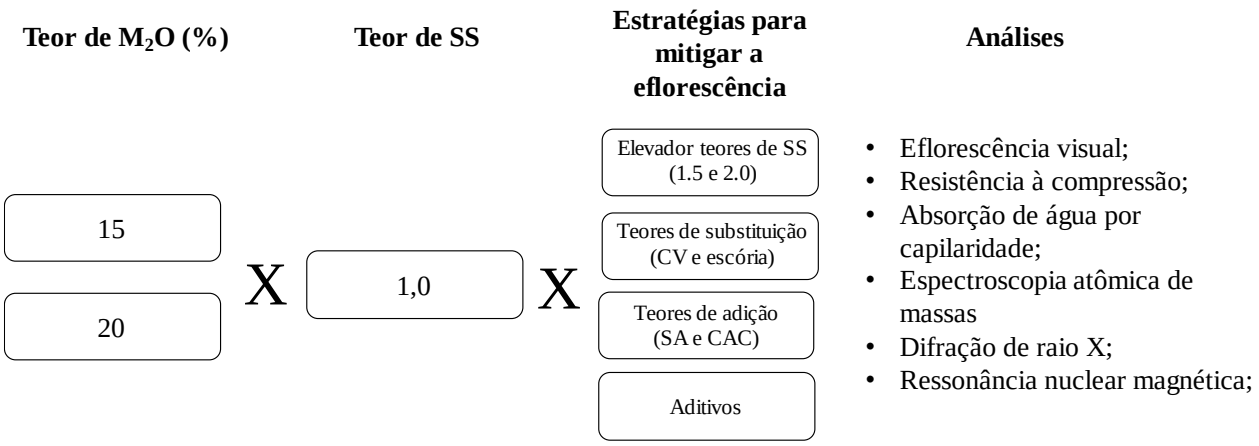

Figura 7 - Fluxograma das combinações e análises realizadas no capítulo 7

3 EFFLORESCENCE OF ALKALI-ACTIVATED CEMENTS (GEOPOLYMERS) AND THE IMPACTS ON MATERIAL STRUCTURES: A CRITICAL ANALYSIS[a]

3.1. INTRODUCTION

Alkali-activated cements (AACs), also broadly termed as geopolymers (mainly for those systems with low content of calcium), have been extensively studied in the past 40 years due to the potential in the development of 'green alternatives' to Portland cement (PC). The formation of geopolymers uses alkalis such as sodium hydroxide, silicate and/or carbonate to activate aluminosilicates precursors usually heated clays, fly ash and slag, at room or elevated temperatures. The environmental benefit of applying AAC technology mainly lies in the reduction of CO_2 emissions and energy consumption, which are issues of wide concern for the Sustainable development of the present cement and concrete industries (DAMTOFT et al. 2008). McLellan et al. (2011) pointed out that the unit emissions of greenhouse gas in making geopolymer binder depend on the location of source materials, the energy source and the mode of transport. The counting of the four mixtures using typical Australian fly ashes indicated potential for a 44–64% reduction in greenhouse gas emissions. Heath et al. (2014) showed that geopolymer manufacture can reduce CO_2 emissions by about 40% when clay minerals are used to replace fly ash and slag. In terms of weight, the manufacture of 1 $m^3$of C25 (compressive strength of 25 MPa at 28 days) geopolymer concrete can reduce 154 kg of CO_2 emissions compared to using PC. This reduction will increase at higher strength design (40 MPa geopolymer concrete reduces 220kg of CO_2). The increasement of the environmental impact can be related to the composition of the alkali-activator, where soluble silicate (such as sodium silicate) is the highest contributor. More recently Passuelo et al. (2017), using a Brazilian calcined clay as precursor and a rice husk ash as part of activator, reported that, per unit of compressive strength, the right design of material can provide a 50-75% reduction of CO_2 emissions. These have been one of the main forces driving the current research and industrial development of geopolymers.

[a] O capítulo já está publicado em formato de artigo e pode ser acessado pelo DOI: 10.3389/fmats.2019.00089

Although the total volume of geopolymer concretes is negligible compared to OPC concretes, there has been rapid growth in the construction of demonstrative structures and buildings in the past decade because of increasing scientific research and environmental driving (PROVIS et al. 2014). Notable examples are the 33 full-scale geopolymer concrete beams installed in the Global Change Institute building at University of Queensland and the flooring of 40,000 m^3geopolymer concrete at Wellcamp airport, Queensland, Australia. From the challenges in supplying consistent raw materials and the cost issues, there are still a variety of technical and political barriers remaining, either unclear or un-solved (VAN DEVENTER et al. 2012). Efflorescence is one such problem which has been raised as a concern in some AAC formulations and this has been discussed briefly by Bernal et al. (BERNAL et al. 2014), systematically investigated by Zhang et al. (2014; 2018).

Looking back to efflorescence occurring in OPC based masonry and concrete, the most common phenomenon is related to the formation of calcium carbonate ($CaCO_3$) on the surface (DOW et al. 2003). To avoid and mitigate efflorescence, the first principle is to reduce the alkali concentration of cements and also to reduce the solubility and absorption rate of CO_2 from the ambient environment (DOW et al. 2003). However, in AAC systems, the concentrations of Na and K in pore solution usually contain much higher soluble alkali metal concentrations than conventional OPC based materials. Burciaga-Díaz et al. (2010) mentioned that alkali-activated slag based materials show significant efflorescence and some have also shown negative impacts on the mechanical properties. It must be noted that alkali-activated slag contains higher concentration of calcium than alkali-activated metakaolin and fly ash systems, and this may lead to certain differences in the specific effects in the development of efflorescence. Škvára et al. (2012) assessed a set of fly ash-based geopolymers, where the acceptable workability and compressive strength above 40 MPa were achieved at a thermal curing (>50°C) and an alkali content of 30 to 150 g/kg, expressed as Na_2O to total mass of paste. These values are up to 42 times higher than in Portland cement paste (assuming 0.5% Na_2O in cement and w/c = 0.4 for paste). Therefore, this raises attention to the efflorescence issue in the application of AAC.

In literature and in the previous research done by these authors, a set of AAC mixtures developed efflorescence rapidly on drying surfaces when samples were in contact with water and under highly humid atmosphere conditions. A number of factors have been reported to affect the extent of efflorescence in AAC: alkali metal type (ŠKVÁRA et al. 2012; ŠKVÁRA et al. 2009), raw materials (ZHANG et al. 2018; TEMUUJIN et al. 2011; KANI et al. 2012)

and reaction conditions (ZHANG et al. 2014; BURCIAGA-DÍAZ et al. 2010; KANI et al. 2012). However there still a lack of consensus when related to the mechanisms of reaction and formation, relationship between activator and reactivity, micro- and macro-structural impact of efflorescence and effective ways to mitigate.

Thus, the aim of this paper is to re-examine the results found in literature and complement the literature analysis with some ongoing experiments. The role of alkalis in AAC (low calcium systems) and the effect of alkali concentration on efflorescence are discussed. Particular interests are given to the different efflorescence behaviours of AACs that were prepared with fly ashes derived from different power stations as well as calcined rich kaolinite clays. The importance of this issue is highlighted by the observations of the microstructural and mechanical properties of AACs that are subjected to efflorescence. The analyses and suggestions made here are based on the understanding of the effect of the curing scheme, design parameters and reaction process of ACC, which is further related to reactivity.

3.2. EFFLORESCENCE IN PC CONCRETE

In Portland cement hydration process, the main constituents, the silicates C_2S (belite) and C_3S (alite) react with water to form the calcium silicate hydrates (C-S-H) and calcium hydroxide (CH, also named as portlandite). The CH is responsible for maintaining the high pH of concrete which plays an important role in the compatibility between concrete and steel for reinforced concrete structures (GALLUCCI et al. 2007). The alkalis in PC concrete are generated into the system by the hydration reaction of anhydrous components, including clinkers and supplementary cementitious materials (SCMs). SCMs are normally used as addition or substitution of cement (or clinker) to consume the content of $Ca(OH)_2$ and produce C-S-H via pozzolanic reaction. On the other hand, the presence of CH within the concrete can promote its leaching, where part of this compound migrate to the surface and precipitate in contact with CO_2, forming a carbonate product as efflorescence. Other phenomena that can be developed is the internal crystallization due to the migration of soluble CO_2 from the environment into the matrix. The reaction of CO_2 with CH starts instantly and leads to formation of calcium carbonate (ZHANG et al., 2017) (CIZER, et al., 2012), further, other calcium phases are susceptible to carbonation (GALLUCCI et al. 2007) (GARCIA-GONZÁLEZ et al. 2006).

To understand the process related to the formation of whitish products, mainly efflorescence products, a model was proposed for Dow and Glasser (2003). According to the authors, efflorescence involves six basic and synergetic stages: dissolution of CO_2 (g) in H_2O at air-water interface on the surface of products, conversion of CO_2 to aqueous species, release of alkali(s), dissolution of $Ca(OH)_2$, diffusion of reactants through solution and precipitation of calcium carbonate, as showed in Figure 8.

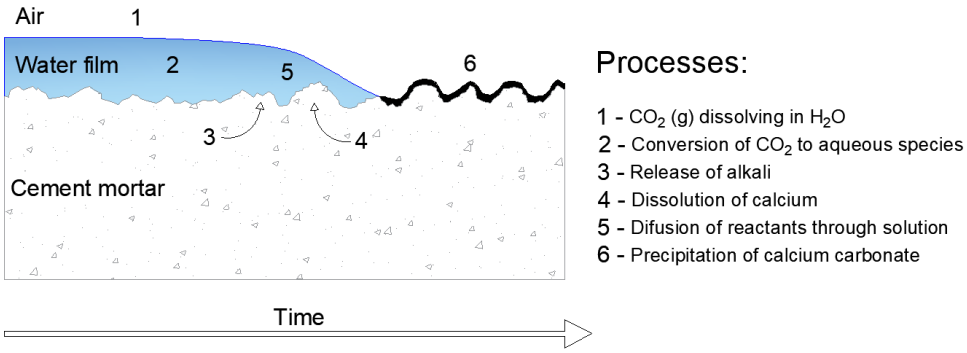

Fig.8 – Schematic process diagram for the formation of efflorescence. Adapted from Dow and Glasser **(Dow, et al., 2003)**

According to the authors, in the first and second stages, the presence of other source of alkali such as NaOH or KOH may increase the dissolution of CO_2 and its absorption in the sample. It is related to the abundance of OH^- group in a high pH solution, which increases the reaction to form H_2CO_3. In other hand, dissolved $Ca(OH)_2$, cannot increase the solubility, due the insolubility of $CaCO_3$. In the third and fourth stages, the leaching of alkalis occurs, the main source is the cement itself. The content of $Ca(OH)_2$ is dependent on other factors as the type of cement, the use of SCMs, as well as the time of curing. Porosity is an important factor, according to Zhang et al. (2014), while the reaction processes, the transport paths become longer if the matrix becomes more porous. The fifth stage is related to the diffusion, which is dependent on factors as the pH of the pore solution and the speciation of CO_2 adjusts to a new equilibrium amongst $(CO)_2$ (aqueous), H_2CO_3 and CO_3^{2-} and then incorporated to the stages 1 and 2 and dissolved Ca^+ species. The final stage is related to the precipitation of $CaCO_3$ species.

The efflorescence in PC is usually observed in recent constructions and is not normally damaging, but, aesthetically undesirable (DOW et al. 2003). However, it is necessary to evaluate the effect by the leaching process and the pore structure of the material, because this process can increase the porosity and accelerate the leaching. As efflorescence is a natural process, the material is exposed to evaporation. According to Dow and Glasser (2003), the efflorescence cycle can be interrupted by loss of liquid film by evaporation, perhaps combined

with suction into porous material. During evaporation, the storage capacity of pure water for CO_2 is sufficiently low and the formation of efflorescence by complete evaporation makes negligible contribution to efflorescence relative to steady-state transportation. However, the concentrations of NaOH or KOH can increase the storage of CO_2. With this, even with evaporation, the content of CO_2 can increase during the wet/dry cycles. The efflorescence cycle can restart by reestablishment of a water film. The precipitated products may, depending on permeability and content of leachable alkalis, affect the reaction kinetics.

On other hand, internal carbonation also induces a neutralizing effect to the highly alkaline environment provided by PC hydration (which in healthy/normal conditions show a pH above 13 in pore solution), thereby increasing the vulnerability of embedded reinforcing steel to corrosion (ZHANG et al. 2017). Internally, the effect is relative to crystallization process. According to Savija and Lukovic (2016) there are two types of carbonation process, (1) passive process when the carbonation causes unwanted and unplanned changes in the surface layer of a concrete structure or an element when exposed to the environment as pH drop, porosity changes, mechanical changes and cracking. However (2) active carbonation assumes controlled exposure of cementitious materials to elevated CO_2 concentrations for certain periods of time, resulting in benefits in terms of mechanical performance or environmental impact of the material. The first one is attributed to deterioration and the second one to utilization. With this, it is evident that the process of carbonation and efflorescence is a complex subject even for PC-based materials, which have a great deal of related research. In fact, besides the reaction between CO_2, water, calcium and alkalis, efflorescence may also involve the reaction with cations sucked from the base of concrete embedded in saline soils and environment. This is a broad issue occurs in many ageing constructions.

3.3. ROLE OF ALKALIS IN AACs

When related to PC, ACCs present some peculiarities and differences in production process, raw material and reactions. AAC formation is a reaction between two parts of materials: reactive aluminossilicate powder (precursor) with a high alkaline solution (activator). The precursor presents negligible or no reactivity with water, and therefore it makes necessary to introduce an alkali material to “activate” the precursor. It means that, the alkali placed in the system is necessary .The main reaction product of AAC is a disordered and highly reticulate structure named M-A-S-(H) gel (where M represents the alkali type, usually Na^+ or K^+) (Provis,

et al., 2005)(PROVIS; LUKEY; VAN DEVENTER, 2005b). The chemical process is well known as alkali activation for CaO-rich systems or geopolymerization for CaO-free systems. This gel is a three-dimensional alumino-silicate network configurated of SiO_4 and AlO_4 tetrahedrons by oxygen bridges with positive alkali ions to compensate the negative balance of Al in a Q^4 molecular coordination (PROVIS et al. 2005; FERNÁNDEZ-JIMENEZ et al. 2006). However, just part of the alkali is bounded to the structure, the other part remains in pores (PROVIS et al. 2014; SAN NICOLAS et al. 2015), as proposed by the model of Rowles et al. (ROWLES et al. 2007). According to the model, in a situation where there is sufficient amount of OH^-, Na^+ is bound superficially to the aluminate (Fig 9a). In situations where OH^- is not directly involved or accessible, Na^+ may associate with part of the silicon in the $SiO\text{-}(Na^+)\text{-}Si^-$ form. In this situation, the negative charge of the AlO_4 tetrahedron can be located on the bridge with the oxygen atom, where Si-O-Si consequently generates the ionic bond with Na^+ (Fig 9b). In fig 9c the model is fully represented, where in some points the ionic bonding with Na^+ occurs, but other part of this element remains free in the pores of the structure.

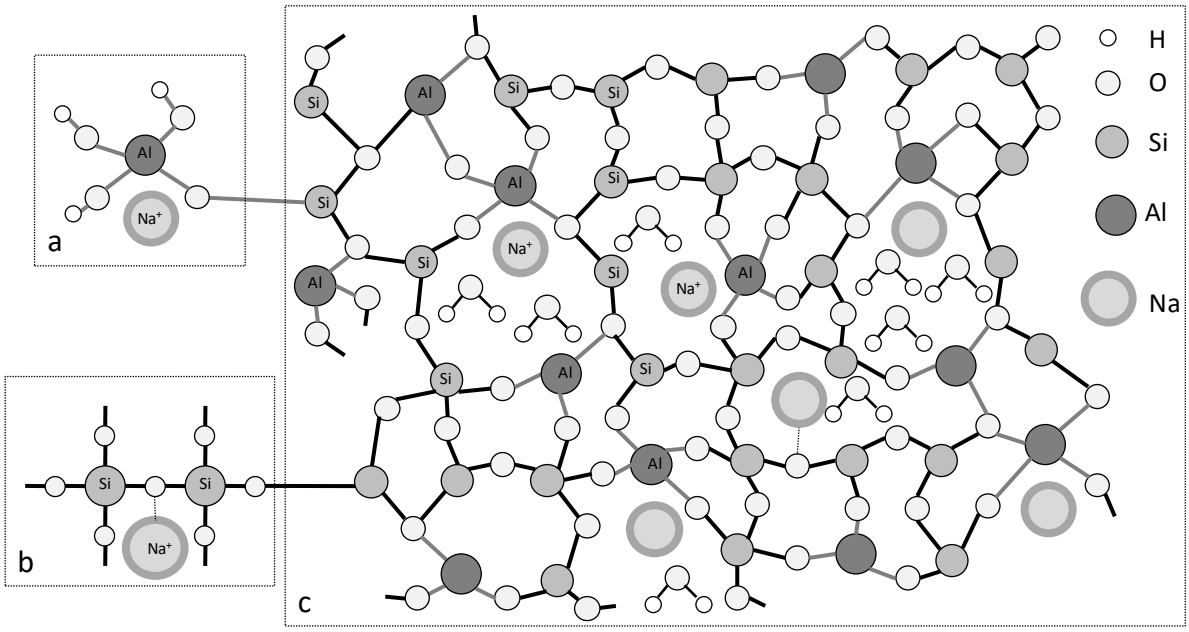

Fig. 9 – Schematical model for aluminossilicates inorganic polymers adapted from Rowles et al. (ROWLES, et al., 2007)

According to Duxson et al. (2005), sodium can be linked with aluminium inside the gel structure, located within the pore solutions, neutralizing the charge of $Al(OH)_4^-$ group. Thus, sodium can be partially Na-O-Al(Si) form in the gel structure, with a relatively stronger Na-O bond, and partially form $Na(H_2O)_n^+$, with a weakly Na^+ associated with molecular water. This is aligned with the leaching result and deconvolution of ^{23}Na MAS NMR spectra for alkali activated fly ash assessed by Fernández-Jiménez et al. (2006). If it is assumed that the Na-O in

gel structure is relatively more stable than in hydration conditions (contact with water molecules), similar to the Na-O in dehydrated zeolite, the soluble sodium must be limited, i.e. a certain fraction of sodium ions are not readily to be leached. Kani et al. (2012) grounded hardened AAC pastes and used stable leaching method at water to solid ratio of 20:1 to evaluate the leaching process. It was reported that after 24 h the leached alkalis were 1-7%, depending on the overall Si/Na and Na/Al molar ratios. Also, Zhang et al. (2014) crushed hardened alkali activated fly ash pastes (after 28 days of curing) into 1.25-1.5 mm particles. The authors used the stable leaching method at water/solid ratio of 25:1 and found that after 24 h the leached sodium was 12-16%, depending on the activator type, curing temperature and amount of slag (added as a substitute for fly ash). These results are in agreement with the above hypothesis.

Škvára et al. (2012) crushed hardened AAC pastes after 28 days of curing and obtained particles under the size of 0.5 mm and used the dynamic leaching method (regularly change leaching solution with fresh water) and found that the alkalis can be almost completely leached from the binder after 150 days. In comparison with zeolite leaching behavior (usually extremely slow in water content), it was concluded that the alkalis (Na^+ and K^+) were only weakly bonded in the form of $Na(H_2O)n^+$.

However, some controversy about the leaching process was reported. Lloyd et al. (2010) measured the alkali concentration in the extracted pore solutions of typical ACC with 7% of Na_2O provided from activator. If it is assumed that all of the sodium presents in the form of $Na(H_2O)_n^+$ in pore solution, the followed analyses can be deduced: assuming 100 g of binder, the pore water (free water) is 10 g and the structural water is 5 g, and the sodium concentration is estimated to be higher than 20000 mM. This value is far from the content identified by Lloyd et al. (2010), which were between 600 to 1600 mM for alkali activated fly ash systems. In fact, it is well known that the alkalis bound in zeolite frame structure may have different states, and each state has its own ion exchange capacity. Therefore, a new hypothesis is proposed here: the alkalis in AAC have different states (maybe more than the two as was discussed above), and each state has its own leaching rate. If the alkali is available in pores of the material or it is weakly bounded, and the pores allow the movement of those alkalis, depending on the intensity and direction of this movement, different phenomena may occur and will alter the integrity of the material.

3.4. EFFLORESCENCE OF AACs

During the last years of rapid development and application of AAC technology, the formation of depositions of material was observed on the surface of the samples. This was initially observed in laboratory conditions and later began to receive attention (BERNAL et al.,2014; ZHANG et al. 2014; ZHANG et al. 2018; ŠKVÁRA et al. 2009; KANI et al. 2012; YAO et al. 2015). This phenomenon is the result of a chemical reaction between free leached alkalis in porous structure with CO_2 in the aqueous form, where alkalis are the result of a physical leaching process, i.e. this only happens when alkalis are free to transport. With this, alkali leaching is relative to the amount of free cations and movement facility within the porous structure. These factors are dependent from synthesis conditions and the reacted products formed after the alkali-activation.

3.4.1 The relation between alkali leaching, design parameters and activation products

The first design parameter is related to precursor. The most used are fly ash, metakaolin and ground granulated blast-furnace slag (GGBFS). All of them have a specific chemical composition, with different oxides content, particle size and geometry, which changes the properties and features of the final reacted product. The reactivity has a wide behaviour due to an internal factor of the material that depends on its generation process. In this regard, particle size has an important function, since smaller particles have a larger specific surface area and consequently a higher initial reactivity. A more reactive material usually can provide a denser matrix, with less porosity. Systems with fly ash and metakaolin are known as low calcium while granulated blast furnace slag is known as high calcium precursor. In low calcium systems, the molar ratio SiO_2/Al_2O_3 is an important indicator of the initial reactivity and microstructural features of the gel formed. According to Criado et al. (2007), the Si-O bond is stronger than the Al-O bond, and this influences the precursor dissolution process, which result in an easier dissolution to precursor with higher content of Al_2O_3. This relation also alters the final product, that is Q^4 linked with different degrees of Al substitution (DUXSON et al. 2005). Relating this and Rowles et al (2007) model, more Al content is believed to result in the higher imprisonment of Na^+.

Precursor with high calcium content exhibits different behavior. Usually, this material needs less content of alkalis for its dissolution. Also, the gels formed are different from low calcium

gels. While low calcium presents the M-A-S-(H), high calcium systems presents gels calcium aluminosilicate hydrate (C-A-S-H). According to Provis and Bernal (2014) this type of products possess a disordered tobermorite structure in layers of coordinated silicon tetrahedral, where, the interlayer region contains Ca^{2+} cations, alkalis and the water chemically incorporated into their molecular structure. This is important to the alkali leaching because cations incorporated into the gel are less leachable in a system where water is also attached to the structure and does not work as a transport agent. Zhang et al. (2014) assessed the efflorescence in geopolymeric systems (free calcium AAC) activated by the use of NaOH and sodium silicate as activators, where a significant reduction of the means particle size and porosity with GGBFS addition was observed, reducing the susceptibility of efflorescence development. When slag is introduced in metakaolin or fly ash systems, the products may contain hydrotalcite-like phases, which have been proven to have ion binding properties. However, there is no report on this aspect, which deserves future insight study.

Besides the addition of slag, a certain amount of MgO in alkali-activated metakaolin-based geopolymers (ZHANG et al. 2010) and slag/fly ash-based geopolymers (SHEN et al. 2011) have shown benefits of reducing autogenous shrinkage and drying shrinkage. An experiment of adding MgO in ambient cured sodium silicate-activated fly ash-based geopolymers has been conducted to examine its effect on efflorescence. Figure 10 shows the appearance of sodium silicate-activated fly ash ACCs with different amounts of MgO. When MgO is used between 2-6%, the efflorescence behaviour does not show a consistent trend. After 2 weeks in contact with 2 mm-deep water at bottom and naturally drying at the ambient conditions (20±10° C, RH=50±20%), the control samples without MgO have sever efflorescence products formed on surface, while the samples with 2 and 6% MgO show more severe efflorescence, and the products formed under surface lead to enough crystallization stress to break the top surface of the sample. Interestingly, the sample with 4% MgO addition have slower and much less severe efflorescence. This behaviour indicates that efflorescence is a complex function of the raw materials, the minerals and the microstructure of the products. The risk of adding MgO in low calcium geopolymers must be considered.

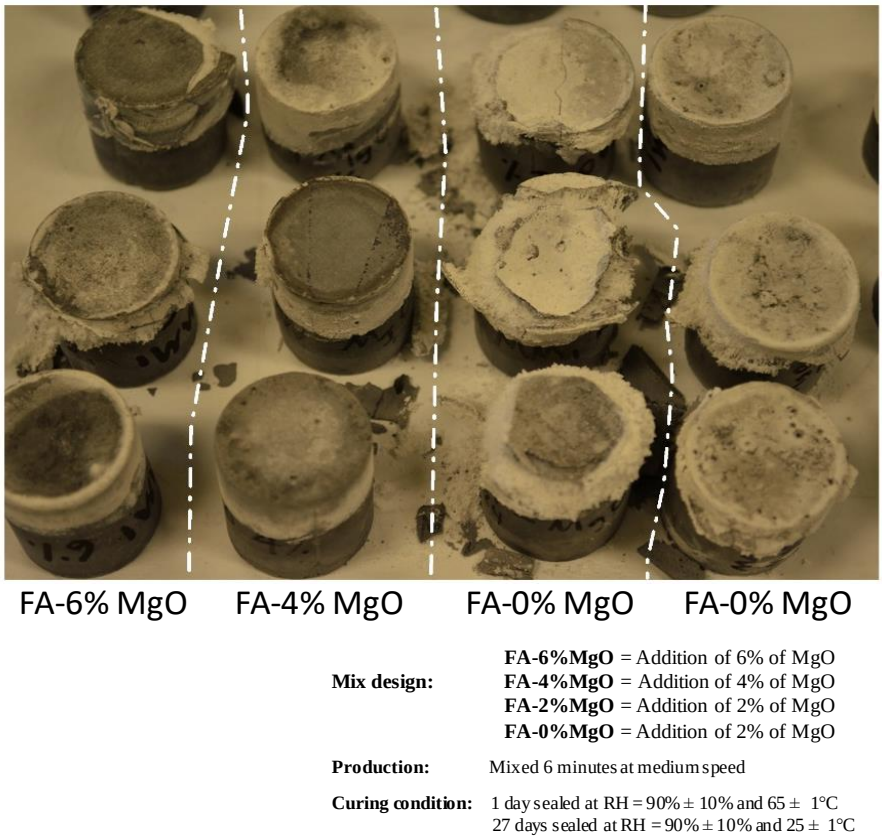

Fig. 10 – Efflorescence formation in fly ash AAC with different contents of external MgO

About the activators, the most usual are sodium and potassium in the form of hydroxide and silicate. Commonly both materials are used combinedly, and the addition of silicates increase the content of soluble silica in the activator, which enhance the compactness of matrix (ZHANG et al. 2013; LONGHI et al. 2016). As molar ratio to characterize the activation content, M_2O/Al_2O_3, represents the fraction between the activator oxide and the Al_2O_3 content of the precursor. This relationship is determined by the stoichiometric equilibrium, where in a fully reacted precursor, each Na^+ can connect with an $[AlO_4]^{5-}$, establishing an ionic bond (ROWLES et al. 2003; DUXSON et al. 2007). In an ideal system, the unit value indicates the consumption of all Na^+ cations. According to Zhang et al. (2013) when $Na_2O/Al_2O_3<1$, the increase in NaOH concentration is effective in increasing the extent of reaction, however, values higher than 1 indicate excess of Na^+, which will not establish connections and will be free in the structure. This part is prone to form efflorescence. However, the results reported by Kani et al. (2012) showed that the extent of leaching alkalis improved with Na/Al increasing from 0.61 to 1.23, and the susceptibility in the development of efflorescence of dry samples after immersion. Though, for this relationship to be chemically possible, during the design process it is important to consider the reactive (or reacted) part of precursor, because other fraction will just work as inert filler. On the same way, different activation design will provide different values of

dissolution and reaction, with changes the effective content of oxides in the geopolymer gel. The relation between design parameters, amount of gel formed and alkali stability is an important topic to be approached and better understood and is directly associated with efflorescence formation.

Another important factor is related to the curing process. The increase of the temperature promotes the reaction and dissolution of oxides and the acceleration of the kinetics of geopolymerization reactions (GRANIZO et al. 2014). This factor was also evaluated for the formation of efflorescence. Kani et al. (2012) observed that the curing temperatures higher than 65°C provided a significant effect in efflorescence reduction and also higher compressive strength using natural pozzolan. This behaviour was also verified by Zhang et al. (2014) from the use of fly ash as precursor and then cured at temperatures between 25°C and 80°C. The use of thermal curing is effective to precursors with low reactivity and its effect can be attributed higher amount of gel formed with associated higher density and higher amount of imprisoned Na^+.

Contextualizing all the information discussed above, two experiments were performed separately, with different precursors and similar alkali activators. Figure 11 shows a current experiment, where the rate of efflorescence development was assessed using fly ash-based as precursor (FA-**3.9**-(1.5) and FA-**4.6**-(1.5)) and fig. 12 shows the experiments using calcined kaolin (CK-20-(**1.0)**, CK-20-(**0.5)** and CK-20-(**0.0)**). The fly ash-based geopolymers were prepared by the activation of sodium silicate (SS) solution at different dosages: FA-**3.9**-(1.5) contained 3.9% Na_2O (expressed as Na_2O to fly ash mass ratio, excluding the Na_2O originating from fly ash) and Ms value of 1.5 (molar SiO_2/Na_2O ratio in the activator), while FA-**4.6**-(1.5) contained 4.6% Na_2O and Ms values of 1.5. The fly ash samples were cured in sealed moulds for initial 24 hours at RH = 90 ± 10%, 25 ± 1°C, followed by 12 hours curing at 75 ± 1°C and naturally cooled down to 25 ± 1°C and allowed further 7 days of ageing. Specimens were removed from moulds and put in ambient air with the bottom immersed in water at a depth of 0.5-1 mm. The efflorescence occurs on the surface of FA-**3.9**-(1.5) more rapidly: tiny white products are observable after 1.5 hours (not presented here), and after only 2 hours, evident efflorescence products can be seen on its surface above the wet line. In comparison, FA-**4.6**-(1.5) starts to exhibit visible efflorescence after 2 hours. The leaching analysis of the crushed samples, as a quantitative method of assessing efflorescence potential, shows that the two AACs have very close sodium releasing rate and fraction (not shown). It means that FA-**4.6**-(1.5) has

higher efflorescence potential as the absolute amount of leached alkali is higher. This result indicates that lowering the alkali concentration in an AAC by reducing the amount of sodium silicate activator may not be a good practical method to mitigate efflorescence. In fact, other factors, such as gel composition (as a result of varied reaction extent of fly ash due to the change of activation conditions) and the pore features (size and volume), can also influence the efflorescence rate.

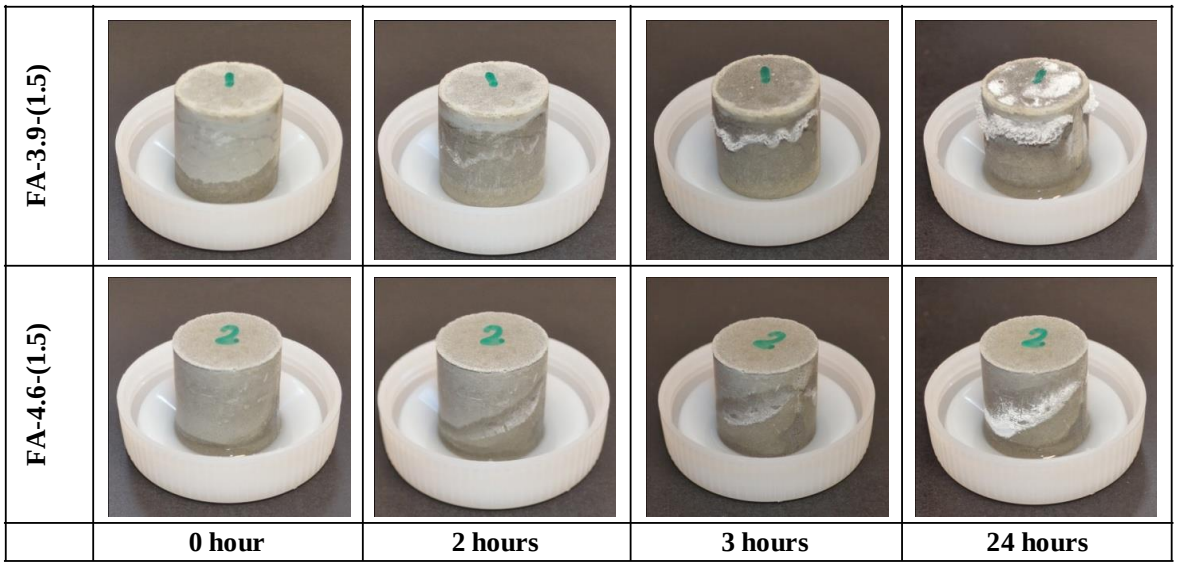

Fig. 11 - Efflorescence of hardened alkali-activated fly ash pastes in contact with water. FA-4.6-(1.5)

Figure 12 shows the experiments on calcined kaolin-based geopolymers (CK). This material was activated with sodium silicate and NaOH, with fixed 20% of Na_2O and different MS values: CK-20-(**1.0**) with MS=1.0, CK-20-(**0.5**) with MS=0.5 and CK-20-(**0.0**) with MS=0.0 (NaOH-based geopolymer without any soluble silicate in the activator). The CK samples were cured for 28 days at RH = 90 ± 10% and 25 ± 1°C in a sealed plastic container. Specimens were removed from moulds and partially immersed in distilled water (at a depth of 5 mm). The system with MS = 1 did not show efflorescence even after 28 days of assessment (not shown here). With MS=0.5 after one day it was able to identify clearly a layer of efflorescence from the middle of the sample. For the system with MS=0, the efflorescence was observed even before contact with water, where the leaching was observed due to the internal moisture of the test specimen. After the immersion, an increase in the formation of efflorescence was rapidly

identified. This makes evident that the effectiveness of silicate soluble when used as activator. In this sense, the system that did not show efflorescence also presented higher mechanical (~52 MPa at 28 days) behaviour. Another factor to be considered when comparing with fly ash systems is that the amount of activator required for calcined clay-based geopolymers is usually two to three times higher.

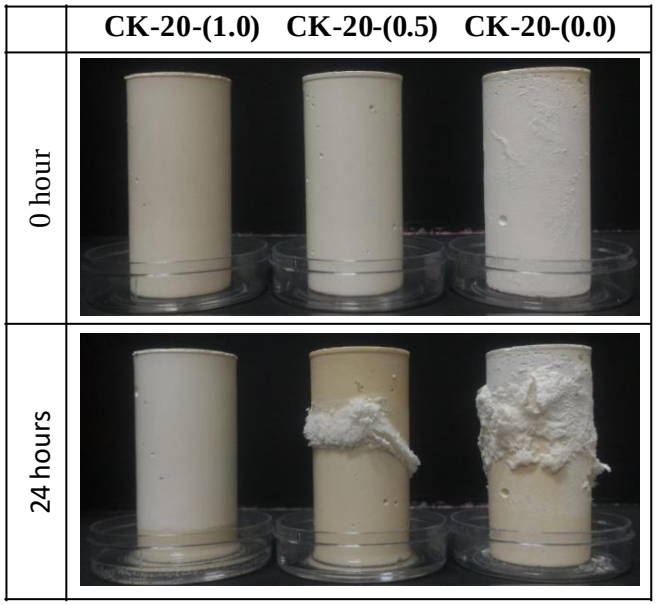

Mix design: **CK-20-(1.0)** = 20% of Na_2O and MS content of 1
CK-20-(0.5) = 20% of Na_2O and MS content of 0.5
CK-20-(0.0) = 20% of Na_2O and MS content of 0.0

Production: Mixed 5 minutes at medium speed

Curing condition: 28 days sealed at RH = 90% ± 10% and 25 ± 1°C

Fig. 12 - Efflorescence of hardened alkali-activated calcined kaolin pastes in contact with water. CK-20-(1.0) means 20% Na_2O in terms of mass ratio to calcined kaolin, and MS is 1.0.

4.4.2 The difference and similarities between efflorescence and subflorescence

Crystallization process is the opposite to the solubilisation of a solid. In a solution when saturation is exceeded, part of solute will be separated from the solution and precipitates as solid crystals to keep the solution saturated. As shown previously, after the leaching process, the alkalis are brought to the surface and are crystallized by carbonation process, generating efflorescence. However, according with Scherer (2004), porous material can be damaged when crystal precipitate from the liquid in their pores. The size of the pores and the magnitude of the repulsive force between the salt and the confining pore surfaces are also important factors. In turn, supersaturation is dependent on the nature of the salt, the rate of the supply of the solution and the evaporation of water (SCHERER, 2004). In this way, the crystallization can occur in two ways: efflorescence, when the internal alkalis are carried towards the surface, providing

Na^+ for the precipitation of sodium carbonates, until an equilibrium (saturation) condition between the pore solution and the crystals is reached (ZHANG et al. 2018); or subflorescence, when the crystallization occurs within pores (DOW et al. 2003), in a depth sufficient to allow the absorption of dissolved CO_2. According to Zhang et al. (2018), efflorescence and subflorescence are both related to the carbonation process, however, the material properties, exposition and environment can determine what will be formed.

Regarding to porosity, in a porous material, water is draw up by capillary pressure, which is dependent on the pore size distribution. The flux ($J=-\kappa.\Delta\rho/\eta$) into the porous material is given by Darcy's law, and is dependent on permeability (κ), viscosity (η) and pressure (ρ). To balance the system, water raises between the pores until an equilibrium height achieved. In the evaporation process, the internal water of pores is brought to surface and reduces the height of equilibrium. When there is the presence of dissolved salts, as water evaporates, the concentration of salt in the liquid rises and the salt concentration at the drying surface until the supersaturation are high enough to cause the salt precipitation (SCHERER, 2004). Summarising this, the water will be transported into the material by capillary pressure. With the evaporation process, the transported salts are precipitated in a spatial sequence according to the ion activities of the salt phases in the system (ARNOLD et al. 1989). However, above the evaporation region, as well as throughout the inner part, due to the presence of remaining soluble salts, is the subflorescence zone. In AACs, if a soluble carbonate is available, it can be transported to the inside and enable the crystallization of the salt, in this case is a carbonate, and the resulting crystallization pressure may exceed the tensile strength of the material (SCHERER, 2004).

In crystallisation process, every salt has an equilibrium relative humidity, which is also relevant to the ambient humidity and temperature. If the relative air humidity is lower than the equilibrium humidity of the salt (RH < Hr eq), the salt will crystallise. Correlating this with AACs, when RH is low, with the availability of a hydrated carbonate provides a movement to inside structure, where with the contact with free alkali, may crystallise internally. If the relative air humidity is higher than the equilibrium humidity of the salt (RH > Hr eq), the salt dissolves and can be brought to the surface by transport agent. This means that the relative humidity of the environment and salt crystallization will define whether there will be efflorescence or internal crystallization (subflorescence). The equilibrium humidity of a specific salt is not always available or has never been evaluated; however, the carbonate $Na_2CO_3{:}10H_2O$, at 25°C, presents Hr eq of 88.2% (ARNOLD et al. 1989). In the same way, the capillarity will determine

the rate of water movement and aqueous CO_2 movement and consequently the depth of subflorescence.

In literature that evaluated the formation of efflorescence in AACs, the main products formed are sodium carbonates. The formation of a hydrated carbonate ($Na_2CO_3.7H_2O$) was observed by Zhang et al. (2014) and Škvára et al. (2009) sodium bicarbonate ($NaHCO_3$) by Kani et al. (2012) and natrite (Na_2CO_3) by Burciaga-Diaz et al. (2010). In system with potassium as activator, it is possible to form potassium carbonate (K_2CO_3) or hydrated potassium carbonate phases, however, this last one does not give rise to visible hydrates as postulated by Škvára et al. (2009), and for this reason, the use of potassium could be indicated for the reduction of efflorescence (or efflorescence visibility). Even without visible efflorescence formation in geopolymers based on potassium as main activator, the leaching process of this element can allow the removal of alkalis and cause microstructural damages.

In short, efflorescence is the crystallization process of alkalis leached from AAC matrix in contact with aqueous carbonate solution in a reaction format as follows (ZHANG et al. 2014).

$$CO_2\,(g) + 2OH^-\,(aq) \rightarrow CO_3^{2-}\,(aq) + H_2O$$

$$2Na^+\,(aq) + CO_3^{2-}\,(aq) + 7H_2O \rightarrow Na_2CO_3.7H_2O\,(s)$$

According to Zhang et al. (2014), this is therefore a partial neutralization for alkaline geopolymers under natural carbonation conditions, as dissolved CO_2 acts as an acid and consumes hydroxides. The main reason for efflorescence in these materials is the availability of mobile Na^+ and OH^-, which are related to the material permeability. In a situation with very aggressive leaching, it can also remove the equilibrium cation (Na^+) and destabilize the aluminium tetrahedral which may damage the matrix structure. This mechanism, however, has not been solidly verified nor highlighted to date.

Internally, the carbonation process may follow the same reactions, but its effect could be different. The formed crystal can be expansive which induces internal stresses. The stress in the megapascal range is only expected in nanometric pores, and lower pressure in larger pores. This pressure can be mechanically damaging depending on the pore structure. According to Scherer theory (SCHERER, 2004), the supersaturation of salts can result from capillary rise and evaporation, or from cycles of wetting and drying. In contact with water, the humidity in the

pores is expected to be very high which support the formation of $Na_2CO_3 \cdot 7H_2O$ as detected by Zhang et al. (2014).

To predict the relation between crystallization pressure and pore diameter, using the estimated liquid interfacial free energy (γ_{CL}=0.09 N/m) of $Na_2CO_3 \cdot 10H_2O$ (RIJNIERS et al. 2005) and Eq. 1 that describes the pressure in a confined spherical crystal with radius of r as proposed by Scherer (2004), it is possible to estimate the crystallisation pressure in a cylindrical. The relation between crystallization pressure and pore diameter is shown in the Figure 13.

$$p = 2\gamma_{CL}/r \qquad \text{(Eq.1)}$$

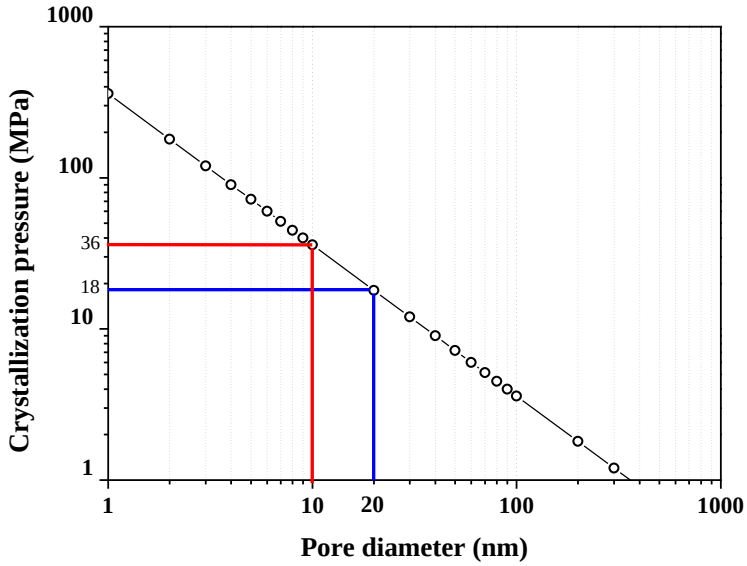

Fig. 13 - Crystallisation pressure as a function of the diameter of a cylindrical pore.

As reported in some previous papers (VAN DEVENTER et al. 2006: SKVARA et al. 2006; ZHANG et al. 2016), the pore sizes in geopolymers determined by mercury intrusion are at a range of several nanometres to 2000 nm. In an experiment conducted using different contents of fly ash and metakaolin, Zhang et al (2014) observed the concentration of 80 to 90% of the pores smaller than 20nm. The crystallization process inside a pore of 20 nm can generate a pressure of 18 MPa and 36 MPa for 10 nm pores. The pressure increases in an exponential relation to the pore diameter. Large pores can permit the growing of crystal with a low crystallisation pressure, however, the crystal formation in small pores can generated a high pressure. The impact on the integrity of the samples, and particularly whether the process will be harmful or harmless, depends on the magnitude of the crystallisation pressure compared to the tensile strength of the geopolymer matrix (ZHANG et al. 2018).

3.5. IMPACTS OF EFFLORESCENCE ON AACs

3.5.1 Microstructural impacts

So far, there has been very limited structural analysis reported in literature related to the formation of efflorescence in ACC. Zhang et al. (2014) analysed the pore structure by scanning electron microscopy (SEM), and made some important considerations. The leaching process is related to the pore size distribution where large pores induces a faster alkali leaching.

The effect of efflorescence on the microstructure of the same material showed in Figure 11, FA-**3.9-(**1.5) and FA-**4.6**-(1.5), is shown in Figure 14. The images correspond to the surface parts of each sample after 28 days of ambient ageing (in the air) and accelerating efflorescence (with bottom immersed in water as described above). The crushed particles near surface were solidified using resin, polished and washed in acetone using an ultrasonic washer to remove loose particles.

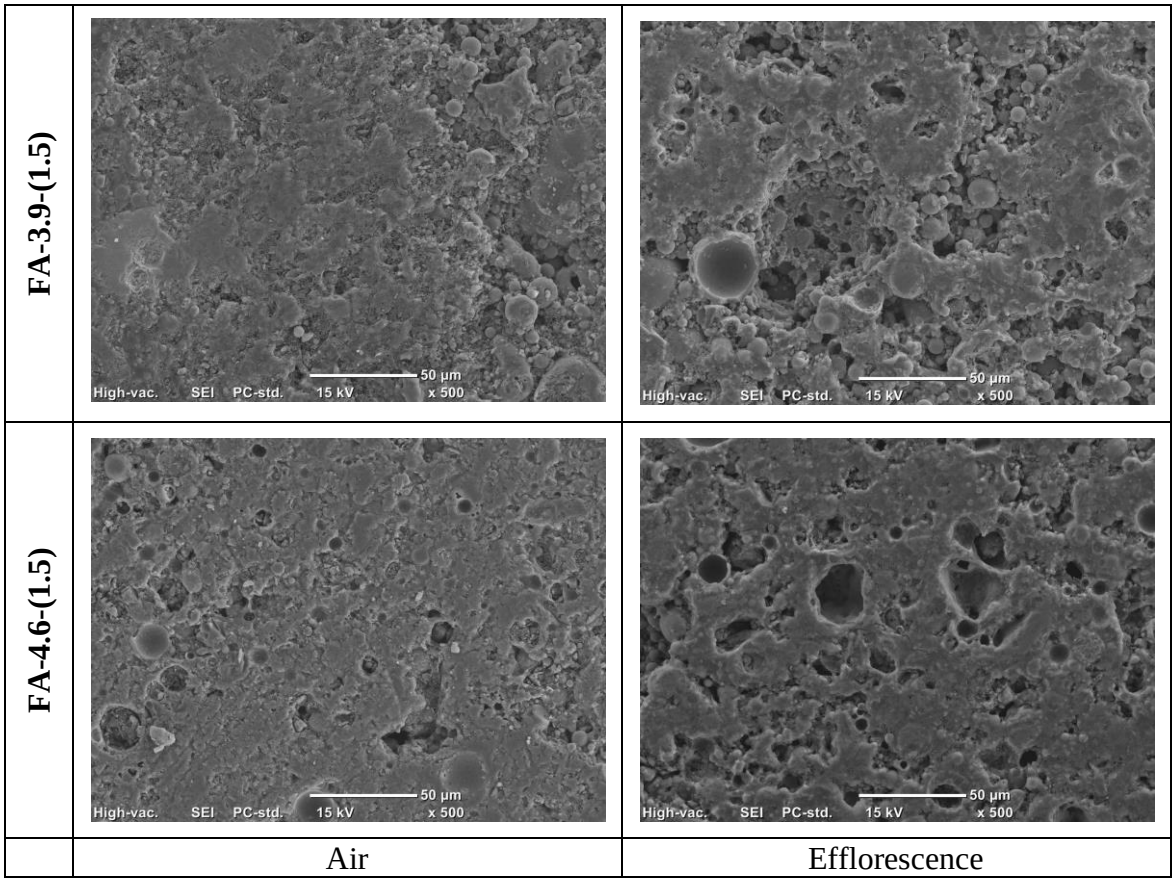

Fig.14 - Scanning electron micrographs of AACs after 28 days of ageing under ambient air and accelerating efflorescence conditions.

After the accelerating efflorescence procedure, FA-**3.9**-(1.5) becomes more porous when compared to the corresponding samples. The same polishing and washing procedures were used for all samples, the porous microstructure in cross-section implies that the binder may be softer or less strong as a consequence of the development of efflorescence. The cross-section of FA-**4.6**-(1.5) after the accelerating efflorescence program shows the same microstructural feature. Zhang et al. (2018) implied that one of the reasons for the increase of large pores is that the later reaction was affected in the specimens with efflorescence, due the consumptions of alkalis to form de $Na_2CO_3 \cdot nH_2O$ reducing the ongoing reaction of gel.

Trying to understand the microstructural effect of efflorescence, Zhang et al. (2018) evaluated the T-O (T=Al or Si) bonding environments by FTIR spectroscopy in systems with intense efflorescence in contact with water. The authors observed a shift of the main band as well as a lower intensity in the systems in contact with water when compared with those samples in air. The author also indicated that efflorescence in geopolymers does not change the main mineralogical composition of the binder, however restricts the later reactions, which is expected to be harmful to the strength development. Unfortunately, the actual mechanical testing on tensile strength change was not reported in the previous study.

Figure 15 shows XRD results of the CK-based geopolymers as presented in Figure 12. The first diffractogram represents the precursor, a calcined kaolin (CK), which shows the presence of kaolinite, anatase and quartz. The hump between 19 and 28 degrees is attributed to the amorphous feature of metakaolin. After the geopolimerization process, another hump is visible between 26 and 34, and attributed to the gel formation. After efflorescence process, it is able to identify a hydrate sodium carbonate ($CaCO_3.nH_2O$). The formation of such carbonate may be from the carbonation of calcium solution as the calcined kaolin contains a certain amount of CaO as impurity, which becomes available after alkali-activation. The system CK-20-(1.0) shows 34.8% of crystalline content, and after efflorescence process it becomes 41.4%. The system CK-20-(0.5) present 39.7% before and 49.7% after efflorescence. This degree of crystallinity was obtained by mathematical peak deconvolution. This increase is visible by the reduction of the main hump near to 28^o in 2θ. This means that there is a reduction in the material amorphic structure after the efflorescence.

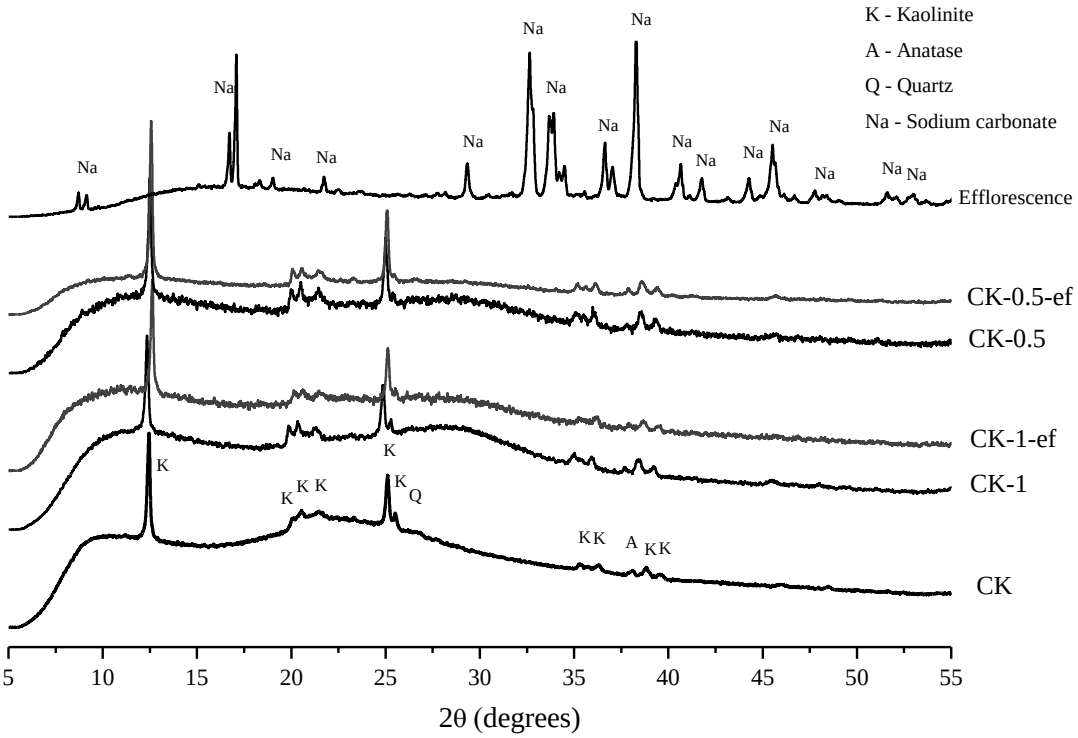

Fig.15 - XRD analysis of precursor, CK-bases geopolymers before and after efflorescence formation and efflorescence product.

Due to the formation of carbonate crystal, microstructural changes become visible in sample integrity. In some systems, after wetting and drying cycles, the process of dissolving alkalis is followed by evaporation of the water, which allows the movement to surface, and it causes severe deterioration. Figure 16 shows a sample produced with the CK subjected to contact with water at the bottom in an environment with approximately 50% RH, so that the movement of water and alkalis by evaporation was forced. The excess of leaching or/and the crystallization in superficial pores may cause this deterioration.

Fig. 16 – Sample with calcined kaolin as precursor and activated with 10% of Na_2O from NaOH with visible surface deterioration

3.5.2 Mechanical impacts

Burciaga-Díaz et al. (2010) evaluated how different formulations affected the development of compressive strength, and found that in slag-based AAC, the addition of more than 5% of Na_2O decreased the compressive strength. This effect was attributed to the excess of alkalis and the consequent efflorescence formation, which was visually observed. In the same work, however, when MK was added as precursor, it required larger amount of Na_2O (15%), while no reduction in the mechanical properties was observed nor efflorescence.

In a long-term exposure for a fly ash-based AAC, Škvára et al. (2012) observed reduction in compressive strength for the water immersed samples when compared with those exposed to air. However, this reduction was attributed to the higher cohesion forces between the gel particles in the dry concrete. To the same authors, as found that Na^+ was replaced by H_3O^+, Škvára et al. (2009) argued that large part of Na are bounded inform of $Na(H_2O)_n^+$, rather than ironic bonds -O-Na^+. It should be noted that in this specific case, the immersed sample only lost the alkalis by leaching, and no crystallization process occurred.

The mechanical properties of fly ash-based geopolymers by different periods of curing, and types of exposure were evaluated by Yao et al. (2015). By comparing the compressive strength results, it was found that the immersed samples and those submitted to bottom contact with water (accelerating efflorescence) presented lower values compared to the control samples that were left in air. The time of exposure also contributed to the strength reduction. The negative effect of immersion was attributed to the instability of sodium aluminosilicate gel in water. For the samples with bottom contacting water, the formation of carbonate crystal and microstructure damage was believed to be the main factor to the reduction of mechanical behaviour. In terms of linear shrinkage, the shrinkage of the samples immersed was smaller than that of efflorescence samples due to the availability to free water in the binder under the immersion condition.

As observed by Yao et al. (2015), the environment of exposure is an import factor that affect carbonation process. A direct comparison by measuring the specimens after demoulding, air-aging and accelerating efflorescence were recently made by the authors. Figure 17 shows the compressive strengths of the fly ash-based AACs, the same as presented in Fig. 2. After 28 days of ageing, the compressive strengths of the pastes in air showed an increase by 20 to 35%

compared with that at demoulding age, while the efflorescence samples showed smaller increase.

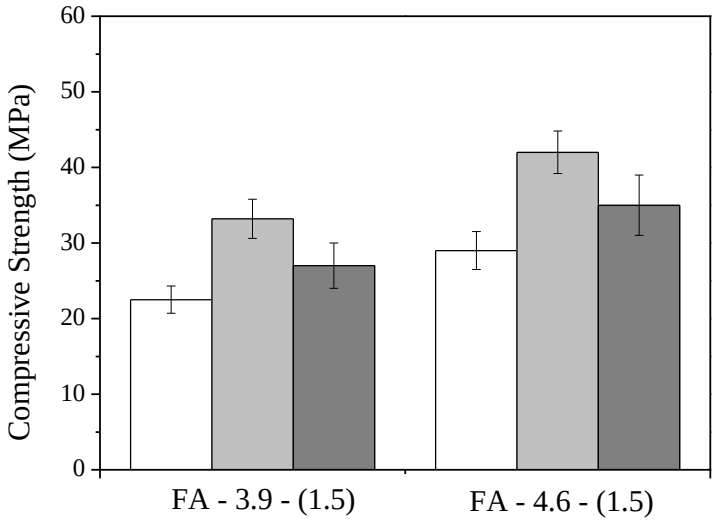

Fig.17 -Compressive strengths of well matured fly ash AACs after demoulding, air-aging and accelerating efflorescence for 28 days

Calcined clays-based AACs were also evaluated by compressive strength (Figure 18). The samples identified as CK-20-(**1.0**), CK-20-(0.5) and CK-20-(0.0) were the same as presented in Figure 12. After 28 days of curing in a sealed plastic container at RH = 90 ± 10% and 25 ± 1°C, followed by 28 days more in contact with water to accelerate efflorescence formation, it was found that the first system (CK-20-(**1.0**)) showed less susceptibility of efflorescence, and this behaviour is attributed to the denser and stronger structure which provides a lower water absorption, and consequently a lower movement of alkalis to the surface. The other systems presented strength reductions of ~25% and extensive effloresce formation. Thus, it is able to confirm that the mechanical behaviour and its susceptibility to efflorescence formation in these systems are related to the design parameters.

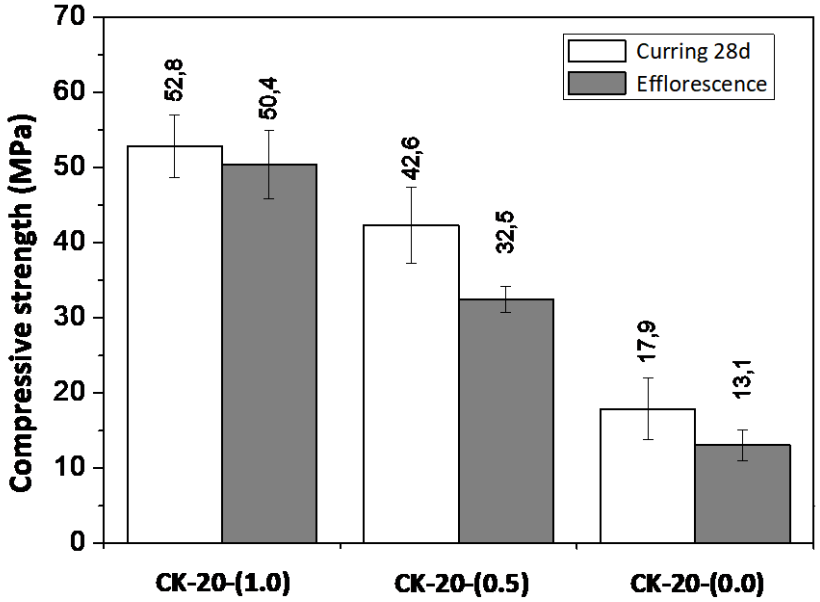

Fig.18 - Compressive strengths of calcined kaolin AACs after curing 28 days and accelerating efflorescence for 28 days

Therefore, it is evident that the efflorescence has negative influence on the strength development. When an AAC paste is placed in accelerating efflorescence conditions, water can be drawn into the pores of the solid matrix by capillary suction and evaporate from the sample surface. The internal alkalis are able to diffuse towards the surface, providing Na^+ for the precipitation of sodium carbonates, until an equilibrium (saturation) condition between the pore solution and the crystals is reached. The reduced alkali concentration in the matrix due to diffusion will affect or suppress the later activation of residual precursors. In addition, the crystallization pressure due to the precipitation of sodium carbonates in the pores of binder may also introduce inner stress, which consequently affects the mechanical properties of AACs.

3.6. CONCLUSIONS

Even with the recent advances in AAC technology, the understanding of the efflorescence phenomenon is still a knowledge gap and distinct from that occurs in PC-based materials. Some progress has been made to understand these efflorescence mechanisms and among the factors that influence them, some topics need to be better clarified. Based on the previous researches and some experimental results, it is clear the importance of the effect of soluble silicates as activator, the hydrothermal curing and the use of slag to reduce the efflorescence rate, when used with the correct design parameters. However, it is necessary to identify micro and nanostructural effect of the materials and the mechanisms, the relation between design parameter and gel formed and the alkalis stability. It is also necessary to understand the

carbonation process, and how the pore network structure is related to external or internal crystallization, and how the humidity is connected to the process and how all of these could be associated to the performance of the material in service. The effect of efflorescence formation on mechanical properties, including compressive strength, tensile strength and linear deformation requires a greater understanding. The use of this material in civil construction needs the understanding of this phenomenon to avoid durability problems.

REFERENCES:

Arnold A. and Zehnder K. Salt Weathering on monuments [Article] // In I' Simposio internazionale Bari. - 1989.

Bernal S A icrostructural changes induced by CO2 exposure in alkali-activated slag/metakaolin pastes [Article] // Frontiers of materials. - 2016. - 3. - Vol. 43.

Bernal S. A., Bílek V. and Criado M. Durability and testing - degradation via mass transport [Book Section] // Alkali Activated Materials: State of the Art Report / book auth. Provis J. L. and Van Deventer J. S. J. - Dordrecht : Springer, 2014.

Burciaga-Díaz O. [et al.] Statistical Analysis of Strength Development as a Function of Varios Parameters on Activated Metakaolin/Slag Cements [Article] // Journal of American Ceramic Society . - 2010. - 93 : Vol. 2.

Cizer Ö [et al.] Real-time investigation of reaction rate and mineral phase modifications [Article] // Construction and Building Materials. - 2012. - 35.

Criado M., Fernandez-Jiménez A. and Palomo A. Alkali activation of fly ash: Effect of the SiO2/Na2O ratio. [Article] // Mocroporus and Mesoporous Materials. - 2007. - 106 : Vols. 1-3.

Damtoft J. S. [et al.] Sustainable development and climate change initiatives [Article] // Cement and concrete research. - 2008. - 38. - pp. 115-127.

Dow C. and Glasser F. P. Calcium carbonate efflorescence on Portland cement and building materials [Article] // Cement and Concrete Research. - 2003. - 33.

Duxson P. [et al.] Effect of alkali cations on aluminus incorporation in geopolymeric gels [Article] // Ind. Eng. Chem. Res. - 2005. - 44.

Duxson P. [et al.] The effect of alkali and Si/Al ratio on the development of mechanical properties of metakaolin-based geopolymers. [Article] // Colloids and Surfaces. - 2007. - 292 : Vol. 1.

Fernández-Jimenez A. [et al.] The role played by the reactive alumina content in the alkaline activation of fly ashes [Article] // Microporous and Mesoporous Materials. - 2006. - 91 : Vols. 1-3.

Gallucci E. and Scrivener K. Crystallisation of calcium hydroxide in early age model and ordinary cementitious systems [Article] // Cement and Concrete Research. - 2007. - 37 : Vol. 4.

Garcia-González C. A. [et al.] Modification of composition and microstructure of Portland cement pastes as a result of natural and supercritical carbonation procedures. [Article] // Ind. Eng. Chem. Res. - 2006. - 45 : Vol. 14.

Granizo N., Palomo A. and Fernandez-Jiménez A. Effect of temperature and alkaline concentration on metakaolin leaching kinetics. [Article] // Ceramics INternational. - 2014. - 40 : Vol. 7.

Heath A., Paine Kevin and McManus Marcelle Minimising the global warming potential of clay based geopolymers [Article] // Journal of Cleaner Production. - 2014. - 78.

Kani N., Allahverdi E. A. and Provis J. L. Efflorescence control in geopolymers binders based on natural pozzolan [Article] // Cement and Concrete Composites. - 2012. - 34 : Vol. 1.

Lloyd R. R., Provis J. L. and Van Deventer J. S. J Pore solution composition and alkali diffusion in inorganic polymer cement [Article] // Cement and Concrete Research. - 2010. - 40 : Vol. 9.

Longhi M. A. [et al.] Valorisation of a kaolin mining waste for the production of geopolymers. [Article] // Journal of Cleaner Production. - 2016. - 115.

McLellan B. C [et al.] Costs and carbon emissions for geopolymers pastes im comparison to ordinary portland cement [Article] // Journal of Cleaner Production. - 2011. - 19.

Passuelo A. [et al.] Evaluation og the potential improvement in the environmental footprint of geopolymers using waste-derived activators [Article] // Journal of cleaner production. - 2017. - 166.

Provis J. L. and Bernal S. A. Geopolymers ans related alkali-activated material [Article] // Annual Review of Material Research . - 2014. - 44.

Provis J. L., Lukey G. C. and Van Deventer J. S. J. Do geopolymers actually contain nanocrystalline zeolites: A reexamination of existing results [Article] // Chem Mater. - 2005. - 17.

Rees C. A. [et al.] In situ ATR-FTIR study of the early stages of fly ash geopolymer gel formation. [Article] // Langmuir. - 2007. - 17. - Vol. 23.

Rijniers L. A. [et al.] Experimental Evidence of Crystallization Pressure inside Porous Media [Article] // Physical Review Letters. - 94.

Rowles M. and O'Connor B. Chemical optimisation of the compressive strength of aluminosilicate geopolymers synthesised by sodium silicate activation of metakaolinite. [Article] // Journal of Material Chemistry. - 2003. - 13 : Vol. 5.

Rowles M. R. [et al.] 9Si, 27Al, 1H and 23Na MAS NMR Study of the Bonding Character in Aluminosilicate Inorganic Polymers. [Article] // Applied Magnetic Ressonance. - 2007. - 32 : Vol. 4.

San Nicolas R and Provis J The interfacial transition zone in alkali-activated slag mortars [Article]. - 2015. - 2. - Vol. 70.

Šavija B. and Lukovic M. Carbonation of cement paste: Understanding, challenge and opportunities [Article] // Construction and Building Materials. - 2016. - 117.

Scherer G. W. Stress from crystallization of salt [Article] // Cement and Concrete Research. - 2004. - 34 : Vol. 9.

Shen W. [et al.] Magnesia modification of alkali-activated slag fly ash cement [Article] // Journal of Wuhan University of Technology-Mater. - 2011. - feb..

Škvára F. [et al.] A weak alkali bond in (N, K)-A-S-H gels: evidende from leaching and modeling [Article] // Ceramics-Silikáty. - 2012. - 56.

Škvára F. [et al.] Aluminosilicate polymers - influence of elevated temperatures, efflorescence [Article] // Ceramics-Silikáty. - 2009. - 53 : Vol. 4.

Skvara F. [et al.] Microstructure of geopolymer materials based on fly ash [Article] // Ceramics - Silikaty. - 2006. - Vol. 50.

Temuujin J. and Van Riessen A. Characterization of glass F fly ash geopolymer pastes immersed in acid and alkali solutions [Article] // Journal of Hazardous Materials. - 2011. - 164.

Van Deventer J. S. J., Lukey G. C. and Xu H. Effect of Curing Temperature and Silicate Concentration on Fly-Ash-Based Geopolymerization [Article] // Ind. Eng. Chem. Res. - 2006. - 45.

Van Deventer J. S. J., Provis J. L. and Duxson P. Technical and commercial progress in the adoption of geopolymer cement [Article] // Minerals Engineering. - 2012. - 29.

Yao X., Yang T. and Zhang Z. Compressive strength development and shrinkage of alkali-activated fly ash-slag blends associated with efflorescence [Article] // Materials and Structures. - 2015. - 49 : Vol. 7.

Zhang D., Ghouleh Z. and Shao Y. Review on carbonation curing of cement-bases materials [Article] // Journal of CO2 Utilization. - 2017. - 21.

Zhang X., Glasser F. P. and Scrivener K. L. Reaction kinetics of dolomite and portlandite [Article] // Cement and Concrete Research. - 2014. - 66.

Zhang Z and Wang H The pore characteristics of geopolymer foam concrete and their impact on the compressive strength and modulus [Article] // Frontiers im materials. - 2016. - 3. - Vol. 38.

Zhang Z. [et al.] Efflorescence and subflorescence induced microstructural and mechanical evolution in fly ash-based geopolymers [Article] // Cement and Concrete Composites. - 2018. - 92.

Zhang Z. [et al.] Fly Ash-based geopolymers: The relation between composition, pore structure ans eflforescence [Article] // Cement and Concrete Research. - 2014. - 64. - pp. 45-56.

Zhang Z. [et al.] Quantitative kinetic and structural analysis of geopolymers. Part 2. Thermodynamics of sodium silicate activation of metakaolin. [Article] // Thermochimica Acta. - 2013. - 565.

Zhang Z. [et al.] Using fly ash to partially substitute metakaolin in geopolymer synthesis [Article] // Applied Clay Science. - 2014. - Vols. 88-89.

Zhang Z., Yao X. and Zhu H. Potential application of geopolymers as protection coatings for marine concrete III. Field experiment [Article] // Applied Clay Science. - 2010. - Vol. 1.

44. **Bernal, S A**. Microstructural changes induced by CO_2 exposure in alkali-activated slag/metakaolin pastes. *Frontiers of materials*. 3, 2016, 43.

4. NEW SELECTIVE DISSOLUTION PROCESS TO QUANTIFY REACTION EXTENT AND PRODUCT STABILITY IN METAKAOLIN-BASED GEOPOLYMERS[a]

4.1 INTRODUCTION

The development of chemically activated reactive aluminosilicate materials has become a technically (BERNAL et al., 2016b; PROVIS; BERNAL, 2014; VAN DEVENTER; PROVIS; DUXSON, 2012) and environmentally (HABERT; OUELLET-PLAMONDON, 2016; HEATH; PAINE; MCMANUS, 2014; MCLELLAN et al., 2011) attractive option for the use of different industrial wastes and calcined clays in manufacturing new binders. These are known as alkali-activated materials (AAMs) or geopolymers. Among the precursors used for geopolymer manufacturing, metakaolin is one of the most commonly used because of its high reactivity and purity, which result in a more homogeneous binder (PROVIS; BERNAL, 2014).

The main reaction product formed in geopolymers is an alkaline aluminosilicate hydrate type-gel (also known as M-A-S-H, where M represents the alkali metal in activator). The alkali metal most commonly used and assessed is sodium, which promotes formation of a structurally disordered and highly cross-linked N-A-S-H gel (PROVIS; LUKEY; VAN DEVENTER, 2005b). When metakaolin is used as the precursor, Al and Si in the M-A-S-H gel structure are present in tetrahedral coordination, with silica in a $Q^4(m\text{Al})$ ($0 \leq m \leq 4$) type environment (DUXSON et al., 2005b). Aluminium plays an important role in the process of dissolution, crystallisation and reaction product formation (PROVIS; BERNAL, 2014). Aluminium also influences the intrinsic mechanical properties, where large amounts of $Q^4(3\text{Al})$ and $Q^4(2\text{Al})$ sites (resulting from a relative increase of Si in the system) provide higher strength to the gel structure than $Q^4(4\text{Al})$ sites (FERNÁNDEZ-JIMÉNEZ et al., 2006).

The composition and quantity of the M-A-S-H gel formed during geopolymerisation is dependent on the degree of reactivity of the precursor, which itself is related to the reactive oxide content, chemical composition and particle morphology. The high pH provided by the

[a] O capítulo já está publicado em formato de artigo e pode ser acessado pelo DOI: 10.1016/j.compositesb.2019.107172

activator facilitates the dissolution Al and Si from the precursor particles, which then precipitate and polymerise via condensation reactions to form the geopolymer gel. During the initial stages of reaction dissolution of Al-O bonds is thermodynamically more favourable than dissolution of Si-O bonds (FERNÁNDEZ-JIMÉNEZ et al., 2006; OELKERS; GISLASON, 2001), indicating a higher initial reactivity for alumina rich precursors. The use of soluble silicates in the activator provides an extra source of silica to the system and induces the incorporation of Si in the gel structure and the subsequent formation of Si-rich tetrahedral sites. The presence of excess alkalis from the activator can facilitate leaching and subsequent efflorescence formation (ZHANG et al., 2013) and changes in the durability of the material due to mechanical performance reduction (YAO; YANG; ZHANG, 2016; ZHANG et al., 2014a, 2018b). The type of alkali affects precursor dissolution kinetics and therefore the microstructure of the final product. In this sense, the synthesis parameters are determinants of gel formation, chemical composition, microstructural features and durability.

Regarding the behaviour of alkalis in the gel structure, sodium can be present as Na-O-Al(Si) or as $Na(H_2O)_n^+$, weakly associated with water molecules. The weak bonding or availability of alkalis in the aqueous phase present in the gel pore network increases the materials susceptibility to leaching. Previous work has shown leaching of between 1 and 16% of alkalis from the gel during the first 24 hours of exposure (NAJAFI; ALLAHVERDI; PROVIS, 2012; ZHANG et al., 2014b), and it has been suggested that complete dissolution is likely after a long exposure time. The wide variation in leaching behaviour in those studies is due to substantially different geopolymers made using materials (fly ash and calcined clay) exhibiting very different chemical composition and mineralogy, under distinct activation and exposure conditions.

Considering all of these factors, determination of the reaction extent is therefore critical for the design of geopolymer gel composition prediction of long-term mechanical properties, chemical and physical durability. A major design parameter in formulating geopolymer reaction mixtures is the Na/Al molar ratio, where the unit value indicates the extent of compensation of the negative charge resulting from the substitution of Al into a Q^4 molecular coordination (FERNÁNDEZ-JIMÉNEZ et al., 2006; PROVIS; LUKEY; VAN DEVENTER, 2005b). However, due to the difficulty in identifying the degree of reaction of the precursor, and the amount of gel formed, this value is typically calculated by assuming that the total amount of Al in the precursor is incorporated into the gel framework and exists in a Q^4 environment. In practice this is unlikely to occur, as much of the Al will remain in unreacted precursor particles

or crystalline phases that are inert under the reaction conditions of alkali activation (e.g. mullite in coal fly ash)(ZHANG et al., 2016). In this case, excess Na remains free in the gel pore solution. However, increasing of reaction mixture pH by the addition of greater amount of Na (i.e. increasing the activator dose) results in greater dissolution of the precursor and consequently more gel formation. This results in a greater charge balancing requirement and hence greater incorporation of alkalis in the gel. There exists an optimum point between maximum particle dissolution and a minimum amount of free alkalis in the pore solution, in regard to the long-term mechanical properties, chemical and physical durability. It is therefore necessary to understand how the different design parameters influence the degree of reaction of the precursor and how the removal of free alkalis can affect the composition and stability of the gel. In addition, the mechanical and physicochemical properties (e.g. chemical durability and permeability) of the geopolymers result from the gel reaction product, and this may be estimated from the reacted portion of the precursor which is not soluble (WILLIAMS; HART; RIESSEN, 2011; ZHANG et al., 2016). Consequently, the degree of reaction during geopolymer formation is fundamental to understand and predict reaction mechanisms and kinetics and mechanical and physicochemical properties in geopolymer systems.

This degree of reaction in geopolymer systems has been assessed in previous work using varying approaches, with chemical methods of selective dissolution and analytical methods of quantification yielding the most promising results. The reactivity of fly ash was evaluated by alkaline dissolution and analytic quantification using X-Ray Diffraction (XRD) and X-Ray Fluorescence (XRF)(CHEN-TAN et al., 2009). In a complementary approach, the reaction extent of fly ash and/or slag based geopolymers was evaluated by selective dissolution and thermogravimetric analysis (TGA), nuclear magnetic resonance (NMR) spectroscopy and scanning electron microscopy (SEM)(GAO; YU; BROUWERS, 2017; LI; LIN; WANG, 2017). The degree of reaction of slag in blended Portland cement was assessed using selective dissolution based on ethylene diamine tetra acetic acid (EDTA) extraction coupled with ^{29}Si MAS NMR (DYSON et al., 2007; LUMLEY; GOLLOP; MOIR, 1996). The extent of reaction of metakaolin-based geopolymers was evaluated using XRD (area ratio method (ARM) and partial or no known crystal structure (PONCKS) methods), SEM and Energy-dispersive X-ray spectroscopy (EDS)(WILLIAMS; HART; RIESSEN, 2011).

Despite the valuable contributions that this work has made to the understanding of the reaction extent in geopolymer systems, some points remain unclear. In particular, a detailed

understanding of the effect on gel formation of the alkali and soluble silicate content in the reaction mixture remains absent from the literature, as does its relation with the amount of readily soluble, poorly soluble and insoluble components of the geopolymer gel and remnant unreacted material within the binder. These relationships dictate the reaction mechanisms and kinetics of gel formation and resistance to degradation in aggressive environments, and therefore have significant implications on geopolymer durability and performance.

Here we use a carefully designed selective dissolution process, coupled with microstructural and spectroscopic techniques probing phase assemblage and nanostructure, to quantify the amount of soluble material, geopolymer gel and unreacted precursor in Ca-free geopolymer systems and assess the susceptibility of geopolymer materials to leaching. We evaluate the reaction extent of a series of metakaolin-based geopolymers produced using different synthesis conditions (different activator content, soluble silicate content, type of alkali, and curing conditions), correlate this with material stability, and evaluate the microstructural and nanostructural changes occurring during a selective dissolution process. This provides new insight about the reaction product formed in metakaolin-based geopolymers, the state of alkalis in the structure and the nature of the selective dissolution processes, knowledge that is essential to define the design parameters and predict the durability of geopolymers materials.

4.2. EXPERIMENTAL PROGRAM

4.2.1 Materials and sample preparation

A commercial metakaolin (MetaMax – BASF) was used as the aluminosilicate precursor, with a mean particle size of 4.56 µm and a specific surface area of 13.49 m^2/g. This material showed a smaller particle size than other calcined clays (LONGHI et al., 2016; ZHANG et al., 2012), which might result in higher water consumption during geopolymer production. The properties and chemical composition are shown in Table 1.

Activating solutions were produced from analytical grade sodium hydroxide pellets (NaOH: ~99%, Chem-Supply, Australia), analytical grade potassium hydroxide pellets (KOH: ~85%, Chem-Supply, Australia), both dissolved in water, and a sodium silicate solution with 29.4 wt.% SiO_2, 14.7 wt.% Na_2O, and 52.7 wt.% H_2O, supplied by PQ Australia.

Table 1 – Chemical composition and particle size of metakaolin

Particle size (µm)	d_{10}	0.82
	d_{50}	3.52
	d_{90}	10.04
	Median particle size	4.56
Composition	Oxide	Wt. %
	SiO_2	54.82
	Al_2O_3	42.47
	TiO_2	1.23
	Fe_2O_3	0.48
	Na_2O	0.35
	K_2O	0.17
	CaO	0.17
	SO_3	0.11
	P_2O_5	0.09
	L.O.I (loss of ignition at 950°C)	0.11

The geopolymers were formulated with different contents of alkali activator (M_2O= 15, 20 and 25%). If metakaolin is assumed to react fully, the final M/Al ratios are between 0.5 to 0.83. The type and content of alkalis were selected according to the literature in order to have a wide range of design parameters (NAJAFI; ALLAHVERDI; PROVIS, 2012; ZHANG et al., 2012, 2013). Activating solutions were designed to give the content of silica in the activator (expressed as MS modulus, representing SiO_2/M_2O molar ratio) as 0.0, 0.5, and 1.0. The alkali activators were produced by blending the NaOH/KOH and sodium silicate solution in proportions to achieve the desired molar ratios. The geopolymer formulations are identified by codes as follows: “Type of activator and curing temperature [content of alkali](MS modulus)”. For example, the system “Na[20](1.0)” was activated using 20% Na_2O, at room temperature, with a MS modulus of 1. The mixes are listed in Table 2. To assess the effect of thermal curing, the systems activated at 20% of Na_2O with different MS were also cured at 50°C for 24 h. This curing process was made with the samples sealed inside a hermetically sealed box with water in the bottom, without contact with the samples. This process was made to avoid the loss of water and evaporation.

Table 2 - Formulation of geopolymer samples

Geopolymers	MK	NaOH or KOH	SS	H_2O
Na [25](1.0)	100	16.6	82.3	42.2
Na [25](0.5)	100	24.5	41.1	64.7
Na [25](0.0)	100	32.3	0.0	79.4
Na [20](1.0)	100	13.3	65.8	44.8
Na [20](0.5)	100	19.6	32.9	63.7
Na [20](0.0)	100	25.8	0.0	75.5
Na[15](1.0)	100	10.0	49.4	54.0
Na [15](0.5)	100	14.7	24.7	62.8
Na [15](0.0)	100	19.4	0.0	71.6
Na+K [20](1.0)	100	15.6	46.2	51.2
Na+K [20](0.5)	100	20.0	21.3	66.9
Na+K [20](0.0)	100	23.8	0.0	74.3
Na 50° [20](1.0)	100	13.3	65.8	44.8
Na 50° [20](0.5)	100	19.6	32.9	63.7
Na 50° [20](0.0)	100	25.8	0.0	75.5

The pastes were produced by mechanically mixing the activator and metakaolin precursor for 5 min (1 min at 140 rpm and 4 min at 280 rpm) and then pouring the resultant mixture into moulds. Cubic samples with a height of 20 mm were produced for compressive strength testing. All the samples were cured at either 25 °C or 50 °C for 24 hours and then stored in a sealed plastic container at room temperature (~25 °C) and RH ≥ 90% for 28 days

4.2.2 Tests conducted

The compressive strength of each hardened sample was measured at 28 days using an MTS universal mechanical testing machine with a loading speed of 0.5 mm/min.

The selective dissolution tests involved dissolving the sample under different pH conditions and assessing the remaining material by micro and nanostructural analysis. The selective dissolution was divided into two different stages:

- Part 1, denoted **process WD** (water dissolution): Extraction of soluble materials in a neutral

pH environment. Two grams of ground binder (passed through a 75 µm sieve) was immersed in 200 g of distilled and deionised water. The solution was stirred using a magnetic stirrer for 5 minutes the pH measured and adjusted to a neutral value of pH = 7 through the addition of HCl (36 vol. %) to neutralise any dissolved alkalis. This process was repeated 5 times until the pH of the solution remained stable (i.e. no further observable dissolution of alkalis occurred), with the quantity of HCl added recorded. The solution was then filtered using a quantitative filter and the extracted solid material was then rinsed once with distilled water, and subsequently rinsed twice with ethanol. The remaining solid material was then dried for 45 minutes in an oven at 40 °C and collected for analysis.

- Part 2, denoted **process AD** (acid dissolution): Dissolution of reaction products by acid attack. One gram of ground geopolymer was immersed for one minute in 100 g of deionised water while stirring using a magnetic stirrer, to which 50 ml of HCl (36 vol. %) was then added while stirring using a magnetic stirrer for another 29 minutes. The solution obtained was then filtered as described above, and the remaining (inert) solid material was collected for analysis.

The geopolymers and the filtered solid material obtained from the selective dissolution processes WD and AD were analysed by:

- X-Ray Fluorescence (XRF) using a Panalytical Axios instrument, with a resolution (Mn Kα) of 35eV, using wavelength dispersive X-ray fluorescence.

- Solid-state single pulse ^{27}Al and ^{29}Si magic angle spinning (MAS) NMR spectroscopy using a Bruker Avance III HD 500 spectrometer at 11.7 T (B_0) with a 4.0 mm dual resonance CP/MAS probe, yielding a Larmor frequency of 130.32 MHz for ^{27}Al and 99.35 MHz for ^{29}Si. ^{27}Al MAS NMR spectra were collected with a 1.7 µs non-selective (π/2) excitation pulse, a measured 5 s relaxation delay, a total of 512 transients and spinning at 12.5 kHz. ^{29}Si MAS NMR spectra were acquired using a 5.5 µs non-selective (π/2) excitation pulse, a measured 60 s relaxation delay, a total of 256 transients and spinning at 12.5 kHz. For all experiments, the spectrometer field was aligned to the ^{13}C resonance of adamantane at 38.48 ppm, and ^{27}Al and ^{29}Si spectra were referenced to 1.0 mol/L $Al(NO_3)_{3(aq)}$ and neat tetramethylsilane (TMS), respectively, at 0 ppm. Gaussian peak profiles were used to deconvolute the NMR spectra, using the minimum number

of peaks possible(MASSIOT et al., 2002). Peak intensities were required to be consistent with the structural constraints described by the thermodynamics of a statistical distribution of Si and Al sites within a Q^4 aluminosilicate network for (N,K)-A-S-H gel products (PROVIS et al., 2005b).

- X-ray diffraction (XRD) using a Bruker D2 Phaser instrument with Cu Kα radiation, a nickel filter, a step size of 0.020° and 0.5 s/step. Data was obtained in the range from 5 to 70° 2θ. Diffracted background intensity at low angles was reduced using an anti-scatter blade, an incident beam divergence of 0.6 mm and a 2.5° Soller slit in the diffracted beam. Phase analysis was performed using X'Pert High Score Plus software with the ICDD PDF-4+ 2016 database.

- Fourier Transformed Infrared Spectroscopy (FTIR) using a Perkin Elmer FTIR-ATR spectrometer in absorbance mode from 4000 to 400cm^{-1}. Using absorbance values, the spectra were fitted using a baseline correction and deconvoluted in the range 600 – 1300 cm^{-1} using Gaussian curves, with the baseline defined and the band position and shape assigned according to the literature (REES et al., 2007b; ZHANG et al., 2012).

- Scanning electron microscopy (SEM) using an EVO MA18 40XVP instrument, with an accelerating voltage of 10 kV. The samples were dried at 60 °C for 2 hours and coated with gold prior to analysis.

4. 3. RESULTS AND DISCUSSION

4.3.1 Compressive strength

The compressive strength results of the geopolymers with different synthesis parameters are shown in Figure 19. Increasing soluble Si content in the activator (provided by sodium silicate) results in a significant increase in compressive strength. The system with MS=1 presents values up to 3.3 times higher compared to MS=0 (sodium hydroxide-based systems). This increase is related to the formation of a denser and more compact geopolymer structure with the use of an activator rich in soluble silicate providing compressive strength values close to 45 MPa for the geopolymer samples investigated here. This behaviour was previously reported in other researches (FERNÁNDEZ-JIMÉNEZ et al., 2006; ZHANG et al., 2012, 2013),

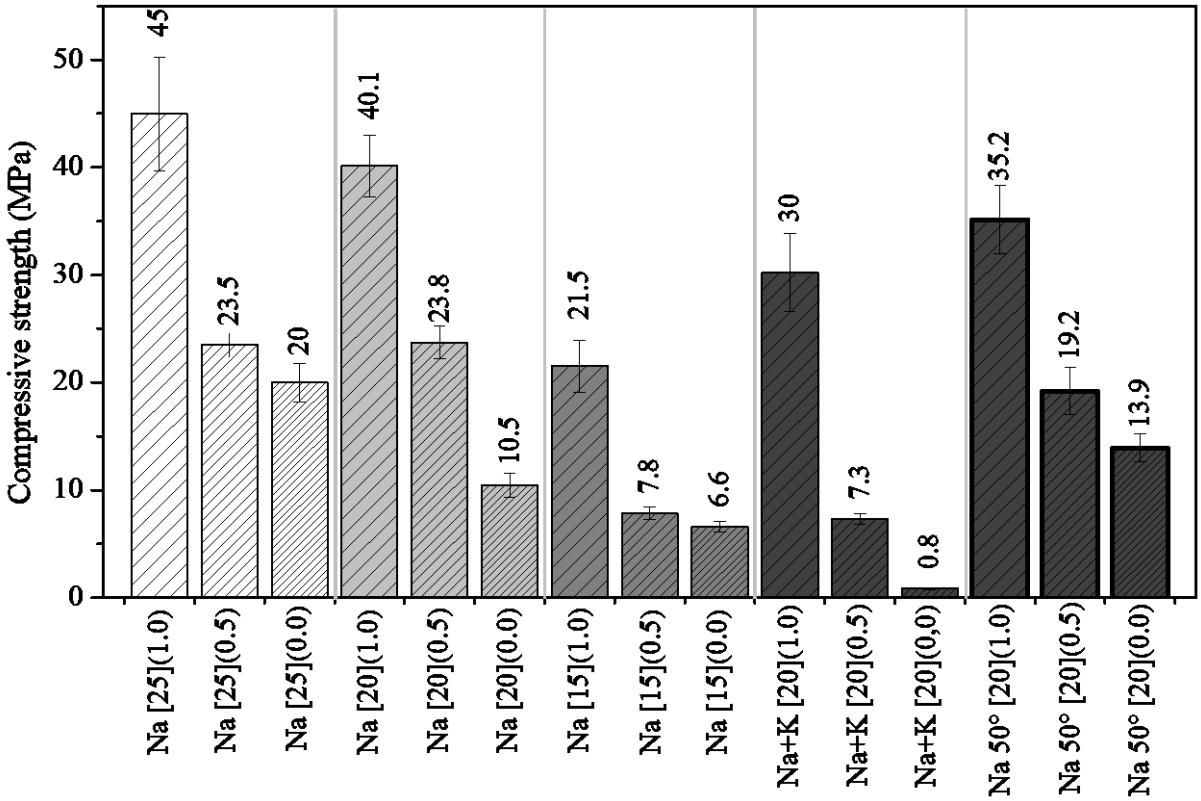

Figure 19– Compressive strength values for geopolymers cured for 28 days

An increase in reaction mixture sodium content also results in an increase in compressive strength. The geopolymers with 25% of Na_2O (Na[25]) exhibit compressive strength values up to 1.2 times higher compared with Na_2O of 20% (Na[20]) and 2.5 times higher when compared with Na_2O of 15% (Na[15]). The increasing in the amount of soluble silicate associated with the alkali content can provide a higher precursor dissolution, more gel formation and higher compressive strength (GAO et al., 2014; WAN et al., 2017). Using potassium as the alkali source results in lower compressive strength values than those observed for samples in which sodium was used as the alkali source (with the alkali content and MS parameters being equal). Curing at 50°C results in a reduction in the compressive strength of the MS>0 systems and a slight increase in the compressive strength of the NaOH-based geopolymers when compared with those samples cured at 25°C.

4.3.2 Selective dissolution

The results of each selective dissolution process are shown in Figure 20. The selective dissolution process WD (part 1) determines the content of soluble material at pH 7. The elements in chemically stable atomic bonds are generally not be removed in a neutral environment. The selective dissolution process WD (part 1) showed that the metakaolin

precursor is insoluble at pH 7, while the aluminosilicate framework formed in metakaolin-based geopolymers is largely hydrolytically stable, due to the high SiO_2/Na_2O of aluminosilicate gel formed, in agreement with other researches (DIMAS; GIANNOPOULOU; PANIAS, 2009; GIANNOPOULOU; PANIAS, 2010), which means that the dissolved material in each sample can be attributed primarily to alkalis leaching from the reaction products, or unreacted alkalis from the pore solution. The soluble alkali content of the system will therefore be proportional to the extent of dissolution at pH 7. Samples with MS=0 (i.e. without any soluble silicate present in the activator) produced from KOH-based activators exhibited a lower extent of dissolution compared to that of samples with MS=0 produced from NaOH-based activators. Curing at 50°C results in a slight increase in soluble material within the geopolymer, the extent of which is more pronounced as the amount of soluble Si in the reaction mixture is decreased. The selective dissolution process WD was applied to finely ground material and consequently the dissolution of soluble material (i.e. alkalis) is faster than the geopolymer gel framework. This is due to the higher surface area and reduced tortuosity of the pore network (and hence the easier release of Si, Al, and alkalis in the pore solution) of the powdered samples. As the potential for efflorescence is directly related to the extent to which alkalis are leached from geopolymer materials, the solubility of ground geopolymer samples in a neutral pH environment provides a reliable indicator of the potential for efflorescence and oxide removal.

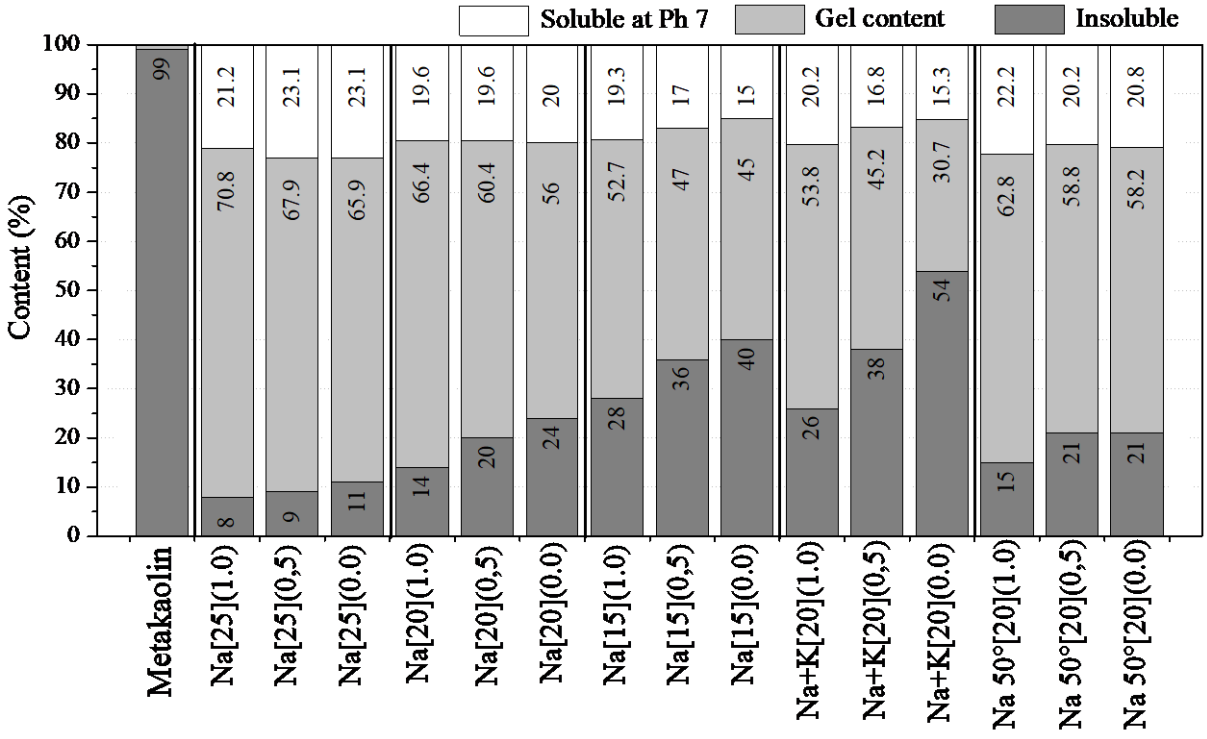

Figure 20 – Relative content of soluble, insoluble and gel material in metakaolin-based geopolymers determined from water dissolution and acid dissolution

In acid dissolution (process AD), the powdered geopolymer was immersed in a concentrated HCl solution to dissolve all the M-A-S-H gel such that the remaining insoluble fraction obtained can then be attributed solely to the unreacted precursor. The metakaolin precursor was treated under the same conditions, and the solubility was shown to be negligible as shown in the first column of Figure 20. The results in Figure 20 show that higher content of Na_2O leads to greater gel formation (i.e. comparing the systems Na[20] and Na[15]). Greater gel formation is also identified at higher values of MS regardless of the Na_2O content. The use of potassium as part of activator results in lower gel formation (consistent with the compressive strength values for these samples), and in the system Na+K[20](0.0) the content of geopolymer formed is only ~30% (c.f. 56% for the system Na[20](0.0)). No significant differences were identified between systems cured at 25ºC and 50ºC.

The quantity of gel formed in each sample determined from the dissolution processes can be used to elucidate the reaction extent of the geopolymers, and related to the mechanical properties, where more content of gel induces the formation of a more compact structure and consequently with more strength and lower permeability (WILLIAMS; HART; RIESSEN, 2011). The data in Figure 20 show that the type of activator (nature of alkali cation and the presence of soluble silicates) and its concentration (%M_2O) used for geopolymer synthesis have a strong influence on the gel structure. Despite the complex phase assemblage and microstructure (discussed in further detail below), a direct relationship between compressive strength and gel formation is observed. Systems with greater MS values showed higher gel formation and compressive strength values when activator content and type are held constant, and systems with greater activator content showed higher gel formation and compressive strength value when MS values and activator type are held constant. Additionally, systems with sodium as the alkali source show higher gel formation and compressive strength values compared to systems where both sodium and potassium are used as the alkali source. The equivalent content of M_2O results in a visible reduction of the compressive strength and gel formation when using hydroxide as the activator rather than soluble silicate. A notable example of this is the system Na+K[20](0.0) which exhibits gel formation of 30.7 wt.% (relative to the total geopolymer mass), yet a compressive strength of less 0.8 MPa. From Zhang et al. (2012), this extremely low strength is related to the highly porous structure and weak binding property of the gel. Additionally, according to Duxson et al. (2007a), the mechanical properties on K-based systems is also dependent on Si/Al molar ratio, where low levels indicate lower reactivity.

This trend is observed for all systems in which potassium is used as an alkali source, also indicating greater effectiveness for systems with higher Si content in the reaction mixture.

The results above show that selective dissolution process allows identification of the soluble, insoluble and gel materials. The susceptibility of geopolymers to efflorescence is related to the leaching characteristics, in particular the specific constituents that are leached from the material. For this reason, it is necessary to identify what constituents are being released in a neutral pH environment (process WD).

Figure 21 shows the SiO_2, Al_2O_3 and Na_2O content, determined using XRF, in the remaining solid phase obtained from the two selective dissolutions processes for the geopolymer systems with 20% of Na_2O. The composition of the dissolved materials shows a large extent of sodium being released, in some cases even greater than 50% of the nominal sodium content, which indicates that a large fraction of sodium is not chemically bound in gel or is weakly bound and is free to move in a neutral pH aqueous environment. The high amount of free sodium in the structure is an indicator of potential efflorescence formation when geopolymers are under high humidity conditions.

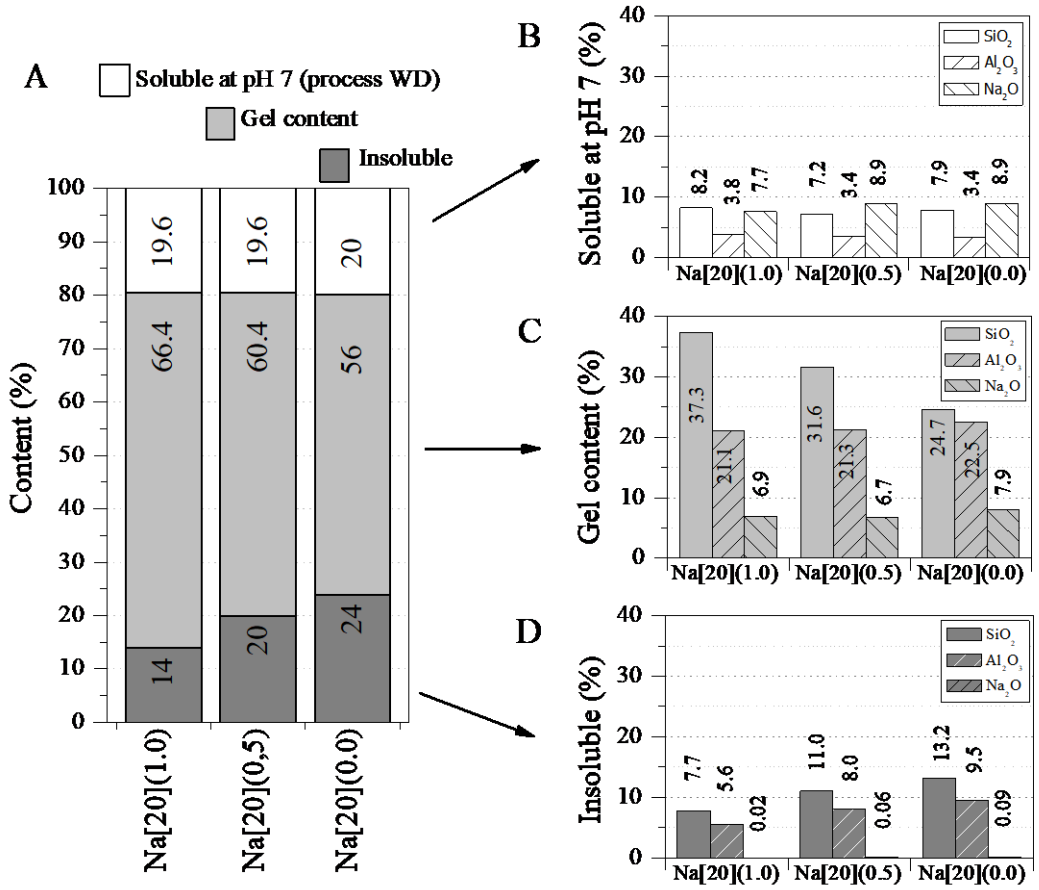

Figure 21 – Oxide compositions (SiO_2, Al_2O_3 and Na_2O, mass basis, as a percentage of either the soluble at pH 7, gel or insoluble content as shown in A, B and C) of the solid phase obtained after the selective dissolution processes. A: The fraction of soluble, gel and insoluble components in geopolymers with Na[20]. B: Oxide compositions in the soluble content (obtained from process WD) (calculated from the gel, insoluble and total content). C: Oxide compositions in the gel content (obtained from process AD). D: oxide compositions in the insoluble content (obtained from process AD). All values are normalised such that the total sample material is 100 wt.%.

The quantity of alkalis within the material dissolved in acid (i.e. the gel content) is 43-47 wt.% (Figure 21C) of the total amount of oxide, along with 54-70 wt.% SiO_2 and 63.5-69 wt.% Al_2O_3. The use of sodium silicate induces the greater formation of a silica-rich gel structure. The content of alumina is relatively constant regardless of the synthesis conditions, and a low fraction (~3 wt.%) is leached at pH 7 (Figure 21B). The insoluble fraction is the remnant metakaolin precursor that is inert under acidic conditions, whose alumina and silica ratios are similar that of the original metakaolin, with a slight increase in the amount of silica. The sodium oxide content in the gel (Figure 21C) is less than half of the nominal sodium content in the initial geopolymer formulation (> 15% of Na_2O). The difference of initial geopolymer formulation and the composition of the resultant gel (oxide content from the filtered solid phase obtained in the acid dissolution) is shown in Figure 22, where it is possible to observe the removal of Na_2O in the geopolymer structure.

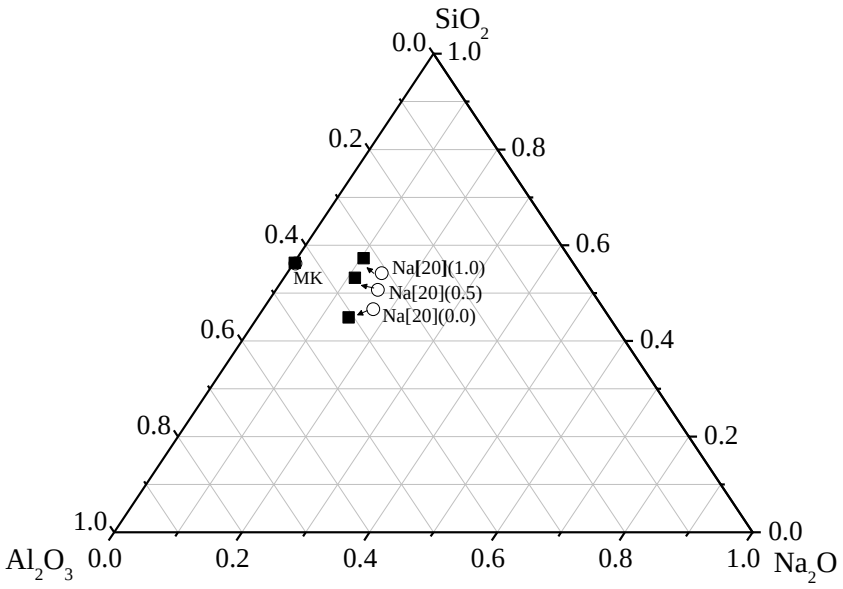

Figure 22 - Ternary diagram showing the chemical composition of the initial geopolymer formulation (white circles) and geopolymer gel formed (black squares) in the SiO_2-Al_2O_3-Na_2O system.

Leaching of components during the selective dissolution process will result in changes to the chemistry (as shown above) and microstructure of the M-A-S-H gel, which will affect the physico-mechanical performance of the geopolymer materials. Therefore, the geopolymers were analysed in their original form (without any dissolution process), after dissolution in pH 7 (process WD) (to examine the gel content) and after dissolution in acidic conditions (process AD) (to examine the unreacted metakaolin). The microstructural analysis was performed for the representative systems Na[20](1,0), Na[20](0,5) and Na[20](0,0) and is discussed in the following sections.

4.3.3 XRD analysis

Figure 23 shows the XRD data for anhydrous metakaolin, the geopolymer samples after 28 days of curing and the samples obtained after each dissolution process. A broad feature due to diffuse scattering is visible between 15° and 35° 2θ in the XRD data for metakaolin, indicating its amorphous nature and hence high reactivity. The crystalline peaks observed in metakaolin are attributed to anatase (TiO_2, Pattern Diffraction File, PDF# 00-021-1272) and halloysite ($Al_2Si_2O_5(OH)_4$, PFD# 00-029-1489). In the metakaolin-based geopolymer samples, a broad feature between 20° and 35° 2θ is observed, indicating formation of an amorphous reaction product consistent with a M-A-S-H gel (ZHANG et al., 2012, 2013). The crystalline phases identified in the unreacted metakaolin are observed in all geopolymers regardless of the synthesis conditions, indicating that these phases are inert under the assessed conditions. The ratio of the intensities of the broad feature at between 20° and 35° 2θ (attributed to M-A-S-H)

and the broad between 15° and 35° 2θ (attributed to unreacted metakaolin) in the XRD data for each geopolymer sample cured for 28 days increases with increasing soluble Si in the activator, indicating a greater reaction extent is promoted by increased soluble Si in the reaction mixture. This is consistent with the data from the selective dissolution processes discussed above.

After selective dissolution under acidic conditions (process AD), the intensity of the crystalline phases increases when related to the intensity of the broad feature and compared with the metakaolin XRD data. During the selective dissolution process, the amorphous M-A-S-H gel is consumed and the intensity of the broad feature due to this phase in the XRD data reduces, while the inert crystalline phases are not consumed, and hence the amount of these crystalline phases relative to the M-A-S-H gel increases, increasing the intensity of the reflections due to these phases in the XRD data. The Na[20](0.0) sample showed the formation of a zeolite phase exhibiting a Linde Type A structure (zeolite A, $Na_{96}Al_{96}Si_{96}O_{384}{\cdot}216H_2O$; PDF# 00-039-0222), which has also been observed in the use of in metakaolin-based geopolymers by Zhang et al. (2012).

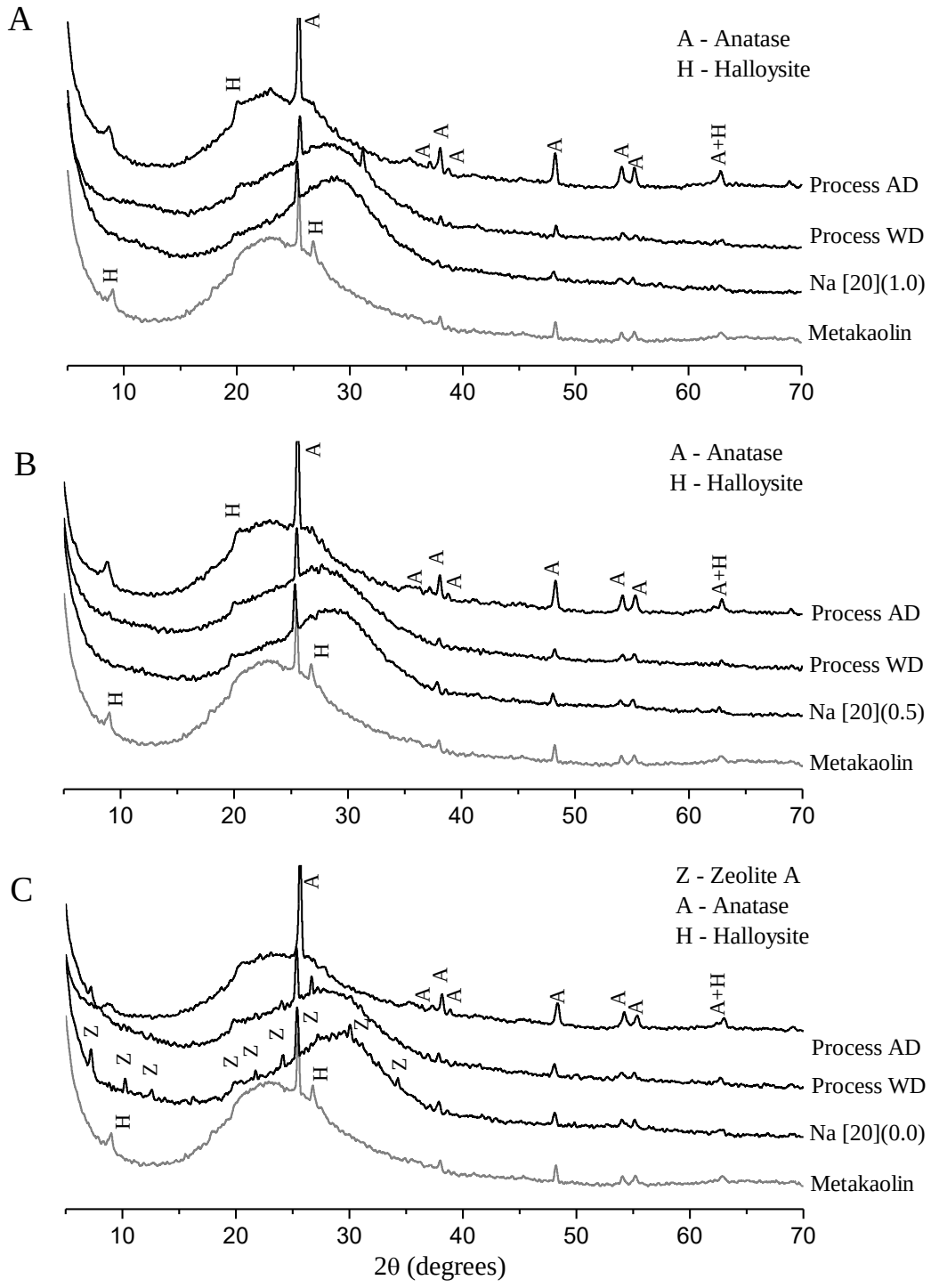

Figure 23 – XRD patterns of the anhydrous metakaolin precursor and geopolymers before and after the selective dissolution processes WD and AD. A: Na[20](1.0), B:Na[20](0.5), C: Na[20](0.0).

Examining the XRD data it is possible to observe the different microstructural transformations occurring during each selective dissolution process, mainly due to the AD process. During the selective dissolution process WD the removal of soluble elements (primarily Na, along with smaller amounts of Al and Si) were observed (Figure 21), however these did not result in any changes in the XRD data. The XRD patterns for the insoluble materials (after selective

dissolution under acidic conditions, process AD) are very similar to that of anhydrous metakaolin, suggesting that the insoluble material comprises unreacted metakaolin. This verifies the efficacy and suitability of the selective dissolution method adopted here. Movement of the broad feature due to diffuse scattering in the XRD data for each geopolymer system to higher or lower values of 2θ after each dissolution processes suggests significant microstructural changes are occurring (discussed in further detail below). The zeolite phase (Z) was identified in Na[20](0.0) (Figure 23C). Formation of zeolite phases is common in geopolymer systems contain nanocrystalline zeolites (PROVIS; LUKEY; VAN DEVENTER, 2005b), and the formation of this phase is therefore unsurprising. After selective dissolution at pH 7 (process WD), the zeolite A phase is partially dissolved, which means that this phase is not stable, possibly due to low crystallinity or small grain size. Dissolution of zeolites at neutral pH conditions has been previously reported, and this can result in degradation of the framework, partial dissolution of Si from the framework, and silicate precipitation (HARTMAN; FOGLER; ARBOR, 2007; YAMAMOTO et al., 1996). A small peak at approximately 31° 2θ is observed in the XRD data for Na[20](1.0) (Figure 23A). This is consistent with the main reflection of magnesium iron oxide (Fe_2MgO_4, PDF# 00-036-0398), and is attributed to minor contamination during preparation of this sample.

4.3.4 Solid state MAS NMR spectroscopy analysis

The ^{27}Al MAS NMR spectra of the anhydrous metakaolin precursor and geopolymer samples before and after each selective dissolution process are shown in Figure 24. Three broad resonances centred at δ_{obs}= 6, 32 and 57 ppm are identified in the spectrum for anhydrous metakaolin, which are assigned to aluminium in tetrahedral (IV), pentahedral (V) and octahedral (VI) coordination. These Al species are usually present in approximately equal proportions due to the highly disordered nature of Al sites in metakaolin (DUXSON et al., 2006, 2005b). According to other authors, halloysite contains Al(VI) sites as the main Al environment (MACKENZIE et al., 2007; NEWMAN; CHILDS; CHURCHMAN, 2006; SMITH et al., 1993) and will therefore, contribute to the intensity of the Al(VI) resonance in the ^{27}Al MAS NMR spectrum for this sample. During the geopolymerisation process, Al(V) and Al(VI) within metakaolin dissolve and react to form Al(IV) species within the geopolymer binder (DUXSON et al., 2005a). This is consistent with the formation of the main ^{27}Al MAS NMR resonance at δ_{obs}= 60 ppm observed in this study. This resonance is assigned to Al(IV) in a Q^4 environment within a highly polymerised N-A-S-H gel framework (DUXSON et al., 2005a; WALKLEY et

al., 2016a). Zeolite A in the system Na[20](0.0) will also contain Al(IV) environments (LIPPMAA; SAMOSON; MAGI, 2005; YANG et al., 2004), and these will contribute to the intensity in this region of the ^{27}Al MAS NMR spectra for this sample. In addition to the main Al(IV) resonance, a low-intensity resonance at δ_{obs}= 6 ppm is also observed in the ^{27}Al MAS NMR spectra for each sample. This resonance has the same line shape as that observed in the spectra of metakaolin precursor and is therefore attributed to the presence of unreacted metakaolin Al(VI) species (DUXSON et al., 2006). The ratio of the intensities of the Al(IV) and Al(VI) resonances (i.e. $I_{Al(IV)}/I_{Al(VI)}$) is greater as the soluble Si content in the activator (i.e. MS) is increased, indicating that the presence of soluble Si in the reaction mixture has promoted a greater reaction extent, consistent with observations from XRD and selective dissolution data discussed above.

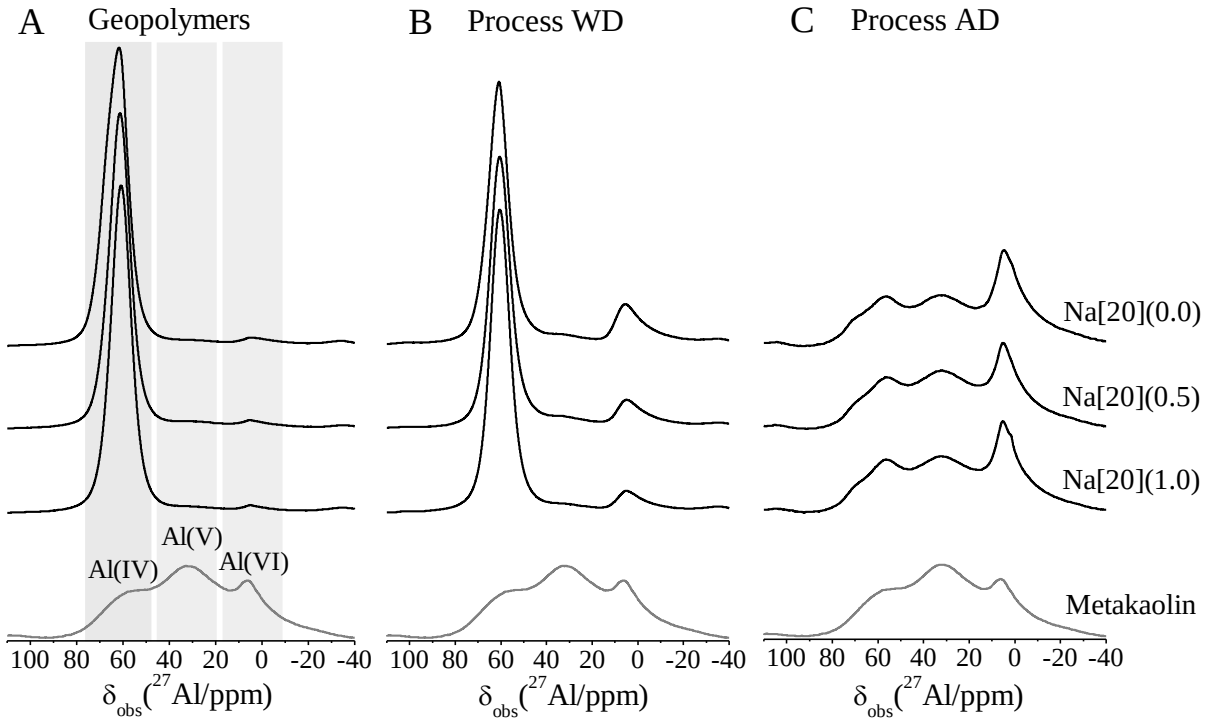

Figure 24 - ^{27}Al MAS NMR spectra (11.7 T, ν_R = 12.5 kHz) of the metakaolin precursor and geopolymers samples after selective dissolution under neutral pH (process WD) and acidic conditions (process AD). A: anhydrous metakaolin and geopolymers, B: after selective dissolution under neutral pH (process WD), C: selective dissolution under acidic conditions (process AD).

After selective dissolution at neutral pH (process WD), a reduction in the intensity of the main Al(IV) resonance is observed for each sample. As shown in Figure 21, soluble Al and Si species are dissolved, and this reduces the relative amount of Al(IV) species present in the solid phase after dissolution. The intensity reduction becomes more pronounced as soluble Si content in the activator is decreased (i.e. moving from MS = 1.0 to MS = 0.5 to MS = 0.0), consistent with the decrease in nominal Si/Al of these samples and thermodynamic preference for dissolution

of Al-O bonds (OELKERS; GISLASON, 2001), as well as previous findings that the amount of silica in the activator determines the speciation of aluminium during the reaction (DUXSON et al., 2005b). This intensity reduction as a consequence of the dissolution can be attributed to the removal of $Al(OH)_{4^-(aq)}$ in the gel pores (DUXSON et al., 2005b) and the removal of weaker or less crosslinked Al species. An intensification of the resonance at approximately δ_{obs}= 6 ppm is also observed after selective dissolution at neutral pH (process WD), which is due to the greater relative amount (and hence easier visibility) of the Al(VI) sites present in the anhydrous metakaolin precursor, which is inert under acidic conditions. This is consistent with the greater thermodynamic stability of Al(VI) when compared with Al(V) and Al(IV)(DUXSON et al., 2005b).

The ^{27}Al MAS NMR spectra of the remnant material obtained after selective dissolution under acidic conditions (process AD) show slight differences when compared to the spectrum of unreacted metakaolin, however the overall lineshape remains very similar. Higher intensity at δ_{obs} = 6 ppm is identified, indicating greater stability of Al(VI) species under acidic conditions when compared to Al(IV) and Al(V) species. The similarity between the residual solid phase after selective dissolution at neutral pH (process WD) and the as-cured geopolymers, and the similarity between the residual solid phase after selective dissolution under acidic conditions (process AD) and the metakaolin precursor, together indicate that the combined selective dissolution processes can quantify the amount of soluble, gel and insoluble content. Quantification of the gel and insoluble content will depend on the proportion of Al(IV), Al(V) and Al(VI) sites in the anhydrous metakaolin, and their relative stability under acidic conditions, however the effect on the quantified results will be minimal.

The ^{29}Si MAS NMR spectra for the metakaolin precursor and geopolymer samples are shown in Figure 25. The spectra for each sample exhibit a broad resonance in a position typically attributed to silicates and aluminosilicates (ENGELHARDT; MICHEL, 1987). Metakaolin exhibits a resonance centred at approximately δ_{iso}= -103 ppm, consistent with that observed by Duxson et al. (DUXSON et al., 2005b). This position is associated with the presence of silicon in tetrahedral coordination (Q^4) and aluminium in a distribution of tetrahedral, pentahedral and octahedral coordination (as observed in ^{27}Al MAS NMR analysis) in the silicate and aluminate layers of metakaolin (WHITE et al., 2010). Metakaolin comprises mainly $Q^4(m\text{Al})$ sites, as aluminosilicates which do not contain alkali or alkaline earth metals do not usually contain lower coordinated Si species (e.g. Q^1, Q^2 and Q^3)(DUXSON et al., 2005b). The position of this

resonance suggests that it comprises primarily Q^4(1Al) silicon sites, however, spectral deconvolution shows a presence of other tetrahedral silicon sites, mainly Q^4(0Al) and Q^4(2Al).

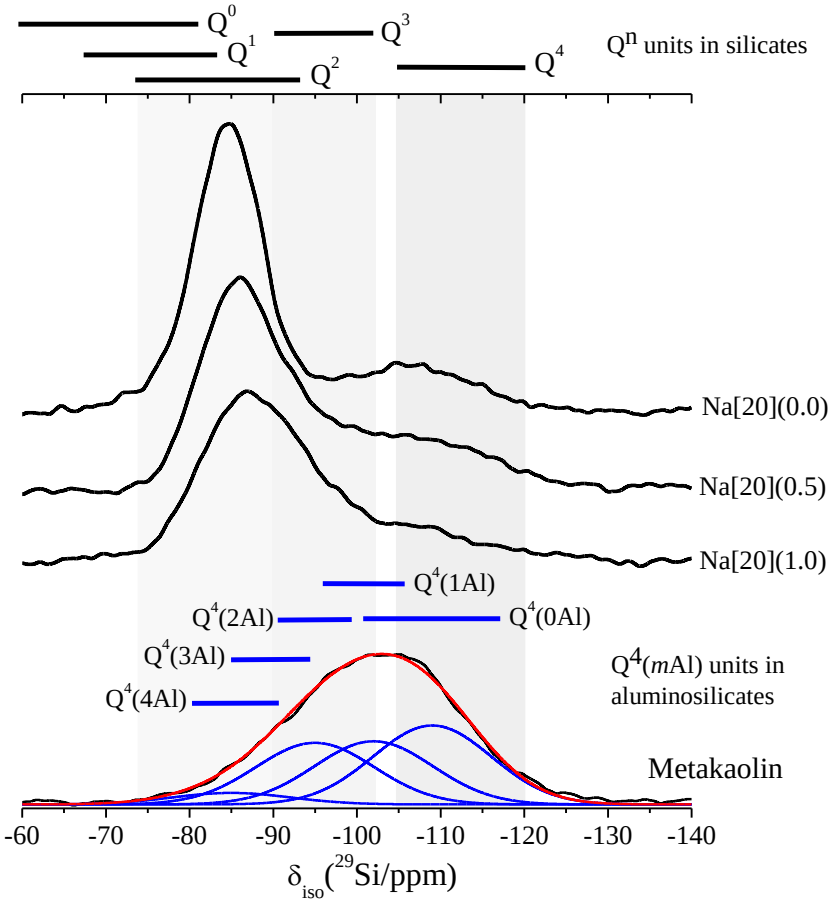

Figure 25 - ^{29}Si MAS NMR (11.7 T, ν_R = 12.5 kHz) data (black lines) of the anhydrous metakaolin precursor and geopolymers. Q^4(*m*Al) assignments are made with reference to the scientific literature as noted in the main text and summarised by Engelhardt et al.(ENGELHARDT, 1989). The simulation (red line) of the ^{29}Si MAS NMR spectra for anhydrous metakaolin precursor and associated spectral devonvolutions (blue lines) are shown at the bottom of the figure.

After geopolymerisation, the main ^{29}Si resonance shifts from δ_{iso} = -103 ppm in the metakaolin precursor to δ_{iso} = -84.8 ppm for Na[20](0.0), -86.1 ppm for Na[20](0.5), and -86.9 ppm for Na[20](1,0), indicating formation of Si sites within the M-A-S-H gel. The shifting of these resonances toward higher ppm is attributed to the replacement of Si by Al within the first coordination sphere of central Si atoms in the three-dimensional M-A-S-H gel framework (DUXSON et al., 2005b; ENGELHARDT; MICHEL, 1987). The intensity and breadth of the main resonance is due to contributions from varying contents of overlapping Q^4(*m*Al) species, whose relative quantities can be determined from spectral deconvolution using Gaussian distributions. Figure 26 shows the ^{29}Si NMR spectra and associated deconvolutions for each geopolymer sample and respective material after selective dissolution at neutral pH (process WD). The remnant unreactive metakaolin precursor (shaded spectra) is accounted for in the

spectral deconvolutions by linearly scaling the intensity of anhydrous metakaolin precursor resonances (the relative intensity of which is determined from the relative amount of insoluble solid phase to gel content, converted from a mass basis to a molar basis, determined from the combined selective dissolution processes) as shown in Figure 20.

The ^{29}Si spectral deconvolution for each sample comprises resonances at δ_{iso}= -70, -85, -90, -95, -100, and -110 ppm. The resonance at approximately -70 ppm is attributed to Q^0 sites and is only observed in the samples with high silicate content (i.e. MS = 1.0). This resonance is therefore attributed to monomer silicate structures (BASS; TURNER, 1997) from dissolved metakaolin and/or remnant soluble silicate that has not reacted. For aluminosilicates and metakaolin-based geopolymers the peaks between δ_{iso} = -85 ppm and δ_{iso} = -110 ppm can be attributed to Q^4(*m*Al) sites, in agreement with other studies (DUXSON et al., 2005b; ENGELHARDT; MICHEL, 1987; WALKLEY et al., 2018) .Q^3 and Q^2 sites resonate in the same region as Q^4(*m*Al) sites, making the coexistence of these species being possible, however the geopolymer framework has been shown to be fully polymerised and hence contains just Q^4 species (DUXSON et al., 2005b; WALKLEY et al., 2018). This is consistent with ^{27}Al MAS NMR data (presented above), which large amount of Al in tetrahedral coordination. Zeolite A contains Q^4(3Al) species (ENGELHARDT; MICHEL, 1987) that resonate at -89.6 ppm in ^{29}Si MAS NMR data, and hence will contribute to the intensity observed in this region in the ^{29}Si MAS NMR data for samples containing this phase. As observed in the XRD data, halloysite is present in the metakaolin precursor and all geopolymer samples. Halloysite contains Q^3(1Al) sites that resonates at -93 ppm (CERVINI-SILVA et al., 2013) and will therefore contribute to the intensity in this region of the ^{29}Si MAS NMR data for all samples. Spectral deconvolution shows that in the systems with sodium silicate as part of the activator there is a greater formation of Q^4 sites with more Si within the second coordination sphere of the central Si atom. This is expected due to the high content of soluble silicates in the reaction mixture and correlates with the observed increase in compressive strength values for these samples (shown in Figure 19).

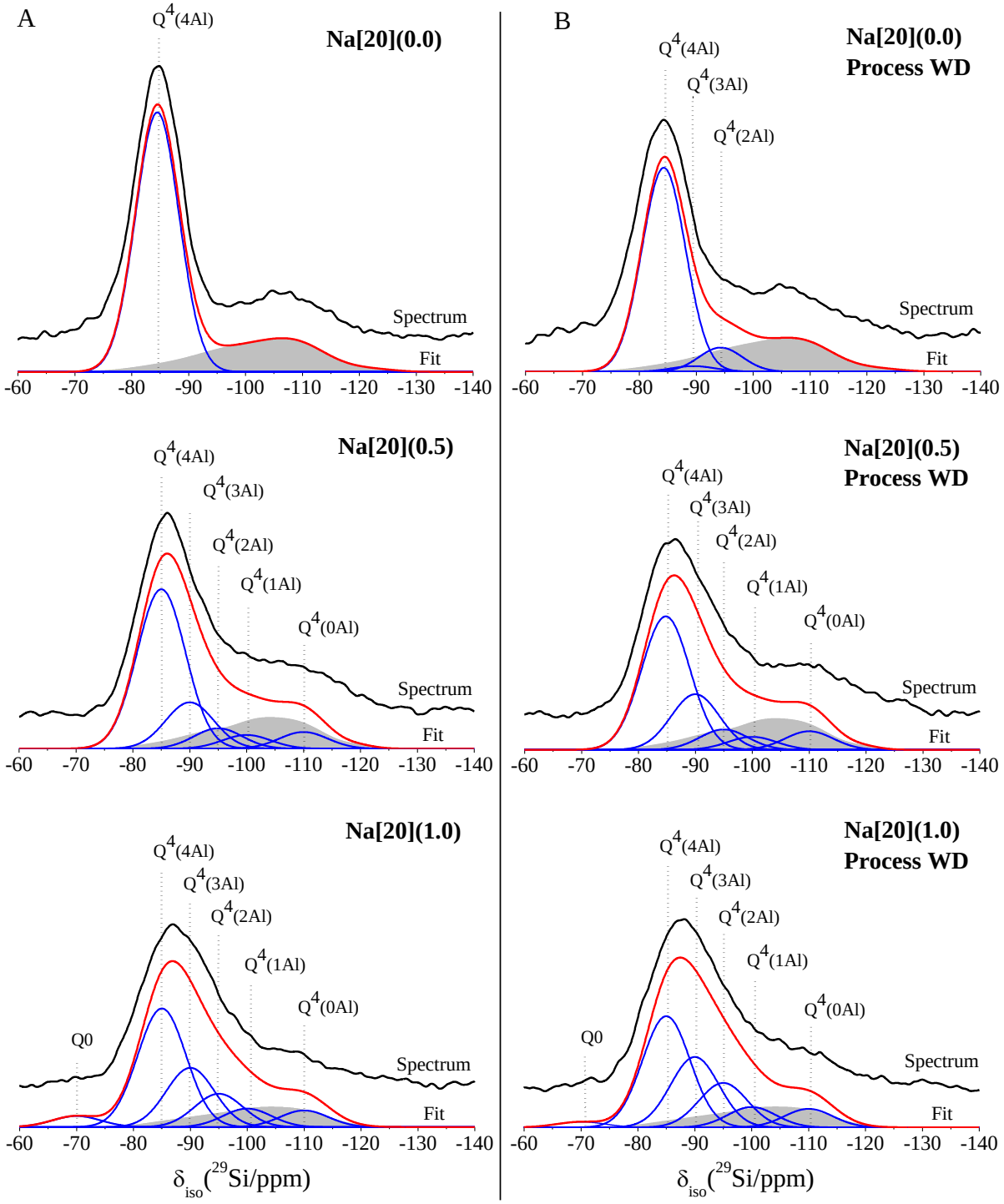

Figure 26 – ^{29}Si MAS NMR (11.7 T, ν_R = 12.5 kHz) data (black lines), simulations (red lines) and spectral deconvolutions (blue lines) for each geopolymer sample before and after selective dissolution at neutral pH (process WD). A: Deconvolution of spectra for the geopolymers and B: deconvolution of spectra for the solid phase obtained after the dissolution process WD. $Q^4(m\text{Al})$ assignments are made with reference to the scientific literature as noted in the main text and summarised by Engelhardt et al.(ENGELHARDT; MICHEL, 1987). The contribution from remnant unreacted metakaolin is shown as the shaded gray area.

The amount of each $Q^4(m\text{Al})$ site in the spectral deconvolutions was quantified and is shown in Figure 27. Engelhardt's formula (ENGELHARDT et al., 1981) (equation 1) was used to

calculate the molar Si/Al ratio of the N-A-S-H gel from the normalised relative integral areas, I_A, of each resonance in the ^{29}Si MAS NMR spectral deconvolutions from $Q^4(m\text{Al})$ sites in the NASH gel (excluding resonances due to $Q^4(m\text{Al})$ sites within remnant anhydrous metakaolin). Previous work has shown that Loewenstein's rulev (LOEWENSTEIN, 1954) (i.e. the absence of Al-O-Al bonds) is obeyed in synthetic alkali aluminosilicate gels with Si/Al > 1 (WALKLEY et al., 2018) and is therefore assumed to be obeyed in the systems studied here.

$$\frac{\text{Si}}{\text{Al}} = \frac{\sum_{m=1}^{4} I_{A_{Q^4(m\text{Al})}}}{\sum_{m=1}^{4} 0.25 \times m \times I_{A_{Q^4(m\text{Al})}}} \quad \text{(equation 1)}$$

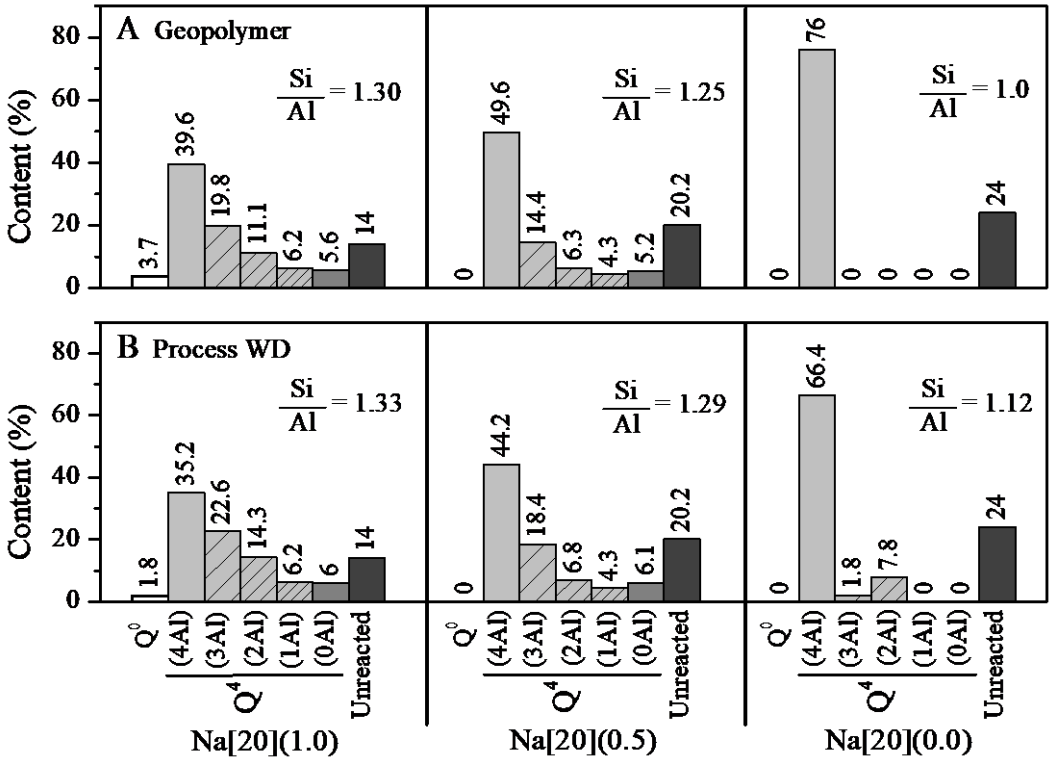

Figure 27 – ^{29}Si MAS NMR (11.7 T, ν_R = 12.5 kHz) peak quantification for each geopolymer sample before and after the selective dissolution at neutral pH (process WD)

These results show that higher values of compressive strength in the geopolymers are associated with a higher gel Si/Al ratio (i.e. greater Si addition in the gel framework), which is in agreement with Duxson(DUXSON et al., 2005b) and Fernandez-Jiménez (FERNÁNDEZ-JIMÉNEZ et al., 2006). This is readily observed in the Na[20](0.0) formulation, which is the system with the lowest content of silica (i.e. lowest nominal Si/Al ratio). The Na[20](0.0) gel consists solely of Q^4(4Al) sites, and exhibits the lowest compressive strength of this series (when activator type and dose are held constant).

XRF analysis (Figure 23) showed the dissolution of a high percentage of Na_2O, SiO_2 and Al_2O_3 during selective dissolution at pH 7 (process WD). This change is also observed in the ^{29}Si and

^{27}Al MAS NMR data by the reduction in intensity of the broad resonances attributed to Q^4(4Al) sites and an increase in the intensity of resonances due to Q^4(3Al) sites and Si-rich sites Q^4(2Al) and Q^4(1Al). This increase in Si-rich sites is not due to the formation of new Si environments, but rather a relative increase to compensate the loss of Q^4(4Al) sites, consistent with the fact that Al-O-Si bonds are weaker than Si-O-Si bonds and will therefore dissolve preferentially. The system with a high content of soluble Si in the activator is less affected due to the lower amount of Q^4(4Al) sites within the gel framework.

To verify the effectiveness of the selective dissolution process, Figure 28 shows the ^{29}Si MAS NMR spectra for the remaining solid material obtained after selective dissolution in acidic conditions (process AD). In all systems, the broad resonance exhibits a position (centred between δ_{iso} = -103 ppm and -108 ppm) and line shape similar to that of metakaolin. A slight shift to lower ppm is observed for all analysed samples after selective dissolution in acidic conditions, and this is attributed to the slight preferential dissolution of Al(IV) species from the remnant unreacted metakaolin precursor. This results in slight reduction in the amount of Q^4(*m*Al) species with high *m* values and a slight increase in the amount of Q^4(*m*Al) species with low *m* values. This is consistent with the observations from ^{27}Al MAS NMR, XRD and XRF data discussed above, which together indicate that the combined selective dissolution processes can quantify the amount of soluble, gel and insoluble content. As discussed above, quantification of the gel and insoluble content will depend on the proportion of Al(IV), Al(V) and Al(VI) sites in the anhydrous metakaolin, and their relative stability under acidic conditions, however the effect on the quantified results will be minimal and is expected to be within the experimental errors inherent in the data used for this analysis.

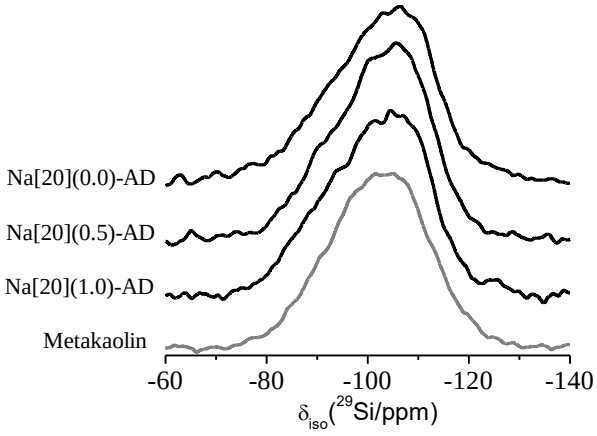

Figure 28 – ^{29}Si MAS NMR spectra (11.7 T, ν_R = 12.5 kHz) of unreacted metakaolin and geopolymer samples after selective dissolution under acidic conditions (process AD).

4.3.5 FTIR analysis

The FTIR spectra for the anhydrous metakaolin precursor and the geopolymer system with an activator dosage of 20% Na_2O are shown in Figure 29. In the spectrum for metakaolin, an intense peak is observed at approximately 1080 cm^{-1} that according to Rees (REES et al., 2007b) is assigned to asymmetric stretching vibrations of Si-O-T bonds, where T= Si or Al in tetrahedral coordination. The band at approximately 800 cm^{-1} is assigned to bending vibrations of Al-O bonds in AlO_6 octahedra (ZHANG et al., 2012). Both of these bands are consistent with the ^{27}Al MAS NMR data for metakaolin discussed above. The geopolymerisation process is observed in the FTIR data by the shift of the main peak in each sample from 1080 cm^{-1} to the region between 950 and 970 cm^{-1}. This change is due to the decrease in the Si/Al ratio (CRIADO; PALOMO; FERNANDEZ-JIMENEZ, 2005) of the tetrahedral Si sites in the sample during geopolymer gel formation (GRANIZO; PALOMO; FERNANDEZ-JIMENEZ, 2014; ZHANG et al., 2012). These were originally surrounded by low amounts of Al atoms (as much of the Al in metakaolin exists in Al(V) and Al(VI) sites). After dissolution of Al(VI) (indicated by the band at approximately 800 $cm^{-1}$and the ^{27}Al MAS NMR data discussed above), Al(V) and Al(IV) (indicated by the ^{27}Al MAS NMR data discussed above) from metakaolin during alkali-activation, the M-A-S-H gel framework is formed, with a larger number (relative to metakaolin) of Al atoms in tetrahedral coordination linked to tetrahedral Si atoms via oxygen bridges. This results in the observed shift of the band due to asymmetric stretching vibrations of Si-O-T bonds towards lower wavenumbers (HAJIMOHAMMADI; PROVIS; VAN DEVENTER, 2011; LEE; VAN DEVENTER, 2002; REES et al., 2007a).

Comparing the different systems evaluated, the movement of the central bands to higher wavenumbers is observed in the systems with activators containing higher contents of soluble Si. This is associated with the higher quantity of Si in the Si-O-T bonds (i.e. higher gel Si/Al ratio). Previous works assigned signals in the range between 1020 cm^{-1} and 998 cm^{-1} to the asymmetric stretching vibrations of Si-O-T (CRIADO; PALOMO; FERNANDEZ-JIMENEZ, 2005; ZHANG et al., 2012, 2013), and 940 cm^{-1} and 979 cm^{-1} to an asymmetric stretching vibration of non-bridging oxygen sites (Si-O-Na in the samples presented here)(ZHANG et al., 2012, 2013). These two bands are identified in the spectra here by deconvolution of the main Si-O-T band. The use of sodium silicate as the alkali activator shifts the centre of this peak to higher wavenumber values. According to this, the addition of soluble silicate results in increased Si in the M-A-S-H gel structure, consistent with the ^{29}Si MAS NMR data discussed

above, and a subsequent higher frequency Si-O-T vibration. The other band observed close to 859 cm^{-1} is attributed to bending of Si-OH bonds (ZHANG et al., 2013). Bands at approximately 690 cm^{-1} are the result of bending of Al-O-Si bonds (BERNAL et al., 2011), and indicate the formation of Al(IV) as the main Al environment in the geopolymer (ZHANG et al., 2012) (consistent with the ^{27}Al MAS NMR data discussed above).

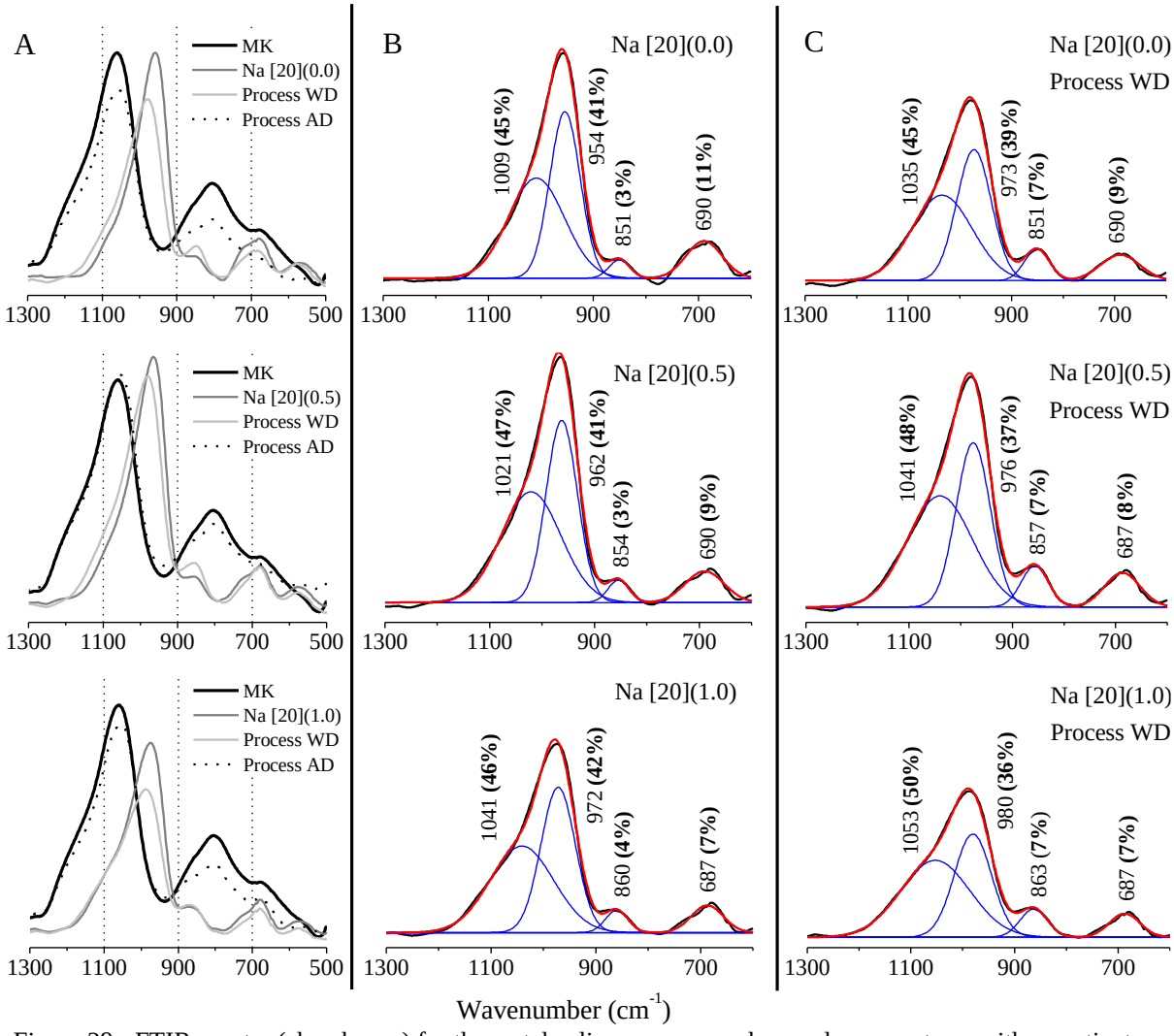

Figure 29 - FTIR spectra (absorbance) for the metakaolin precursor and geopolymer systems with an activator dose of 20% Na_2O before and after each dissolution process. A: The anhydrous metakaolin, geopolymer and solid material obtained after the dissolution processes WD and AD, B: Deconvolution of spectra for the geopolymers and C: deconvolution of spectra for the solid material obtained after selective dissolution at neutral pH (process WD).

According to Figure 29, the FTIR data for the solid material remaining after the selective dissolution process at neutral pH (process WD) exhibits a reduction in the intensity of the two main bands, which also shift to higher wavenumbers. This movement and change in intensity indicates the release of alkalis from Si-O-Na non-bridging oxygen sites (which result in the bands at approximately 940 cm^{-1} and 979 cm^{-1}), as well as dissolution of a small amount of Al(IV) sites (observed via ^{27}Al and ^{29}Si MAS NMR above) which results in a reduction of Si-

O-Al bonds. As observed in the ^{27}Al NMR results, aluminium is primarily present in tetrahedral coordination within the M-A-S-H gel structure, indicating the presence of a net negative charge due to Al^{3+} substituting for Si^{4+} that has been shown to be charge balanced by Na^{+} ions in sodium silicate and sodium hydroxide activated metakaolin (DUXSON et al., 2005b; ZHANG et al., 2013). Previous work has shown that in the presence of sufficient quantities of Al the negative charge on tetrahedral Al in N-A-S-H gel systems can also be balanced by an extra-framework Al atom, coordinated by six framework oxygen atoms (i.e. Al(IV) species)(WALKLEY et al., 2018). Thus, the removal of alkalis induces the distortion of the aluminosilicate framework where the Si asymmetric stretching vibration (Si-O-T) is shifted to higher wavenumbers, which is also consistent with the reduction of Al(IV) environment. This was also observed by the reduction from the band intensity associated with Al(IV) in ^{27}Al MAS NMR analysis and can be associated with conversion of Al in tetrahedral to non-tetrahedral environments bonding to Si (ZHANG et al., 2012).

After selective dissolution under acidic conditions (process AD), the FTIR spectra for the residual materials are very similar to that of anhydrous metakaolin. The shift of the bands that were present in the FTIR spectra of the geopolymers to lower wavenumbers, and similar lineshape of the FTIR spectra of the solid material after selective dissolution under acidic conditions to that of anhydrous metakaolin demonstrates the efficacy of the combined selective dissolution process, consistent with the XRD and NMR results discussed above.

4.3.6 SEM analysis

Figure 30 shows the SEM secondary electron images of anhydrous metakaolin and the geopolymer system Na[20](1.0) before and after the selective dissolution under neutral pH (process WD) and acidic conditions (process AD). As expected, metakaolin figure 12A) comprises plate-shaped particles. For the geopolymer samples (which were ground and passed through a75 μm sieve prior to analysis) the particle size is larger than those of metakaolin. After selective dissolution at neutral pH (process WD), the particle size and shape remained the same as that of the geopolymer, indicating that the removal of the soluble elements did not cause a morphological change in the material. After selective dissolution under acidic conditions (process AD), the particle size is reduced when compared to the geopolymer and the original metakaolin. Some particles still remain plated-shaped, indicating a portion of unreacted material.

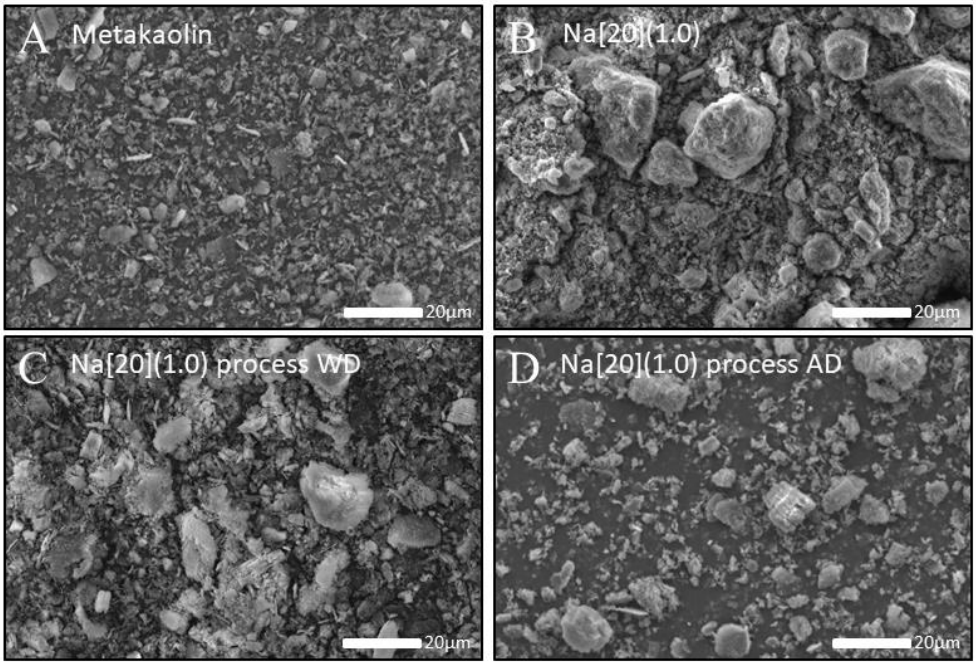

Figura 30 - SEM secondary electron images of A: anhydrous metakaolin, B: geopolymer Na [20](1.0), C: Na [20](1.0) after selective dissolution at neutral pH (process WD) and D: Na [20](1.0) after selective dissolution under acidic conditions (process AD).

4.6. CONCLUSIONS

This study developed a selective dissolution process to systematically investigate the reaction extent of metakaolin-based geopolymers produced with different design parameters and curing conditions. The selective dissolution process, based on dissolution under neutral (pH 7) conditions to remove the water-soluble materials and dissolution under acidic conditions (pH 0) using a strong acid to remove the geopolymer gel, is an effective method and its efficacy is confirmed by a range of detailed spectroscopic and microstructural analyses. This approach provides a method for accurate quantification of soluble materials, gel content and insoluble materials within geopolymers.

The compressive strength is dictated by the gel nanostructure. The use of soluble silicate in the activator plays an important role in relation to the Si/Al ratio within the gel, observed via differing amounts of $Q^4(m\text{Al})$ sites. The Si/Al ratio of the geopolymer gel increases by the higher degree of reaction provided as a result of the addition of soluble silicate to the reaction mixture. Higher amounts of soluble silicate results in increased gel formation; however, this can results in an excess of alkali, due to reduced need for charge balancing of Al^{3+} in tetrahedral sites, which is reflected in the large amount of soluble alkali content. The compressive strength

is also directly proportional to the amount of gel formed, although this effect is not as pronounced as that of the microstructural changes observed.

The content of soluble material in neutral pH conditions is mainly composed of M_2O, SiO_2 and Al_2O_3, where the alkalis are the main soluble fraction (representing values up to 50% of the total alkali content used) and the amount of alkali dissolution is dependent on the content of alkalis and soluble silicate of the activator. Spectroscopic and microstructural characterisation of the geopolymers shows that the extraction of alkalis from the geopolymer through a neutral dissolution process (water dissolution) results in a distortion of the framework structure with marked changes in the Al and Si environments. The removal of alkalis under neutral conditions shows nanostructural changes, including the reduction of Q^4(4Al) and Al(VI) species as observed by ^{29}Si and ^{27}Al MAS NMR and FTIR analysis. As the content of soluble silicate in the alkali activator is increased (i.e. higher MS content) the stability of Al-rich Q^4(*m*Al) sites is enhanced. This is visible in the system Na[20](1.0), with a high content of soluble silicate, which presents less nanostructural change when subjected to the dissolution process in a neutral environment.

Subsequent selective dissolution in acidic conditions dissolves the geopolymer gel content, leaving only the remnant unreacted metakaolin precursor which may then be quantified. Dissolution in acidic conditions also results in slight reduction in the amount of Al-rich Q^4(*m*Al) species from the remnant unreacted metakaolin precursor, and as such quantification of the gel and insoluble content will depend on the proportion of Al(IV), Al(V) and Al(VI) sites in the anhydrous metakaolin, and their relative stability under acidic conditions. The effect on the quantified results will, however, be minimal and is expected to be within the experimental errors inherent in the data used for this type of analysis.

The combined selective dissolution process provided here can therefore quantify the amount of soluble material, geopolymer gel and unreacted precursor in Ca-free geopolymer systems. This provides valuable new insight into the reaction product formed in metakaolin-based geopolymers, the state of alkalis in the structure and the nature of the selective dissolution processes, knowledge that is essential to define the design parameters and predict the durability of geopolymers materials.

REFERENCES:

ARBI, Kamel et al. A Review on the Durability of Alkali-Activated Fly Ash / Slag Systems : Advances , Issues , and Perspectives. **Ind. Eng. Chem. Res.** v. 55, p. 5439–5453, 2016.

BARATA, M. S.; ANGÉLICA, R. S. Caracterização dos resíduos cauliníticos das indústrias de mineração de caulim da amazônia como matéria-prima para produção de pozolanas de alta reatividade (Characterization of kaolin wastes from kaolin mining industry. **Cerâmica**, v. 58, p. 36–42, 2012.

BERNAL, Susan A. et al. Management and valorisation of wastes through use in producing alkali-activated cement materials. **Journal of Chemical Technology and Biotechnology**, 2016.

BERNAL, Susan A. Microstructural Changes Induced by CO2 Exposure in Alkali-Activated Slag/Metakaolin Pastes. **Frontiers in Materials**, v. 3, n. September, p. 1–10, 2016.

BUCHWALD, Anja et al. Purdocement: application of alkali-activated slag cement in Belgium in the 1950s. **Materials and Structures**, 2013.

CRIADO, M.; FERNÁNDEZ-JIMÉNEZ, A.; PALOMO, A. Alkali activation of fly ash: Effect of the SiO2/Na2O ratio. **Microporous and Mesoporous Materials**, v. 106, n. 1–3, p. 180–191, 2007.

CRIADO, M.; PALOMO, A.; FERNANDEZ-JIMENEZ, A. Alkali activation of fly ashes . Part 1 : Effect of curing conditions on the carbonation of the reaction products. v. 84, p. 2048–2054, 2005.

CRISTIANE, Kelly et al. Ativação alcalina de residuos de caulim. n. January, 2007.

CRISTIANE, Kelly et al. Activation Alkaline Waste Kaolin for Fabrication of Building Blocks. n. June, 2012.

DAMTOFT, J. S. et al. Sustainable development and climate change initiatives. **Cement and Concrete Research**, v. 38, n. 2, p. 115–127, 2008.

DAVIDOVITS, Joseph. Geopolymers: Inorganic polymeric new materials. **Journal of thermal analysis**, v. 37, n. 8, p. 1633–1656, 1991.

DOW, C.; GLASSER, F. P. Calcium carbonate efflorescence on Portland cement and building materials. **Cement and Concrete Research**, v. 33, n. 1, p. 147–154, 2003.

DUXSON, P. et al. Geopolymer technology: the current state of the art. **Journal of Materials Science**, v. 42, n. 9, p. 2917–2933, 2006.

DUXSON, Peter et al. The role of inorganic polymer technology in the development of 'green concrete'. **Cement and Concrete Research**, v. 37, n. 12, p. 1590–1597, 2007.

DUXSON, Peter; PROVIS, JL Jhon L. Designing precursors for geopolymer cements. **Journal of the American Ceramic Society**, v. 91, n. 12, p. 3864–3869, 2008.

FROENER, Muriel. **Valorização de Cinza de Fundo por meio da sintese de ligantes geopoliméricos: Otimiação de traços em pastas e avaliação dos sistemas em argamassa**. 2016. 2016.

GAO, Kang et al. Effects SiO2/Na2O molar ratio on mechanical properties and the microstructure of nano-SiO2 metakaolin-based geopolymers. **Construction and Building Materials**, v. 53, p. 503–510, 2014.

GARTNER, Ellis M.; MACPHEE, Donald E. A physico-chemical basis for novel cementitious binders. **Cement and Concrete Research**, v. 41, n. 7, p. 736–749, 2011.

GRANIZO, N.; PALOMO, A.; FERNANDEZ-JIMENEZ, A. Effect of temperature and alkaline concentration on metakaolin leaching kinetics. **Ceramics International**, v. 40, n. 7, p. 8975–8985, 2014.

IEA; WORLD BUSINESS COUNCIL FOR SUSTAINABLE DEVELOPMENT (WBCSD).; INTENATIONAL_ENERGY_AGENCY_(IEA). Cement Technology Roadmap 2009 Carbon emissions reductions up to 2050. 2009, p. 26.

IPCC. **Chapter 10 Industry, In "Intergovernamental panel on climate change)** Berlin, 2014.

JUENGER, M. C. G. et al. Advances in alternative cementitious binders. **Cement and Concrete Research**, v. 41, n. 12, p. 1232–1243, 2011.

LONGHI, Márlon et al. Geopolymers based on calcined kaolin sludge/ bottom ash blendsandan alternative sodium silicate activator. In: 34TH CEMENT AND CONCRETE SCIENCE CONFERENCE 2014, Sheffield. United Kingdom. **Anais**. Sheffield. United Kingdom

LONGHI, Márlon A. Málon A. M. A. et al. Valorisation of a kaolin mining waste for the production of geopolymers. **Journal of Cleaner Production**, v. 115, 2016.

LONGHI, Marlon Augusto Márlon Augusto. **Álcali-ativação de lodo de caulim calcinado e cinza pesada com**

ativadores convencionais e silicato de sódio alternativo. 2015. Universidade Federal do Rio Grande do Sul, Porto Alegre, 2015.

MOLIN, Dal et al. Cinzas volantes álcali-ativadas com solução combinada de NaOH e Ca (OH)2. p. 462–469, 2007.

MÜLLER, N.; HARNISCH, J. A blueprint for a climate friendly cement industry. **Report for the WWF–Lafarge Conservation Partnership.** 2008.

NAJAFI, Ebrahim; ALLAHVERDI, Ali; PROVIS, John L. Efflorescence control in geopolymer binders based on natural pozzolan.pdf. v. 34, p. 25–33, 2012.

PROVIS, John L.; BERNAL, Susan a. Geopolymers and Related Alkali-Activated Materials. **Annual Review of Materials Research**, v. 44, n. 1, p. 140205180727009, 2014.

SCRIVENER, Karen L.; JOHN, Vanderley M.; GARTNER, Ellis M. **Eco-efficient cements: Potential economically viable solutions for a low-CO2 cement-based materials industryUnited Nations Environment Programme**. Paris.

SCRIVENER, Karen L.; KIRKPATRICK, R. James. Innovation in use and research on cementitious material. **Cement and Concrete Research**, v. 38, n. 2, p. 128–136, 2008.

SCRIVENER, Karen L.; NONAT, André. Hydration of cementitious materials, present and future. **Cement and Concrete Research**, v. 41, n. 7, p. 651–665, 2011.

SHI, Caijun; JIMÉNEZ, A. Fernández; PALOMO, Angel. New cements for the 21st century: The pursuit of an alternative to Portland cement. **Cement and Concrete Research**, v. 41, n. 7, p. 750–763, 2011.

SHI, Caijun; KRIVENKO, Pavel; ROY, Della. **Alkali-activated Cement and concretes**. 1. ed. New York: Taylor & Francis, 2006.

ŠKVÁRA, František et al. Aluminosilicate polymers - Influence of elevated temperatures, efflorescence. **Ceramics - Silikaty**, v. 53, n. 4, p. 276–282, 2009.

ŠKVÁRA, František et al. A weak alkali bond in (N, K)-A-S-H gels: Evidence from leaching and modeling. **Ceramics - Silikaty**, v. 56, n. 4, p. 374–382, 2012.

VAN DEVENTER, Jannie S. J.; PROVIS, John L.; DUXSON, Peter. Technical and commercial progress in the adoption of geopolymer cement. **Minerals Engineering**, v. 29, p. 89–104, 2012.

YAO, Xiao et al. Geopolymerization process of alkali-metakaolinite characterized by isothermal calorimetry. **Thermochimica Acta**, v. 493, p. 49–54, 2009.

ZHANG, Zuhua et al. Quantitative kinetic and structural analysis of geopolymers. Part 1. The activation of metakaolin with sodium hydroxide. **Thermochimica Acta**, v. 539, p. 23–33, 2012.

ZHANG, Zuhua et al. Quantitative kinetic and structural analysis of geopolymers. Part 2. Thermodynamics of sodium silicate activation of metakaolin. **Thermochimica Acta**, v. 565, p. 163–171, 2013.

ZHANG, Zuhua et al. Fly ash-based geopolymers: The relationship between composition, pore structure and efflorescence. **Cement and Concrete Research**, v. 64, p. 30–41, 2014.

ZHANG, Zuhua et al. Efflorescence and subflorescence induced microstructural and mechanical evolution in fly ash-based geopolymers. **Cement and Concrete Composites**, v. 92, n. March, p. 165–177, 2018.

5. METAKAOLIN-BASED GEOPOLYMERS: RELATION BETWEEN EFFLORESCENCE FORMATION, DESIGN PARAMETERS AND PHYSICOCHEMICAL PROPERTIES [a]

5.1. INTRODUCTION

Geopolymer cements are engineered, sustainable alternatives to Portland cements that have proven application in a large scale in civil construction (GLASBY et al., 2015; PASSUELLO et al., 2017). These materials are well recognized in terms of mechanical performance and lower environmental impact resulting from low carbon dioxide (CO_2) emissions (BERNAL et al., 2016a; DUXSON et al., 2007b; HABERT; D'ESPINOSE DE LACAILLERIE; ROUSSEL, 2011; HABERT; OUELLET-PLAMONDON, 2016; HEATH; PAINE; MCMANUS, 2014; PASSUELLO et al., 2017; PROVIS, 2013; VAN DEVENTER; PROVIS; DUXSON, 2012). However, widespread implementation remains impeded due to a lack of knowledge related to some of its durability properties, as alkali-aggregates reaction, carbonation, acid attack and efflorescence, as well as the absence of standards for their characterization and production, and inhomogeneity of a materials supply chain (VAN DEVENTER; PROVIS; DUXSON, 2012).

Enhanced durability is one of the key drivers for adoption of this technology. Some authors (BAKHAREV, 2005; BERNAL; PROVIS, 2014; FERNANDEZ-JIMENEZ; PALOMO, 2009; PROVIS; BERNAL, 2014; PROVIS; VAN DEVENTER, 2014; ZHANG et al., 2014a; ZHANG; YAO; ZHU, 2010) have investigated geopolymer durability when these materials were exposed to several aggressive environments (marine condition, sulfate exposure and chloride ingress) and carbonation conditions. However, the design parameters controlling susceptibility of geopolymers to leaching of alkalis when exposed to water and subsequent efflorescence are still not fully understood. In particular, an effective methodology for efflorescence reduction remains absent from the literature.

Efflorescence results from leaching of free alkalis present in the pore structure when in contact with water. These leached alkalis then react with carbonic acid (formed by dissolution of

[a] O capítulo já está publicado em formato de artigo e pode ser acessado pelo DOI: 10.1016/j.compositesb.2019.107671

atmospheric carbon dioxide), forming alkali salts which crystallize on the geopolymer surface (LONGHI et al., 2019a; ŠKVÁRA et al., 2009; ZHANG et al., 2014b). Alkali salt crystals can also form within the pore network due to diffusion of dissolved CO_3^{2-} ions, a phenomenon known as subflorescence (ZHANG et al., 2018b). Efflorescence is observed in Portland cement (DOW; GLASSER, 2003), however the high concentrations of alkalis in geopolymer cements (the excess of which may not be chemically bound in the gel structure) makes them particularly susceptible to this phenomenon. Work to date has shown that the free movement of alkalis due to excess or non-effective reaction and extraction of the alkalis during leaching is influenced by the pore structure, where a denser structure and more tortuous pore network difficult the alkali movement (BERNAL; PROVIS, 2014; NAJAFI; ALLAHVERDI; PROVIS, 2012; ŠKVÁRA et al., 2009, 2012; YAO; YANG; ZHANG, 2016; ZHANG et al., 2014a, 2018b). Physical and chemical properties, which are related to formation of efflorescence, are dependent on design parameters and geopolymer formulation. This relation is complex, and effect directly the efflorescence formation, however poorly discussed, so this relation will be more investigated in this work.

Geopolymer production requires alkali activation of an amorphous aluminosilicate material (typically fly ash or metakaolin) with an alkaline solution (mainly blends of NaOH/KOH and sodium/potassium silicate (PROVIS; BERNAL, 2014)). The high content of alkalis used during activation can result in substantial leaching of the excess alkalis, with leaching of between 7 and 16 wt. % of the total alkalis as observed in previous studies (NAJAFI; ALLAHVERDI; PROVIS, 2012; ZHANG et al., 2014a). This can result in removal of alkalis from both the pore network and gel framework and affecting the geopolymer service life aesthetically due to the visual efflorescence formation or superficial deterioration and mechanically due to the reduction in compressive strength (YAO; YANG; ZHANG, 2016; ZHANG et al., 2018b). Very recently, we demonstrated that this deleterious process promotes significant changes in the chemical environment of the Al ions presented in the geopolymer gel. The removal of alkalis induces the reduction of Q^4(4Al) and Al(VI) species as observed by ^{29}Si and ^{27}Al MAS NMR and FTIR analysis (LONGHI et al., 2019c).

Geopolymers contain a pseudo-zeolitic three-dimensional aluminosilicate network comprising SiO_4 and AlO_4 tetrahedra. The negative charge arising from substitution of Al^{3+} for Si^{4+} in tetrahedral coordination is compensated by an alkali cation (commonly Na^+ or K^+) (FERNÁNDEZ-JIMÉNEZ et al., 2006). Therefore, the maximum content of Na^+ bound to the

gel framework is defined by the molar ratio $Al_2O_3/Na_2O=1$. Sodium can also be partially associated in the form of $Na(H_2O)_n^+$ with Na^+ in a hydrogen bond (FERNÁNDEZ-JIMÉNEZ et al., 2006) and associated with a framework oxygen bonds (WALKLEY et al., 2018). Excessive alkali ions are present in the pore solution and are not chemically bound (DUXSON et al., 2005a). The amount of geopolymer gel formed, the gel structure, the tortuosity of the pore network and the consequent susceptibility of the geopolymer cement to alkali leaching is also dependent on the reactivity degree of the precursor (which results in the presence of excess alkalis) (ZHANG et al., 2018b). On the same way, the reaction degree is dependent on the curing conditions and the amount alkalis and soluble silicate in the activator (NAJAFI; ALLAHVERDI; PROVIS, 2012; ZHANG et al., 2014b).

Despite the recent advances in understanding efflorescence formation, there remains an absence of knowledge about the fundamental relationships between precursor chemistry, reaction mixture formulation, gel microstructure and efflorescence. This knowledge can only be obtained through a systematic study varying design parameters in a simplified model system. Previous studies have primarily examined geopolymer cements produced from highly chemically and physically heterogeneous industrial by-products such as fly ashes and granulated blast furnace slag (BERNAL; PROVIS, 2014; NAJAFI; ALLAHVERDI; PROVIS, 2012; ŠKVÁRA et al., 2009, 2012; YAO; YANG; ZHANG, 2016; ZHANG et al., 2014a, 2018b). In contrast metakaolin derived from high purity kaolinitic clays exhibits a Si/Al ratio close to 1.0, high purity and reactivity, and provide a reliable and reproducible precursor for production of high purity geopolymers.

In the study presented here, we evaluate the efflorescence formation in series of metakaolin-based geopolymers (systematically varying the alkali and soluble silicate content of the activator, the type of alkali in the activator and the curing temperature) and correlate this phenomenon with the physical, chemical and microstructural properties of the gel. The effect of different design parameters of the extent of efflorescence formation was assessed by visual observation of efflorescence, characterisation of alkali leaching using pH measurements and measurement of alkali concentration by atomic absorption spectroscopy (AAS), compressive strength, water absorption, mercury intrusion porosimetry (MIP), scanning electron microscopy (SEM) and Fourier transformed infrared spectroscopy (FTIR).

5.2. EXPERIMENTAL PROGRAM

5.2.1 Materials and sample preparation

A commercial metakaolin (MetaMax – BASF) was used as the aluminosilicate precursor. The metakaolin has a mean particle size of 4.56 µm, specific surface area of 13.49 kg/m² and an oxide composition of 54.82% wt.% SiO_2, 42.57 wt.% Al_2O_3, 1.23 wt.% TiO_2, 0.48 wt.% Fe_2O_3 with 0.11 wt.% loss of ignition at 1000°C. This material exhibits a smaller particle size than other calcined clays used as a geopolymer precursor in previous studies (LONGHI et al., 2016; ZHANG et al., 2013), which results in a higher water consumption during geopolymer production. The particle morphology is shown in Figure 31.

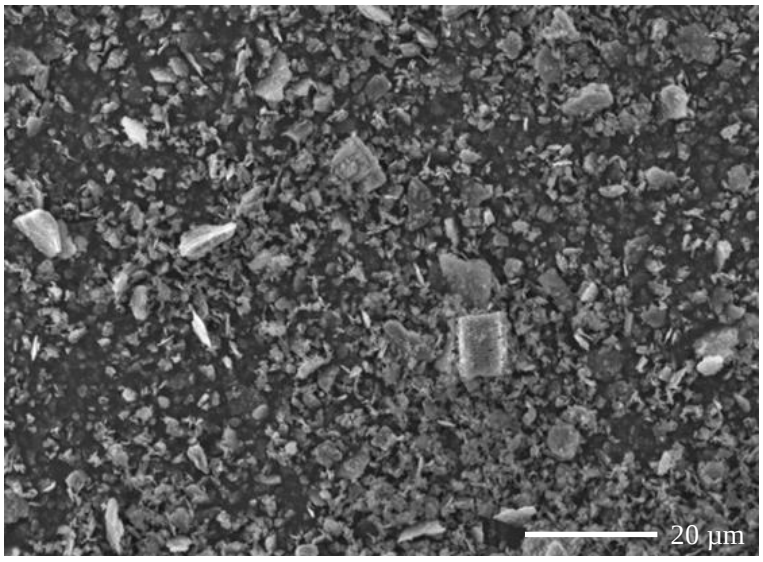

Figura 31– Scanning Electron Microscope (SEM) using secondary electron image of commercial metakaolin used in this study

The alkali activating solutions were prepared by initially mixing sodium hydroxide pellets (NaOH: ~99%, Chem-Supply, Australia) with distilled water to form a sodium hydroxide solution, and subsequently mixing the sodium hydroxide solution with a commercial sodium silicate solution (29.4 wt.% SiO_2, 14.7 wt.% Na_2O, and 55.9 wt.% H_2O, PQ, Australia) in proportions to reach the desired molar ratios.

Geopolymers were formulated with different alkali contents (M_2O= 15, 20 and 25 wt.%), using Na^+ as main alkali and K^+ in some mixtures. The content of soluble silicate in the activator (expressed by the modulus of silica MS, the SiO_2/M_2O molar ratio in the activator) was varied such that MS = 0.0, 0.5 and 1.0. The geopolymers were cured at either ambient temperature (~25°C) and relative humidity (RH) ≥ 90% or at 50°C. The increasing of temperature was made

in an oven, with a hermetically sealed box with water in the bottom, without contact with the samples. This process provides a high humidity and avoid the loss of water. The geopolymers were identified according to the content of sodium (H- high, 25%; M-medium, 20% and L- low, 15%) or sodium and potassium (Na+K) and the MS modulus (0.0, 0.5 and 1.0). The mix formulations of the geopolymers and their compressive strength (details of which are provided below) are shown in Table 3.

Tabela 3- Formulation of geopolymer samples

Geopolymers	Design parameters				Compressive strength (MPa)	Standard deviation (MPa)
	wt. % M_2O	MS modulus	Alkali	Temperature (°C)		
HA 0.0	25	0	Na	25	20.00	1.8
HA 0.5	25	0.5	Na	25	23.50	1.1
HA 1.0	25	1	Na	25	44.97	5.3
MA 0.0	20	0	Na	25	40.13	2.9
MA 0.5	20	0.5	Na	25	23.75	1.5
MA 1.0	20	1	Na	25	10.45	1.1
LA 0.0	15	0	Na	25	6.59	0.5
LA 0.5	15	0.5	Na	25	7.84	0.6
LA 1.0	15	1	Na	25	21.52	2.4
Na+K 0.0	20	0	Na+K	25	0.83	0.1
Na+K 0.5	20	0.5	Na+K	25	7.29	0.5
Na+K 1.0	20	1	Na+K	25	30.2	3.6
50°C 0.0	20	0	Na	50	13.92	1.3
50°C 0.5	20	0.5	Na	50	19.18	2.2
50°C 1.0	20	1	Na	50	35.15	3.2

M_2O= $Na_2O + K_2O$, **MS modulus=** SiO_2/M_2O molar ratio.

HA=25% Na_2O, **MA**=20% Na_2O, **LA**=15% Na_2O, **Na+K**=20%Na_2O+K_2O, **50°C**= 20% Na_2O + curing at 50°C.

Pastes were mixed or 5 min using a mechanical mixer and then were poured into molds. Geopolymers cured at 50°C were sealed with plastic film, stored in a plastic container and stored inside an oven for 24h. After one day, the samples were removed from the molds, sealed

with plastic film and stored during 27 days in room temperature (~25 °C) and RH ≥ 90% controlled during 24h per day.

5.2.2 Tests conducted

The efflorescence formation was assessed by visual observation of the samples after curing for 28 days. The environmental conditions were controlled at 20 ± 5 °C and RH of 65 ± 20%. The samples were subsequently submitted to two different treatments, as follows: (i) partial immersion in 5mm height of water, which was replaced every day to permit cycles of wetting and drying as well as alkali leaching; (ii) contact with air only to reduce alkali leaching and increase CO_2 diffusion of CO_2 into the pore solution (simulating natural carbonation).

Efflorescence was also evaluated by monitoring alkali leaching through the measurement of solution pH. A cylindrical sample of 20×35 mm (10 ml) was completely immersed in 500 ml of distilled water. The pH of this solution was measured every 10 minutes during the first hour, every hour during the first 6 hours and then daily until 30 days using a Eutech PC 2700 pH and conductivity analyser. To quantify the alkali concentration in the solution surrounding the sample, 10 ml of solution was removed after 30 min, 6 h, 24 h and 28 days and analysed by Shimatzu Atomic Absorption Spectrophotometer (AAS, AA-7000) for the elements Na and K using the emission method. The calibration curve was made using 4 points using distilled water and pure reagents.

Water permeability was quantified using the capillary absorption method where the dried cylindrical samples (28mm diameter and 55 mm height) were partially immersed in 5mm of water. This test was performed in a sealed plastic container to prevent water loss and evaporation. The amount of absorbed water was measured every 10 minutes in the first hour and then every hour up to achieve constant mass. The data are reported as the quantity of water absorbed (g) per the cross-sectional area of the sample (cm^2). The pore size distribution was also characterised using mercury intrusion porosimetry (MIP).

The compressive strength of hardened samples (20 mm cubes) was tested at 28 days of curing using an MTS universal mechanical testing machine with a loading speed of 0.5 mm/min. The density was calculated using the mass and volume of the dried sample used during the water absorption test. The sample was dried in an oven, with 50°C until obtain the mass constancy.

The open porosity was calculated from the ratio of the water mass absorbed to the sample volume, using the same samples of water absorption test.

The products formed under the surface of the samples during the partial immersion (treatment i) and carbonation (treatment ii) were analysed at the Brazilian Nanotechnology National Laboratory LNNano (Laboratório Nacional de Nanotecnologia), using a high resolution FEI Quanta 650 FEG scanning electron microscope (SEM). The instrument was equipped with an Everhart Thomley SED (secondary electron detector) and an In-column detector (ICD) for secondary electrons in bean deceleration (BD) mode. Working with a high resolution Schottky field emission (FEG), accelerating voltage of 10kV in a probe current ≤ 200 nA. The samples used were a fracture surface of the specimen. Prior to analysis the sample was a dried at 60 °C for 2 hours, placed on a carbon tab and coated with gold for 60s at a current of 40A. And a JEOL-JMC-6000PLUS instrument, with a voltage of 10kV.

The samples were analysed by X-ray diffraction (XRD) using a Siemens D5000 diffractometer with Cu Ka radiation (λ=1.54178 Å), with a step size of 0.02°, and a scanning speed of 0.5°/min for a 2θ range of 5 to 70°. Fourier transformed infrared spectroscopy (FTIR) data was acquired using a Perkin Elmer FTIR spectrometer in absorbance mode from 4000 to 400 cm^{-1}. The data between 600 – 1400 cm^{-1} were deconvoluted using Gaussian curves according to the literature (Rees, et al., 2007).

5.3. RESULTS AND DISCUSSION

5.3.1 Efflorescence formation

5.3.1.1 Visual inspection

Figure 32 and Figure 33 show the efflorescence formation in the samples after partial immersion in water (treatment i) and exposure to ambient air (treatment ii), respectively. Figure 32 shows the evolution of efflorescence formation in the system with 20 wt.% of Na_2O cured at room temperature, in ambient conditions, which is also defined as the reference system hereafter. After 28 days of partial immersion in water it is possible to identify severe efflorescence formation on the surface of the samples regardless of the synthesis conditions (MS content). However, after 7 days of partial immersion in water, the system MA 0.0 and MA 0.5 showed higher efflorescence formation when compared to the corresponding systems with MA 1.0. This

indicates that addition of soluble silicate in the activator therefore reduces the extent of efflorescence.

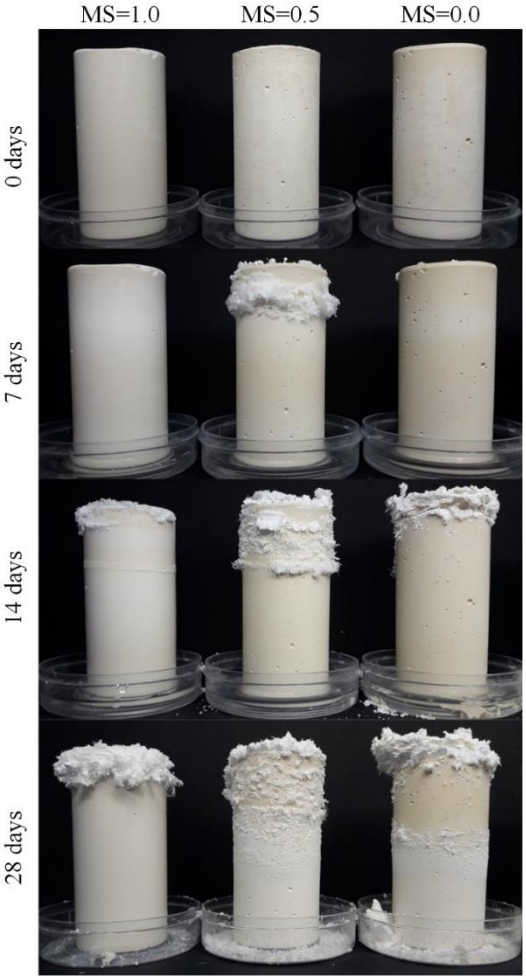

Figura 32 – Images of the evolution of efflorescence during 28 days for the systems with 20% of Na_2O and different contents of soluble silicate (MS = 0, 0.5, and 1.0). All samples were partially immersed in water as described in the main text.

The differences in extent of efflorescence result from differences in the rate of movement of the alkalis through the pore network in each system. According to (SCHERER, 1990), the transport process and rate of movement of fluid and in this case alkalis obeys the Darcy's Law, where the flux ($J=-\kappa.\Delta\rho/\eta$) into the porous material is dependent on permeability (κ), viscosity (η) and pressure (ρ). The constant permeability is an intrinsic property dependent on the material and can be associated to the size of the pores and tortuosity of the pore network. On the other way, pressure is dependent on external condition. In case of porous materials as geopolymers the main pressure associated to fluids movement is from capillary pressure. To this situation, according to Scherer (SCHERER, 1990), in evaporation condition, due to the energetic solid/vapor interface, liquid tends to spread from the interior to prevent the increasing of pressure. In the correct conditions of humidity where evaporation is possible, the drying

process allows the movement of fluids to the surface of the geopolymer cement, and consequently results in a high concentration of alkalis on the surface (typically to the point of saturation). Efflorescence then occurs when the carbonic acid (formed due to diffusion of atmospheric CO_2 into water) reacts with alkalis in the solution at the surface of the sample to form alkali salts (typically sodium or potassium carbonates) that crystallize and precipitate (defined by humidity and temperature). Efflorescence is therefore dependent on geopolymer microstructural features (pore size and pore network tortuosity). The content of soluble silicate in the activator has been shown to control the density (and hence pore size) and therefore plays an important role in retarding efflorescence formation, especially when large quantities of this material (or higher values of MS) are used. These findings are consistent with previous work examining efflorescence in fly ash-based geopolymers (ZHANG et al., 2014a).

Figure 33 shows a comparison of the evolution of efflorescence formation for all systems where the samples are partially immersed in water (treatment i) and exposed to ambient air (treatment ii). When exposed to ambient air systems with the highest alkali content (Na_2O = 25%) and MS values of 0.5 and 0.0 showed higher efflorescence formation. The systems with higher content of soluble silicate (MS=1.0) did not show any efflorescence formation regardless the alkali concentration (Na_2O = 15, 20 or 25%). This indicates that the addition of soluble silicate in the activator therefore also provides higher resistance to efflorescence formation in samples exposed to ambient air. The samples partially immersed in water (treatment i) showed significantly higher efflorescence formation than those exposed to ambient air. Systems in which only Na was used as the alkali source (HA, MA and LA) showed the most severe superficial deposition of efflorescence, even at higher values of MS.

Figura 33 – Images of efflorescence of geopolymer samples after 28 days of either partial immersion in water or exposure to ambient air. HA= 25% Na_2O, MA= 20% Na_2O, LA= 15% Na_2O, Na+K=20% Na_2O+K_2O, 50°C= 20% Na_2O + curing at 50°C.

A significant reduction in efflorescence formation in samples both partially immersed in water and exposed to ambient air is identified for systems with 20% of Na+K (i.e. when the alkali source is both Na and K). Of these mixed alkali systems, the system with Na+K 0.0 showed the highest efflorescence and sample degradation both when partially immersed in water and

exposed to ambient air. The system with 20% of Na+K and MS=0.5 showed a significant reduction in the extent of efflorescence (consistent with the above observation of reduced efflorescence when soluble silicate is added to the activator). However, an unexpected increase in efflorescence was identified for the geopolymer Na+K 1.0. According to (ŠKVÁRA et al., 2009), the efflorescence formation can be partially prevented by the replacement of Na with K due to the high solubility of potassium carbonate (K_2CO_3) compared with sodium carbonate ($Na_2CO_3.nH_2O$).

The systems with 20% of Na_2O cured at 50°C exhibit a reduction in the efflorescence formation compared to those cured at 20°C, with a reduction of efflorescence again observed with the addition of soluble silicate. This indicates that curing at elevated temperatures reduces the susceptibility of geopolymers to efflorescence. This observation is consistent with previous work from (ZHANG et al., 2014b) and (NAJAFI; ALLAHVERDI; PROVIS, 2012), where the reduction was attributed to the pore refinement.

The characteristics of the efflorescence formation differs depending on the geopolymer formulation, as shown in Figure 33. The results indicate that lower content of sodium silicate influence the mechanical behaviour and aesthetic of geopolymers. In the first case (see Figure 34A), a layering process is identified due to the excess of efflorescence in the top of the sample and excessive crystals growing into the porosity. In the second case (see Figure 34B), the excess of alkali movement, high evaporation throughout a sample with high porosity and low mechanical strength promoted a deeper degradation (~ 3 mm) and higher delayering process even in most of the faces of the sample. In the last case (see Figure 34C) is identified a foamier white efflorescence with delayed degradation, due to the excessive alkali content used as activator.

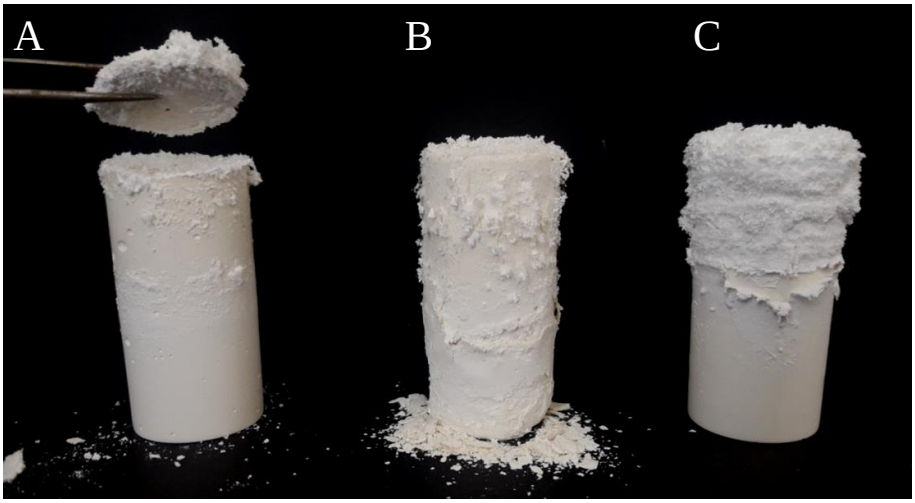

Figura 34 - Different types of deterioration in NaOH-based geopolymer samples: A. MA 0.0, B. Na+K 0.0 and C. HA 0.0

The extent of efflorescence formation is also dependent on the precursors used. In this study using metakaolin precursors, a larger quantity of alkali activator (between 15-25% of Na_2O) was used when compared with studies using pozzolan-based or fly ash precursors which typically use between 5 and 13% (NAJAFI; ALLAHVERDI; PROVIS, 2012)(ZHANG et al., 2014b). Alkali activation of metakaolin requires larger quantities of activator when compared to other precursors (such as fly ash or slags) due to the high reactivity and high amount of alumina (PROVIS; BERNAL, 2014). Thus, the systems under investigation in the study are therefore more susceptible to efflorescence than work utilising lower amounts of alkali activator.

Related to the compensation of the negative ion from Al in a tetrahedral coordination, the molar ratio of Na/Al ranges between 0.67 (Na_2O=15%), 0.88 (Na_2O=20%) and 1.11 (Na_2O=25%), giving nominal values close to or less than the maximum content of Na^+ that can be bound to the gel framework (i.e. such that the molar ratio Al_2O_3/Na_2O=1) when fully reacted (FERNÁNDEZ-JIMÉNEZ et al., 2006). As the extent of reaction does not progress to 100%, a significant amount of excess alkali (i.e. those not chemically bound to the gel framework) is expected, and will be particularly susceptible to leaching. When lower values are used, the extent of reaction is also lower, inducing less formation of gel, as observer by (LONGHI et al., 2019c). The same author observed that the alkali available to efflorescence formation is derived from the excess of alkali used as activator or from the solubility of this material in weak bond when in a neutral environment.

In addition to the visible surface efflorescence during carbonation, subflorescence (internal carbonation) can also occur, with carbonate crystals forming inside of the pore network. This

results in a significant pressure increase within the pore network (SCHERER, 2004) that can cause significant structural damage (ZHANG et al., 2018b). During the development of efflorescence, some geopolymers samples exhibited a delayed degradation, which is attributed to the pressure promoted by carbonates crystal formation into a porous structure.

The different concentration of soluble alkalis generates the formation of different types of crystals. Figure 35 shows the XRD diffractograms of the superficial efflorescence products for the geopolymers in system MA 1.0, MA 0.5 and MA 0.0 (SEM images shown in Figure 35A, B, and C, respectively). The results indicate that all systems are composed of sodium carbonate (Na_2CO_3, Pattern Diffraction File, PDF # 01-086-0301), sodium carbonate monohydrate (thermonatrite, $Na_2CO_3.H_2O$, PDF # 01-070-2148) and sodium carbonate decahydrate (natron, $Na_2CO_3.10H_2O$, PDF # 00-015-0800), aligning with previous observations of efflorescence products in geopolymers produced from fly ash (BURCIAGA-DÍAZ et al., 2010; ŠKVÁRA et al., 2009; ZHANG et al., 2014a). Is also observed broad feature near to 22 degrees, which can be attributed to leached products during the efflorescence formation. This extent of hydration of sodium carbonate is dependent on the content of alkali concentration, temperature, humidity, and capillary pressure. According to some previous studies (KOBE; SHEEHY, 1948; MAHMOUDKHANI; KEITH, 2009; WELLS; MCADAM, 1907), the crystallization of decahydrate sodium carbonate happens from low concentration, initiating near to 0.6 Na_2CO_3 mol/l at 0 °C to 4.3 Na_2CO_3 mol/l at 32 °C. The increasing of this temperature induces the formation of monohydrates ($Na_2CO_3.H_2O$) and anhydrous (Na_2CO_3) phases. To this study, systems with lower amounts of soluble silicate in the activator exhibit higher intensity reflections in the diffractograms, indicating that lower amounts of soluble silicate in the activator results in formation of a higher amount of sodium carbonate phases. According to Scherer (2004) and Zhang *et al.* (2018) the amount of sodium carbonate phase formation is controlled by the crystallization pressure and humidity within the pore network, while the extent of carbonation and pore size controls the deterioration of the geopolymers cement. These statements are consistent with that observed here, where the extent of efflorescence is dependent on the properties of the formed gel, therefore consistent with the decreased levels of efflorescence and sample deterioration with increased amounts of soluble silicate in the activator discussed above.

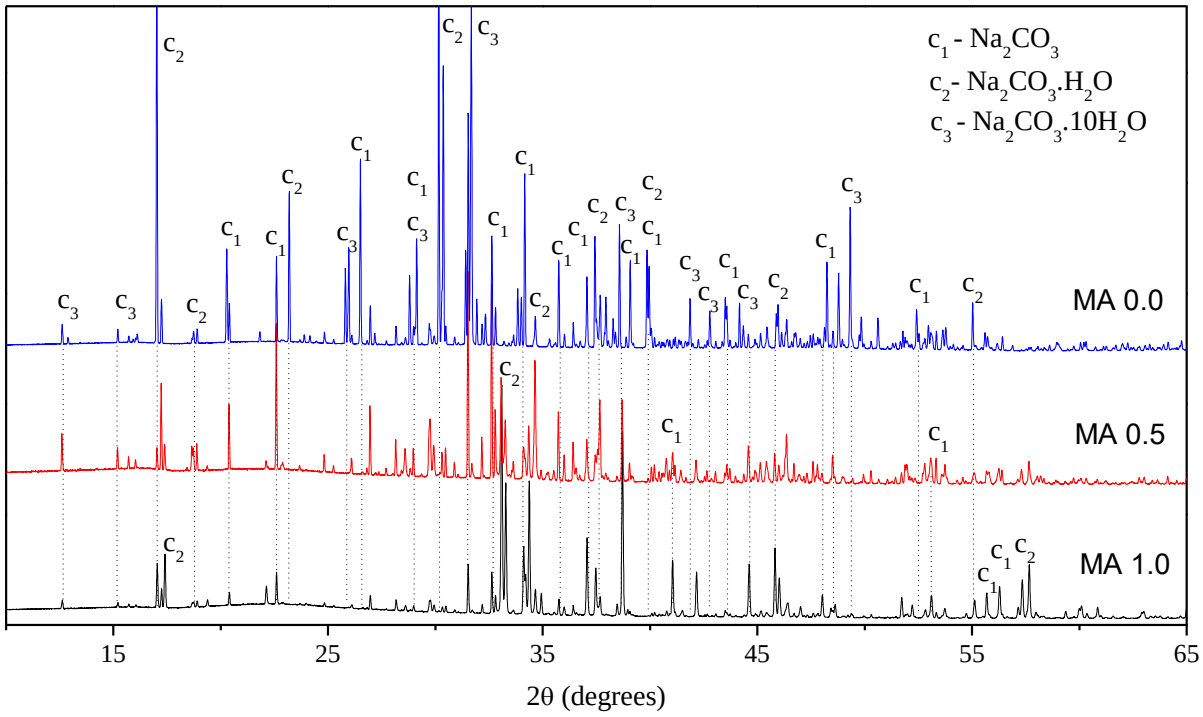

Figura 35 – XRD patterns of the efflorescence products from the surface of geopolymers MA 1.0, MA 0.5 and MA 0.0

Additionally to XRD data, sections of the degraded samples (exclusively from the Na_2O 20% system) were analysed by SEM (Figure 36A, B and C) to observe their morphology and the presence of any crystalline phases. For comparison, a drop of each activator was allowed to evaporate and crystallize in ambient air to investigate alkali salt precipitation and crystallization in the absence of the geopolymer cement or metakaolin precursor. These phases were also analysed by SEM (Figure 36 D, E, and F).

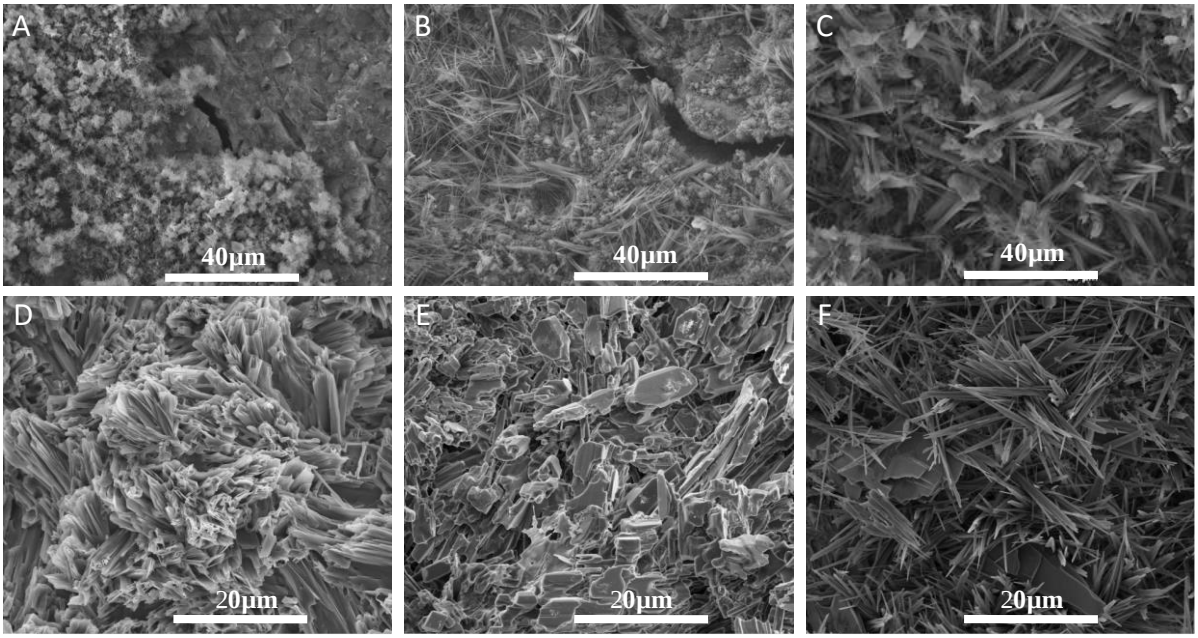

Figura 36 – Scanning electron microscopy using secondary electrons images of efflorescence products formed on the surface of geopolymers samples synthesized at different conditions: A: geopolymer MA 1.0, B: geopolymer MA 0.5, C: geopolymer MA 0.0, D: activator MA 1.0, E: activator MA 0.5, F: activator MA 0.0.

Figure 36A (geopolymer) and Figure 36D (crystallised activator) correspond to the system MA 1.0 (high amounts of soluble silicate, Figure 32). The crystals formed on the geopolymer surface (Figure 34A) are small crystals (< 10 µm). Figure 36D shows bigger crystals formed after crystallisation of the activator in contact with air, where layers of crystals in different directions can be observed. The formation of larger crystals is observed on the surface of the geopolymer and the crystallised activator for the system MA 0.5 (moderate amounts of soluble silicate, Figure 36B and Figure 36E), with crystallised activator exhibiting the larger crystals of the two. The geopolymer and crystallized activator for the system MA 0.0 (no soluble silicate, Figure 36C and Figure 36F) show the formation of the largest crystals of all systems analysed in form of both needles and platelets (> 20 µm) , consistent with the higher degree of degradation identified for the NaOH-based geopolymers (MS=0.0). Both the geopolymer and crystallised activator that do not contain soluble silicate exhibit a different morphology when compared to the crystallised activator containing soluble silicate, showing the formation of needle-like crystals rather than plate-like crystals. The crystal formation is associated with the amount of leached material and its composition, where the different shapes and sizes of the crystals indicate the formation of different products. The differing activator compositions and reaction extents of the geopolymers results in differences in extent of alkali solubility and hence formation of different carbonate crystals. To the crystallization of the activator, is observed the formation of different shapes, due to the presence of different amount of sodium silicate.

However, in the degraded samples, the main material leached to the geopolymers surface is the free alkali, resulting in the formation of needle-like crystals.

5.3.1.2 Evaluation of efflorescence potential using pH measurement

As efflorescence formation results from movement of free alkalis to the surface, the susceptibility of geopolymers to efflorescence may be quantified by measuring the pH of the solution in contact with the sample. The pH analysis of the solutions in which geopolymer samples fully immersed for up to 600 hours are shown in Figure 37. Each solution exhibited a rapid rise in pH, with a value of ~10.5 being reached after only two minutes. In all systems, geopolymers with MS content of 1.0 (high amounts of soluble silicate) exhibit lower pH values than those prepared with lower amounts (MS = 0.5) or without sodium silicate (MS = 0.0). This is consistent with the visual appearance of the samples (Figure 33), where the efflorescence formation takes a longer time for geopolymers with MS = 1.0. The values measured also showed a direct relation between pH and alkali concentration in the activator, where highest alkalinity in the solution was identified for the samples activated at 25% of Na_2O. Therefore, higher alkali leaching rates were observed in samples with larger alkali content in the activator. Increased amounts of soluble silicate in the activator in mixed alkali systems ($Na^+ + K^+$) results in lower pH values when compared those where the only alkali source was Na^+ (consistent with the visual observations of efflorescence in Figure 33). The systems with thermal curing (50 °C for the first 24 hours, then 20 °C thereafter) also exhibit lower pH values when compared to the corresponding systems cured at 20 °C, in agreement with visual observations of efflorescence (Figure 33). In general, the results show increasing pH values (and therefore alkali leaching) over time for all samples assessed. Previous work reports pH values between 11 and 12 up to 3 days of analysis using fly ash as a precursor and the amount of alkalis (represented by the percentage in mass of alkalis relative to precursor) between Na_2O/precursor relation between 5.8 and 6.5 wt.% and particles sizes between 1.2 and 1.5 mm (ZHANG et al., 2014a). The values observed in the study presented here are higher than that observed by Zhang et al. (ZHANG et al., 2014a) and result from the increased alkali content in the activator (between 3 and 4 times higher), longer exposure time and smaller particle size, which increases the contact area and facilitates the leaching process.

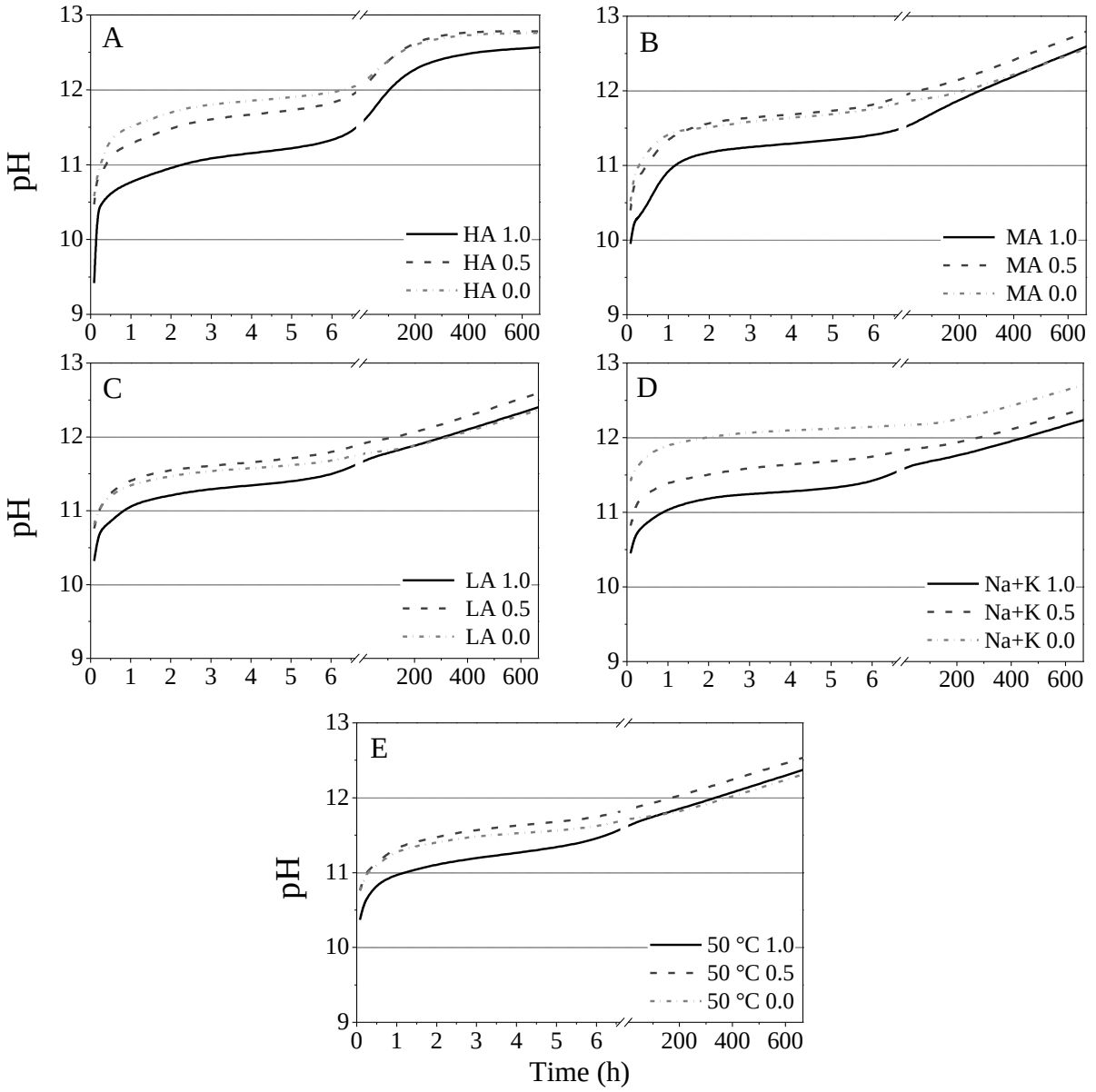

Figura 37 – pH values of the solutions in which each geopolymer system was immersed over time: A. 25% Na_2O, B. 20% Na_2O, C. 15% Na_2O, D. 20% Na_2O + K_2O and E. 20% Na_2O + thermal curing 50°C

5.3.1.3 Evaluation of efflorescence potential by alkali concentration

In additionally to measuring the pH of the solutions in which the samples were immersed, the concentration of Na^+ and K^+ in the solutions were quantified using atomic absorption spectroscopy (AAS) (Figure 38). The analysis was performed according to the type of alkali used as the activator (Na, K or Na + K).

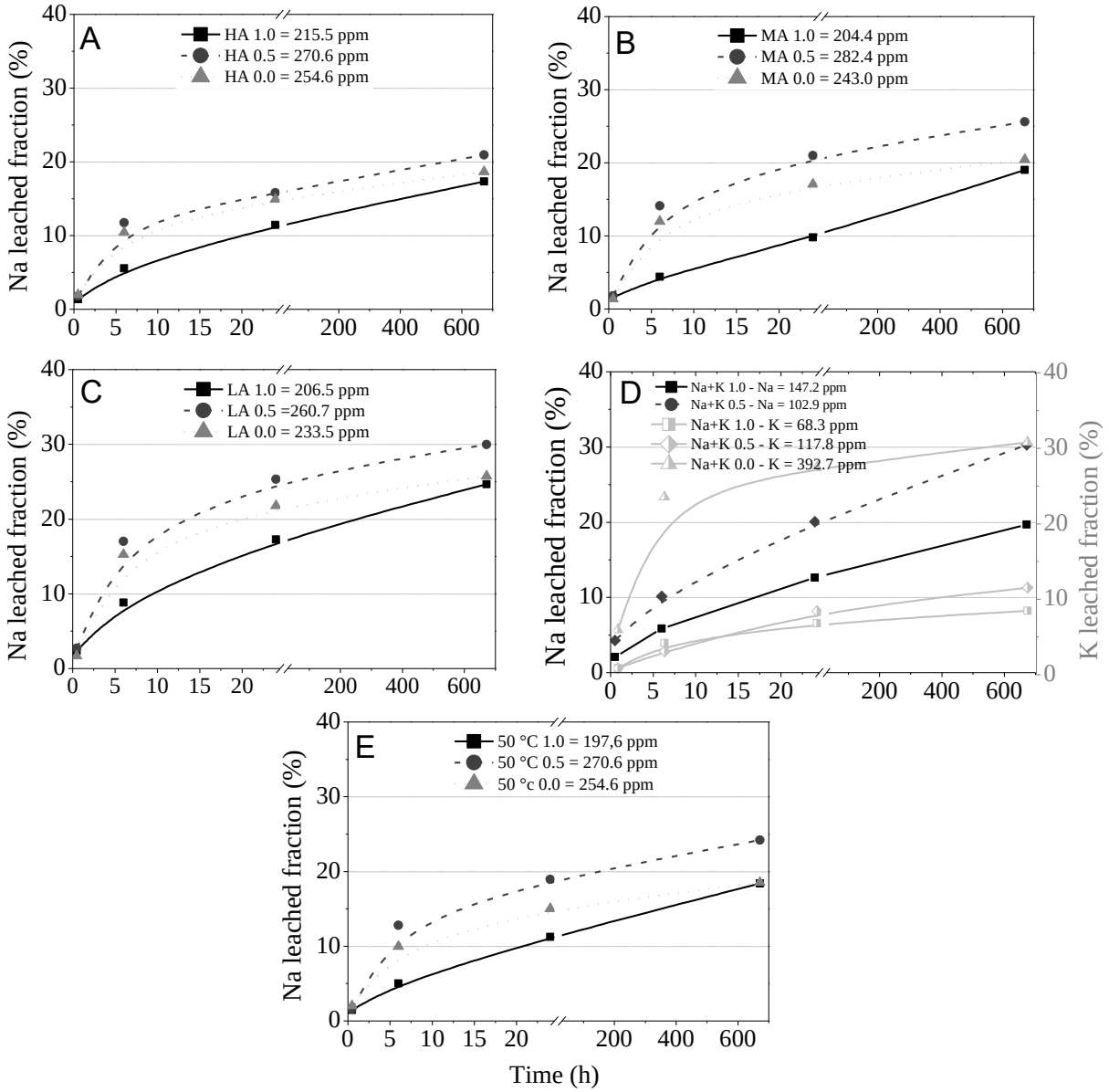

Figura 38 – Concentration of Na^+ and K^+ measured using atomic absorption spectroscopy: A. 25% Na_2O, B. 20% Na_2O, C. 15% Na_2O, D. 20% Na_2O + K_2O and E. 20% Na_2O + thermal curing 50 °C

The increasing in the use of soluble silicate results in lower alkali concentration in solution (and hence lower alkali leaching), and is particularly evident during the early stages of leaching. on average, the addition of sodium silicate (MS = 1.0) provides a reduction of approximately 14% when compared to hydroxide-based systems. This is consistent with the pH values discussed above and is attributed to the stronger chemical bonding of the alkalis to the gel framework, the greater sample density (consistent with the higher compressive strength) and pore network tortuosity in geopolymers with MS > 0.0. The reduction in alkalis leached from the geopolymer with increasing soluble silicate in the activator is also observed in mixed alkali (Na^+ + K^+) systems. However, in the absence of soluble silicates mixed alkali systems (Na+K 0.0) showed higher alkali leaching. This is attributed to a lower extent of reaction and geopolymer formation,

consistent with the behaviour observed by Longhi et al., (2019b), where the use of KOH as the main alkali activator does not provide an effective dissolution of precursor and gel formation. Minimal efflorescence formation was observed visually in these mixed alkali systems (Figure 33), even with high alkali concentrations. According to Škvára *et al*., (2009), K_2CO_3 presents a high solubility when compared with Na_2CO_3 at 20°C, which results lower precipitation of K_2CO_3 crystals and hence a lower extent of visible efflorescence, as observed by. According to Zeng and Zheng (2009), the solubility of the salt K_2CO_3 (112g/l at 20°C) is much higher than Na_2CO3 (30g/l at 20°C) and provides a smaller crystallization area. The systems with thermal curing (50 °C for the first 24 hours, then 20 °C thereafter), reduced alkali leaching (with a final Na^+ concentration of 220 ppm after 28 days). This is ~9% lower than the alkalis leached in the reference system (with a final Na^+ concentration of 240 ppm after 28 days). Therefore, it is clear that the amount of sodium silicate and the use of additional temperature of curing are the most effective synthesis parameter related to leaching reduction.

For the MK-based geopolymers assessed in this work, a dissolved alkali concentration of between 197.6 ppm (50 °C 1.0) and 392.7 ppm (Na+K 0.0) was observed, corresponding to 17% and 30% of the original alkali concentration used in the activator. Zhang *et al.* (2014b) reported a concentration of 12% and 16% of sodium and potassium, respectively, in fly ash-based geopolymers after 24 hours of immersion in water (concentrations of around 100 to 150 ppm). However, the authors evaluated crushed samples with particles of 1.2 to 1.5 mm, leading to a faster alkali leaching than in the cylindrical samples (due to the greatly reduced surface area in the latter). Another previous study published by Zheng *et al*. (2011) found leaching of between 40 and 60% of the original sodium concentration from cylindrical fly ash-based geopolymer samples after immersion in a nitric acidic solution with pH adjusted to 4 during the time of 45h. The authors attributed the high leaching levels to the low reactivity of the precursor and geopolymer sample immersion in an acidic solution, which accelerates alkali dissolution when compared with immersion of geopolymers in water.

Together, the pH and alkali concentration measurements indicate that the extent of alkali leaching is directly controlled by the geopolymer synthesis parameters, as these determine the amount of free alkalis within the geopolymer cement and the pore size and tortuosity of the pore network through which they must migrate. The addition of sodium silicate as part of the activator is found to be the primary synthesis parameter that can be used to reduce the content

of free alkalis, increase sample density and pore network tortuosity, and hence susceptibility to efflorescence and subsequent material degradation.

5.3.2 Physical properties

The physical properties of geopolymer cements are important to predict their behaviour during service life. According to previous studies, the sample porosity and pore structure significantly affect the extent of efflorescence formation, as lower permeability results in a reduction in alkali leaching and internal carbonation (ZHANG et al., 2014a).

5.3.2.1 Capillarity water absorption.

The water absorption of each sample by capillarity is shown in Figure 39. In the systems with less amount of sodium silicate, the mass increased with time up to 24 hours, and then remained unchanged beyond this point, indicating the saturation point. To systems with high amount of sodium silicate (MS=1) the absorption process is slower, requiring a much longer time for the same amount of water. Regardless the alkali concentration (15% to 25% of Na_2O), the absorption of water is significantly reduced (mainly during the first hours) in samples where the activator higher amounts of soluble silicate (MS = 1.0). The MA 1.0 and HA 1.0 geopolymers showed the lowest water permeability with values of approximately 2 g/cm². The use of mixed alkali ($Na^+ + K^+$) as part of activator provided a slower absorption at the beginning of the measurements, but after 24 h the Na+K 1.0 geopolymer showed up to 25% higher values when compared to the corresponding Na-based systems. The use of thermal curing (50 °C for the first 24 hours, then 20 °C thereafter) showed the same behaviour when compared to the reference system, and final water absorption is slightly higher. The trends of water absorption correlate directly with the pH measurements, extent of alkali leaching and visual observation of efflorescence, consistent with the degree of water permeability controlling the extent of alkali leaching and hence efflorescence in these systems.

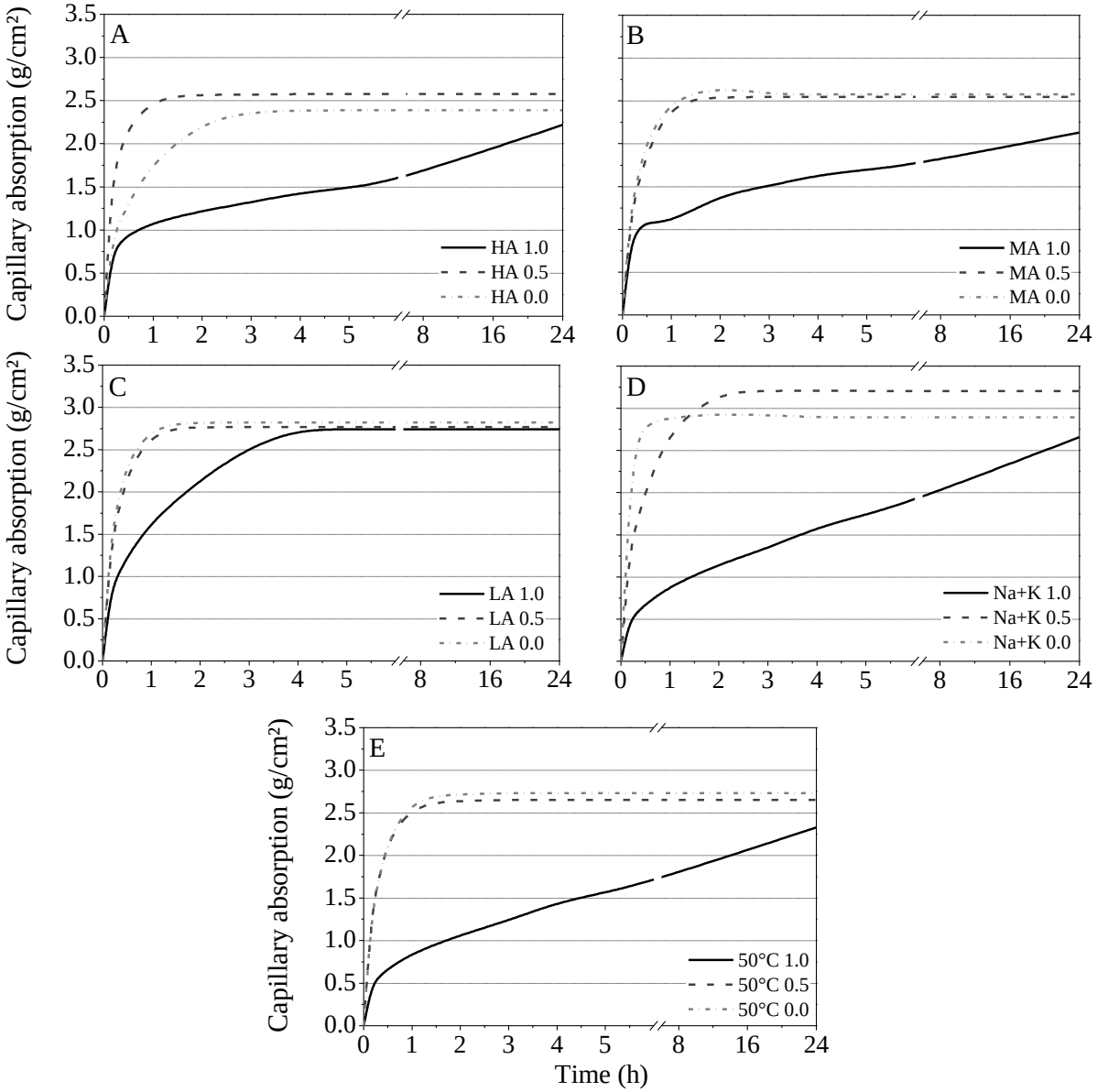

Figura 39 - Capillarity absorption of geopolymers after 28 days of curing: A. 25% Na_2O, B. 20% Na_2O, C. 15% Na_2O, D. 20% Na_2O + K_2O and E. 20% Na_2O + thermal curing 50 °C

5.3.2.2 Density and total porosity

The density and total porosity of each sample, measured by water absorption, are shown in Figure 40, while the compressive strength of each sample is presented in table 1. Summarising the compressive strength data, the higher values were obtained in systems with greater Na_2O content. This is because increased activator Na_2O content results in an increased activator pH, which drives increased precursor dissolution and consequently greater gel formation. Also, the addition of soluble silicate induces the formation of a microstructure with more tetrahedral bounded Si in $Q^4(1Al)$ and $Q^4(2Al)$ coordination, providing a stronger material (LONGHI et

al., 2019c). The use of potassium as part of the activator significantly decreased the compressive strength, as did thermal curing (50 °C for the first 24 hours, then 20 °C thereafter).

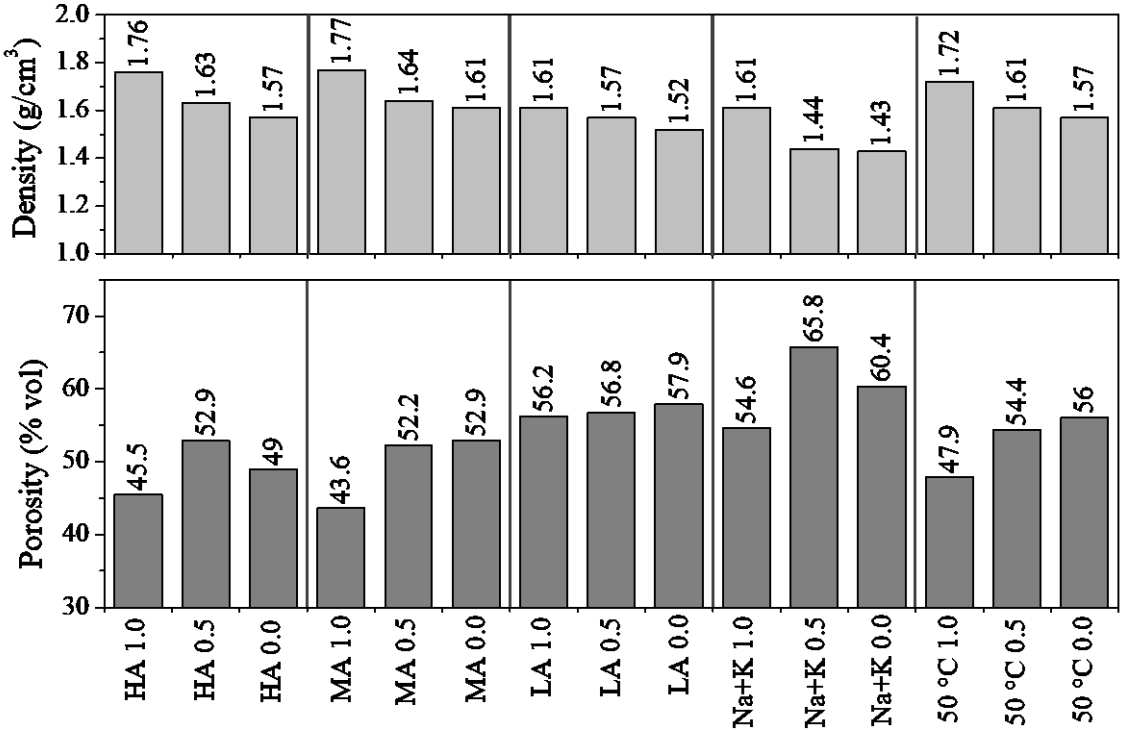

Figura 40 - Density (A) and porosity (B) of geopolymers with 28 days of curing

As expected, higher density is aligned to higher compressive strength. A higher density was identified in the systems with medium content of sodium (20%) and is reduced with less sodium content or the presence of potassium in the activator. The porosity presented in Figure 40 represents the void volume or open porosity in relation to the volume of the sample. The behaviour is also consistent with the other analyses and confirms a lower porosity is observed in denser and stronger systems. The values observed here are higher than those published by Zhang *et al.* (2018), where the open porosity of fly ash geopolymers was between 17 and 45%. This is consistent with the higher rate of water absorption and higher alkali leaching observed in metakaolin-based geopolymers when compared to fly ash-based geopolymers.

In addition to the open porosity calculated using water absorption, the mercury intrusion porosimetry (MIP) data were also obtained for each sample and are shown in Figure 41. The absorption values determined by MIP are lower than those determined by water absorption. The dimensional limit of MIP in this analysis is 5.5 nm, and smaller pores than this are not able to be quantified. Additionally, MIP can only measure the total accessible or percolated pore volume and not the total pore volume (i.e. including those not connected to the sample surface (SCRIVENER; SNELLINGS; LOTHENBACH, 2016). Thus, the difference observed between

water absorption and MIP can be attributed those pores that are not connected and pores with diameter size smaller than 5.5 nm.

The medium pore determined by MIP data indicates that using higher content of alkali and soluble silicates in the activator results in the formation of smaller pore, consistent with the density values for each sample (Figure 40). The effect of a bigger pore dimension is reflected in the reduction of compressive strength values. These values indicate easier fluid movement and removal of alkalis, also it is compatible with the extent of alkali leaching presented in Figure 38.

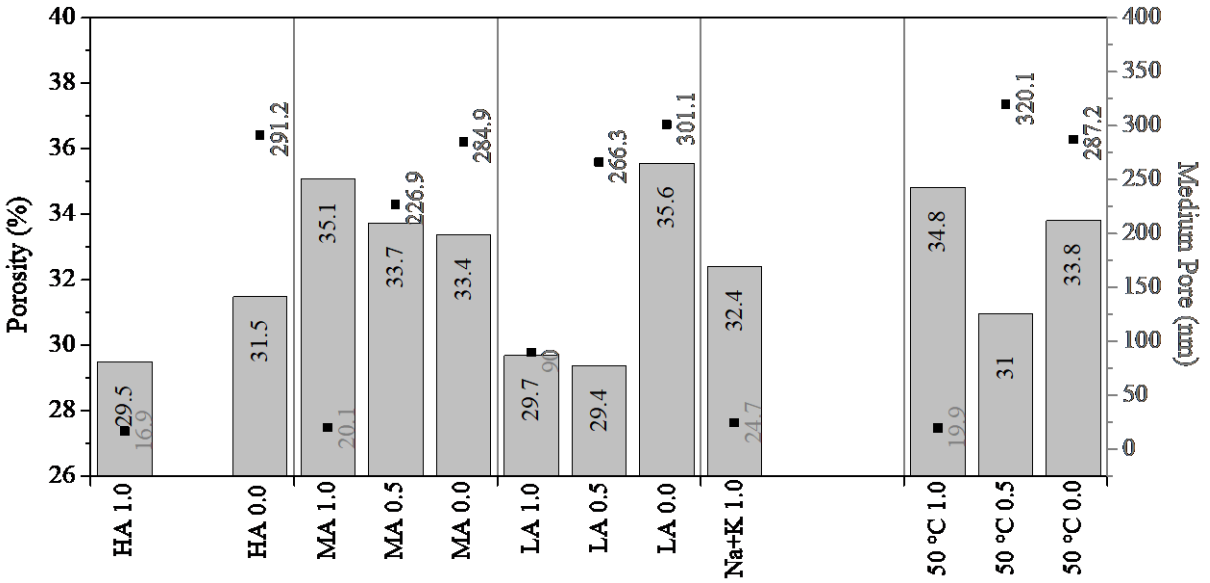

Figura 41 – Porosity and medium pore distribution of each geopolymer system determined by mercury intrusion porosimetry

The relation between physical properties and efflorescence formation is also important. The systems with 25% of Na_2O presented the higher compressive strength, however, in all systems, the efflorescence formation was observed, even when only exposed to air. This indicates an excess of alkalis in these systems. Regardless of all other samples with sodium as the activator, the efflorescence formation is independent of compressive strength, however, is less aggressive or located just at the top for more resistant systems. The use of potassium within the activator decreased the compressive strength but also reduced the visual efflorescence formation. Therefore, even though the compressive strength is directly related to density and porosity, cannot be used as an index for efflorescence formation. In this sense, only the porosity and water absorption are related to sample susceptibility to efflorescence development. These

relations between leaching potential and physical properties show that it is possible to reduce the leaching process if a denser geopolymer material is synthesized.

The morphology of selected geopolymer samples were also examined using by SEM (figure 42). The homogeneity of the material indicates the large extent of reaction between the activator and the precursor. In a system with a lower reaction degree, the matrix looks less compact and unreacted MK particles can be observed, which is consistent with what was previously observed by Longhi et. al (Longhi et al 2019-paper 2). In the geopolymer HA 1.0 (Figure 42A) the formation of a strong and dense matrix is visible, without any unreacted MK particles. The geopolymers MA 1.0 (figure 42B) and LA 1.0 (figure 42C) also shows a homogeneous and dense structure, but with the presence of more free unreacted MK particles (lighter grey particles in the images). Geopolymer systems MA 0.5 (Figure 42 D) and MA 0.0 (Figure 42E) show increased amounts of unreacted particles and a less compact structure compared with the MA 1.0 system, consistent with the reduction in density and extent of reaction with a reduction of soluble silicates in the activator. This is also consistent with the lower mechanical performance and higher water absorption in these samples, as discussed above.

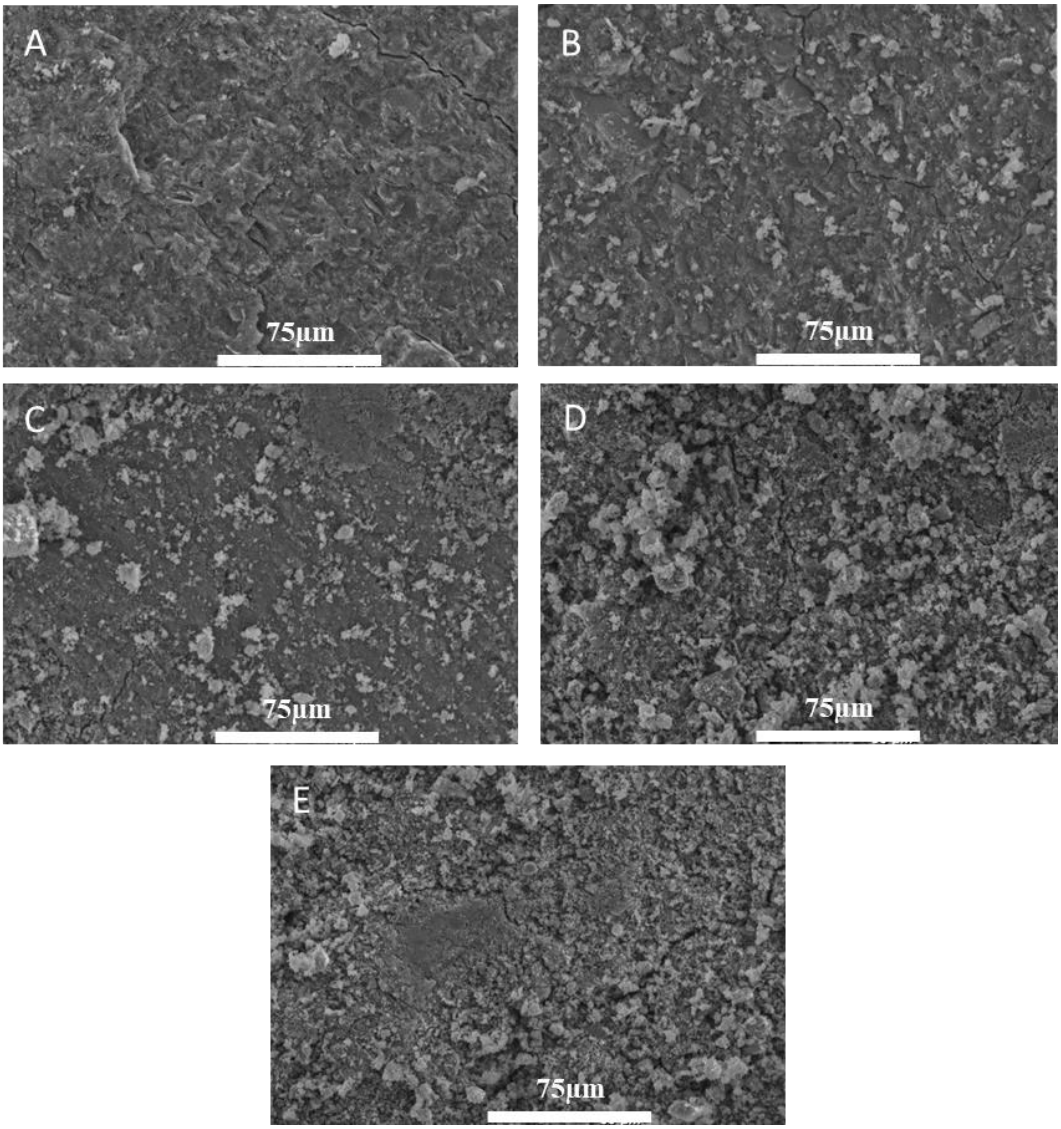

Figura 42– Scanning electron microscopy by secondary electron images of geopolymers a) HA 1.0, (b) MA 1.0, (c) LA 1.0, (d) MA 0.5, (e) MA 0.0

5.3.3 Microstructural properties

A detailed analysis of geopolymer microstructure and its relation to mechanical and chemical properties was performed, and correlated with the efflorescence formation to elucidate the underlying mechanisms of efflorescence formation.

5.3.3.1 XRD

The x-ray diffractograms of the geopolymer and the unreacted MK precursor are shown in Figure 43. The metakaolin exhibits the formation of a broad feature due to diffuse scattering between 15 and 35° 2θ, indicating the predominant amorphous nature, as well as reflections due to the crystalline phases as anatase (TiO_2, Pattern Diffraction File, PDF# 00-021-1272) and halloysite ($Al_2Si_2O_5(OH)_4$, PDF #00-029-1489). After alkali activation a broad feature due to

diffuse scattering is observed at approximately 30° 2θ and is attributed to formation of an alkali aluminosilicate (geopolymer) gel framework.

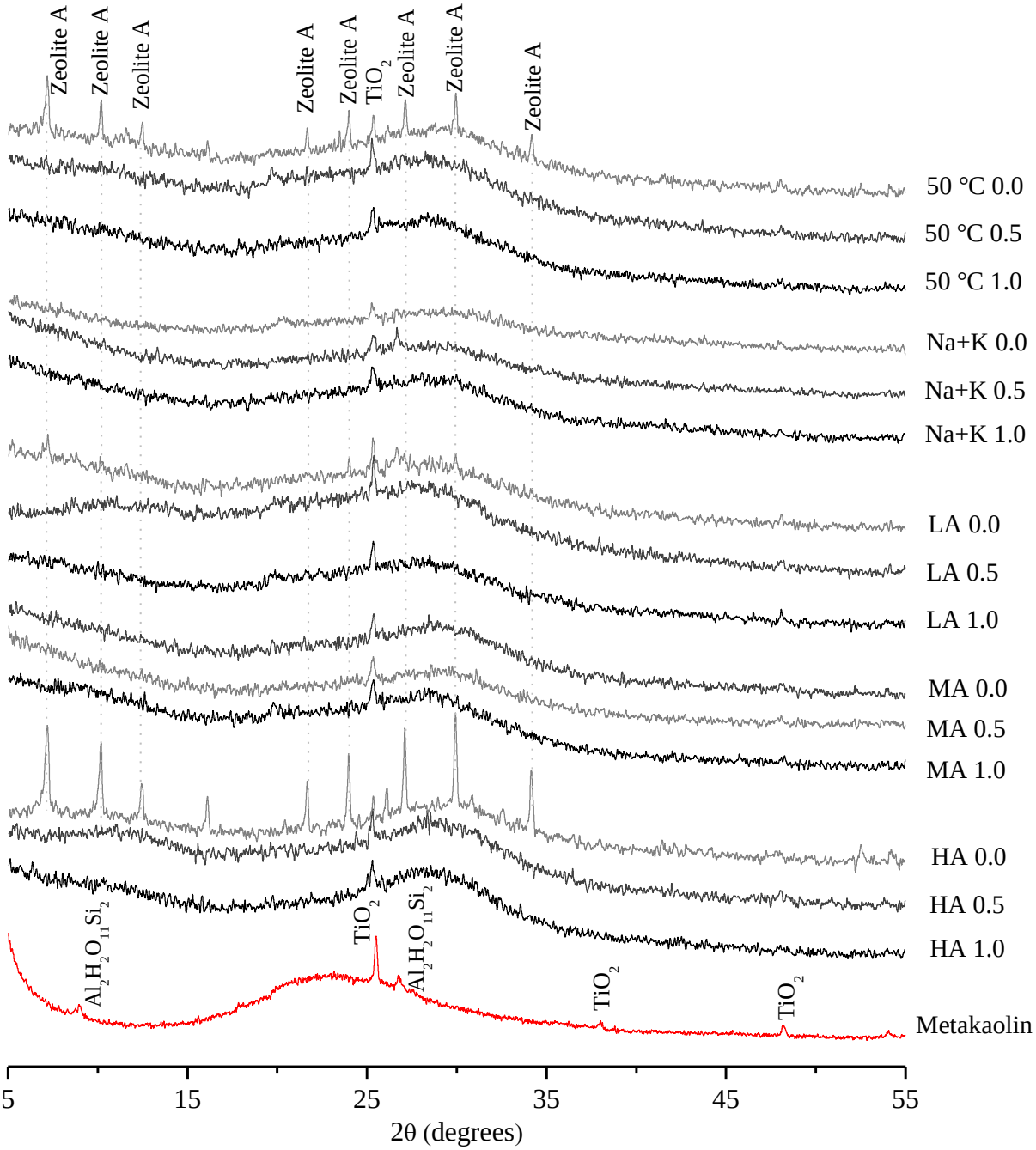

Figura 43 – X-ray diffraction data of metakaolin and each geopolymer system

Reflections due to anatase are also observed in the XRD data for the geopolymer samples, indicating that this phase is largely inert during alkali activation. Reflections due to zeolite A ($Na_{96}Al_{96}Si_{96}O_{384}{\cdot}216H_2O$; PDF# 00-039-0272) are also observed in the hydroxide-based geopolymer systems, and the formation of this phase is enhanced in systems with thermal curing and containing higher amounts of alkali in the activator (HA 0.0). Formation of zeolites in geopolymers is relatively common, due to their pseudo-zeolitic structure, and zeolite A has

been previously reported as a reacted product formed in MK-based geopolymers with hydroxide as the activator (ZHANG et al., 2012). The XRD characterization of geopolymer can not define the extend of efflorescence formation, however, is an important analysis to identify the products formed and their possible influence on the phenomenon formation.

5.3.3.2 FTIR

The results of the FTIR spectra of geopolymers systems are shown in Figure 44. The metakaolin is presented in the first spectrum, and exhibits a main peak around 1080 cm^{-1}, attributed to the asymmetric stretching vibration of Si-O-T (T=Si or Al) (REES et al., 2007a). The second broad peak in the bands around 800 cm^{-1} is attributed to the Al-O bending of AlO_6 octahedral sites within metakaolin (ZHANG et al., 2012). After alkali activation, all systems exhibit a main peak between 900 and 1000 cm^{-1} that is attributed to the asymmetric stretching vibration mode of Si-O-T bonds, characteristic of geopolymer gel formation (CRIADO; PALOMO; FERNANDEZ-JIMENEZ, 2005). The peak between 660 and 730cm^{-1} represents the O-Si-O bond band, corresponding to quartz or zeolite species (CRIADO; PALOMO; FERNANDEZ-JIMENEZ, 2005). The peak near to 1400 cm^{-1} can be attributed to asymmetric stretching of the O-C-O bond, and related to the sample carbonation (ZHANG et al., 2012), however, this carbonation was generated during the sample preparation and is not related to efflorescence. The peaks near to 1650 cm^{-1} are attributed to the surface hydroxyl groups hydrogen-bonded to the adsorbed water (GIANNOPOULOU; PANIAS, 2010; ZHANG et al., 2012).

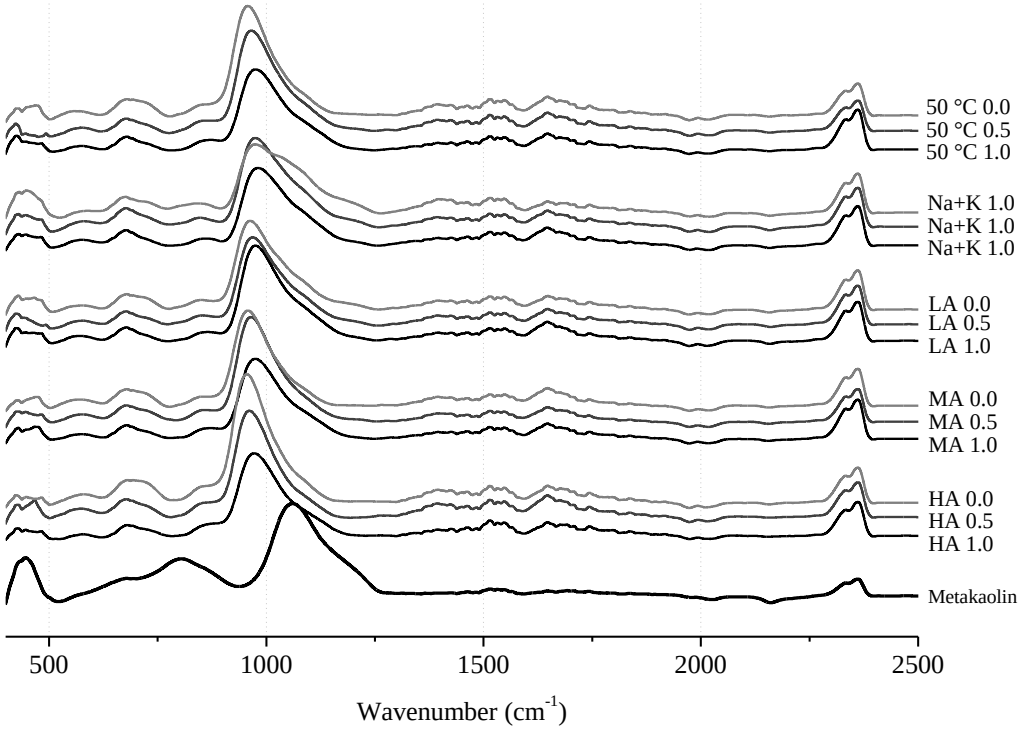

Figura 44 – Fourier transform infrared spectroscopy data of metakaolin and each geopolymer system between 400 and 2500 cm^{-1}

Figure 45 shows the FTIR spectra and associated deconvolutions between 1300 and 500 cm^{-1}. The spectrum was fit manually with the minimum number of peaks possible, with the requirement that the fit of the original curve be represented by a coefficient of determination higher than 0.99. The systems with 20% of Na_2O in the activator show the formation of five main peaks, with some differences according to the addition of soluble silicate (or MS value used during the synthesis). The two main peaks are between 1041 cm^{-1} - 1009 cm^{-1} and 971 cm^{-1} - 955 cm^{-1}. The band between 1020 - 998 cm^{-1}) is assigned to asymmetric stretching vibrations of Si-O-T (CRIADO; PALOMO; FERNANDEZ-JIMENEZ, 2005; ZHANG et al., 2012, 2013) and the band at 940 - 979 cm^{-1} to asymmetric stretching vibrations of non-bridging oxygen sites, in this case Si-O-Na (ZHANG et al., 2012, 2013). The addition of sodium silicate (MS>0.0) promotes the shift of these bands to higher wavenumbers, due to the addition of soluble silicate and provides a higher amount of Si in the vibration associated with Si-O-T, consistent with other studies (ZHANG et al., 2013). Likewise, the characteristic vibration of Si-O-Na, indicated more content of bounded Na by the addition of extra Si. This microstructural change has a strong effect on the mechanical properties of geopolymers and the alkali leaching potential. Thus, better performance is observed from the addition of soluble silicates and indicates a more resistant structure in the presence of greater quantities of Si bounded to the structure. The bands near to 859 cm^{-1}, can be associated to the bending in the Si-OH group

(ZHANG et al., 2013) and the peak near to 690 cm^{-1} represents the bending of Al-O-Si bonds (BERNAL et al., 2011).

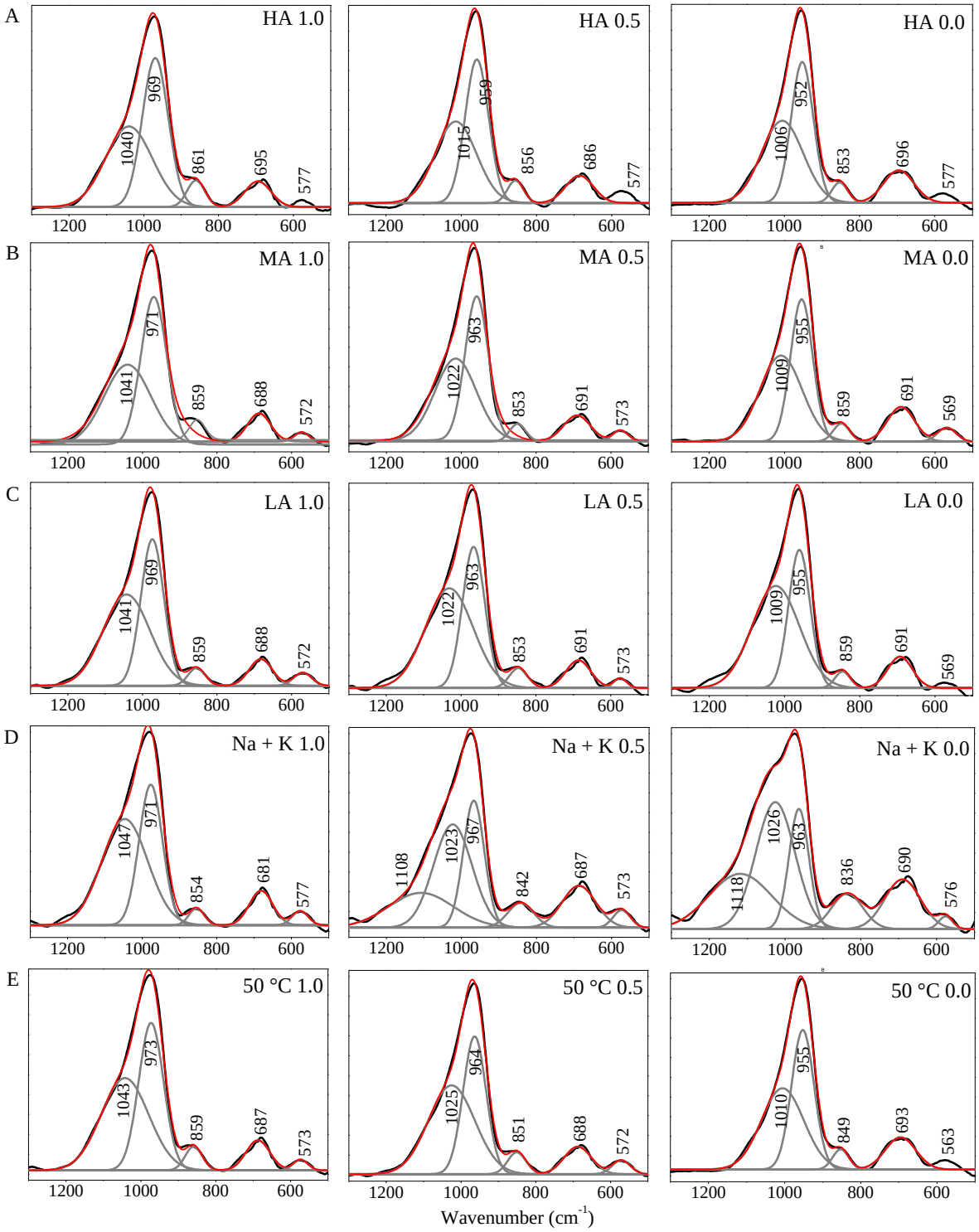

Figura 45 – Fourier transform infrared spectroscopy data (black line) and associated deconvolutions for each geopolymers system: A. 25% Na_2O, B. 20% Na_2O, C. 15% Na_2O, D. 20% Na_2O + K_2O and E. 20% Na_2O + thermal curing 50 °C. The red line is the simulated spectrum, and the grey lines are the fitted peaks

Regardless of the activator composition, the deconvoluted FTIR spectra are generally similar. The main difference is related to the peak near to 855 cm^{-1}, characteristic of bending in Si-OH

group and associated with the soluble silicate content used as activator. More amount of Na_2O indicates more Si-OH bonds, which indicates the excess hydroxyl groups provided by the activator. The spectra for the system with medium alkali with and without thermal curing did not show significant differences, which is consistent with the other analyses discussed above. The geopolymers synthetized with KOH as part of the activator showed different bands in the FTIR spectra. The use of high content of sodium silicate provides a spectrum similar to the "Na system", however, the addition of more potassium in the mixture generates the formation of a new peak near to 1100 cm^{-1} and the shift of other peaks. The new peak located at 1126 cm^{-1} can be attributed to the formation of Si-O-K bound, where the intensity is relative to the quantity of KOH used. Also, it is possible to find a reduction of Si-O-Na bonds, it is in agreement with the design contents.

The relation between FTIR analysis and efflorescence formation is associated with the structure type formed. A more amount of Si-O-T bonds induce the formation of a denser and stronger material, with less water absorption and consequently fewer alkalis movement. The addition of extra Si source induces the amount of alkali bonded to the framework structure, which reduces the leaching potential. These results are in agreement with the alkali leaching content and visual efflorescence formation.

5.4. CONCLUSIONS

In this work in order to improve the knowledge on the efflorescence formation in metakaolin-based geopolymers, a set of 15 geopolymers was investigated. Efflorescence formation is a visible phenomenon in form of carbonate deposition formed by the movement of free alkalis in a porous structure in contact with CO_2 present in the air. The carbonate phases identified as crystals are anhydrous sodium carbonate (Na_2CO_3) monohydrate sodium carbonate ($Na_2CO_3.H_2O$) and decahydrate sodium carbonate (natron, $Na_2CO_3.10H_2O$).

Overall, this work provides that the efflorescence formation is dependent on chemical and physical properties as the amount of free alkalis, density, porosity and water absorption. Also, these properties are associated to precursor and activator content. In other words, the efflorescence formation is totally dependent on design parameters.

The increasing of sodium silicate provides a geopolymer with less efflorescence formation. This reduction is associated with the higher amount of Si in the gel, improving physical

properties as compressive strength and porosity, retarding the leaching process. In the same way, the increasing of alkali amount, provide a strong material, associated with the higher amount of precursor dissolved and gel formed, however, a higher amount of alkalis can induce the higher amount of free alkalis.

The cation presents in the alkaline activator shows influence on the visual efflorescence formation and mechanical behaviour. The design parameters with potassium hydroxide shows a false benefit. Even though the use of potassium as part of activator is effective when combined with sodium silicate to reduce the visual efflorescence formation, increasing potassium content in the samples reduces the density and mechanical strength. The reduction of efflorescence formation is due to high dissolution of the carbonate formed.

The use of thermal curing (50 °C) looks effective for a specific sample, consistent to the reduction of alkali leached, however, in the other nanostructural and physical analysis, the behaviour is similar when compared to the geopolymers cured in ambient temperature. Due to the high reactivity of the metakaolin used and the high amount of activator, the improvement of properties using additional temperature is not so expressive.

Thus, every geopolymer presents an amount of free and leachable alkali, the correct design parameters can optimize the amount of alkali in the framework structure and provides physical and chemical properties that can reduce the alkali movement and consequently the efflorescence formation. The effect of this formation remains unclear, so it is important to investigate how free alkali can affect the durability of the material due to leaching and efflorescence processes and find ways to reduce the potential of efflorescence formation.

REFERENCES:

BAKHAREV, T. Durability of geopolymer materials in sodium and magnesium sulfate solutions. **Cement and Concrete Research**, v. 35, n. 6, p. 1233–1246, 2005.

BERNAL, Susan. et al. Management and valorisation ofwastes through use in producing alkali-activated cementmaterials. **Journal of Chemical Technology & Biotechnology**, v. 91, p. 2365–2388, 2016.

BERNAL, Susan a. et al. 5-Bernal S.A. et al. 2011 - Evolution of binder structure in sodium silicate-activated slag-metakaolin blends.pdf. **Cement and Concrete Composites**, v. 33, n. 1, p. 46–54, 2011.

BERNAL, Susan A.; PROVIS, John L. Durability of alkali-activated materials: Progress and perspectives. **Journal of the American Ceramic Society**, v. 97, n. 4, p. 997–1008, 2014.

BURCIAGA-DÍAZ, Oswaldo et al. Statistical analysis of strength development as a function of various parameters on activated metakaolin/slag cements. **Journal of the American Ceramic Society**, v. 93, n. 2, p. 541–547, 2010.

CRIADO, M.; PALOMO, A.; FERNANDEZ-JIMENEZ, A. Alkali activation of fly ashes . Part 1 : Effect of curing conditions on the carbonation of the reaction products. v. 84, p. 2048–2054, 2005.

DOW, C.; GLASSER, F. P. Calcium carbonate efflorescence on Portland cement and building materials. **Cement and Concrete Research**, v. 33, n. 1, p. 147–154, 2003.

DUXSON, P. et al. Effect of alkali cations on aluminum incorporation in geopolymeric gels. **Industrial & Engineering Chemistry Research**, v. 44, n. 4, p. 832–839, 2005.

DUXSON, Peter et al. The role of inorganic polymer technology in the development of ‘green concrete’. **Cement and Concrete Research**, v. 37, n. 12, p. 1590–1597, 2007.

FERNÁNDEZ-JIMÉNEZ, A. et al. The role played by the reactive alumina content in the alkaline activation of fly ashes. **Microporous and Mesoporous Materials**, v. 91, n. 1–3, p. 111–119, 2006.

FERNANDEZ-JIMENEZ, A.; PALOMO, A. Nanostructure/microstructure of fly ash geopolymers. In: PROVIS, John L.; VAN DEVENTER, Jannie S. J. (Eds.). **Geopolymers: Structure, processing, properties and industrial applications**. 1. ed. Oxford - Cambridge - New Delhi: Woodhead Publishing Limi, 2009. p. 89–117.

GIANNOPOULOU, I.; PANIAS, D. Hydrolytic stability of sodium silicate gels in the presence of aluminum. **Journal of Materials Science**, v. 45, n. 19, p. 5370–5377, 2010.

GLASBY, T. et al. EFC geopolymer concrete aircraft pavements at Brisbane West Wellcamp Airport. **Concrete Conference**, v. 11, n. 1, p. 1–9, 2015.

HABERT, G.; D’ESPINOSE DE LACAILLERIE, J. B.; ROUSSEL, N. An environmental evaluation of geopolymer based concrete production: reviewing current research trends. **Journal of Cleaner Production**, v. 19, n. 11, p. 1229–1238, 2011.

HABERT, Guillaume; OUELLET-PLAMONDON, Claudiane. Recent update on the environmental impact of geopolymers. **Rilem Technical Letters**, v. 1, p. 17–23, 2016.

HEATH, Andrew; PAINE, Kevin; MCMANUS, Marcelle. Minimising the global warming potential of clay based geopolymers. **Journal of Cleaner Production**, v. 78, p. 75–83, 2014.

KOBE, Kenneth; SHEEHY, Thomas. Addendum - Thermochemistry of Sodium Carbonate and It’s Solutions. **Industrial & Engineering Chemistry**, v. 40, n. 12, p. 2370–2370, 1948.

LONGHI, Márlon A. et al. Efflorescence of Alkali-Activated Cements (Geopolymers) and the Impacts on Material Structures : A Critical Analysis. v. 6, n. April, p. 1–13, 2019. a.

LONGHI, Márlon A. et al. New selective dissolution process to quantify reaction extent and product stability in metakaolin-based geopolymers. **Composites Part B: Engineering**, v. 176, p. 107172, 2019. b.

LONGHI, Márlon A. Málon A. M. A. et al. Valorisation of a kaolin mining waste for the production of geopolymers. **Journal of Cleaner Production**, v. 115, 2016.

MAHMOUDKHANI, Maryam; KEITH, David W. Low-energy sodium hydroxide recovery for CO2 capture from atmospheric air-Thermodynamic analysis. **International Journal of Greenhouse Gas Control**, v. 3, n. 4, p. 376–384, 2009.

NAJAFI, Ebrahim; ALLAHVERDI, Ali; PROVIS, John L. Efflorescence control in geopolymer binders based on natural pozzolan.pdf. v. 34, p. 25–33, 2012.

PASSUELLO, Ana et al. Evaluation of the potential improvement in the environmental footprint of geopolymers using waste-derived activators. **Journal of Cleaner Production**, v. 166, p. 680–689, 2017.

PROVIS, John L. Geopolymers and other alkali activated materials: why, how, and what? **Materials and Structures**, v. 47, n. 1–2, p. 11–25, 2013.

PROVIS, John L.; BERNAL, Susan a. Geopolymers and Related Alkali-Activated Materials. **Annual Review of Materials Research**, v. 44, n. 1, p. 140205180727009, 2014.

PROVIS, John L.; VAN DEVENTER, Jannie S. J. **Alkali Activated Materials State of the Art Report, RILEM TC 224-AAM**..

REES, Catherine A. et al. Attenuated Total Reflectance Fourier Transform Infrared Analysis of Fly Ash Geopolymer Gel Aging. **Langmuir**, n. 10, p. 8170–8179, 2007.

SCHERER, George W. Theory of Drying. v. 14, 1990.

SCHERER, George W. Stress from crystallization of salt. **Cement and Concrete Research**, v. 34, n. 9, p. 1613–1624, 2004.

SCRIVENER, Karen; SNELLINGS, Ruben; LOTHENBACH, Barbara. **A Practical Guide to Microstructural Analysis of Cementitious Materials - Chapter 5: Thermogravimetrix Analysis**. Taylon and ed. Boca Raton: CRC press, 2016.

ŠKVÁRA, František et al. Aluminosilicate polymers - Influence of elevated temperatures, efflorescence. **Ceramics - Silikaty**, v. 53, n. 4, p. 276–282, 2009.

ŠKVÁRA, František et al. A weak alkali bond in (N, K)-A-S-H gels: Evidence from leaching and modeling. **Ceramics - Silikaty**, v. 56, n. 4, p. 374–382, 2012.

VAN DEVENTER, Jannie S. J.; PROVIS, John L.; DUXSON, Peter. Technical and commercial progress in the adoption of geopolymer cement. **Minerals Engineering**, v. 29, p. 89–104, 2012.

WALKLEY, Brant et al. New Structural Model of Hydrous Sodium Aluminosilicate Gels and the Role of Charge-Balancing Extra-Framework Al. v. 4, 2018.

WELLS, R. C.; MCADAM, D. J. Phase relations of the system: Sodium carbonate and water. **Journal of the American Chemical Society**, v. 29, n. 5, p. 721–727, 1907.

YAO, Xiao; YANG, Tao; ZHANG, Zuhua. Compressive strength development and shrinkage of alkali-activated fly ash–slag blends associated with efflorescence. **Materials and Structures/Materiaux et Constructions**, v. 49, n. 7, p. 2907–2918, 2016.

ZENG, Ying; ZHENG, Zhiyuan. Phase Equilibria for the Aqueous System Containing Sodium , Potassium , Carbonate , and Sulfate Ions at 273 . 15 K. **J. Chem. Eng. Data**, n. 54, p. 1244–1248, 2009.

ZHANG, Zuhua et al. Quantitative kinetic and structural analysis of geopolymers. Part 1. The activation of metakaolin with sodium hydroxide. **Thermochimica Acta**, v. 539, p. 23–33, 2012.

ZHANG, Zuhua et al. Quantitative kinetic and structural analysis of geopolymers. Part 2. Thermodynamics of sodium silicate activation of metakaolin. **Thermochimica Acta**, v. 565, p. 163–171, 2013.

ZHANG, Zuhua et al. Cement and Concrete Research Fly ash-based geopolymers : The relationship between composition , pore structure and efflorescence. v. 64, p. 30–41, 2014. a.

ZHANG, Zuhua et al. Fly ash-based geopolymers: The relationship between composition, pore structure and efflorescence. **Cement and Concrete Research**, v. 64, p. 30–41, 2014. b.

ZHANG, Zuhua et al. Efflorescence and subflorescence induced microstructural and mechanical evolution in fly ash-based geopolymers. **Cement and Concrete Composites**, v. 92, n. March, p. 165–177, 2018.

ZHANG, Zuhua; YAO, Xiao; ZHU, Huajun. Potential application of geopolymers as protection coatings for marine concrete II. microstructure and anticorrosion mechanism. **Applied Clay Science**, v. 49, n. 1–2, p. 7–12, 2010.

ZHENG, Lei et al. Immobilization of MSWI fly ash through geopolymerization: Effects of water-wash. **Waste Management**, v. 31, n. 2, p. 311–317, 2011.

6. METAKAOLIN-BASED GEOPOLYMERS: EFFLORESCENCE FORMATION AND ITS EFFECT ON MICROSTRUCTURE AND MECHANICAL PROPERTIES

6.1. INTRODUCTION

Efflorescence formation is a visible phenomenon observed mostly on the surface of cementitious and ceramics materials. This formation can be found in concrete made with Portland cement (PC) and usually responsible for aesthetic damage or superficial deterioration. Efflorescence results from the reaction between leached alkalis and CO_2 present in the environment, resulting in the formation carbonate phases. In hydrated PC, the alkali is present as calcium hydroxide ($Ca(OH)_2$), generated by the hydration process of anhydrous PC components and summarized by Dow and Glasser (DOW; GLASSER, 2003).

In geopolymers, efflorescence formation is still not fully understood due to the different mechanism of reaction and formed product. Geopolymer formation involves the reaction (often called “activation”) of a reactive aluminosilicate with high alkalinity solutions (or ‘activators’) (DUXSON et al., 2007b; PROVIS, 2013). Thus, the need to use alkaline activators as one of the components induces the presence of alkalis in the structure of the geopolymers. The alkali is present in the disordered reaction product, an alkali aluminosilicate hydrate gel denoted M-A-S-(H) gel, with M representing alkali metals, most commonly Na^+ or K^+ (DUXSON et al., 2005c). The state of Na^+ or K^+ in the geopolymer gel is associated with the neutralization of the excess negative charge resulting from Al in tetrahedral coordination in the alkali aluminosilicate gel framework (DUXSON et al., 2005c). Thus, in an ideal system, the stoichiometric equilibrium of alkalis is determined by the Na/Al ratio of 1.0 (FERNÁNDEZ-JIMÉNEZ et al., 2006). Sodium can also be present in Na-O-Al(Si) form with a relative stronger Na-O ionic bond or partially as $Na(H_2O)_n^+$ form, with a weakly bond o Na^+ associated with molecular water and present in the pores (ROWLES; BRIAN H. O’CONNOR, 2009)(ROWLES, M. R. HANNA, J. V. PIKE, K. J, SMITH, M. E, 2007). The availability of free alkalis was measured by leaching potential, and values between 1 and 16% related to the total alkali in the system were reported in previous studies (NAJAFI; ALLAHVERDI; PROVIS, 2012; ZHANG et al., 2014a) using ground hardened AAC with different materials and design parameters. In a

previous analysis of leaching potential of metakaolin-based geopolymers (LONGHI et al., 2019c) using an ionic equilibrium method for the determination of leachable alkalis, observed values around 55% related to free alkalis and 45% related to the stable alkalis in the framework structure. The high values of potentially leachable alkalis associated with porosity properties of geopolymers and specific environmental condition can allow the efflorescence formation and can affect the properties of geopolymers.

The first process of efflorescence formation involved is the alkali leaching. The free alkalis present within the capillary porosity can be leached, and this process can be facilitated in a liquid environment. The capillary pressure induces the water transportation and alkali movement, which is accelerated when the material is exposed to cycles of wetting/drying. The porosity also plays an important role in this movement, where large pores are connected by microcracks and contribute to the faster alkali leaching (ZHANG et al., 2014a). Leaching process can also be damaging to the gel structure due to the nanostructural transformation associated to the removal of alkalis and changes of the chemical environment of the aluminosilicates species (LONGHI et al., 2019c). After leaching, the presence of aqueous phases of alkalis in contact with the CO_2 present in the air and dissolved in an aqueous form allows the carbonations process. The carbonation process is mainly controlled by reactivity and diffusivity of CO_2, where the diffusivity is related to the interconnectivity of pore structure and carbonation exposure conditions, and reactivity of CO_2 mainly to concentration and chemistry of pore solution (ARBI et al., 2016). The diffusivity is an exponential function of porosity (HOUST; WITTMANN, 1994). The relative humidity is also an important factor, a partially saturated moisture condition accelerates the carbonation reaction process, where the RH values of 65 ± 5% was observed as critical using GBFS/MK-based geopolymers (BERNAL; PROVIS, 2014). Thus, depending on the porosity, alkali concentration of geopolymers and diffusivity of CO_2, the carbonates deposition can be internal (subflorescence) or external (efflorescence) (ZHANG et al., 2018b). Subflorescence is induced by the reaction between the free alkalis and CO_3^{2-} absorbed from the atmosphere and can generate an internal pressure during crystallization and this formation can damage the matrix, specially the tensile strength (ZHANG et al., 2018b).

In efflorescence, the products formed are predominantly carbonates associated with the alkali used as activator. The formation of a hydrated carbonate ($Na_2CO_3 \cdot 7H_2O$) was observed by (ZHANG et al., 2014a) and (ŠKVÁRA et al., 2009) sodium bicarbonate ($NaHCO_3$) by (NAJAFI; ALLAHVERDI; PROVIS, 2012) and natrite (Na_2CO_3) by (BURCIAGA-DÍAZ et

al., 2010). Visible formation of crystal is also related to the relative humidity (RH) in the air. Low values of RH make difficult this diffusion of CO_2. On the other way, the high values of RH can dissolve the crystal formed. This crystallization occurs at a specific RH equilibrium, which is dependent on the type of carbonate crystal formed. Thus, the efflorescence formation is a phenomenon associated to different processes and their effects are dependent on the combinations between geopolymer properties, microstructure, exposure conditions, magnitude/type of crystallization and carbonation.

In previous studies, the effect of efflorescence formation was evaluated for some specific geopolymeric materials and conditions, an is already reported that efflorescence formation reduces the compressive strength (YAO; YANG; ZHANG, 2016; ZHANG et al., 2018b). In fly ash-slag based alkali activated materials leaching process does not contribute to the reduction of compressive strength and does not allow the development of resistance over time (YAO; YANG; ZHANG, 2016). In the same study, the shrinkage is more evident to samples with efflorescence formation than with alkali leaching. In other study, using metakaolin as precursor, some microstructural changes are attributed to the excessive leaching process (LONGHI et al., 2019c). Using three different class F fly ashes, with different design parameters, Zhang et al.(ZHANG et al., 2018b) evaluated the compressive strength under different exposure conditions (air contact, ambient air with water in the bottom and fully immersed). The results showed an increase of compressive strength in air contact condition and reduction for samples in water contact and immersed. The negative influence of efflorescence formation was attributed to multiple factors as loss of alkalis and subflorescence formation. Even with all the knowledge provided by the previous studies, there are still doubts related to the effect of efflorescence on other mechanical properties in metakaolin-based geopolymers, such as tensile and flexural strength, as well as the need for a greater understanding of microstructural effects.

This study aims to evaluate the effect of efflorescence formation and alkali leaching on the mechanical properties and microstructure of metakaolin-based geopolymers. The understanding of effects caused by geopolymer exposure associated with microstructure transformation will allow the knowledge about this phenomenon and indicate the behaviour in real scale applications.

6.2. EXPERIMENTAL

6.2.1 Materials and sample preparation

Metakaolin (MK) used as precursor to make geopolymers had a mean particle size of 4.56 µm, specific surface area of 13.49 kg/m² and consisted of 54.82% wt.% SiO_2, 42.57 wt.% Al_2O_3 and 0.11 wt.% loss of ignition at 1000 °C. The complete characterization and more detailed description were previously reported (LONGHI et al., 2019c).

Alkali activators used were analytical grade NaOH (~99%) dissolved in water and a sodium silicate solution with 29.4 wt% SiO_2, 14.7 wt% Na_2O and 52.7 wt% H_2O supplied by PQ Australia. The composition of the alkali activators was adjusted by blending the NaOH and sodium silicate solution in proportions to reach the desired molar ratios.

The formulations of the geopolymers were based on previous reports (LONGHI et al., 2019c, 2020), and formulated with unique alkali concentration of 20% of Na_2O with a MS (SiO_2/Na_2O ratio) of 1.5, 1.0, 0.5, and 0.0. Different parameters formulation where used to provide different physical and chemical properties to the geopolymers. The pastes were produced by mechanical mixing for 5 min, stored in a sealed plastic container at room temperature (~25 °C) and RH ≥ 90%. In order to assess the effect of thermal curing, the geopolymer produced with a MS of 1 was also cured at 50 °C during 24 h and then stored under environmental temperature. The content of water was adjusted with a water/binder ratio of 0.55, where binder is represented by the MK and anhydrous fraction of the alkali activator. The Table 4 shows the system ID and synthesis formulation.

Table 4 - formulation of geopolymer samples

Geopolymer	Silica Modulus (MS)	Curing temperature (°C)	Materials (g)			
			MK	NaOH	SS*	H_2O
MS_1.5	1.5	25	100	7.1	98.7	24.9
MS_1.0	1.0	25	100	13.3	65.8	44.8
MS_0.5	0.5	25	100	19.6	32.9	63.7
MS_0.0	0.0	25	100	25.8	0.0	75.5
MS-1.0-50°	1.0	50	100	13.3	65.8	44.8

*SS: Sodium silicate solution

After 28 days of curing, samples were exposed to different exposure conditions during extra 28 days, as is shown in Figure 46. We believe that efflorescence formation is a phenomenon controlled by different mass transport processes, summarized in this study as air carbonation, external efflorescence and leaching. As a **reference** system (without contact with damaging environment) the samples were exposed under environmental conditions (25 ºC ± 5 and RH of 65 ± 15%) in the laboratory. The development of **efflorescence** was induced by the partial immersion of the sample (~5 mm of depth) in an ambient condition (20±5 °C and RH= 65 ± 15%). The level of water was adjusted every 24 h. In this condition by the high absorption and cycles of wetting and drying is possible to provide an alkali movement and carbonation deposition on the surface. As a third condition, the samples were exposed to natural **carbonation** by the contact with the air. In this condition, due to the presence of CO_2 in the air, the carbonation process is developed in the first layer of the samples where the pore-structure partially filled by carbonate-type products (LONGHI et al., 2020). The leaching process in the fourth condition, which is developed by the complete immersion in deionized water. In this condition, the free or weakly bonded alkali in geopolymer is removed from the structure to the solution, as observed in previous study (LONGHI et al., 2019c).

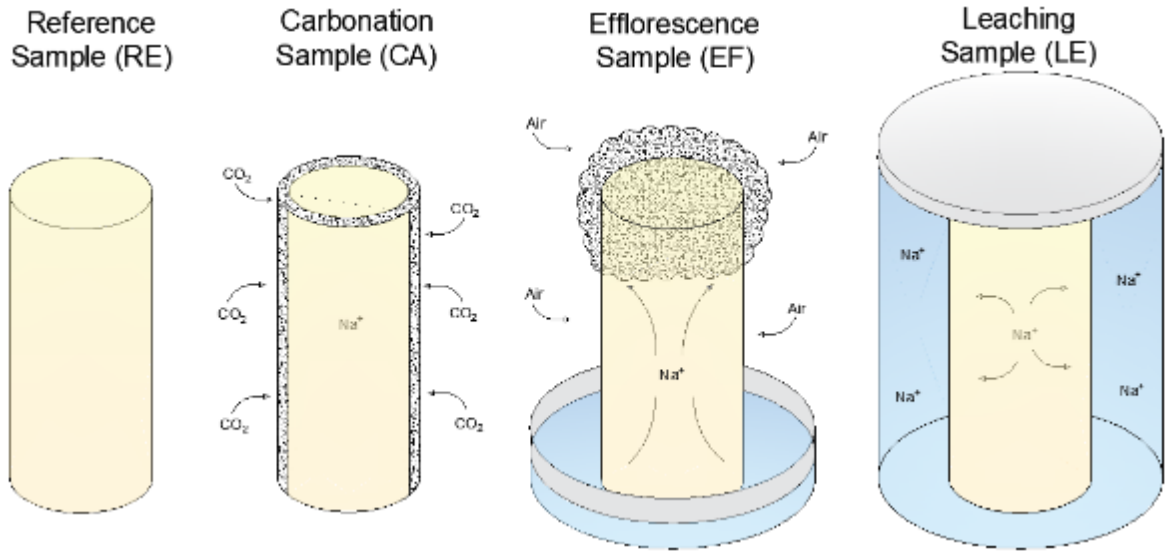

Figura 46 - different conditions of ambient exposure (reference, carbonation, efflorescence and leaching).

6.2.2 Tests conducted

After exposure conditions (Figure 46) the samples were cleaned with paper and placed in ambient conditions (~25 °C and RH= 65 ± 15%) for 24 h. The analyses conducted were:

- **Compressive strength** in five cubic samples of 20 mm of height for each system and exposure condition. The test using an MTS universal mechanical testing machine with a loading speed was 0.5 mm/min.

- S**plitting tensile strength**, in four cylindrical samples with 20 mm of diameter and 35 mm of height. For this analysis the samples were tested in the longitudinal direction. The splitting tensile strength was calculated using the equation according to the NBR 7222, 2011 Eq. (1):

  Splitting tensile strength (MPa) =$ft = \frac{2P}{\pi DL}$ (1)

  where P is the load applied to the sample in N, D is the diameter in mm and L is the height in mm. A tape of neoprene of 2 mm thickness was used in order to distribute homogeneously the load.

- **Flexural strength** in three prismatic samples of 20×20×80 mm. The flexural strength was calculated using the Eq. (2) according to NBR 12142, 2010:

  Flexural strength (MPa) = $ff = \frac{3PL}{2bd^2}$ (2)

  where P is the load applied in N, L is the length of the support span, b is width, d is thickness.

- **Linear deformation** was applied in prismatic samples of 20×20×80 mm measured using a length comparator along the longitudinal direction.

Microstructural features were evaluated using:

- **High resolution scanning electron microscopy (SEM)** using a FEI Quanta 650 FEG, in the Brazilian Nanotechnology National Laboratory LNNano (Laboratório Nacional de Nanotecnologia). The equipment was equipped with an Everhart Thomley SED (secondary electron detector) and an In-column detector (ICD) for secondary electrons in BD mode. Working with a high resolution Schottky field emission (FEG), accelerating voltage between 200V and 30kV in a probe current ≤ 200 nA. The samples used were a superficial fragment of the specimen. The sample was a dried at 60 °C during 2 hours, placed in carbon tab and coated with gold during 60 s with a current of 40 A.

- **Solid-state single pulse ^{23}Na, ^{27}Al and ^{29}Si magic angle spinning (MAS) NMR spectroscopy** using a Bruker Avance III HD 500 spectrometer at 11.7 T (B_0) with a 4.0 mm dual resonance CP/MAS probe, yielding a Larmor frequency of 132.26 MHz for ^{23}Na, 130.32 MHz for ^{27}Al and 99.35 MHz for ^{29}Si. ^{23}Na MAS NMR spectra were collected with a 3.0 μs non-selective (π/2) excitation pulse, a measured 10 s relaxation delay, a total of 128 scans and spinning at 12.5 kHz. ^{27}Al MAS NMR spectra were collected with a 1.7 μs non-selective (π/2) excitation pulse, a measured 5 s relaxation delay, a total of 512 scans and spinning at 12.5 kHz. ^{29}Si MAS NMR spectra were acquired using a 5.5 μs non-selective (π/2) excitation pulse, a measured 60 s relaxation delay, a total of 256 scans and spinning at 12.5 kHz. For all experiments, the spectrometer field was aligned to the ^{13}C resonance of adamantane at 38.48 ppm, and ^{23}Na, ^{27}Al and ^{29}Si spectra were referenced to 1.0 $NaCl_{(aq)}$, 1.0 mol/L $Al(NO_3)_{3(aq)}$ and neat tetramethylsilane (TMS), respectively, at 0 ppm. Gaussian peak profiles were used to deconvolute the NMR spectra, using the minimum number of peaks possible (MASSIOT et al., 2002). Peak intensities were required to be consistent with the structural constraints described by the thermodynamics of a statistical distribution of Si and Al sites within a Q^4 aluminosilicate network for (N,K)-A-S-H gel products (DUXSON et al., 2005b).

- **X-ray diffraction (XRD)** using the XRD1 beamline at the Brazilian Synchrotron Light Laboratory (LNLS). The LNLS is a second-generation synchrotron source, which operates with the energy of 1.37 GeV. The XRD1 beamline is installed on D12B bending magnet (1.67 T) operates in the 5.5–14 keV range and has a photon flux of 7.8 x 10^9 photons s^{-1} (with 100 mA) at 12 keV, which is one of the typical working energies. At 8 keV (the other typical working energy) the photon flux at the sample position is 3.4 x 10^{10} photons s^{-1} and the energy resolution $\Delta E/E = 3 \times 10^{-4}$ (CARVALHO et al., 2016; CARVALHO; NUNES; COELHO, 2017).

- **Thermogravimetry analysis (TGA)**, using a Tam Air Discovery SDT 650, with the heating rate of 10 C/min up to 1000 °C and 90μm alumina crucibles. Simultaneous thermal analysis (**STA**), with a Tam Air Discovery SDT 650, using the heating rate of 10 ºC/min up to 1000 °C and 90 μml alumina crucibles.

- **The X-ray microtomography (XRμT)** was developed in the Brazilian synchrotron LNLS (Laboratório Nacional de Luz Síncrotron) at Campinas using beamline IMX. A

monochromatic beam of 4 to 20keV with a pixel size of 0.82 μm^2 and field view (horizontal x vertical) of 1.64 mm^2. As a detector a 7.4 μm pixel, 2048×2048 pixel, 14-bit CCD (PCO.2000) camera was used. Tomography images were obtained point-to-point with an angle range of 360º along its vertical axis with a step size of 0.1758 degrees (or 2048 projections) up to achieve 310000 counts. Three Si(111)Xia Filters were used, consisting one of 200 μm and two of 350μm . Cylindrical geopolymer samples of ~1.70 mm of diameter were produced, cured and treated (RE, EF and LE) as same conditions described previously. Sample heights were between ~7 and 11 mm and the beam was adjusted approximately in the middle of the specimen. A set of images 3048×3048×2048 were obtained and adjusted to the 3D volume generation. In order to reduce the size of the data to be analyzed, a prismatic voxel of 1024×512×512 was extracted. The images and segmentation analyses were executed using Avizov 9.5.0 software package and adjusted using different filter plug-in tools based on the variation on grey scale intensity.

6.3. EFFLORESCENCE FORMATION

6.3.1 Visual efflorescence

Figure 47 shows the visual aspect of geopolymers under different exposure conditions after 28 days. The reference condition (RE) did not show any efflorescence formation for all the geopolymer assessed. When the samples were in contact with water (EF), most of the systems exhibited the efflorescence formation on the surface, which correspond to carbonate-type products as was identified previously(LONGHI et al., 2020). The images elucidate that the content of sodium silicate in the alkali activator plays an important role in the reduction of efflorescence formation. Geopolymer MS_1.5 does not show any efflorescence formation, while, MS_0.0 (hydroxide-based geopolymer) shows a severe carbonates formation and surface deterioration. This behaviour was classified by Zhang et al.(ZHANG et al., 2018b) and named as subflorescence which can be attributed to the crystallization of carbonate within the first layer external pore structure inducing stress and subsequent cracking. As observed in previous studies(LONGHI et al., 2019c, 2020), the use of silicate-rich activators reduce the amount of leachable alkalis due to the higher density and less porosity when compared to geopolymers with lower content of soluble silicate. The use of higher curing temperature (50 ºC for 24 h) did

not show an expressive reduction in the efflorescence formation and showed a similar behaviour of the corresponding geopolymer cured at room temperature (MS_1.0).

The samples exposed to the air carbonation condition (CA), where the air carbonation process is induced, also showed a thin layer of carbonates deposition distributed in the sample (not only on the top of the specimens as observed before) regardless the alkali activation parameters (%Na_2O and MS). The high porosity of these systems allows the movement of water and free alkalis to the surface, which contributes to the development of efflorescence. Taking into account the limited content of free water, the formation of carbonate-type products on the surface is less severe when compared to systems immersed partially.

The samples exposed to leaching conditions (LE) does not show any superficial change, however, the contact with water induces the removal of free alkalis. In a previous study was observed the removal around 17 to 30% using cylindrical samples (LONGHI et al., 2020) and higher than 50% using powder (hardened geopolymer previously grounded) (LONGHI et al., 2019c). Due to the high removal of alkalis imposed by the leaching process, as well as the absence of CO_2 in the aqueous solution, the formation of efflorescence is not expected, however, the movement and quantity of leached alkalis is determinant for the understanding of the susceptibility of the efflorescence formation and the effect associated to alkalis removal.

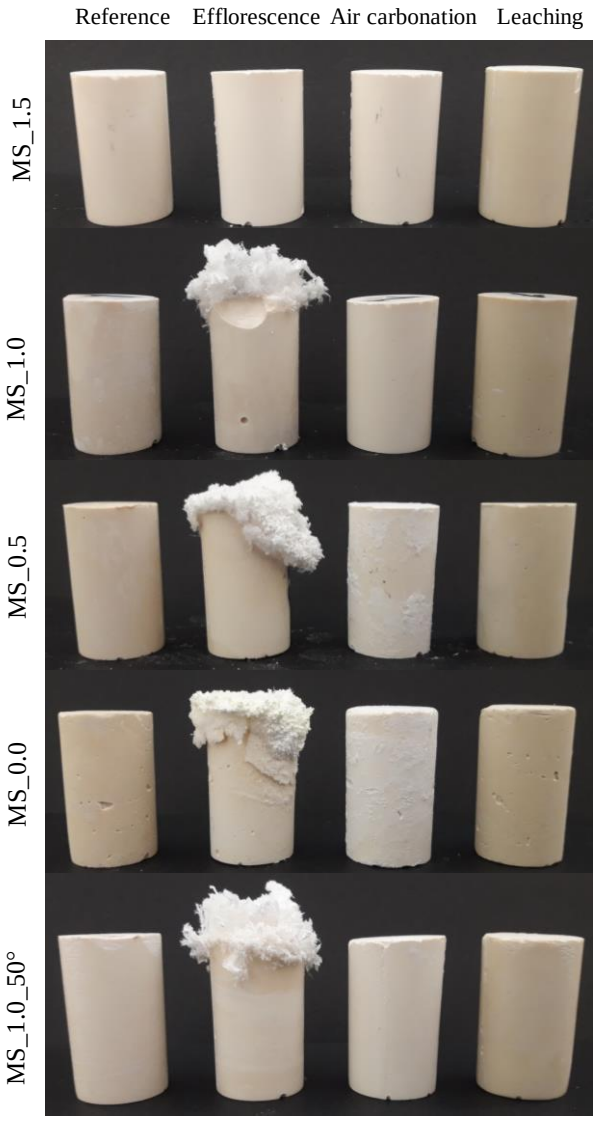

Figura 47 - visual efflorescence formation in geopolymeric samples. (Cylindrical sample with a diameter of 30 mm and 60 mm of height).

6.3.2 Compressive strength

The compressive strength of geopolymers after the different exposure conditions is shown in Figure 48. Geopolymer produced with different contents of sodium silicate in the activator and curing conditions provides different levels of strength when exposed to the RE exposure condition. The maximum value of compressive strength achieved was 49.9 MPa the geopolymer MS_1.5, which is up to 5.6 times higher compared to the geopolymer MS_0.0. This increasing was discussed in previous studies (LONGHI et al., 2019c, 2016) and also for other researchers (FERNÁNDEZ-JIMÉNEZ et al., 2006; ZHANG et al., 2012, 2013) and attributed to high amount of Si in the atomic structure to the formation of three-dimensional aluminosilicate framework structure, resulting in denser and stronger microstructure. Figure 48 also shows that in most of the cases the reference exposure conditions exhibit the higher

compressive strength which elucidates that the efflorescence formation, carbonation and leachability affect negatively the mechanical performance of the geopolymers. Therefore, the exposure condition has a strong effect on the compressive strength results. The most expressive reduction in this case is associated to efflorescence formation, where the highest reduction in most of the cases is observed mainly in the systems with the lower content of soluble silicates, MS_0.5 and MS_0.0. The accelerated formation of efflorescence identified under the EF exposure condition reduces the compressive strength up to 45% for the systems MS_0.5 and MS_0.0. Additionally, in the geopolymers MS_1.0 and MS_0.0, is observed in Figure 48 the presence of some broken parts, which can be attributed to the internal crystallization and excessive internal stress within the pore network.

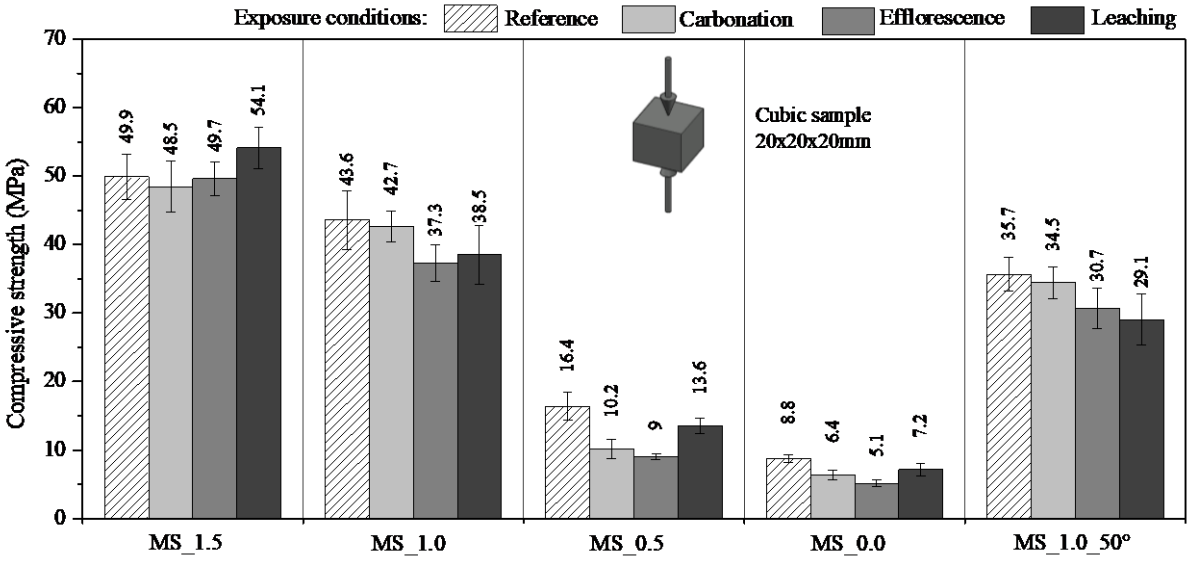

Figura 48 - compressive strength of geopolymers in different conditions of exposure.

Even though, the air carbonation conditions (CA) seems to be less aggressive, as was shown in Figure 48 for the geopolymers MS_0.5 and MS_0.0, a reduction up to 53% in the compressive strength is observed. These geopolymeric systems showed the efflorescence formation as a homogeneous thin layer (1 mm) covering the samples. In this sense, is identified a slight deterioration of this external surface due to the formation of crystals into the porosity network, which was also previously reported by Zhang *et al.* (ZHANG et al., 2018b) as subflorescence formation.

For the leaching condition (LE), was also observed the reduction of compressive strength, specially to the geopolymers MS_0.5 and MS_1.0_50°. It is important to highlight that the geopolymer with the highest content of soluble silicate (MS_1.5) does not show notable changes in the compressive strength, regardless the exposure conditions.

The effect of exposure conditions was also evaluated in previous papers using fly ash-based systems (ŠKVÁRA et al., 2012; YAO; YANG; ZHANG, 2016), and the reduction of compressive strength was also reported. According to Yao, Yang and Zhang (YAO; YANG; ZHANG, 2016), the efflorescence formation induces the carbonate crystallization and an internal stress can be developed. This behaviour is also consistent with the subflorescence formation observed by Zhang et al. (ZHANG et al., 2018b) and the phenomena observed in this study. The different levels of alkali leaching, environmental conditions and carbonates formation determines the level of degradation and the effect observed.

6.3.3 Flexural strength

The flexural strength measures the transverse rupture strength of the sample when subjected to load in three different points. The results are shown in Figure 49. All the exposure condition affects the flexural strength, where if observed significant loss of ~45% when exposed to the leaching condition (LE), ~12% to carbonation exposure and ~29% to efflorescence exposure. These results are consistent with those observed by compressive strength where the efflorescence formation and superficial carbonation can damage the material surface due to the excessive crystal formation in the surface and within the pores.

Interestingly, the most marked loss of flexural strength was observed to the leaching condition. With the absence of crystals formation, this behaviour can be attributed to the alkali removal from the framework structure. This is associated to the leaching of free-alkali and some soluble compounds within the geopolymeric gel, as observed previously (LONGHI et al., 2019c). The leachability process can achieve values up to 20%, including the extraction of sodium, silica and alumina, which promotes mass and density reduction and consequently the depletion of mechanical properties. As also observed by Longhi et al.(LONGHI et al., 2019c), the leaching process induces the reduction of Q^4(4Al) and Q^4(3Al) sites within the geopolymeric matrix, indicating a structural change due to the alkali removal. This microstructural change can also be attributed to the instability of sodium aluminosilicate gel in water.

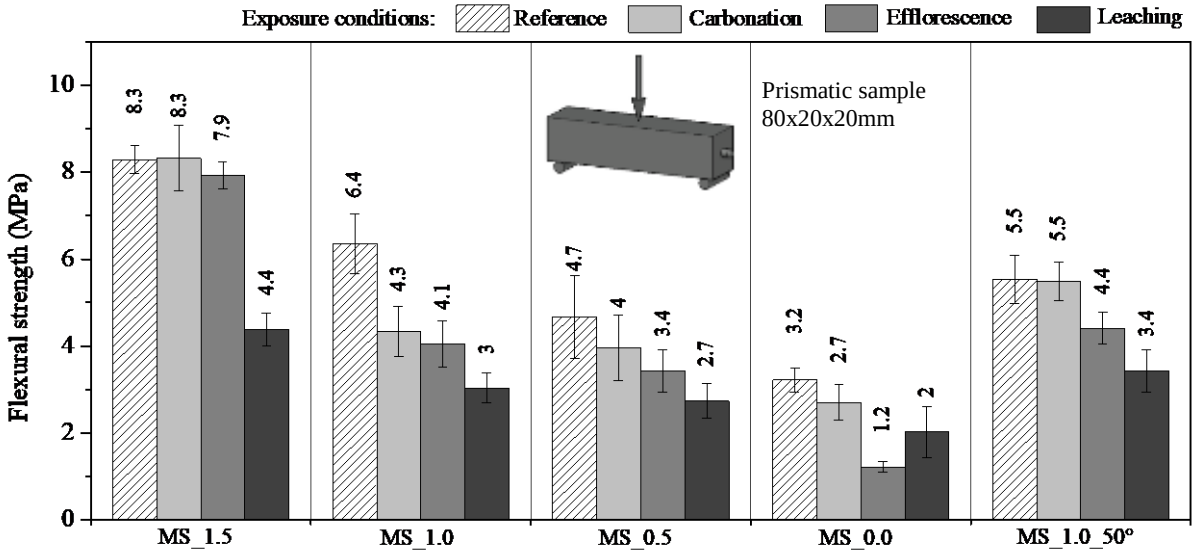

Figura 49 - flexural strength of geopolymers in different conditions of exposure.

Differently than efflorescence and carbonation, due to the open porosity and presence of high amount of free alkalis on metakaolin-based geopolymer, the leaching exposure may be more in-depth than the other exposure conditions. The flexural stress is progressive from the surface to the centre of the sample, thus, the micro-structural and chemical changes developed during the different exposure conditions (mainly EF, LE and CA) on the surface have a stronger effect for the mechanical performance. Therefore, the depth of geopolymer affected determinates the reduction in tensile strength.

In order to understand this behaviour, and the extent of the effect, the geopolymer system MS_0.5, submitted to the three exposure conditions was analysed by TGA at three different depths, as shown in Figure 50A (where the cross section of the sample is showed in the figure). Each TG/DTG curve corresponds to a sample collected in three different points from one specimen the piece extracted (~5 g) was milled in an agate mortar, the reaction stopped using isopropanol and dried in the oven during 45 min at 60 °C. To allow the direct comparison between the depths in each exposure condition, the data was normalized between 0 and 1. The TG/DTG curves indicates the decomposition of carbonates-type phases at temperatures between 500 °C and 700 °C, which is more clear for the external fraction of samples (represented by the black line) exposed to air carbonation (CA) and efflorescence (EF) exposure conditions. Lower content of carbonate products and therefore less carbonation is observed in the samples extracted from the internal fraction (represented by grey lines). Therefore, the superficial part is more highly affected than the internal part when submitted to air contact and efflorescence formation. On the other hand, the extraction of free alkalis during the leaching

process did not show loss of mass related to carbonation (Figure 50C). The loss of mass is consistent to the sample independent of the depth analysed, which elucidates that all the sample is exposed to the same condition. Additionally, by DTG analysis, in leaching exposure, as observed in the peak near to 150 °C, the amount of adsorbed water is higher and homogeneous in the 3 different depths when compared to carbonation and efflorescence exposure. Thus, the leaching exposure promotes the effect to the whole sample, independent of the depth, which can be more damaging to the tensile strength than the other exposure conditions evaluated.

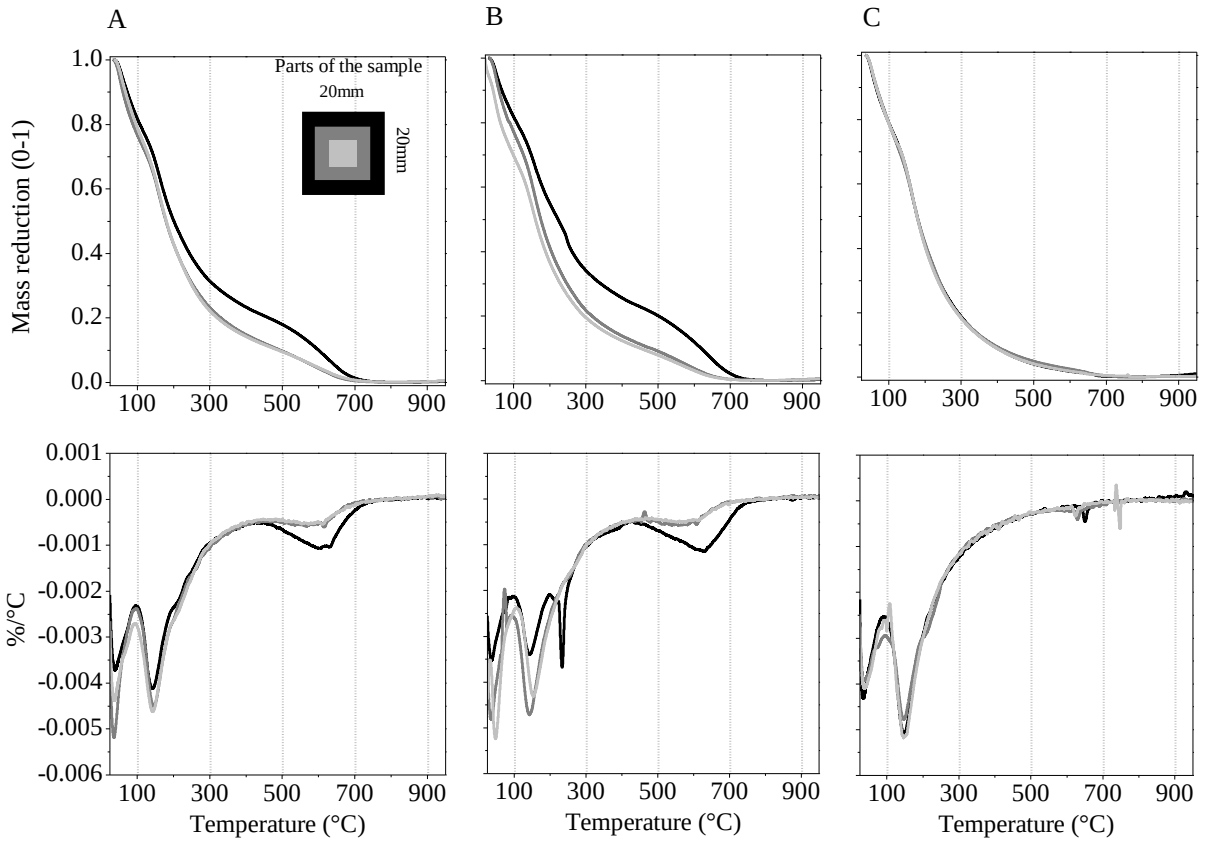

*As is shown in the upper-left corner, the darker line corresponds to the most external area collected (or most damaged) in the prismatic samples exposed to the different conditions and the brighter line to the most internal area (or with less attack).

Figura 50 - TGA analysis of the geopolymer MS_0.5 exposed to different exposure conditions in different depths. A. Carbonation, B. Efflorescence and C. Leaching.

6.3.4 Splitting tensile strength

The splitting test, also known as Brazilian test, is based on the tensile strength from a compression load in the diametral direction of cylindrical sample in Figure 51. The results are aligned to the other mechanical tests data where the reference exposure condition (RE) showed higher values when compared to the other exposure conditions. The geopolymer with high content of soluble silicates (such as MS_1.5 and MS_1.0) also achieved the higher strength.

According to the average values, the splitting tensile strength is approximately 10% of the compressive strength. The samples exposed to the carbonation process shows a very slight reduction (~12%), however, due to the variability of the results, the values vary in the same range and cannot be considered statistically different. The efflorescence condition developed in the EF exposure exhibited a similar behaviour to carbonation exposure, except in the system MS_0.0, where it is observed a reduction in strength of more than 50%. A slight reduction is also identified in the system with thermal curing. By leaching exposure, is observed a reduction near to 50% for all systems. Even the geopolymer MS_1.5 is susceptible to the leaching exposure, which is not observed by compressive strength. This result is consistent with the values observed in flexural strength, and reflects the susceptibility of geopolymers when exposed to leaching.

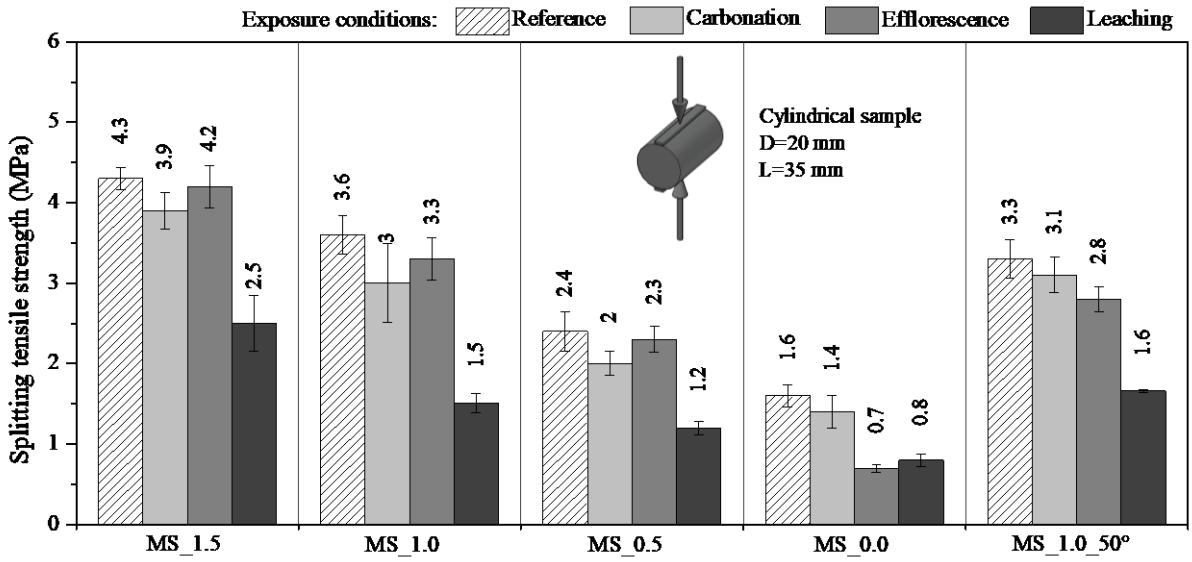

Figura 51 – splitting tensile strength of geopolymers in different conditions of exposure.

The results of mechanical strength presented in this study, it is clear that the efflorescence formation is dependent on different mechanisms (summarized were as superficial efflorescence, carbonation and leaching) and each one presents different effects. In the same way, the effect is different according to the mechanical properties, where carbonation and efflorescence are more damaging to compressive strength and leaching more damaging to flexural and tensile strength.

6.3.6 Linear deformation

The results of linear deformation when the samples were exposed to the different exposure conditions are shown in Figure 52. The dotted line in 0 represents the dimension after 28 days

of curing, without any exposure condition (or the initial system without shrinkage or expansion). After this, the samples were exposed to the specific exposure conditions during 28 and 56 days. In the reference sample the highest shrinkage (~0,25%) is observed in the geopolymers with more amount of sodium silicate. According to Kuenzel et al., (KUENZEL et al., 2012), higher values of Si/Al ratio requires more amounts of bounded water to prevent the drying shrinkage, which is consistent with the behaviour observed in this study, where the addition of sodium silicate increases the shrinkage. The samples exposed to carbonation condition shows a similar shrinkage (between ~0.20 and 0.12%, except the system MS_1.0_50°, where the value is approximately much lower (~0.05%) when compared to the corresponding system MS_1.0 without thermal curing. Similar behaviour is observed in systems exposed to efflorescence conditions, with the shrinkage reduced by the addition of sodium silicate. Due to the extensive efflorescence formation observed in Figure 47, it was expected expansion due to internal strength caused by crystals growing, however, this is not observed here. As indicated by Figure 47 for the systems MS_1.0 and MS_0.0, the efflorescence formation can induces the carbonates formation within the pores and sample degradation, however, as indicated in Figure 50, the presence of carbonate phases is predominantly superficial. Thus, the internal pressure is not enough to present an important change in the sample dimension. To the leaching exposure, mainly to the systems with more amount of sodium silicate, is observed a slight expansion, however this effect cannot be attributed to crystal formation.

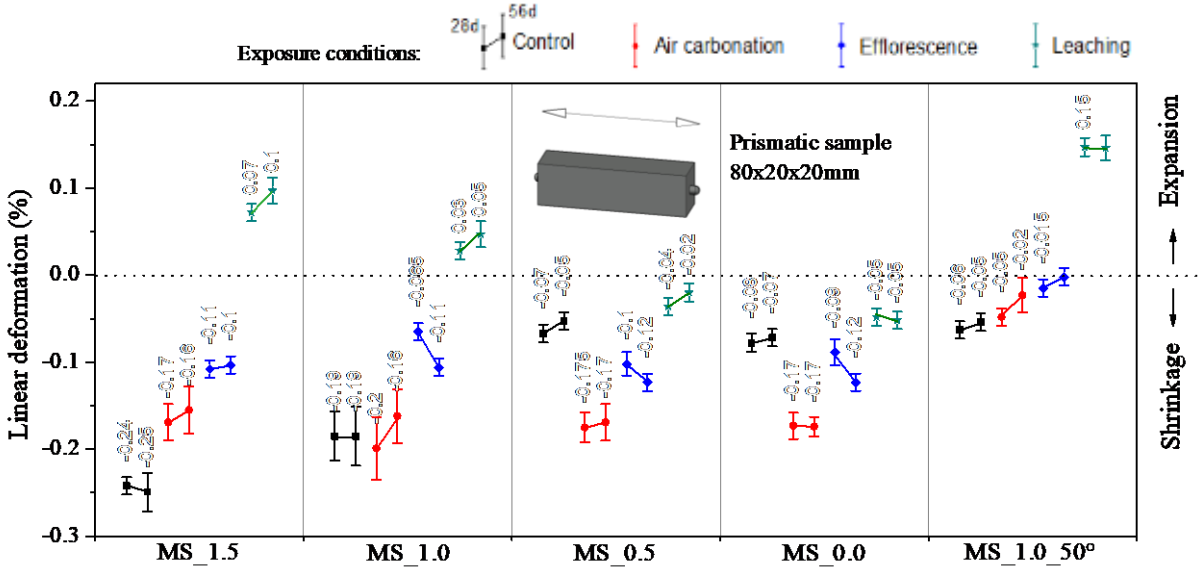

Figura 52 - linear deformation of geopolymers in different conditions of exposure.

6.4. MICROSTRUCTURE

Due to the strength reduction observed by the effect of air carbonation, efflorescence formation and leaching in geopolymers, the microstructure was analysed to elucidate the process of deterioration and identify the origins of this behavior.

6.4.1 Scanning Electron Microscopy

By SEM, the geopolymers (MS_1.5, MS_1.0, MS_0.5 and MS_0.0) were analysed under exposure conditions. The images are shown in Figure 53. Related to reference exposure, with the samples sealed during 56 days and without contact with air or water, is possible to observe that the addition of sodium silicate (MS_1.5 and MS_1.0) in the activator induces the formation of a denser and stronger structure. The images obtained correspond to the most external part of the samples exposed to the different conditions (darker section as was shown in figure 5A. In the systems with less content of SS (MS_0.5 and MS_0.0) is visible a less consistent matrix, with the insufficient dissolution of the precursor, with higher porosity and lesser density in the geopolymeric matrix. In general, the system MS_1.5 do not show marked differences after exposure. In the other systems, the air carbonation exposure shows the formation of different sodium carbonate crystals as also observed in previous studies (LONGHI et al., 2020) and superficial shrinkage. In efflorescence exposure, it is also observed the crystal formation and a superficial deterioration. In the leaching condition, is observed the morphology change, which indicates that the soluble part of the material is being partially removed.

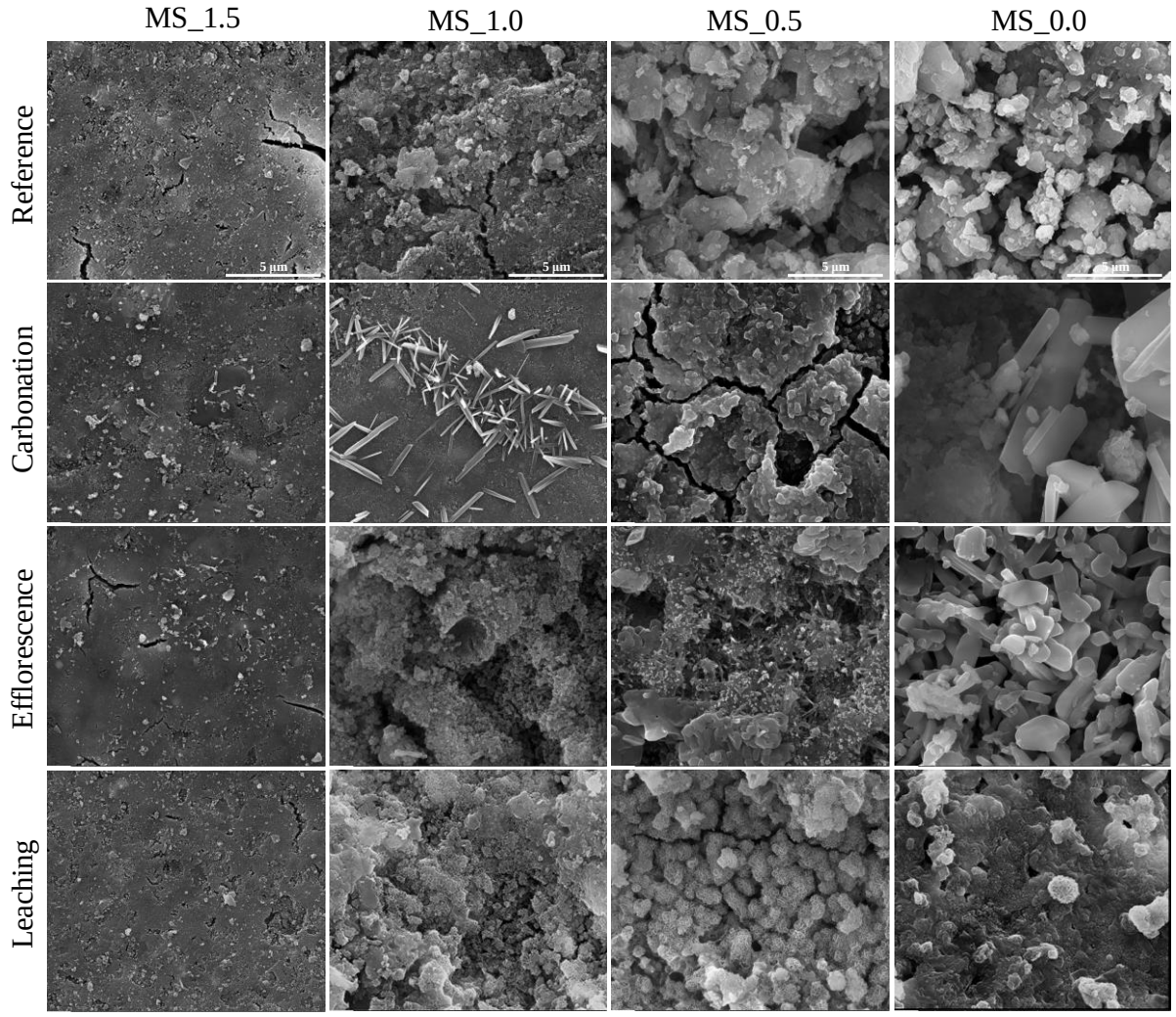

Figura 53 - SEM images of geopolymer samples (MS_1.5, MS_1.0, MS_0.5 and MS_0.0) in different exposure conditions.

To evaluate individually the effect of the different exposure conditions, the geopolymers MS_0.5 was investigated in more detail, Figure 54 to Figure 58. According to Figure 54, related to the system MS_0.5 in a reference exposure, the SEM shows a geopolymers structure formed by layered structure. The elemental composition determined by EDS in specific points (showed as small circles in the Figure 54A) indicate some differences in the percentage, related to the formation of gel or different degrees of the reaction of the precursor but do not represent the entire material. Using the SEM/EDS mapping technique (Figure 54B, C, D and E), is observed the homogeneity of the geopolymer matrix due to the presence of Si, Al and Na. According to the mapping and point EDS from Figure 54A, is observed some traces of carbonates, attributed to the carbonation during the sample preparation. As observed with more details between the Figure 54F to 9H, the reacted gel is formed by grain nucleation, however, due to the design

parameters, this gel does not provide a fully dense matrix. By the morphology of the particles, part of the precursor is not reacted and in retained in the structure as filler.

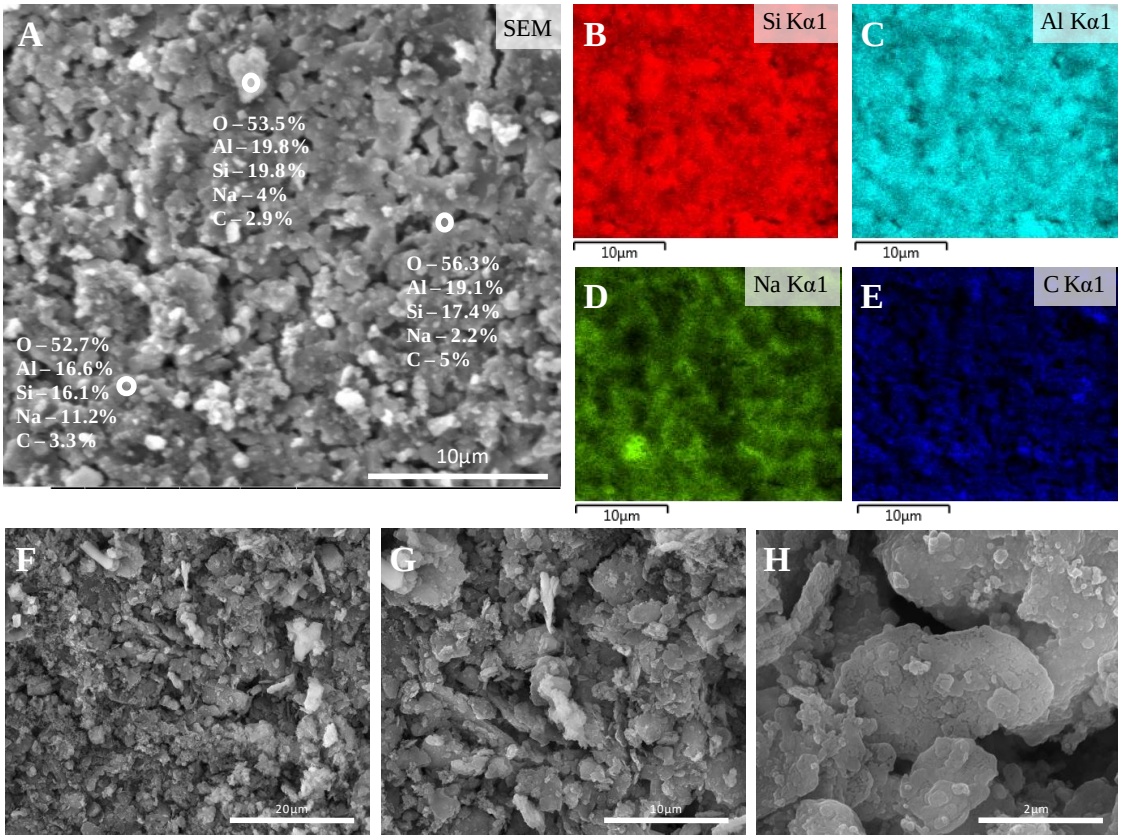

Figura 54 - SEM images and EDX elemental maps of the geopolymer MS_0.5 exposed to reference condition.

The carbonation is more pronounced in this first layer of the material, and this difference is visible by SEM image in Figure 55. In part A, the image shows 2 different morphologies. According to EDS, the left area is formed mostly by sodium carbonate crystals, with small amounts of Si and Al. On the other hand, in the right area is observed the presence of a higher amount of Si and Al and less amount of C, which indicates the presence of carbonated geopolymer gel. Additionally, in Figure 55 A-E, using EDS mapping is visible the difference between elemental composition in the carbonate crystal area and partially carbonated geopolymers. The extended carbonation induces the cracking on the surface as shown in Figure 55F and G and the formation of crystals (Figure 47) due to the excessive alkali movement from the sample to the surface induced by the moisture variation.

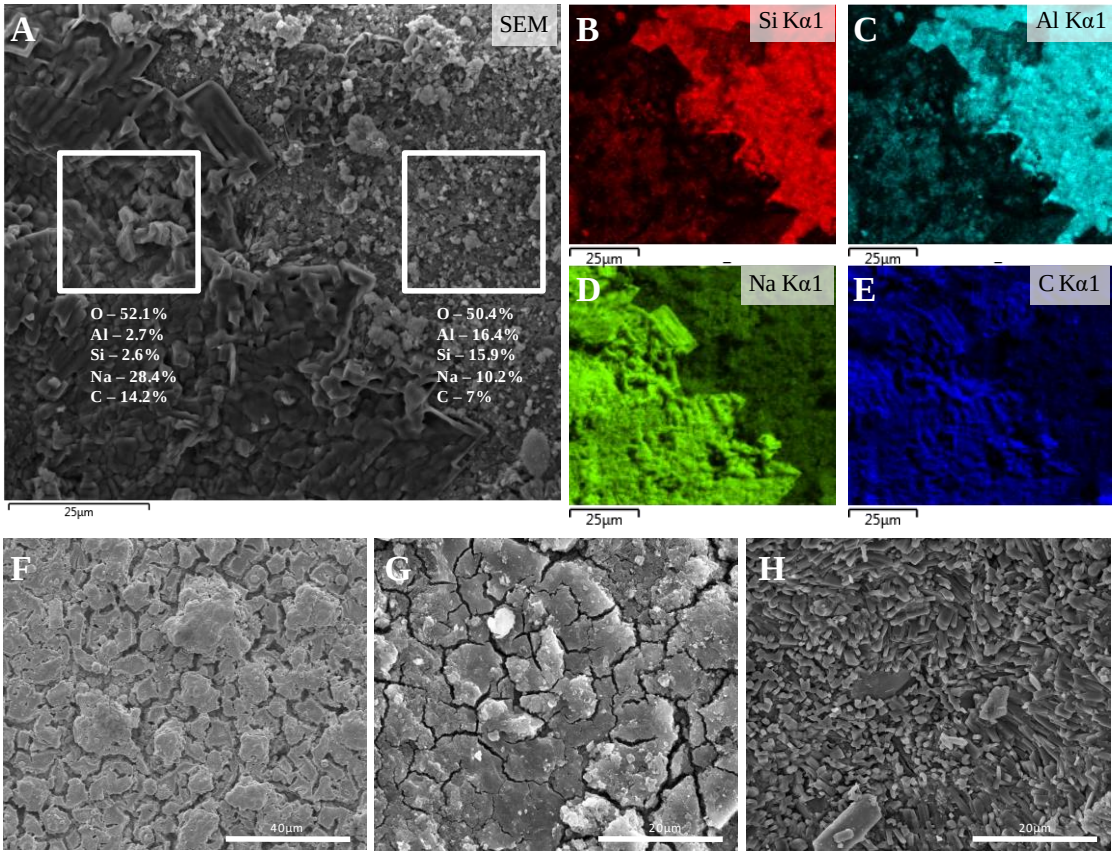

Figura 55 – SEM images and EDX elemental maps of the geopolymer MS_0.5 exposed to carbonation condition.

The efflorescence exposure also affects the mechanical strength as shown previously due to the superficial deterioration and breaking of sample parts. As shown in Figure 56A–E, the crystal is composed by Na and C, in form of sodium carbonate with the growing of carbonate crystals on the surface where sodium availability is higher and in a correct concentration to allows the crystalization. As observed in Figure 56 F-H, the composition of the crystal confirms the formation of sodium carbonate, with different shapes and sizes, related to the availability of sodium, dissolved carbon dioxide, amount of water and humidity (LONGHI et al., 2019c)(LONGHI et al., 2020). As observed in the SEM images, the carbonate crystal growing into the surface can be damaging to the structure due to the high pressure imposed during the crystal formation.

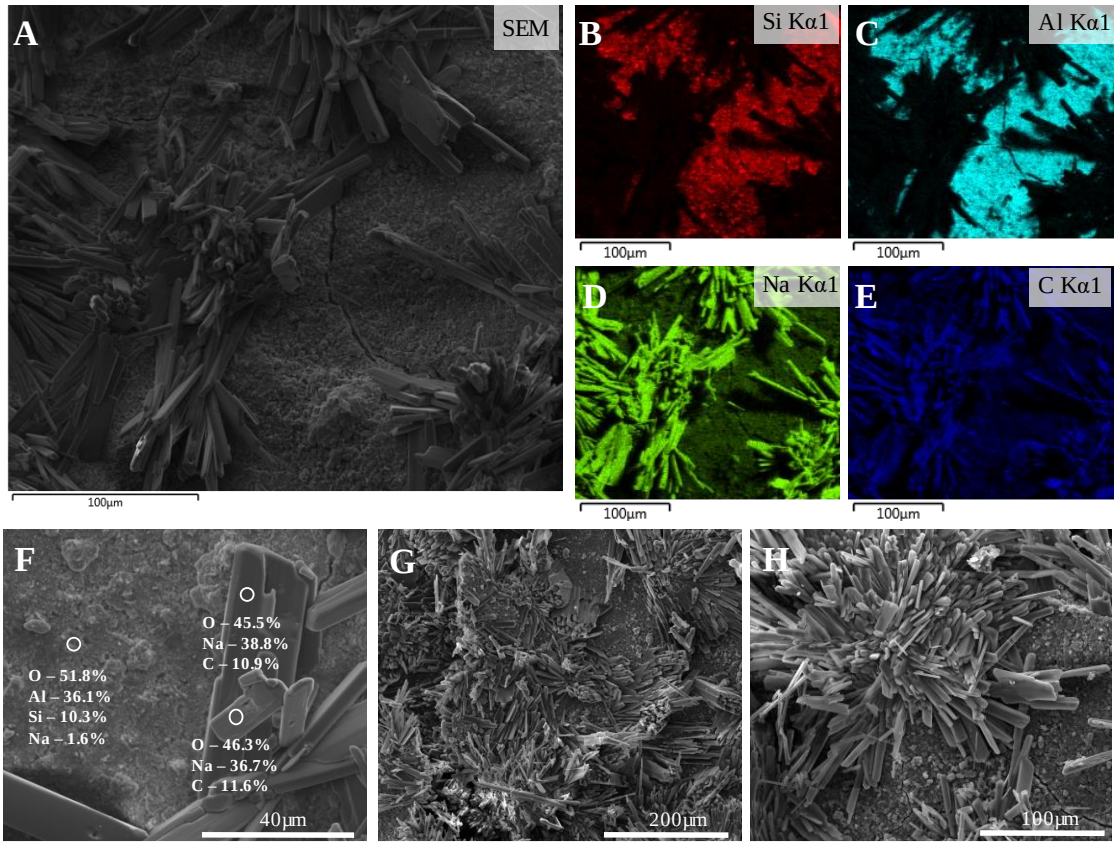

Figura 56 - SEM images and EDX elemental maps of the geopolymer MS_0.5 exposed to efflorescence condition.

The leaching exposure condition is shown in Figure 57 and does not presents the formation of carbonates crystals. This is expected due to the high amount of sodium leached when immersed in water, as well as the absence of dissolved CO_2 within the solution. As observed in SEM mapping (Figure 57 A-E), some points have a different concentration of materials. As the sample was immersed in water, the presence of carbon is attributed to the contact with air during the sample preparation. In Figure 57 F, it is observed a different morphology and elemental composition for each SEM image. In the left area is observed a structure more similar to the reference geopolymer, however, in the right micrograph, the morphology is changed to non-connected spherical type grains. In Figure 57 G-H, it is possible to identify this structure formed, which is constituted by not connected nuclei. Some studies about zeolite synthesis, specially chabazite and sodalite, show a similar morphology (HUO; XU; LV, 2013; LUO; ZHANG; YANG, 2016), however this is just a hypothesis that requires further investigation. Another possibility is that due to high amount of soluble material (or leached components after the immersion) and the change in the Q^n units observed previously by ^{29}Si MAS-NMR (LONGHI et al., 2019c), the microstructure obtained may be the result of the extraction of the more leachable part or the rearrangement of the entire structure. In details the Figure 57 I and J shows the remaining part after the leaching condition, which is constituted with similar

morphology than geopolymer without leaching and is progressively being transformed to spherical grain. The morphology formed can also be associated to the mechanical behaviour observed in flexural and tensile strength. The removal of some of the gel reduces the bond between the grain, which directly affects the tensile strength of the material.

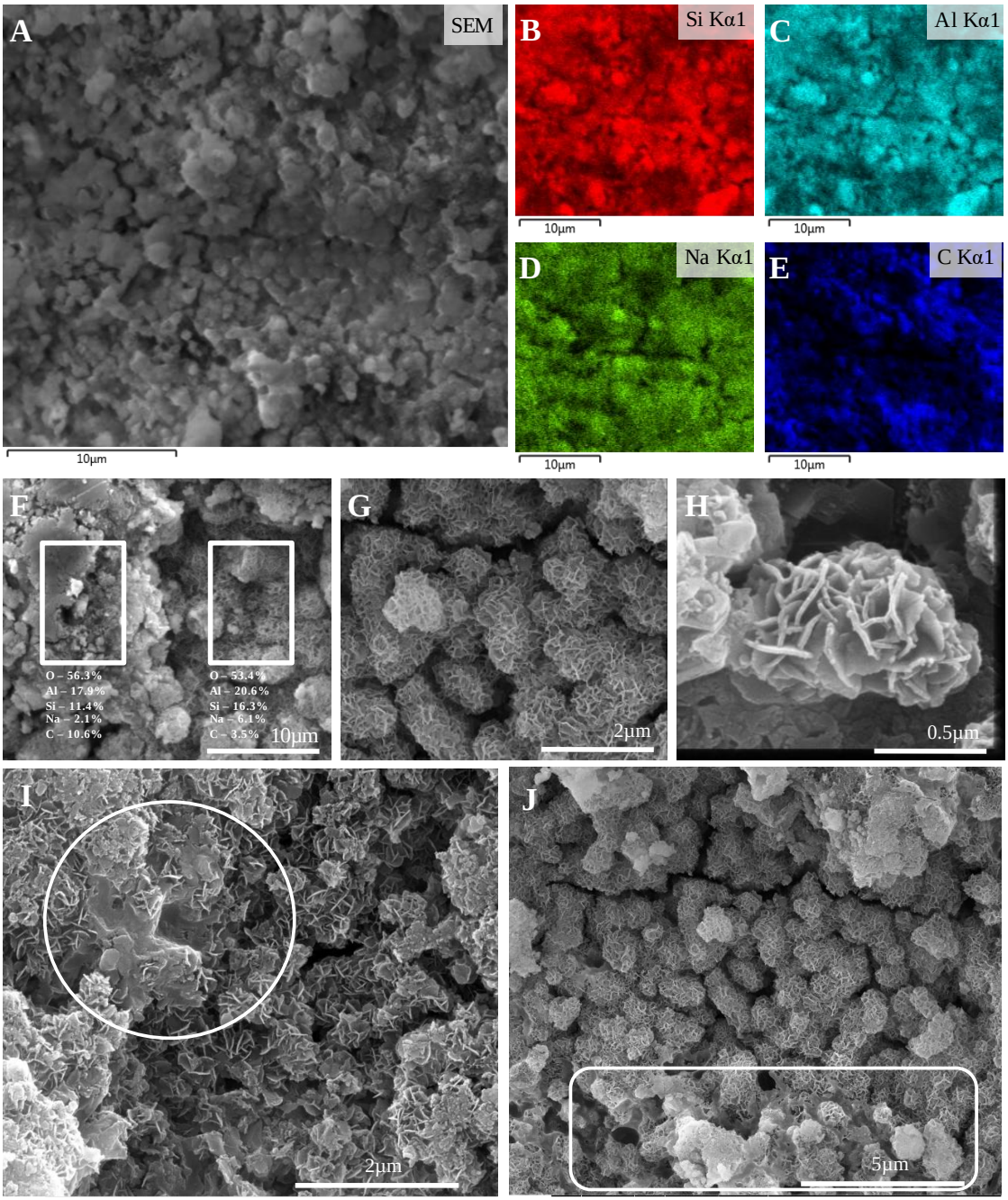

Figura 57- SEM images and EDX elemental maps of the geopolymer MS_0.5 exposed to leaching condition.

Summarising, the SEM analysis evidence important morphology transformations and helps to identify the phenomena related to exposure conditions. During carbonation and efflorescence exposure, the formation of crystals or a carbonate layer were observed and related to the amount of released compounds. The crystals formation into the structure can generate an excessive

stress and can affect the mechanical behaviour. The leaching exposure condition induced the transformation of morphology and formation of a different structures.

6.4.2 Solid state MAS NMR spectroscopy analysis

The **^{27}Al MAS NMR** spectra of the anhydrous metakaolin precursor and the geopolymer sample MS_0.5 in reference, carbonation, efflorescence and leaching exposure condition are shown in Figure 58 The anhydrous metakaolin spectrum exhibits three broad resonances centred at δ_{obs}= 6, 32 and 60 ppm, attributed respectively to aluminium in tetrahedral (IV), pentahedral (V) and octahedral (VI) coordination, which is in agreement with other researches (DUXSON et al., 2005a; WALKLEY; PROVIS, 2019). By the geopolymerisation process, Al(V) and Al(VI) are dissolved to react with other elements to form predominantly Al(IV) species of geopolymer binder (DUXSON et al., 2005a; LONGHI et al., 2019c; WALKLEY; PROVIS, 2019). As reported previously, the presence aluminium in Al(IV) coordination with a negative charge allow the equilibrium of Na^+ and reduce the availability of free alkalis (FERNÁNDEZ-JIMÉNEZ et al., 2006; LONGHI et al., 2019c).

The exposure to different conditions induces some changes associated to the state of aluminium sites. The leaching exposure condition reduces the intensity of the main peak associated to Al(IV) and makes visible the peaks associated with the nonreactive portion of the precursor and corresponding to Al (V) and Al (VI). The reduction in Al(IV) was observed and reported previously ((LONGHI et al., 2019c)(DUXSON et al., 2005b) and associated to the removal of $Al(OH)^-_{4(aq)}$ in the pores and the removal of weaker or less crosslinked Al species. This behaviour is consistent with SEM analysis (Figure 58), where is observed a morphology change associated to microstructural transformations or partial phases removal.

The carbonation of geopolymers in contact with air and the excessive efflorescence formation are associated to the consumption of free or weakly bounded alkalis to form carbonate phases. This phenomenon induce some changes associated to the formation of a new broad peak near to 10 ppm, in Al(VI) region (indicated with a + in the figure). At these conditions, Na^+ ions are removed from the charge-balancing sites within the N-A-S-H gel (as a consequence of efflorescence or carbonation), there is a residual negative charge on the Al ions which must be balanced. As the N-A-S-H gel is now deficient in Na^+, it appears that some of the Al in tetrahedral coordination moves into the charge balancing sites in octahedral coordination,

becoming the charge balancing extra framework Al sites observed previously in geopolymer systems (WALKLEY et al., 2018).

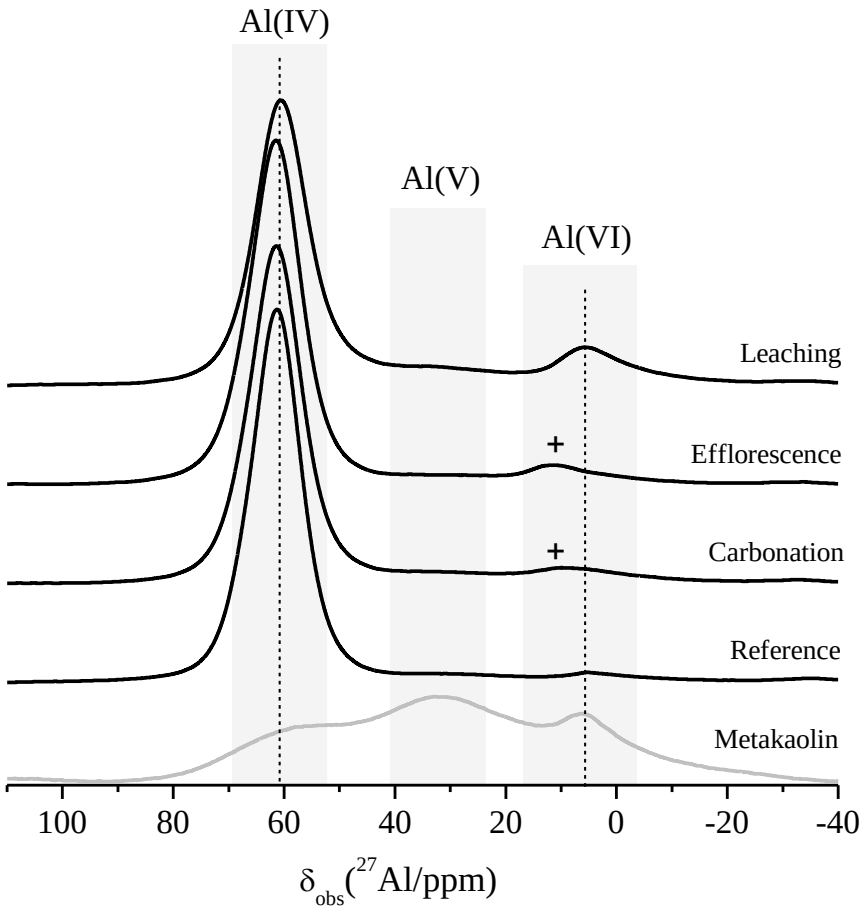

Figura 58 – ^{27}Al MAS NMR of the metakaolin precursor and geopolymer system MS_0.5 after reference, carbonation, efflorescence and leaching exposure conditions.

The **^{29}Si MAS NMR** spectra for the reference geopolymer and after exposure conditions are shown in Figure 59. All the geopolymers shows a different spectrum associated to the different amounts of tetrahedral Si sites formations with a main broad peak, located at -86 ppm to the reference system, -84.9 ppm to carbonation, -84.9 ppm to efflorescence and -85.6 ppm to leaching exposure. This broad peak is composed of Q^4(mAl) species, which are deconvoluted using Gaussian distribution by resonances at δ_{iso} = -85 (4Al), -90 (3Al), -95 (2Al), -100 (1Al), -105 (0Al). The main formation is associated to the tetrahedral coordination with aluminium (Q^4(4Al)), which is consistent with the amount of Al_2O_3 observed by XRF and by ^{27}Al MAS NMR, where the presence of aluminium is predominantly in tetrahedral form Al(IV) in all geopolymer systems.

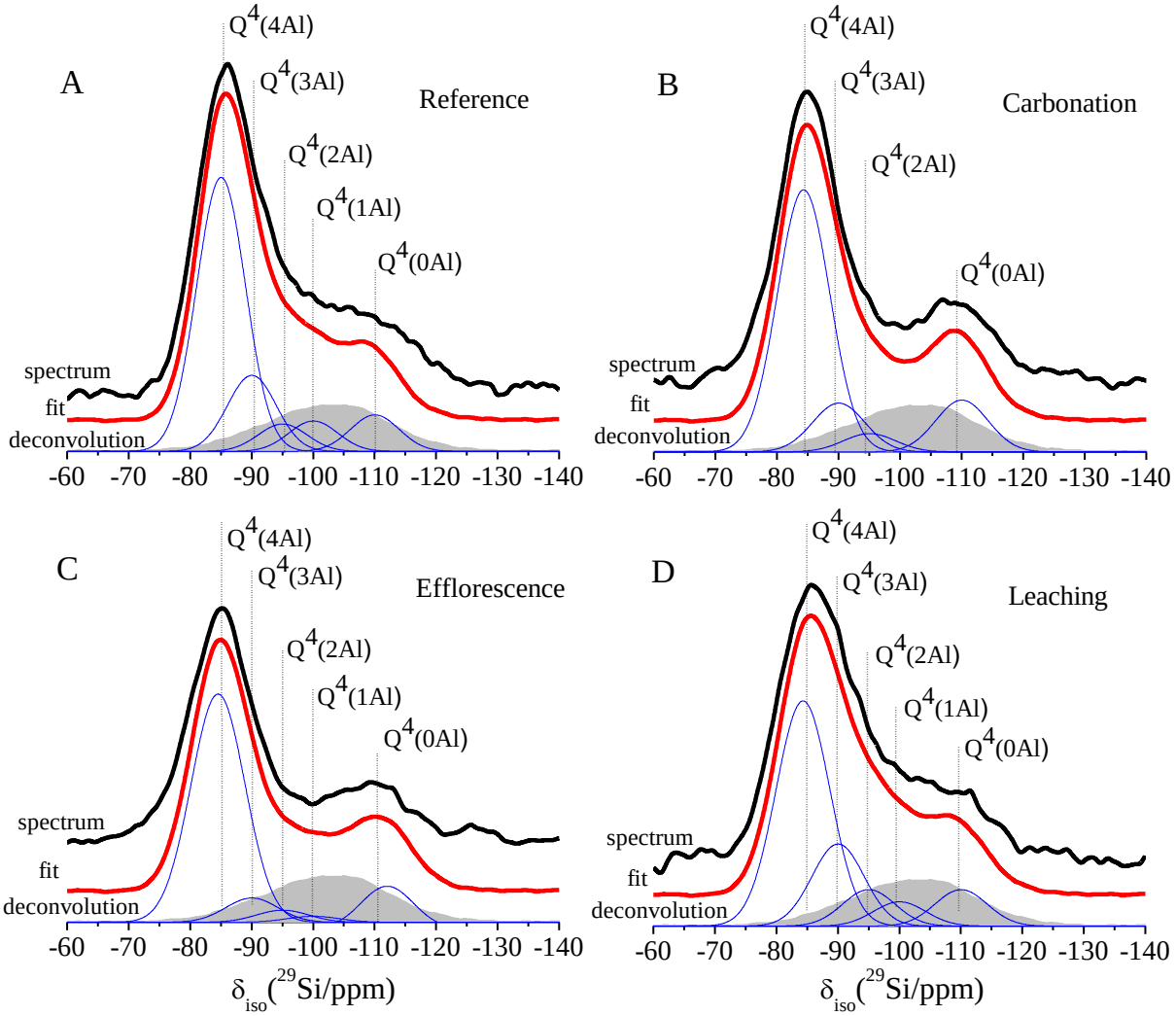

Figura 59 – ^{29}Si MAS NMR of spectrum (black lines), simulation (red lines) and spectral deconvolution blue lines for geopolymer MS_0.5 as reference geopolymer and after carbonation, efflorescence and leaching exposure conditions.

The **^{23}Na MAS NMR** spectra of the reference geopolymers and after exposure condition are shown in Figure 60. The geopolymers exhibit a single broad resonance between -2.48 to -4.5 ppm, which can be attributed to sodium associated to the aluminium-centred tetrahedra in a charge balancing, providing the Na^+ necessary to the equilibrium of the gel framework (DUXSON et al., 2005a; WALKLEY et al., 2016b). According to Duxson et al. (DUXSON et al., 2005a), the resonances near to -4 ppm are attributed to sodium associated to the aluminium in charge-balancing and the resonances near to 0 ppm can be associated to the isotropic sodium located in the pore solution. Thus, after leaching exposure condition the main broad peak is observed in -4.5 ppm, indicating Na^+ mostly associated to the tetrahedral aluminium Al(IV). On the other way on reference system and after leaching and carbonation exposure conditions, the resonance is reduced indicating that in carbonation and efflorescence conditions the sodium carbonate is overlapping with the main resonance due to sodium in charge balancing sites and increasing the main peak. According to Duxson et al. (DUXSON et al., 2005a) the Na^+(aq) can

be present in the solution associate to $Al(OH)_4^-$. The presence of Na^+ and aqueous sodium and aluminium and partially soluble is consistent with the results observed by ^{27}Al MAS NMR (Figure 58) and ^{29}Si MAS NMR (Figure 59).

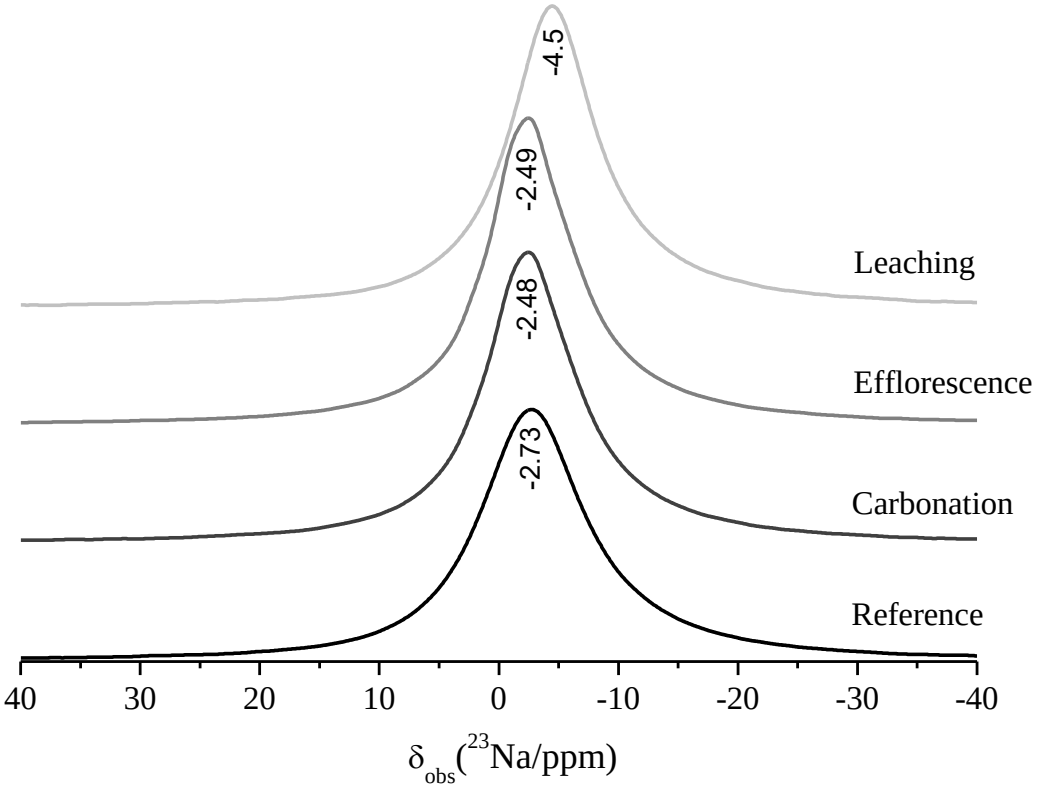

Figura 60 – ^{23}Na MAS NMR spectra of the geopolymer binder MS_0.5 in reference conditions and after exposure.

6.4.3 XRD

In Figure 61 is shown the XRD data for metakaolin and geopolymers exposed to different conditions. In metakaolin precursor is observed the main hump between 10 and 30°, attributed to the amorphous part of the material. Some traces of anatase (TiO_2, Pattern Diffraction File, PDF# 00-021-1272) and halloysite ($Al_2Si_2O_5(OH)_4$, PDF# 00-029-1489) are observed, indicating a crystalline and nonreactive part. After the geopolimerization process, the amorphous hump is reduced and shifted to higher values, indicating the consumption of metakaolinite and formation of N-A-S-H type gel. The crystalline phases (anatase and halloysite) remain in the structure.

After exposure condition, the main difference is attributed to efflorescence condition (EF), where is observed the formation of crystals, related to the formation of sodium carbonate (Na_2CO_3, PDF # 01-086-0301), thermonatrite ($Na_2CO_3 \cdot H_2O$, PDF # 01-070-2148) and natron

($Na_2CO_3 \cdot 10H_2O$, PDF # 00-015-0800). This formation is more visible in the systems MS_0.5-EF and MS_0.0-EF, which were the systems with the highest formation of external efflorescence. The same products were also observed in other studies (BURCIAGA-DÍAZ et al., 2010; ŠKVÁRA et al., 2009; ZHANG et al., 2014b)

In carbonation exposure, even with the visible superficial carbonation observed in figure 5, it is not identified the formation of carbonates phases, probably due to the low amount of carbonates compared to the total mass of the sample. By leaching exposure, the microstructure transformation is visible by SEM, however, this transformation is not visible by XRD. The leaching exposure does not generate a new crystalline phase, the SEM presented in Figure 61 indicates the dissolution of the part of the gel, resulting in different morphology. The dissolved gel for each geopolymer was already quantified and reported in a previous paper (LONGHI et al., 2019c), which also is aligned with the XRD results.

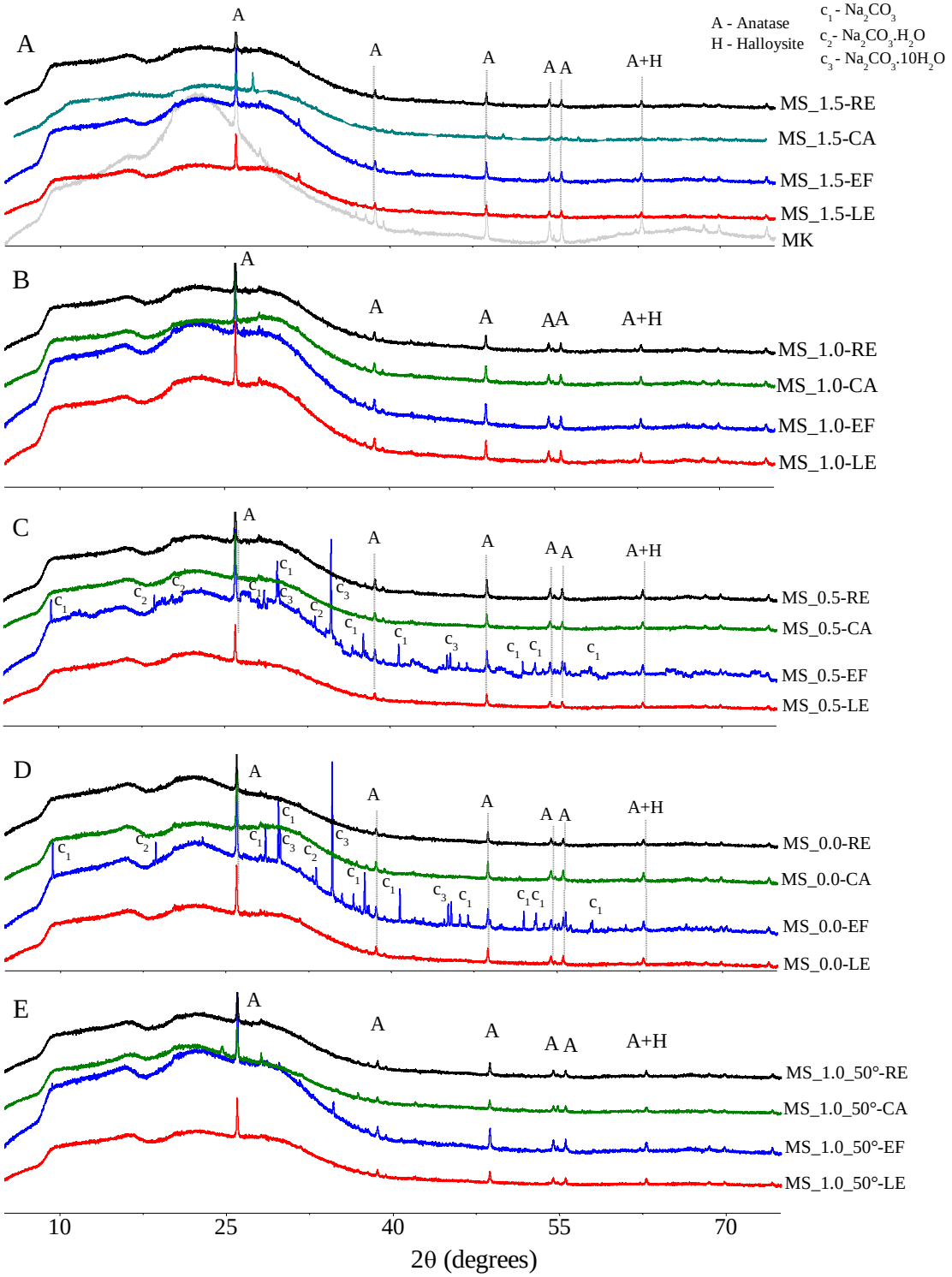

Figura 61 - XRD patterns of the metakaolin geopolymers before exposure condition; A: MS_1.5, B: MS_1.0, C: MS_0.5, D: MS_0.0, E: MS_1.0_50°.

6.4.4 MIP

The MIP analysis is shown in Figure 62. Even with some limitations related to the ink botte effect (SCRIVENER; SNELLINGS; LOTHENBACH, 2016) and the presence of different sizes and shape pores, which will increase the measured volume of very small pores (DIAMOND,

2000). This technique is widely used to identify differences in pore sizes when different conditions or parameter are assessed (or as a comparison purposes). By MIP is possible to estimate the permeable porosity (Figure 62A), were the lower values are observed in high sodium silicate geopolymers. This property is consistent with mechanical behaviour shown in Figure 48, 49 and 51, 4 and 6, indicating the relation between mechanical strength and porosity. Under the exposure conditions, was observed the reduction of porosity due to carbonation, efflorescence formation and leaching, except to the system MS_1.0, where the porosity increased due to carbonation and leaching. The porosity reduction is more sensitive to carbonation and efflorescence than leaching which can be associated to the formation of carbonate crystals, especially in the systems MS_0.5 and MS_0.0, consistent with carbonates formation identified by XRD (Figure 61).

Using the relative volume of pore size in different ranges (Figure 62B), is possible to observe the effect of design parameters and exposure conditions on pore size formation. The high content of sodium silicate provides the formation of small pore sizes when compared to the geopolymer with low MS. The pore size of MS_1.5 consists basically of smaller pores than 50 nm, with a large volume of pores smaller than 10 nm. Similar behaviour is observed in the geopolymer MS_1.0, however, with less content of small pores than 10 nm. On the other hand, the geopolymers MS_0.5 and MS_0.0, present pores basically on the range between 100 nm and 1000 nm. The geopolymers with thermal curing (MS_1.0_50°) presents the same behaviour as the respective geopolymer cured under environmental conditions (MS_1.0). Related to different exposure conditions, the geopolymers MS_1.5 showed the more notable changes, due to the presence of smaller pores in carbonation, efflorescence and leaching when compared to the reference exposure.

The presence of small pores also indicates more reactivity of the precursor and more gel formation, inducing a denser and stronger structure. The presence of pores in smaller diameter is important to durability, considering that the diffusion of aggressive agents inside the binder structure usually takes place through the larger pores (RODRÍGUEZ et al., 2013).

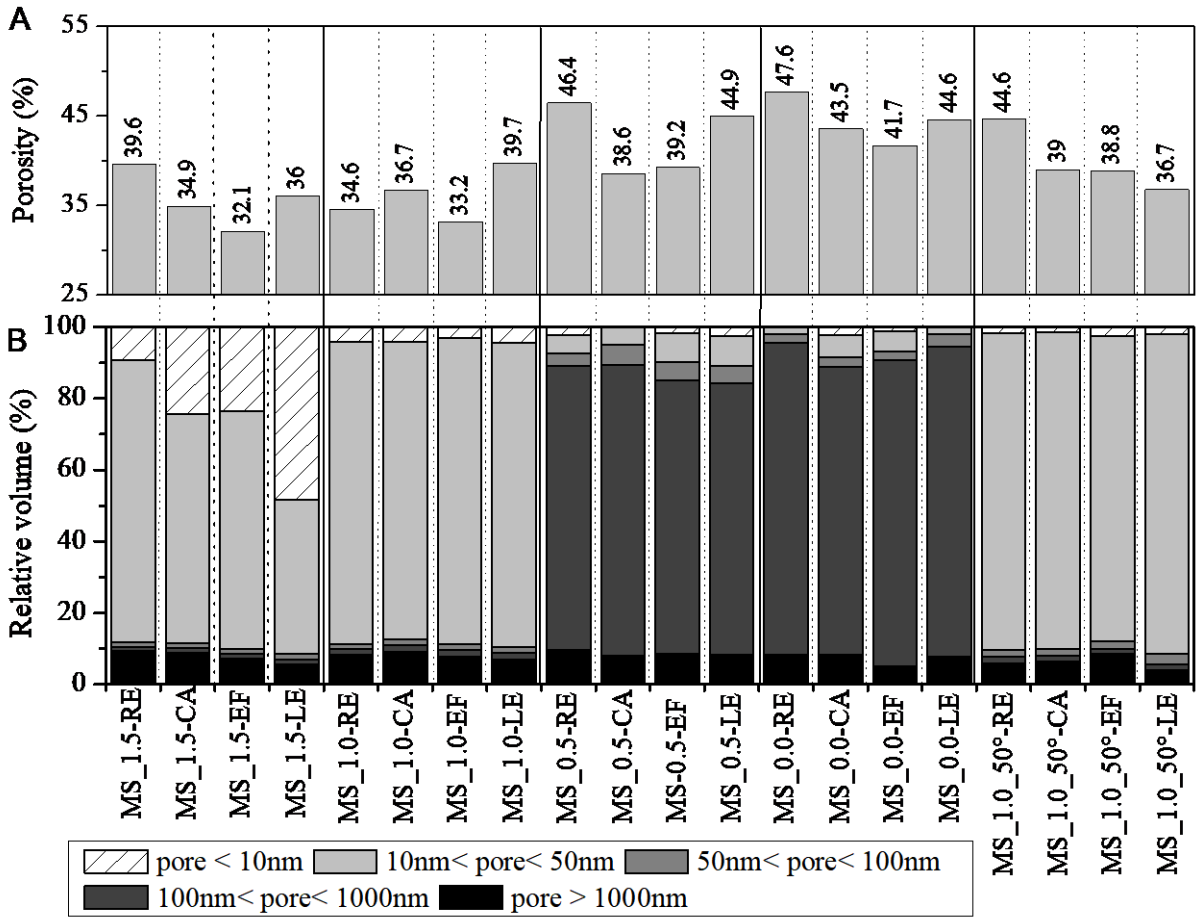

Figura 62 – Porosity and pore size distribution measured by MIP. A. Porosity (%), B. relative volume of pore size distribution (%).

6.4.5 X-Ray microtomography

Figure 63 shows the 3D image rendering for the geopolymer assessed (MS_0.0) under reference, efflorescence and leaching exposure conditions. The air-entrained during the mixing is identified easily as larger bubbles, which were extracted selectively using a watershed filter segmentation technique. The volume fraction of this voids is calculated between 2.4 to 2.9% for the geopolymers assessed. These voids are generated during the mixing and samples production and can be attributed to the insufficient air removal process by vibration. This value will not be considered in the total porosity due to its size and origin of this voids. Content of air entrained between the sample is identified and can be attributed to the different viscosity that the material exhibits due to the nature and concentration of the alkali activator (ZHANG et al., 2018a). The unreacted MK-particles and large-pores (with sizes higher than 4 µm) were assessed by the selection of point-based threshold based on a high grey level transition ("or transition point"). The calculated volume of unreacted metakaolin in the samples under reference (RE), efflorescence (EF) and leaching (LE) exposure conditions, is 11.2, 19.0 and

11.8%, respectively. The calculated volume fraction of this pores is 3.3, 1.4 and 1.2%, respectively. Transition point identification based on the gray-scale histogram is a method used often for segmentation. However, this technique may not be appropriate for geopolymers materials since its porosity network exhibits sizes smaller than the voxel resolution, and the sample produces a wide range of greyscale intensities for different phases (unreacted and partially unreacted particles, as well as reacted products) (DAS et al., 2015; PROVIS et al., 2012). Taking into account that the images acquired in the XRµT are also limited to 0.84 µm by voxel/pixel, a detailed analysis of pore network is not reliable for this material. The 3D pore-network volume, connectivity and tortuosity quantification are limited in this study due to the high heterogeneity of the MK-based geopolymer as well as the presence of a pore size distribution smaller than 1 µm (as was shown in MIP). Therefore, the images and pore volume reported here, correspond to voids with sizes larger than 3 µm, where the statistics and consistency during the application of the segmentation algorithm showed coherence between images, results derived from other techniques, and previous reports (DAS et al., 2015; PROVIS et al., 2012)

This analysis aims to identify if the porosity or the gel structure changes due to the exposure of the geopolymers to the process of efflorescence and leaching. According to Provis et al. (2013), the complete distinction between the phases (unreacted and partially particles, N-A-S-H gel and micro-porosity) is quite difficult and represent the main limitation of XRµT for this type of material.

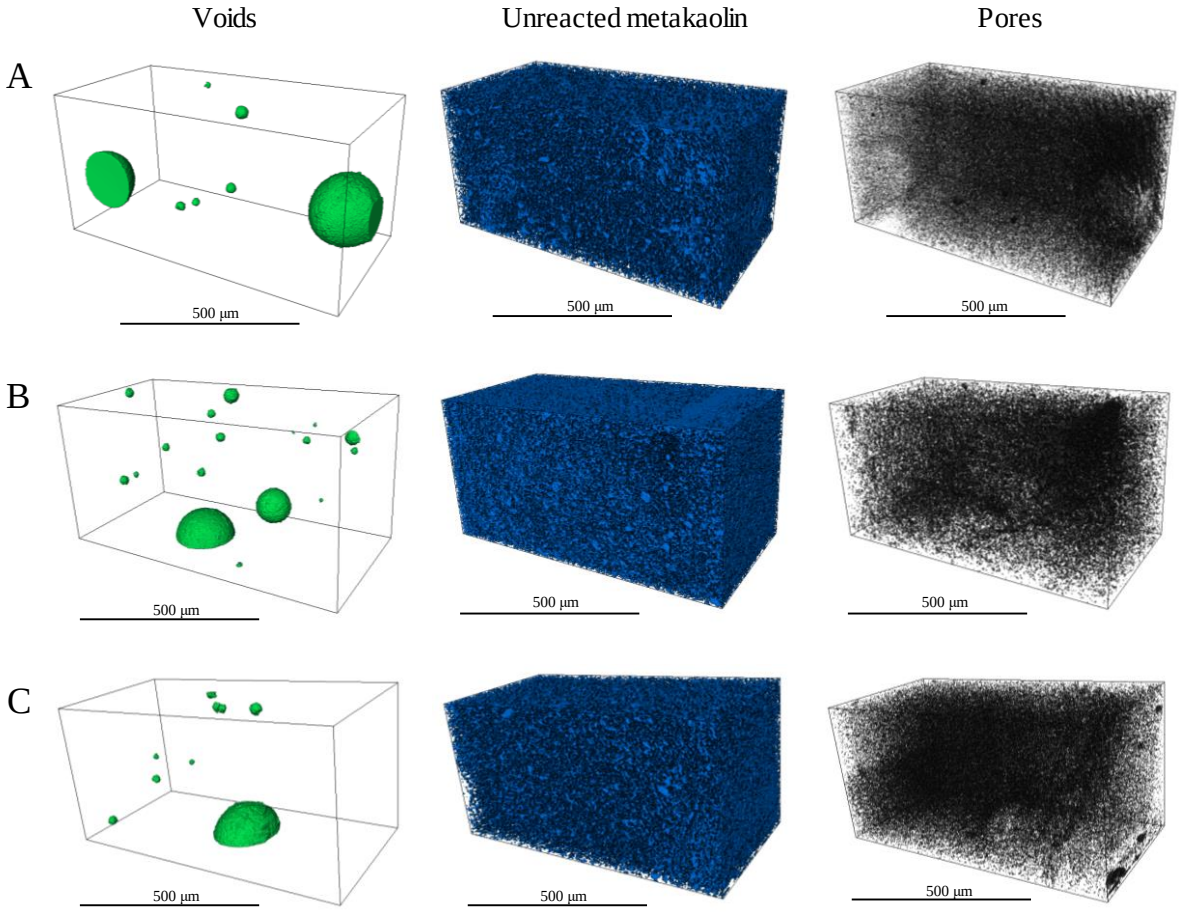

Figura 63 – Images of voids, unreacted metakaolin and pores of a prismatic region of the geopolymer MS_0.0 exposed to: A. Reference, B. Efflorescence, C. Leaching.

6.5. CONCLUSIONS

This study evaluated the effect of efflorescence formation associated with air carbonation and leaching in metakaolin based geopolymers by mechanical strength and micro/nanostructure. The efflorescence formation associated with different exposure conditions in a mechanical and nanostructural scale, provides a new understanding related to the effect caused by these phenomena and helps to predict durability features.

Leaching can be indicated as the first process associated with efflorescence formation. This exposure condition induces the removal of free or weakly bounded alkalis which affect the mechanical and microstructural properties. The flexural and tensile strength of geopolymers are sensitive to exposure to leaching condition. An important reduction in these properties is observed and associated with the excessive alkali removal and dissolution of weak parts of gel. The excessive removal of soluble sodium can change the equilibrium of aluminium in the framework structure, consequently, the stability of some phases in the gel. The removal of the

less stable portion resulted in the formation of a structure based on non-connected grains. A morphological transformation of gel can be observed by SEM. The addition of sodium silicates provides an improvement in the mechanical properties, however, even systems with high levels of sodium silicate are susceptible to the leaching process.

The condition of exposure to air carbonation induces the process of carbonation associated with the efflorescence formation. This phenomenon occurs in the first layers of the material and affects the mechanical performance of geopolymers. The main property affected is compressive strength, which is also dependent on the content of sodium silicate used. Geopolymers with more amount of sodium silicate is less susceptible to effects in mechanical strength. According to porosity, the excessive loss of water allows the leaching process and induces the carbonates crystals growing. The formation of this carbonates can be superficial or within the pores in the first geopolymer layer, which can generate internal stress and superficial deterioration.

The efflorescence formation is the main phenomenon investigated were, however directly associated to leaching and carbonation processes. The efflorescence formation is strongly dependent on design parameters, where the addition of sodium silicate associated to the correct content of alkali can reduce the extent of efflorescence formation. It is also a superficial formation than can affect all mechanical properties, especially compressive strength, which is strongly affected to some geopolymers. This effect is associated to excessive superficial deterioration and crystal formation within the pores, also associated to internal carbonation, which generates internal stress greater than tensile strength of the material and causes the rupture of fragments or parts. The main product associated to efflorescence is sodium carbonates and hydrated sodium carbonate, which grow on the surface in different shapes and sizes.

The effect of efflorescence formation and its associated mechanisms is easily identified by the formation of visual efflorescence, mechanical resistance and microstructural properties. The occurrence of this formation is negative for the durability of the material and may limit its use under specific conditions. However, some geopolymers are less susceptible to effects, which indicates the possibility of improving properties. More researches should be conducted with the aim of reducing the susceptibility to efflorescence formation.

REFERENCES:

ARBI, Kamel et al. A Review on the Durability of Alkali-Activated Fly Ash / Slag Systems : Advances , Issues , and Perspectives. **Ind. Eng. Chem. Res.**, v. 55, p. 5439–5453, 2016.

BERNAL, Susan A.; PROVIS, John L. Durability of alkali-activated materials: Progress and perspectives. **Journal of the American Ceramic Society**, v. 97, n. 4, p. 997–1008, 2014.

BURCIAGA-DÍAZ, Oswaldo et al. Statistical analysis of strength development as a function of various parameters on activated metakaolin/slag cements. **Journal of the American Ceramic Society**, v. 93, n. 2, p. 541–547, 2010.

CARVALHO, A. M. G. et al. X-ray powder diffraction at the XRD1 beamline at LNLS. **Journal of Synchrotron Radiation**, v. 23, n. 6, p. 1501–1506, 2016.

CARVALHO, A. M. G.; NUNES, R. S.; COELHO, A. A. X-ray powder diffraction of high-Absorption materials at the XRD1 beamline off the best conditions: Application to (Gd, Nd)5Si4 compounds. **Powder Diffraction**, v. 32, n. 1, p. 10–14, 2017.

DAS, Sumanta et al. Effective properties of a fly ash geopolymer: Synergistic application of X-ray synchrotron tomography, nanoindentation, and homogenization models. **Cement and Concrete Research**, v. 78, p. 252–262, 2015.

DIAMOND, Sidney. Mercury porosimetry An inappropriate method for the measurement of pore size distributions in cement-based materials. v. 30, p. 1517–1525, 2000.

DOW, C.; GLASSER, F. P. Calcium carbonate efflorescence on Portland cement and building materials. **Cement and Concrete Research**, v. 33, n. 1, p. 147–154, 2003.

DUXSON, P. et al. Effect of alkali cations on aluminum incorporation in geopolymeric gels. **Industrial & Engineering Chemistry Research**, v. 44, n. 4, p. 832–839, 2005. a.

DUXSON, Peter et al. Si NMR Study of Structural Ordering in Aluminosilicate Geopolymer Gels. p. 3028–3036, 2005. b.

DUXSON, Peter et al. Understanding the relationship between geopolymer composition, microstructure and mechanical properties. **Colloids and Surfaces A: Physicochemical and Engineering Aspects**, v. 269, n. 1–3, p. 47–58, 2005. c.

DUXSON, Peter et al. The role of inorganic polymer technology in the development of 'green concrete'. **Cement and Concrete Research**, v. 37, n. 12, p. 1590–1597, 2007.

FERNÁNDEZ-JIMÉNEZ, A. et al. The role played by the reactive alumina content in the alkaline activation of fly ashes. **Microporous and Mesoporous Materials**, v. 91, n. 1–3, p. 111–119, 2006.

HOUST, Yves F.; WITTMANN, Folker H. Influence of porosity and water content on the diffusivity of CO2 and O2 through hydrated cement paste. **Cement and Concrete Composites**, v. 24, n. 6, p. 1165–1176, 1994.

HUO, Zhiping; XU, Xiangyu; LV, Zhi. Thermal study of NaP zeolite with different morphologies. p. 365–369, 2013.

KUENZEL, Carsten et al. Ambient temperature drying shrinkage and cracking in metakaolin-based geopolymers. **Journal of the American Ceramic Society**, v. 95, n. 10, p. 3270–3277, 2012.

LONGHI, Márlon A. et al. New selective dissolution process to quantify reaction extent and product stability in metakaolin-based geopolymers. **Composites Part B: Engineering**, v. 176, p. 107172, 2019.

LONGHI, Márlon A. et al. Metakaolin-based geopolymers: Relation between formulation, physicochemical properties and efflorescence formation. **Composites Part B: Engineering**, v. 182, n. October 2019, 2020.

LONGHI, Márlon A. Málon A. M. A. et al. Valorisation of a kaolin mining waste for the production of geopolymers. **Journal of Cleaner Production**, v. 115, 2016.

LUO, Jie; ZHANG, Haijun; YANG, Jian. Hydrothermal synthesis of sodalite on alkali-activated coal fly ash for removal of lead ions. **Procedia Environmental Sciences**, v. 31, p. 605–614, 2016.

MASSIOT, Dominique et al. Modelling one- and two-dimensional solid-state NMR spectra. **Magnetic Resonance in Chemistry**, v. 40, n. 1, p. 70–76, 2002.

NAJAFI, Ebrahim; ALLAHVERDI, Ali; PROVIS, John L. Efflorescence control in geopolymer binders based on natural pozzolan. v. 34, p. 25–33, 2012.

PROVIS, John L. et al. Cement and Concrete Research X-ray microtomography shows pore structure and tortuosity in alkali-activated binders. **Cement and Concrete Research**, v. 42, n. 6, p. 855–864, 2012.

PROVIS, John L. Geopolymers and other alkali activated materials: why, how, and what? **Materials and Structures**, v. 47, n. 1–2, p. 11–25, 2013.

RODRÍGUEZ, Erich D. et al. Cement & Concrete Composites Effect of nanosilica-based activators on the performance of an alkali-activated fly ash binder. v. 35, p. 1–11, 2013.

ROWLES, M. R. HANNA, J. V. PIKE, K. J, SMITH, M. E, O'connor B. H. Si, Al, 1 H and 23 Na MAS NMR Study of the Bonding Character in Aluminosilicate Inorganic Polymers 27. **Applied Magentic Resonance**, v. 32, p. 663–689, 2007.

ROWLES, Matthew R.; BRIAN H. O'CONNOR. Chemical and Structural Microanalysis of Aluminosilicate Geopolymers Synthesized by Sodium Silicate Activation of Metakaolinite ReadCube Articles. **Journal of the American Ceramic Society**, v. 92, n. 10, p. 2354–2361, 2009.

SCRIVENER, Karen; SNELLINGS, Ruben; LOTHENBACH, Barbara. **A Practical Guide to Microstructural Analysis of Cementitious Materials - Chapter 5: Thermogravimetrix Analysis**. Taylon and ed. Boca Raton: CRC press, 2016.

ŠKVÁRA, František et al. Aluminosilicate polymers - Influence of elevated temperatures, efflorescence. **Ceramics - Silikaty**, v. 53, n. 4, p. 276–282, 2009.

ŠKVÁRA, František et al. A weak alkali bond in (N, K)-A-S-H gels: Evidence from leaching and modeling. **Ceramics - Silikaty**, v. 56, n. 4, p. 374–382, 2012.

WALKLEY, B.; PROVIS, J. L. **Solid-state nuclear magnetic resonance spectroscopy of cementsMaterials Today Advances**, 2019.

WALKLEY, Brant et al. Phase evolution of Na_2O–Al_2O_3–SiO_2–H_2O gels in synthetic aluminosilicate binders. **Dalton Transactions**, v. 45, n. 13, p. 5521–5535, 2016.

WALKLEY, Brant et al. New Structural Model of Hydrous Sodium Aluminosilicate Gels and the Role of Charge-Balancing Extra-Framework Al. v. 4, 2018.

YAO, Xiao; YANG, Tao; ZHANG, Zuhua. Compressive strength development and shrinkage of alkali-activated fly ash–slag blends associated with efflorescence. **Materials and Structures/Materiaux et Constructions**, v. 49, n. 7, p. 2907–2918, 2016.

ZHANG, Da Wang et al. Rheology, agglomerate structure, and particle shape of fresh geopolymer pastes with different NaOH activators content. **Construction and Building Materials**, v. 187, p. 674–680, 2018. a.

ZHANG, Zuhua et al. Quantitative kinetic and structural analysis of geopolymers. Part 1. The activation of metakaolin with sodium hydroxide. **Thermochimica Acta**, v. 539, p. 23–33, 2012.

ZHANG, Zuhua et al. Quantitative kinetic and structural analysis of geopolymers. Part 2. Thermodynamics of sodium silicate activation of metakaolin. **Thermochimica Acta**, v. 565, p. 163–171, 2013.

ZHANG, Zuhua et al. Cement and Concrete Research Fly ash-based geopolymers : The relationship between composition , pore structure and ef fl orescence. v. 64, p. 30–41, 2014. a.

ZHANG, Zuhua et al. Fly ash-based geopolymers: The relationship between composition, pore structure and efflorescence. **Cement and Concrete Research**, v. 64, p. 30–41, 2014. b.

ZHANG, Zuhua et al. Efflorescence and subflorescence induced microstructural and mechanical evolution in fly ash-based geopolymers. **Cement and Concrete Composites**, v. 92, n. March, p. 165–177, 2018. b.

7. STRATEGIES OF SYNTHESIS PARAMETERS FOR THE CONTROL AND MITIGATION OF EFFLORESCENCE DEVELOPMENT IN METAKAOLIN-BASED GEOPOLYMERS

7.1. INTRODUCTION

Efflorescence is a phenomenon that occurs due to the movement of free alkali through the pore network to the surface and when in contact with the carbon dioxide from the environment can form carbonate-type phases on the surface. Previous studies in geopolymers cements show that the leaching of the alkalis presented in the reacted products and the pore structure plays a significant role in the efflorescence formation (LONGHI et al., 2019c; ZHANG et al., 2014b, 2018b). The susceptibility of alkalis leachability is related to the synthesis parameters, mainly the alkali metal type (such as Na^+ or K^+) (LONGHI et al., 2020; ŠKVÁRA et al., 2009, 2012), raw materials used (BERNAL, 2016; NAJAFI; ALLAHVERDI; PROVIS, 2012; ZHANG et al., 2018b), and synthesis conditions (BURCIAGA-DÍAZ et al., 2010; NAJAFI; ALLAHVERDI; PROVIS, 2012; ZHANG et al., 2014b). The composition of the alkali activator, mainly the content of M_2O (where M can be Na^+ and/or K^+) and the presence of soluble silicates (LONGHI et al., 2019c, 2020) can be considered the most important parameters.

During the geopolymerization, the constituent responsible for the activation of the aluminosilicate precursor, is the same one that will provide the development of this pathological manifestation. The alkali is provided by the activator solution, which reacts with the amorphous aluminosilicate precursor to start the stages of dissolution, reorientation and polycondensation to form the geopolymeric gel (DUXSON et al., 2006). The main product formed is a highly reticulate M-A-S-H gel (PROVIS; LUKEY; VAN DEVENTER, 2005a), where M represents the alkali type used. Part of this alkali can be present in the framework structure to compensate the negative balance of Al^- in a Q^4 molecular coordination (DUXSON et al., 2005b; FERNÁNDEZ-JIMÉNEZ et al., 2006; ROWLES, M. R. HANNA, J. V. PIKE, K. J, SMITH, M. E, 2007; WALKLEY et al., 2016a). Other fraction of the alkalis remain within the pores weakly associated with water molecules in form of $Na(H_2O)_n^+$ (PROVIS; BERNAL, 2014;

ROWLES, M. R. HANNA, J. V. PIKE, K. J, SMITH, M. E, 2007). Stoichiometrically, the limit of Na^+ in equilibrium with the negative balance of Al is represented by the molar ratio Na_2O/Al_2O_3=1. However, this limit consider that all Al is reactive (or soluble) and exhibits a Q^4 molar coordination, where is assumed a perfect reaction through total dissolution of precursor. In practice it may be different and relative to the effectiveness of the activation and contents of activator used.

Considering that a small portion of the aluminosilicate precursors is non-reactive (or non-dissolved) during the geopolymerization process, it is expected that portion of the alkalis remain free or easily leach from the M-A-S-H gel network. The leachability of alkalis was investigated previously, where values between 12 to 16% of the total alkali used were observed by Zhang *et al.* (ZHANG et al., 2014a), 40 to 60% by Zheng *et al*. (ZHENG et al., 2011) in fly ash based-geopolymers, as well as 17 to 30% by Longhi *et al*. (LONGHI et al., 2020) in metakaolin-based geopolymers. Thus, the leachability of alkali cations (Na^+) associated with the high amount of free or weakly bounded alkalis is evident.

Other factor that can be considered for efflorescence formation is the high alkali mobility within the pore structure, which is also aesthetically undesirable and harmful to the performance of geopolymers. According to other studies (LONGHI et al., 2020; YAO; YANG; ZHANG, 2016; ZHANG et al., 2018b), the excessive degree of efflorescence formation, associated to leaching and excessive carbonation on the surface and inside the pores can reduce the compressive and tensile strength. The main phenomena associated to this reduction is related to the microstructural changes due to the alkali removal and the superficial deterioration by excessive crystallization of the surface.

The reduction of efflorescence formation was previously investigated by Najafi *et al.* (NAJAFI; ALLAHVERDI; PROVIS, 2012) using natural pozzolan based-geopolymers. The most effective method observed by the authors were the addition of alumina-rich admixtures or by hydrothermal curing, both responsible to enhance the framework structure. The alumina addition improves the extent of crosslinking and reduce the alkali mobility due to the increasing of Al in a tetrahedral molecular coordination and the hydrothermal curing increase the amount of gel formed and the pore structure refinement. As an initial alternative for control the efflorescence, the adopted strategies are related to the reduction of the quantity of free alkalis and refinement of the porosity to reduce the leachability. As observed by Najafi *et al.* (NAJAFI; ALLAHVERDI; PROVIS, 2012), the addition of an reactive extra source of aluminium

increases the ability of Na^+ to the equilibrium on the negative balance of Al(IV). On the same way, according to Lloyd *et al.* (LLOYD; PROVIS; VAN DEVENTER, 2010), more amount of soluble silica in the activator can improve the reaction degree and gel formation. Similar behaviour was observed by Longhi *et al.* (LONGHI et al., 2020) where the addition of silica soluble from the activator generates more amount of gel and the formation of higher amount of Q^4(mAl) rich in Si. The increasing of silica in the framework structure does not reduce the amount of bounded Al(IV) sites or Na^+ in equilibrium with the negative balance, but induces the formation of a more reticulate and denser framework structure, which provides stronger chemical bonding of the alkalis and greater difficulty in fluid movement. The pore refinement can also be improved reducing the porosity by the optimization of particles morphology or by use of chemical barriers to reduce the fluid movement.

Two alternatives are the most plausible to reduce this phenomenon, the first related to reducing the amount of free alkali, and the second, related to improving the gel and pore refinement porosity. In this sense, this work assessed the potential alternatives to mitigate or control the formation of efflorescence in metakaolin based-geopolymers from the improvement of alkali stability and physical properties. For this, optimization it was assessed the synthesis parameters and the addition of three different materials: (1) supplementary cementitious materials (SCM's), such as granulated blast furnace slag (GBFS), silica fume (SF), fly ash (FA), (2) cement, as calcium sulfoaluminate cement (CAC), and (3) additives.

7.2. EXPERIMENTAL PROGRAM

7.2.1 Materials and sample preparation

A commercial metakaolin (MetaMax – Basf) was used as a main amorphous aluminosilicate precursor. Other materials, such as fly ash (FA), granulated blast furnace-slag (GBFS), silica fume (SF) and calcium aluminosilicate cement (CAC) were used in substitution or addition to metakaolin in different proportions. The use of these materials was adjusted to provide the achievement of specific mechanical properties and/or formation of reacted products. The physical properties and chemical composition of these aluminosilicate materials are shown in the Table 5.The materials were used as received without any thermal and mechanical treatment; thus, the difference in particle size distribution and specific surface area can affect their reaction degree. The alkali activators were prepared by the dissolution of sodium hydroxide pellets (NaOH ~99%) dissolved in water and a sodium silicate solution with 29.4 wt% SiO_2, 14.7 wt%

Na_2O, and 52.7 wt% H_2O, supplied by PQ Australia. The composition of the alkali activators was adjusted by blending the NaOH and sodium silicate solution in proportions to reach the desired molar ratios. Complementary, silicon oil (from Sigma- Aldrich, Merck) or a dispersive/hydrophobic polymer (from VINNAPAS) were used as additives for the mitigation of efflorescence formation in some specific geopolymeric systems.

Tabela 5 - Chemical composition and particle size of metakaolin

		Metakaolin (MK)	Fly ash (FA)	Silica fume (SF)	Granulated blast furnace slag (GBFS)	Calcium aluminate cement (CAC)
Particle size (µm)	Dv(10)	0.82	4.55	11.01	2.54	8.82
	Dv(50)	3.52	19.11	46.02	15.65	44.63
	Dv(90)	10.04	43.84	122.26	35.02	131.81
	Median particle size	4.56	22.10	58.21	17.53	59.04
Composition (%)	Óxide					
	SiO_2	54.82	67.6	97.02	36.46	0.94
	Al_2O_3	42.47	21.7	0.67	12.01	64.78
	TiO_2	1.23	1.78	-	0.98	0.12
	Fe_2O_3	0.48	3.68	0.1	1.72	0.22
	Na_2O	0.35	-	0.2	0.15	0.3
	K_2O	0.17	2.45	0.65	0.34	0.08
	CaO	0.17	1.53	0.34	41.84	31.3
	SO_3	0.11	0.36	0.13	1.76	0.14
	P_2O_5	0.09	0.16	-	0.01	-
	MgO	-	-	-	4.2	0.29
	L.O.I (loss of ignition at 950°C)	0.11	0.22	0.15	0.23	0.32

The synthesis of the geopolymers were adjusted using two alkalis contents, represented by the overall content of Na_2O of 15 and 20 wt%. The presence of silicate soluble in the activator (expressed by the modulus MS, which is the SiO_2/Na_2O molar ratio in the activator solution) was 1.0, 1.5, and 2.0. The content of water was adjusted by the w/b ratio of 0.55, where *w* corresponds to the free water and the water present in the sodium silicate solution; and *b* makes reference to the binder, which is the MK and the anhydrous phase of the alkali activator. These

synthesis parameter are chosen based on a previous studies (LONGHI et al., 2019c, 2020). The pastes were produced mechanically using a high shear mix during 5 min. The curing process was executed at room temperature (~25°C), inside a sealed box and relative humidity (RH) ≥ 90%.

The optimization of synthesis parameters was assessed by the production of six geopolymeric systems with different content of soluble silicate in the alkali activator to provide the formation of a Si-rich framework structure. The FA was used as secondary aluminosilicate precursors (source of Al and Si), which were included as substitution of MK in 25 wt% in the geopolymeric system activated at 15% of Na_2O with two different MS ratio in the alkali activator (1.0 and 1.5). The main goal for the FA presence is the reduction of required Na_2O content and improve the pore refinement due to the particle morphology. The GBFS is used as calcium source to promote the formation of C-A-S-H-type phases, which coexist with the N-A-S-H phase derived from geopolymerization (YIP; LUKEY; VAN DEVENTER, 2005). The GBFS was also included as substitution of MK at 5 and 10 wt. As is widely reported in the open literature, the high amorphous FA (CRIADO et al., 2008; PALOMO; ALONSO; FERNANDEZ-JIMÉNEZ, 2004), and GBFS (BERNAL et al., 2013; BURCIAGA-DÍAZ et al., 2010), require lower alkalinity for their dissolution, when compared to MK, the geopolymeric system activated at 15% of Na_2O, was used as reference condition. On the other hand, the SF was used as an extra source of high-reactive silicate species in order to increase the amount of Si-rich gel. Alternative sources of soluble silica derived from industrial by-products have been shown to be effective with similar or even higher performance when compared to traditional silicate solutions (BERNAL et al., 2020; BOUZÓN et al., 2014; DAHLAN et al., 2009; MEJÍA; MEJÍA DE GUTIÉRREZ; PUERTAS, 2013; PUERTAS; TORRES-CARRASCO, 2014). The SF was added at 5, 10 and 15 wt% respect to the aliminosilicate precursor. The CAC is used as a calcium/aluminium source in order to provide extra Al/Ca during the geopolimerization to increase the amount of Al(IV) and reduce the content of free Na^+ (NAJAFI; ALLAHVERDI; PROVIS, 2012). The CAC was also added at 5, 10 and 15 wt% respect to the aliminosilicate precursor. The use of a dispersive/hydrophobic additive and silicone oil were made to allow a better particle dispersion, which improves the workability of the pastes in fresh state and subsequently the production of denser and more compact geopolymer is obtained as a consequence of lower w/b ratio. Silicone oil was used as addition in contents between 0.5 and 1.5% of the binder. On the same way, a dispersive/hydrophobic polymer additive (VINNAPAS series) was used in contents of 0.5 and 1.0%. The effect of SF, CAC and the additives in the

effloresecnece formation was assessed in the geopolymeric system activated at 15% of Na_2O with a MS ratio of 1.o in the alkali activator. The systems ID, mix formulation and amount of material for 100 g of the overall geopolymer systems assessed are listed in Table 6, where the nomenclature is constituted by MK-(alkalis concentration; 15 or 20% of M_2O)-(MS)-(content of secondary precursor or additive).

Tabela 6 - formulation of geopolymer samples

Synthesis parameter to be considered	Geopolymer	Design parameters			Materials (g)				
		MS content	Na_2O content (wt.%)	MK	FA, GBFS, SF or CAC	NaOH	SS	H_2O	Oil-Aditive
Alkali content (%Na_2O)	MK-20Na-1.0ms	1.0	20	100		13.3	65.8	37.5	
	MK-15Na-1.0ms	1.0	15	100		10.0	49.4	44.8	
Content of soluble silicate (MS ratio)	MK-20Na-1.5ms	1.5	20	100		7.1	98.7	24.9	
	MK-20Na-2.0ms	2.0	20	100		0.0	131.7	11.8	
	MK-15Na-1.5ms	1.5	15	100		5.3	74.1	31.1	
	MK-15Na-2.0ms	2.0	15	100		0.0	98.7	21.3	
Use of FA and different MS ratio	MK/25FA-15Na-1.0ms	1.0	15	75	25	10.0	49.4	44.8	
	MK/25FA-15Na-1.5ms	1.5	15	75	25	5.3	74.1	31.1	
Use of GBFS	MK/5GBFS-15Na-1.0ms	1.0	15	95	5	10.0	49.4	44.8	
	MK/10GBFS-15Na-1.0ms	1.0	15	90	10	10.0	49.4	44.8	
Use of SF	MK/5SF-20Na-1.0ms	1.0	20	100	5	13.3	65.8	37.5	
	MK/10SF-20Na-1.0ms	1.0	20	100	10	13.3	65.8	37.5	
	MK/15SF-20Na-1.0ms	1.0	20	100	15	13.3	65.8	37.5	
Use of CCA	MK/5CAC-20Na-1.0ms	1.0	20	100	5	13.3	65.8	37.5	
	MK/10CAC-20Na-1.0ms	1.0	20	100	10	13.3	65.8	37.5	
	MK/15CAC-20Na-1.0ms	1.0	20	100	15	13.3	65.8	37.5	
Use of additives (Dispersant or Si-oil)	MK-20Na-1.0ms - 0.5Ad	1.0	20	100		13.3	65.8	37.5	0.67
	MK-20Na-1.0ms - 1.0Ad	1.0	20	100		13.3	65.8	37.5	1.33
	MK-20Na-1.0ms - 0.5Si-Oil	1.0	20	100		13.3	65.8	37.5	0.67
	MK-20Na-1.0ms - 0.5Si-Oil	1.0	20	100		13.3	65.8	37.5	1.33
	MK-20Na-1.0ms - 0.5Si-Oil	1.0	20	100		13.3	65.8	37.5	2.00

7.2.2 Tests conducted

C**ompressive strength** of hardened cubic samples (of 20 mm of height) was determined at 7, 28 and 90 days using an MTS universal mechanical testing machine with a loading speed of 0.5 mm/min.

The **susceptibility of efflorescence formation** was assessed in cylindrical samples with 28 mm of diameter and 55 mm of weight after 28 days of curing, which were exposed under accelerated test, where each sample was partially immersed in distilled water. This method was successfully used in previous studies (LONGHI et al., 2019b), through the evolution of efflorescence growing in the top surface of the samples and continuous visual inspection. The images were obtained at room temperature of 20±5 °C and RH of 65 ± 15% during 28 days. To provide cycles of wetting and drying and a faster process of efflorescence formation, the samples were individually immersed 5 mm, where the water was replaced every day due to the high absorption and evaporation. The set of experiments (mainly the efflorescence formation) were programmed to assessed all geopolymers at the same time and under the same environmental conditions to avoid any difference of ambient exposure (temperature and humidity).

The efflorescence potential was also evaluated through the measurement of the leachable alkali. Cylindrical samples of 20×35 mm (or 10 ml) was individual and completely immersed in 500 ml of distilled water. To quantify the alkali concentration of leached material, 10 ml of solution were removed after 28 days and analysed by atomic absorption spectroscopy (AA-7000) for the element Na using the emission method.

Water absorption was used to quantify the capillarity of the geopolymers, where the dried cylindrical samples with 28 mm of diameter and 55 mm of weight were exposed to 5 mm of contact with water. This test was performed in a sealed plastic container to prevent water loss and evaporation. The amount of absorbed water was measured every 10 minutes in the first hour and then every hour up to achieve constant mass. The results reported are the ratio between the quantity of water absorbed (in g) and the cross-section area of the sample (in cm^2).

Solid-state single pulse ^{27}Al and ^{29}Si magic angle spinning **(MAS) NMR** spectroscopy were determined using a Bruker Avance III HD 500 spectrometer at 11.7 T (B_0) with a 4.0 mm dual resonance CP/MAS probe. ^{27}Al MAS NMR spectra were measured with a 1.7 μs non-selective ($\pi/2$) excitation pulse, 5 s relaxation delay, a total of 512 transients and spinning at 12.5 kHz

and yielding a Larmor frequency of 130.32 MHz. The ^{29}Si MAS NMR spectra were obtained using a 5.5 μs non-selective (π/2) excitation pulse, a measured 60 s relaxation delay, a total of 256 transients, spinning at 12.5 kHz and yielding a Larmor frequency of 99.35 MHz. The spectrometer field was aligned to the ^{13}C resonance of adamantane at 38.48 ppm, and ^{27}Al and ^{29}Si spectra were referenced to 1.0 mol/L $Al(NO_3)_{3(aq)}$ and neat tetramethylsilane (TMS), respectively, at 0 ppm. Gaussian peak profiles were used to deconvolute the NMR spectra, using the minimum number of peaks possible (MASSIOT et al., 2002). Peak intensities were required to be consistent with the structural constraints described by the thermodynamics of a statistical distribution of Si and Al sites within a Q^4 aluminosilicate network for (N,K)-A-S-H gel products (PROVIS et al., 2005b).

A superficial fragment of some specimens was carefully selected and collected to be assessed through scanning electron microscopy (SEM), using a FEI Quanta 650 FEG, in the Brazilian Nanotechnology National Laboratory LNNano (Laboratório Nacional de Nanotecnologia). The sample was a dried at 60 °C during 2 hours, placed in carbon tab and coated with gold during 60 s with a current of 40 A. The microscope was equipped with an Everhart Thomley secondary electron detector (SED) and an In-column detector (ICD) for secondary electrons in BD mode. Working with a high resolution Schottky field emission (FEG), accelerating voltage between 200 V and 30 kV in a probe current ≤ 200 nA.

7.3. EFFLORESCENCE FORMATION

7.3.1 Visual efflorescence

Figure 64 shows the efflorescence formation in the geopolymers systems produced with different synthesis parameters, such as the effect of alkali content (Figure 64 A); higher silicate soluble in the activator at lower (15% of Na_2O in Figure 64 B) and higher (20% of Na_2O in Figure 64 C) alkalinity condition. From the images showed in Figure 64A, the system with lower amount of sodium (MK-15Na-1.0ms) induces the growing of more efflorescence (white foamed products) predominantly on the top of the sample and superficial deterioration is not expressive. Based on previous results sodium carbonate (Na_2CO_3), sodium carbonate monohydrate ($Na_2CO_3 \cdot H_2O$, thermonatrite) and sodium carbonate decahydrate ($Na_2CO_3 \cdot 10H_2O$, natron) are the main carbonates generated (LONGHI et al., 2020). This two systems showed the formation of more gel at the higher amount of activator (LONGHI et al., 2019c), which provides a denser and more stable material and the subsequent reduction of

efflorescence formation. The increase of MS ratio in the geopolymers MK-20Na-1.5ms and MK-15Na-1.5ms contributes to the reduction of efflorescence formation, where no visible efflorescence is observed (Figure 64 B and C). However, the excessive addition of sodium silicate induces a severe efflorescence deposition, as observed in the systems MK-20Na-2.0ms and MK-15Na-2.0ms (Figure 64 B and C). During the reaction process, it was observed the need for more time for the hardening of the sample, indicating a reduction in the rate of reactions. According to Provis *et al.* (PROVIS et al., 2005a), the reaction extent to geopolymers activated with excess of sodium silicate solution is much lower than when activated with NaOH. These systems also present superficial deterioration. The crystal formation in the mid-sample height indicates the equilibrium between capillarity pressure and evaporation, inducing the movement of alkalis and crystallization.

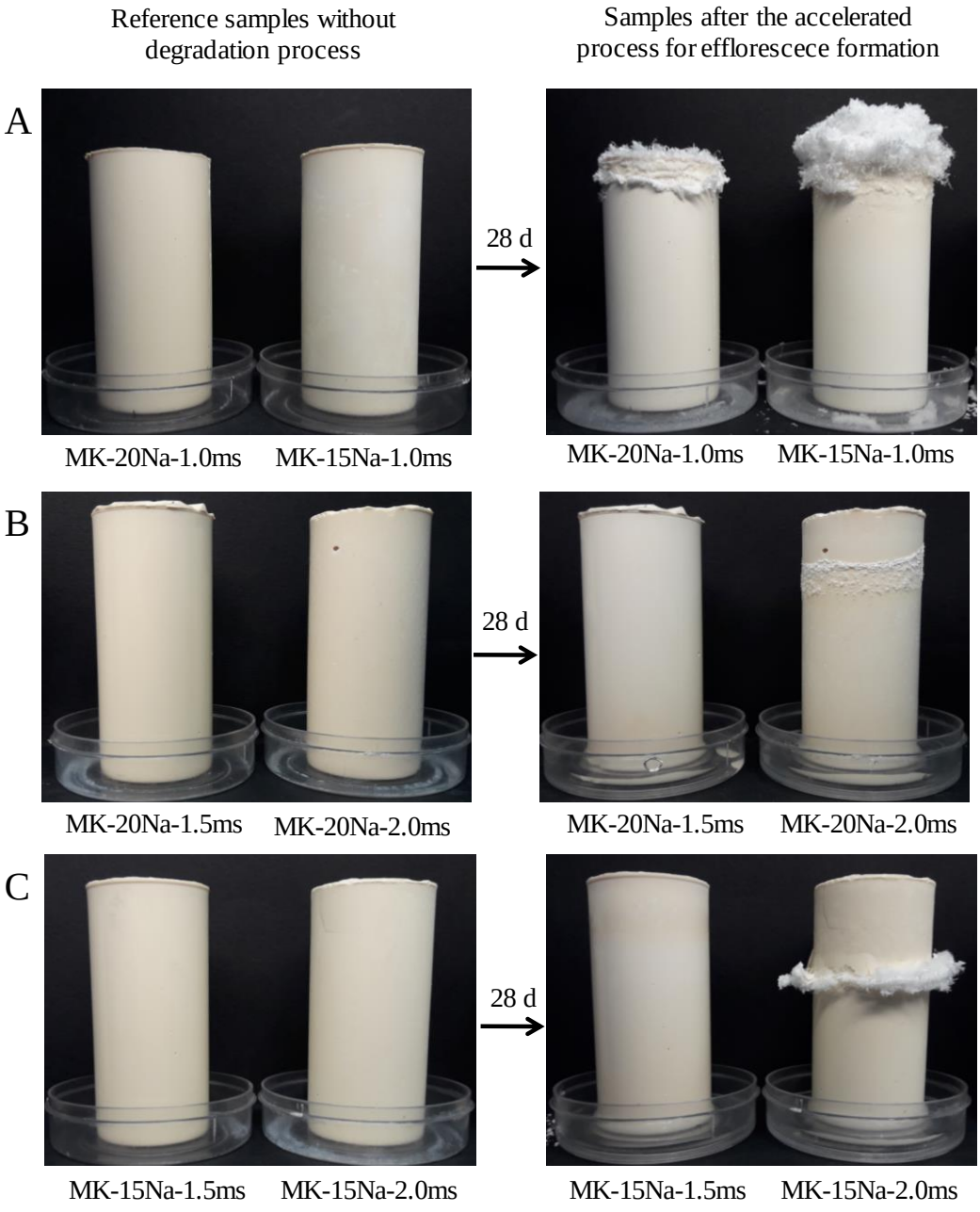

Figura 64 - Geopolymers after 28 days of the accelerated test for efflorescence formation: A. REF1 and REF 2, B. R1- 1.5 and R1- 1.5, C. R2- 1.5 and R2- 1.5

In Figure 65 is shown the efflorescence formation in geopolymers with the substitution of MK by different amounts of FA or GBFS, as well as the systems with the addition of SF or CAC. The substitution of 25% of MK for FA Figure 65A) does not exhibited a reduction or mitigation of efflorescence formation, when compared to the corresponding MK-based geopolymer (MK-15Na-1.0ms system showed in Figure 65A) . The increase of silica provided by the precursor and the different particle morphology does not contribute to the efflorescence reduction. The lower reactivity of FA precursor does not allow the effective increase in silica in the framework structure. Even in MK/FA-based geopolymers, the addition of more amount of sodium silicate

through the adjustment of higher MS ratio is not effective. Neither, the substitution of MK for small amounts of GBFS (5 and 10 wt%) and the reduction of sodium in the activator does not reduce the content of soluble alkalis and provides higher carbonates deposition (Figure 65B). In a previous study, Zhang *et al.* (ZHANG et al., 2014b) observed the reduction of efflorescence formation in FA-based geopolymers by the addition of 35% of GBFS, behaviour attributed to pore refinement and matrix densification. On the other way, Yao *et al.* (YAO; YANG; ZHANG, 2016), observed the increasing of efflorescence formation to percentages higher than 50% and attributed to the weak binding capability of the alkalis in the C-A-S-H type gel than the N-A-S-H type gel. The addition of GBFS in fly ash systems can improve the precursors reactivity due the high crystallinity of fly ash, however, in this study, due to the high amount of alkali required to activate MK based-geopolymers the behaviour of the GBFS as part of the precursor is not effective. The simultaneous formation of N-A-S-H and C-A-S-H gels is not beneficial to the conditions evaluated.

Considering the effectiveness of higher contents of soluble silicate for the efflorescence mitigation, the addition of small amounts of SF as a source of active silica species was also evaluated (Figure 65C). Important to note that the SF used here exhibited a high densification degree, which reduce its reactivity (RODRÍGUEZ et al., 2012), and the subsequent dissolution in alkaline solutions. Even though the sodium silicate solution exhibits better performance as a source of soluble silicates, the addition of SF in the geopolymers can be considered effective to reduce the efflorescence formation. The carbonate crystallization on the surface (efflorescence formation) is clearly reduced when compared to the corresponding systems produced with sodium silicate solution (MK-20Na-1.0ms). The addition of calcium aluminate cement (5, 10 and 15%) provides an extra source of calcium and alumina (Figure 65D), which is also effective to reduce significatively the efflorescence formation and carbonates type products on the surface were not observed. The extra source of reactive aluminium during the geopolymerization may allow the presence of more Na^+ to compensate the negative balance of Al(IV), as reported previously (NAJAFI; ALLAHVERDI; PROVIS, 2012), however, this behaviour needs as better understanding and further detailed studies should be developed.

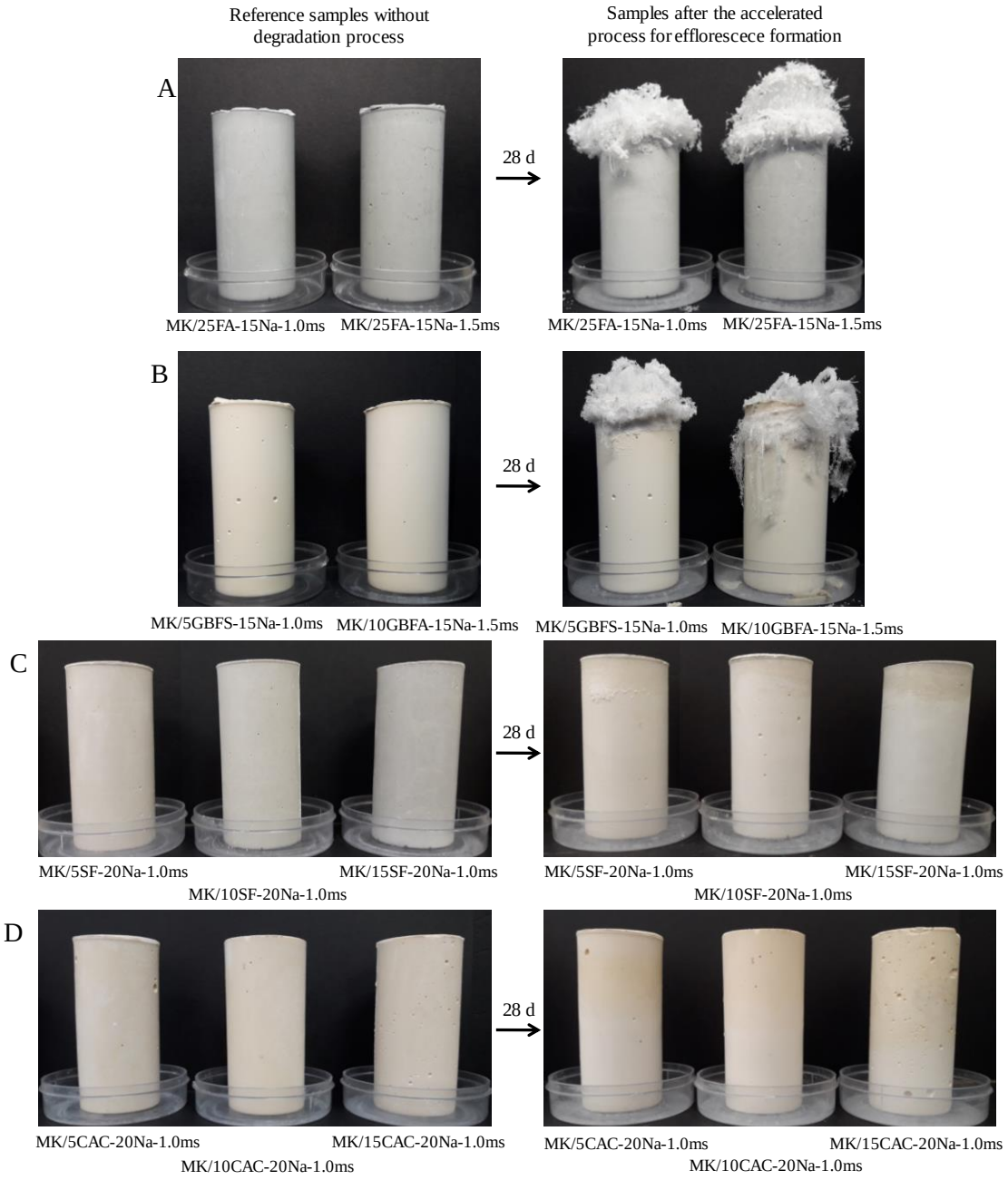

Figura 65 - efflorescence formation for geopolymers after 28 days of exposure: A. R2-25FA and R2-25FA-MS 1.5, B. R2-5GBFS and R2-10GBFS, C. R1-5SF, R1-10SF and R1-15SF, D. R1-5CAC, R1-10CAC and R1-15CAC

In Figure 66 is shown the geopolymers with the use of dispersive/hydrophobic additive exposed to efflorescence formation conditions. The addition of small amounts of additive (0.5 and 1.0%) contributes to the reduction of efflorescence formation, which is lesser when compared to the corresponding system without additive (compare the behaviour of the MK-20Na-1.0ms between the Figure 64A and Figure 66A). The effect can be associated to the improvement in the mixture provided by a better dispersion of particles, the reduction of water absorption and delay of water movement promoted by the hydrophobic properties of the additive. The use of silicone oil (0.5, 1.0 and 1.5%) also reduces efflorescence formation. This reduction can be

associated with filling the pores with a material with a different density of water, which makes it difficult to move it. However, was observed that the small parts breaking at the top of the sample, which can initially attributed to a superficial carbonation process and the subsequent stress related to crystallization within the pore network.

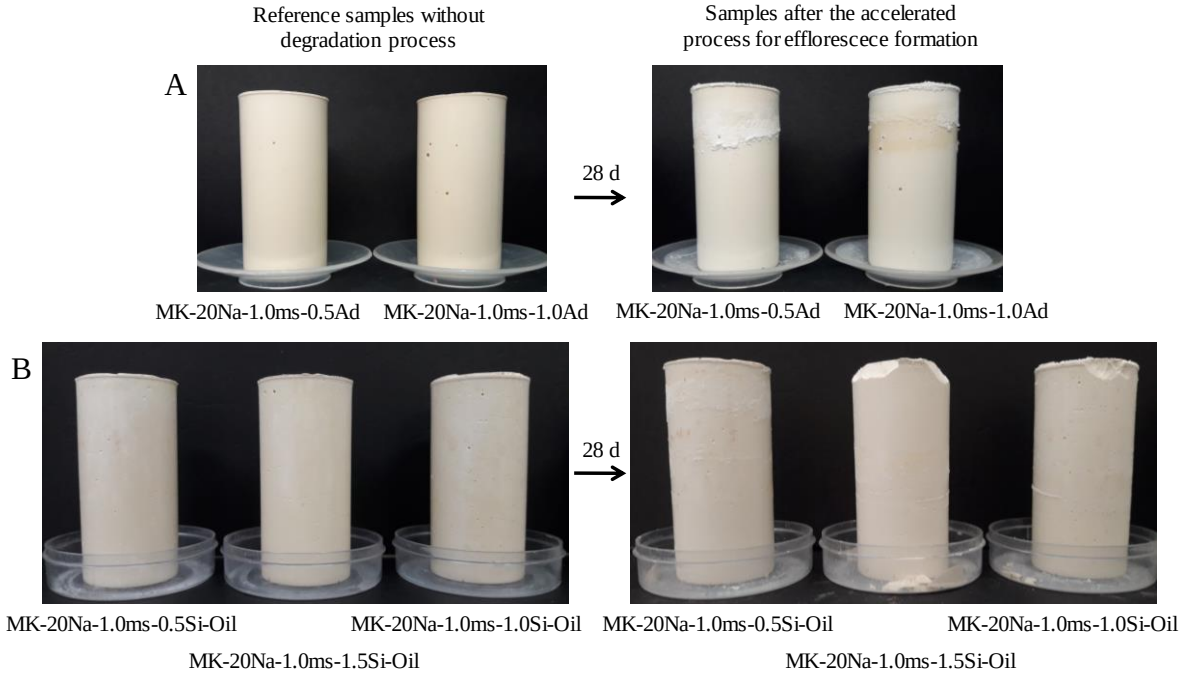

Figura 66 - efflorescence formation for geopolymers after 28 days of exposure: A. R1-0.5AD and R1-1.0AD, B. R1-0.5Si Oil, R1-1.0Si Oil and R1-1.5Si Oil

7.3.2 Compressive strength

The compressive strength of all geopolymers is shown in Figure 67, Figure 68 and Figure 69. The addition of sodium silicate (MS=1.5) promotes an expressive increase in compressive strength related to reference system (MS=1.0), approximately 40% after 90 days of curing. The increment of compressive strength is even more expressive for lower amount of sodium (Na_2O=15%), with an increase of 117% after 90 days. However, the excessive addition of sodium silicate (MS=2.0) reduces the rate of reaction and compressive strength values, especially at early ages. This behaviour can be attributed to lower pH at higher contents of sodium silicate when compared to NaOH-based systems. According to Zhang *et al.* (ZHANG et al., 2013) the use of sodium silicate in the activator reduce the alkali cation available, which makes the reaction slower. This behaviour is consistent to the efflorescence formation observed and indicates that due to the addition of high amount of soluble silicate the time required for the complete geopolymerization process is higher and the more amount of sodium remains free to be released.

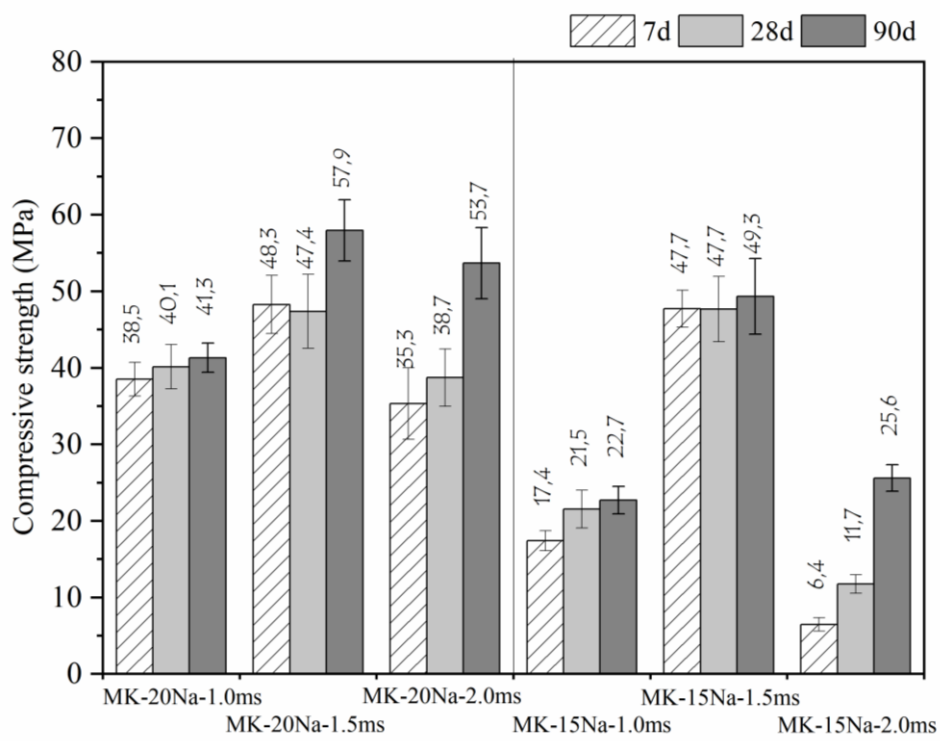

Figura 67 - compressive strength of geopolymers with different design parameter after 7, 28 and 90 days of curing.

In Figure 68 is shown the compressive strength results for the binary geopolymers MK/FA, MKK/GBFS, MK/SF, and MK/CCA. After 90 days the use of 25% of fly ash as substitution provides an increase of 24%, when compared to corresponding MK-based geopolymer with MS=1.0. The use of FA associated with the increase o sodium silicate does not show an expressive increase in the compressive strength (when compared to the MK-15Na-1.5ms system). In the case of GBFS the compressive strength increased up to 28% and 38% to the substitution of 5 and 10%, respectively. Even with a better mechanical behaviour, the use of FA and GBFS as secondary precursor did not reduce the susceptibility for efflorescence formation, which elucidates that does not exist a direct relation between effloresce formation and mechanical performance.

Alternative sources of silica during geopolymerization does not have a clear effect under the compressive strength, where the addition of 10% of SF increase approximately 10% in the mechanical performance, however at higher contents (15%) a reduction of 6% in the mechanical performance is identified. This behaviour is similar to that observed in the addition of sodium silicate. As observed previously, the larger particle size of silica fume can reduce the effectiveness of its dissolution. The addition of 5 and 10% of CAC presents slightly higher strength when compared to the corresponding MK-based geopolymer (MK-20Na-1.0ms), and

a reduction of ~14% with higher contents of CAC (15%). Similar behaviour was identified in other studies (CAO et al., 2018; HE et al., 2020). In both cases (SF and CAC), is identified that the addition of high contents (>10%) of these secondary precursors have a negative effect on the mechanical performance.

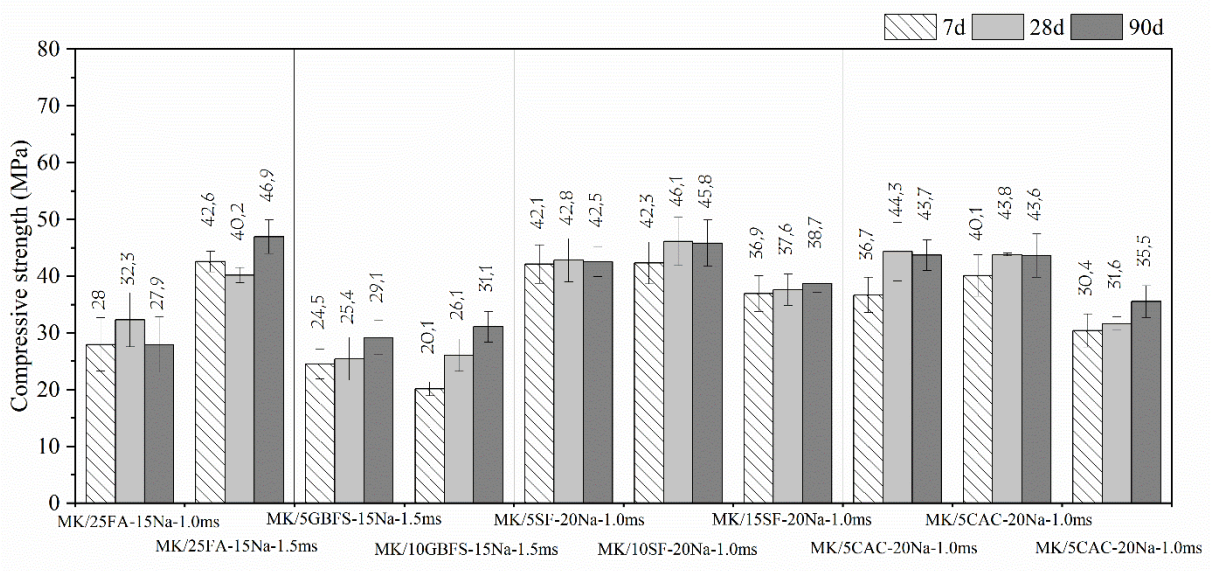

Figura 68 - compressive strength of geopolymers with the substitution of MK for small contents of fly ash and GBFS an addition of SF and CAC after 7, 28 and 90 days of curing.

By the use of additives (Figure 69), after 90 days of curing, was observed an increasing of 16% to the percentage of addition of 0.5%. Higher values of addition do not have significant effects. The addition of silicone oil, does not show expressive differences when compared to the corresponding geopolymer without additive (MK-20Na-1.0ms), however, is observed a slightly increasing by the addition of 1.5%.

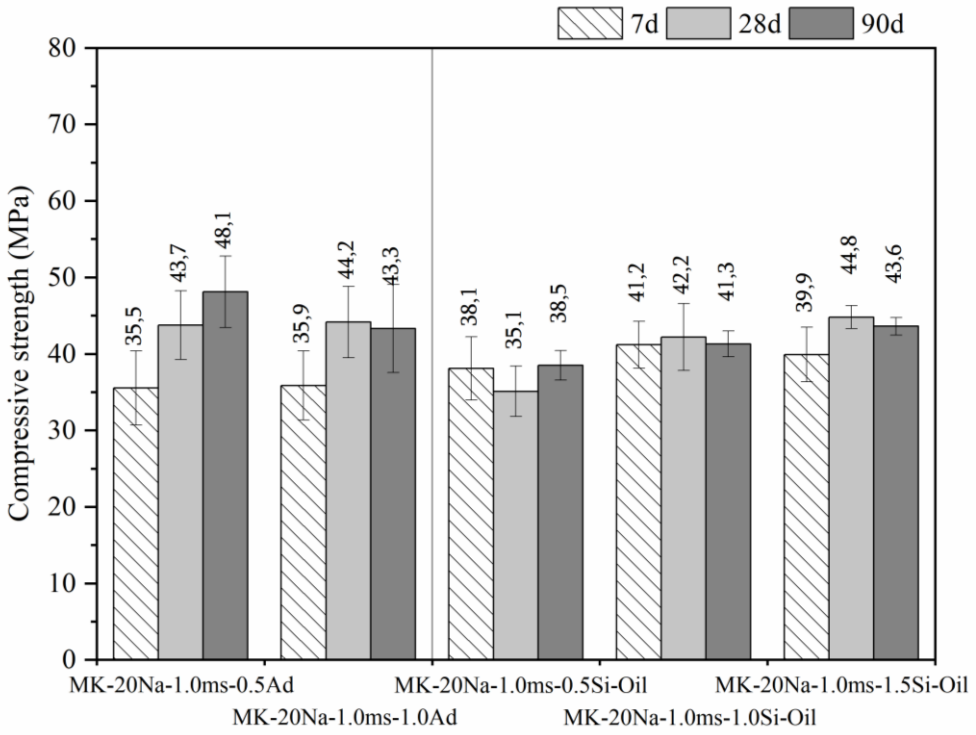

Figura 69 - compressive strength of geopolymers with additives after 7, 28 and 90 days of curing.

7.3.3 Capillarity water absorption

The water absorption can give an indication about the open porosity (or capillarity); thus, the alkali movement through the pore structure. The open porosity was calculated as a ratio between the water absorbed and the sample volume. The results are shown in Figure 70. The MK-based geopolymers produced with high alkalis content (MK-20Na-1.0ms) presents ~22% less water absorption than the system MK-15Na-1.0ms (15% of Na_2O). As observed previously (LONGHI et al., 2019c), the increase in the alkali content provides a greater amount of gel, which plays an important role in the physical and mechanical properties. The optimization of synthesis parameters by different content of sodium (expressed here as %Na_2O) and sodium silicate (assessed here by the MS ratio), shown a refinement in pore structure. In these geopolymers (Figure 70A), the rate of water absorption and the open porosity is reduced when higher alkalinity and higher content of soluble silicates are used in the activator solution. The use of MS=1.5 presented the lower level of water absorption regardless the alkali concentration (15 and 20% of Na_2O). Even though, systems with high content of soluble silicates (high MS in MK-15Na-2.0ms and MK-20Na-2.0ms) showed lower porosity, the development compressive strength takes longer time, the high cost due to the amount of sodium silicate and the formation of efflorescence, exclude this option as a reliable alternative.

The use of FA and GBFS (Figure 70 B) also shown a reduction of water absorption when compared to the MK-based geopolymers. Higher amounts of SS and GBFS presented the most effective results. However, even with less water absorption, these systems showed a high efflorescence formation in the surface, indicating that additionally to the water absorption, is important to analyse the alkali leaching from the reacted products formed. The addition of SF and CAC (Figure 70 C) presents a similar behaviour in the capillarity absorption when compared to the MK-based geopolymer. Even with similarities in water absorption in compressive strength, the use of SF and CAC provides and expressive improvement related to the reduction of efflorescence formation.

The use of additive reduced the permeability, where the water absorption values are approximately 25% lower than the MK-based geopolymer (MK-20Na-1.0ms). By the use of silicone oil, the values are slightly lower than MK-based geopolymer (MK-20Na-1.0ms). In this case, it is possible that the oil, which has a higher density from water, remains in the pores and act as a barrier for the water movement. Is also possible to see an expressive reduction in the rate of absorption which is reflected in the reduction of efflorescence formation.

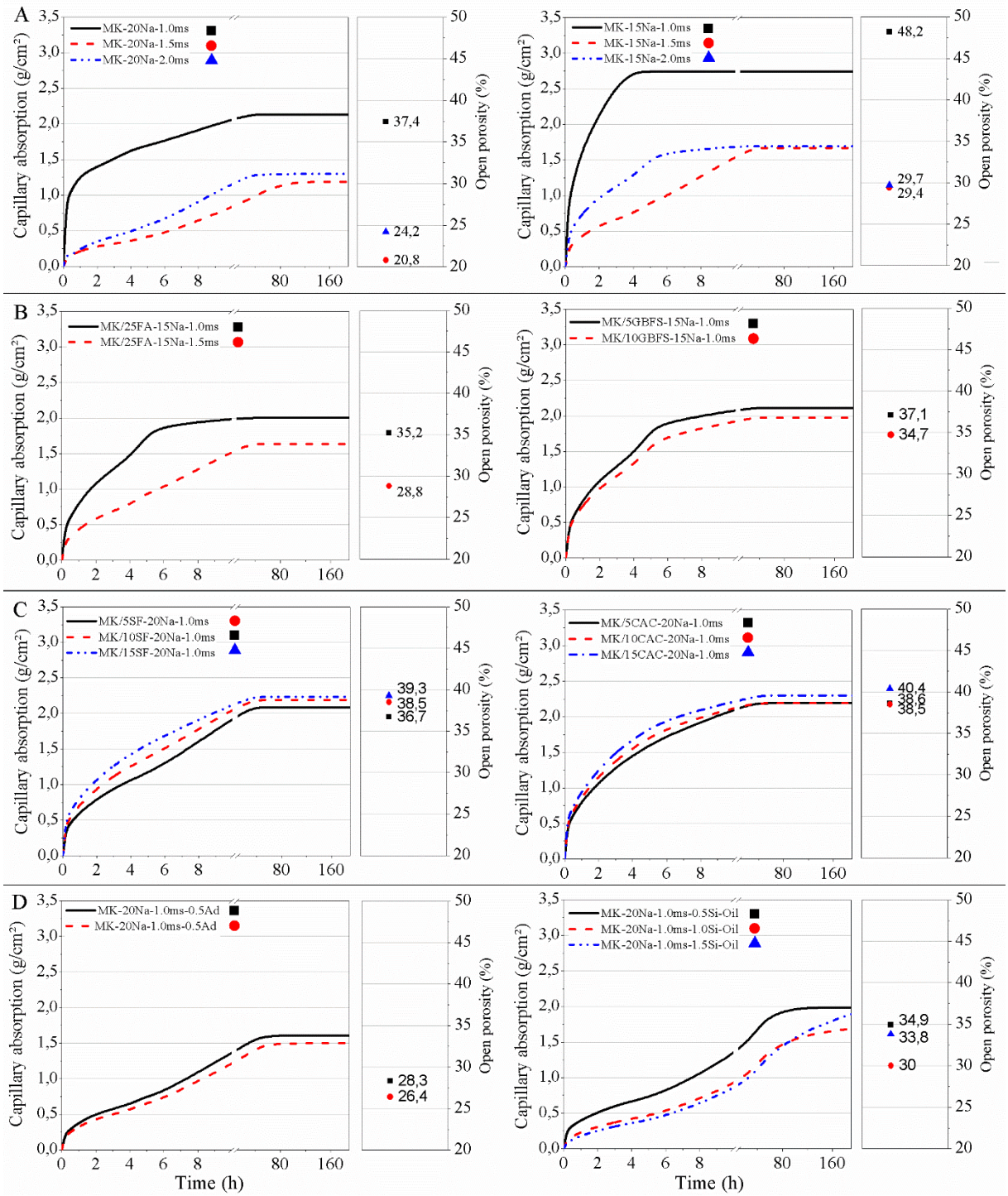

Figura 70 - capillary absorption and open porosity for geopolymers samples: A. Different design parameters, B. Substitution of MK for fly ash and GBFS, C. Addition of SF and CAC, D. Use of additives.

7.3.4 Atomic Absorption Spectroscopy

In addition to the capillary absorption that indicates the movement of fluids and alkalis, it is important to identify and quantify the amount of leachable alkali. The quantification of free alkalis by atomic absorption spectroscopy is shown in the Figure 71. The MK-based systems (MK-20Na-1.0ms and MK-15Na-1.0ms) showed similar values of alkalis leachable (~206.5 ppm) although the synthesis parameters were adjusted at different Na_2O concentrations. IN this sense, the MK-20Na-1.0ms showed a higher imprisonment of Na^+ in the framework structure. Regardless the alkali concentration FA content, the adjustment of sodium silicate to MS ratio of 1.5 reduces the alkalis leachability up to 22%. However, the excess of soluble silicate in the alkali activator, as is shown in the systems with a to MS ratio of 2.0 (MK-20Na-2.0ms and MK-15Na-2.0ms), showed a higher susceptibility of leachable alkalis, which is coherent with the efflorescence formation, although its water absorption elucidates a lower permeability (Figure 70A). The link between the pore refinement and alkalis imprisonment provides a geopolymers more resistant to the efflorescence formation.

The increasing of leachable alkali is also visible by the use of FA and GBFS, consistent with visual observation of efflorescence (Figure 65). The higher content of soluble silicate (through higher MS ratio in the alkali activator) contributes to reduce the leaching, which is also coherent with water absorption values. The addition of silica fume (MK/SF) contributes to reduce the alkali leaching up to ~9% and reduce the visual efflorescence formation (Figure 65C), when compared to the MK-based geopolymer. This improvement is due to reduction in the absorption rate and the reduction of alkali leaching. On the other way, the addition of CAC increased the amount of leachable alkalis. Even with higher leachability and slightly higher water absorption, the CAC/MK-based geopolymers did not show efflorescence formation (Figure 65D).

The use of additives and silicone oil reduce slightly (<4%) the alkali leaching when compared to MK-based geopolymers. This reduction associated to the lower rate of water absorption contributes to mitigate the efflorescence formation. According to the results obtained, the mitigation of efflorescence formation is more effective when the alkali leachability is reduced and even more effective if the permeability and tortuosity of the pore network are improved.

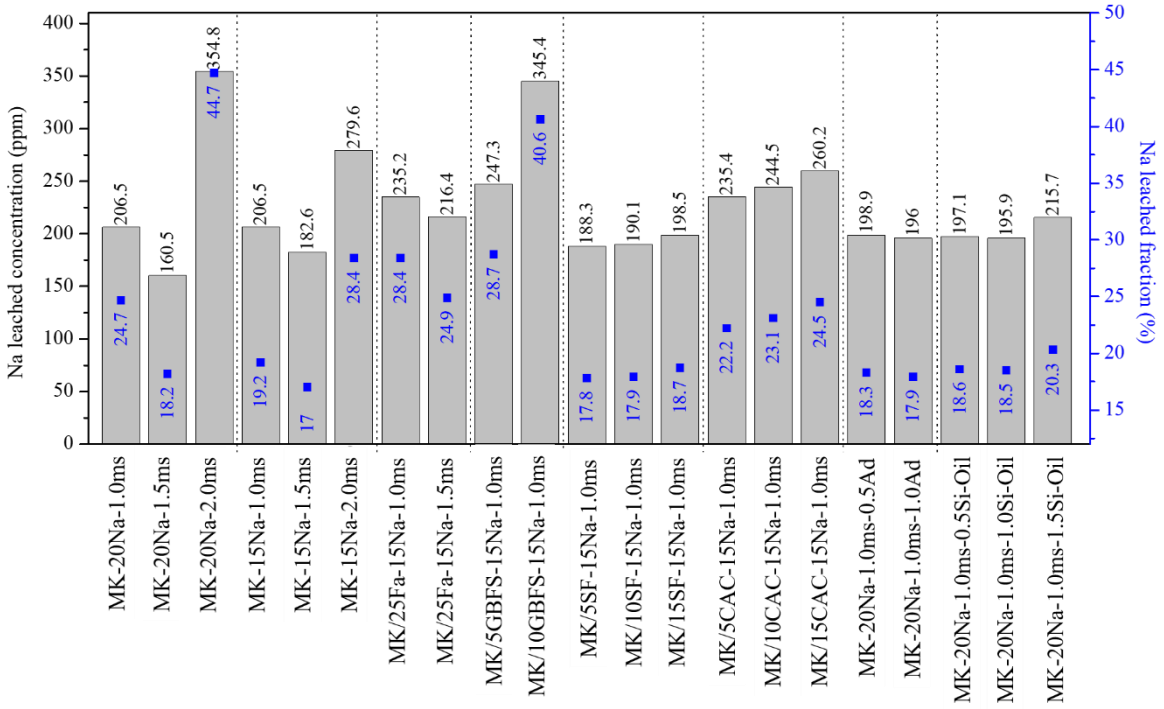

Figura 71 - Na leached concentration and leached fraction measured by AAS

7.3.5 Solid-state magic angle spinning Nuclear Magnetic Resonance (MAS NMR)

The ^{27}Al MAS NMR spectra of those geopolymers systems that showed a significant reduction in efflorescence formation are presented in the Figure 72. For these geopolymers, the spectrum shows a higher and well-defined peak and sensible variation in two regions. Generally, the geopolymer spectra exhibit three main regions, approximately at δ_{obs}= 60, 32 and 6 ppm, attributed respectively to aluminium in tetrahedral (IV), pentahedral (V) and octahedral (VI) coordination (DUXSON et al., 2005b; LONGHI et al., 2019c; WALKLEY; PROVIS, 2019). The mean broad peak formed during geopolymerisation process of metakaolin-based materials is attributed to Al(IV) species.

Associated to the MK-based geopolymers analyzed, is possible to observe in MK-20Na-1.0ms, more amount of Al(IV) species and for MK-15Na-1.0ms some traces of Al(V) and Al(VI). This behavior can indicate a more effective metakaolin consumption during geopolymerization process. The increasing of sodium silicate in reference systems, presents some small changes. The geopolymer MK-20Na-1.5ms, shifted to lower ppm concentration, which can indicate a partial geopolymerisation or uncompleted MK dissolution of Al(V) and Al(IV) species. To geopolymer MK-15Na-1.5ms (higher content of silicate soluble), similar behavior than MK-15Na-1.0ms is observed, with an increase in intensity of Al(IV) species. Related to the addition

of small amounts of silica fume (MK/5SF-20Na-1.0ms) and CAC (MK/5CAC-20Na-1.0ms and MK/10CAC-20Na-1.0ms) the behavior is similar than the MK-based geopolymers. However, the addition of 10% of CAC lead the formation of a sensible peak at 10 ppm, which is different of the peak close to 6 ppm associated to Al(VI) formed in metakaolin-based geopolymer. This new formation is also attributed to Al(VI), however, in different sites of Al as CAH_{10}, C_2AH_8, C_3AH_6 (PENA et al., 2008; WALKLEY; PROVIS, 2019).

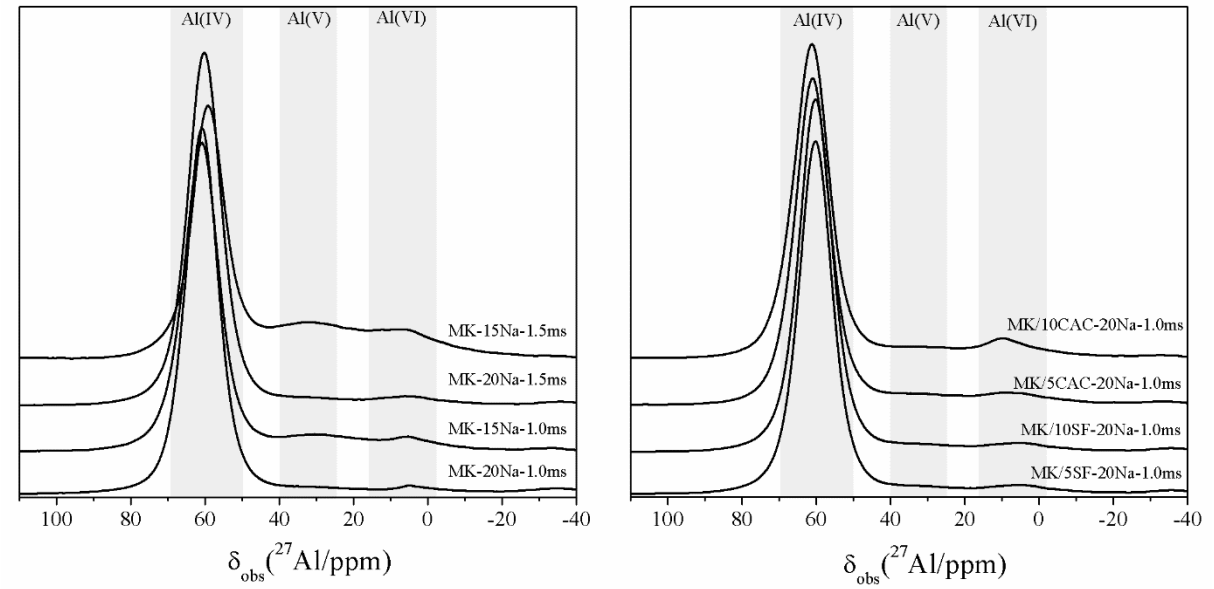

Figura 72 - ^{27}Al MAS NMR of geopolymer systems

The ^{23}Na MAS NMR spectra the geopolymers assessed are shown in 23Na MAS **NMR**. All geopolymers exhibit a simple broad resonance located between -2 and -5 ppm. According to other researches, this location can be attributed to a charge balancing of sodium associated to the aluminium-centred tetrahedra balancing (DUXSON et al., 2005b; WALKLEY; PROVIS, 2019; WALKLEY et al., 2016b). The spectra exhibits similar behavior with very slightly differences based on synthesis parameters and precursors used.

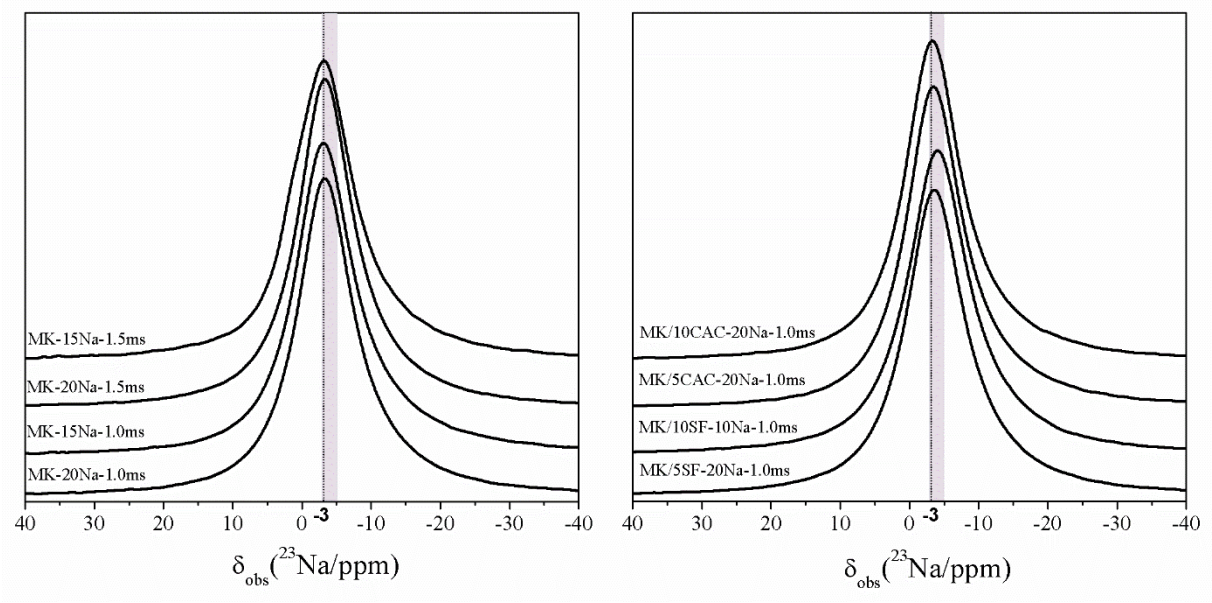

Figura 73 - ^{23}Na MAS NMR of geopolymer systems

The ^{29}Si MAS NMR spectra collected show different Si sites formation associated to the different raw-materials used and different synthesis parameters (Figure 74). The main broad peak is composed of Q^4(mAl) species, which were deconvoluted using Gaussian distributions. According to other studies (BRUS et al., 2016; PALOMO et al., 2008; PALOMO; ALONSO; FERNANDEZ-JIMÉNEZ, 2004; WALKLEY; PROVIS, 2019; WALKLEY et al., 2016b), these resonances are attributed to different silicon species δ_{iso} and Al degree substitutions, including -85 (4Al), -90 (3Al), -95 (2Al), -100 (1Al), -105 (0Al). Due to the high amount of alumina in precursor and the presence of aluminium predominantly in tetrahedral form as observed in Figure 74, the main formations are associated to coordination with high amount of aluminium as Q^4(4Al) and Q^4(3Al).

Related to the improvements in the MK-based geopolymers, it is observed that the addition of higher sodium silicate content (higher MS values in the alkali activator) increases the number of sites with more Si and reduces de amount of Al. In MK-15Na-1.5ms it is observed a slight reduction in Q^4(4Al) and an increase in Q^4(3Al) species. In the systems synthetized at higher alkalinity the presence of more soluble silicates (compare the MK-20Na-1.0ms and MK-20Na-1.5ms spectra in Figure 72) this effect is more pronounced, where Q^4(4Al) and Q^4(3Al) were consistently reduced and Q^4(1Al) and Q^4(0Al) is increased. This behavior associated to compressive strength indicates that higher Si/Al ratio can improve the compressive strength, with is in agreement with other researches (DUXSON et al., 2005b; FERNÁNDEZ-JIMÉNEZ et al., 2006; LONGHI et al., 2019c). It can be also associated to the efflorescence formation, where these two systems with more amount of sodium silicate does not show any trace of

efflorescence formation. However, the excess of sodium silicate, regardless the alkalinity content (MK-15Na-2.0ms and MK-20Na-2.0ms) increase consistently the amount of $Q^4(0Al)$ (in form of silicate monomers from de activator), which reduce the effectiveness of activation and subsequently increase the amount of leachable alkalis, as observed in Figure 74.

The addition of silica fume (MK/5SF-20Na-1.0ms and MK/10SF-20Na-1.0ms) presents a similar behaviour when compared to the MK-based geopolymer (MK-20Na-1.0ms) and significant differences are not identified. The increasing in the amount of $Q^4(0Al)$ is consistent and clearly identified, due to the increase in compressive strength and reductions of efflorescence formation. The dissolution and reaction of silica fume is reduced to be compared to SS, so the effective reaction is also dependent on the design parameters and morphological properties. The addition of small amount of CAC, also increase the content of Al, and the subsequent higher intensities for $Q^4(4Al)$ sites and $Q^4(0Al)$, when compared to the MK-based geopolymers.

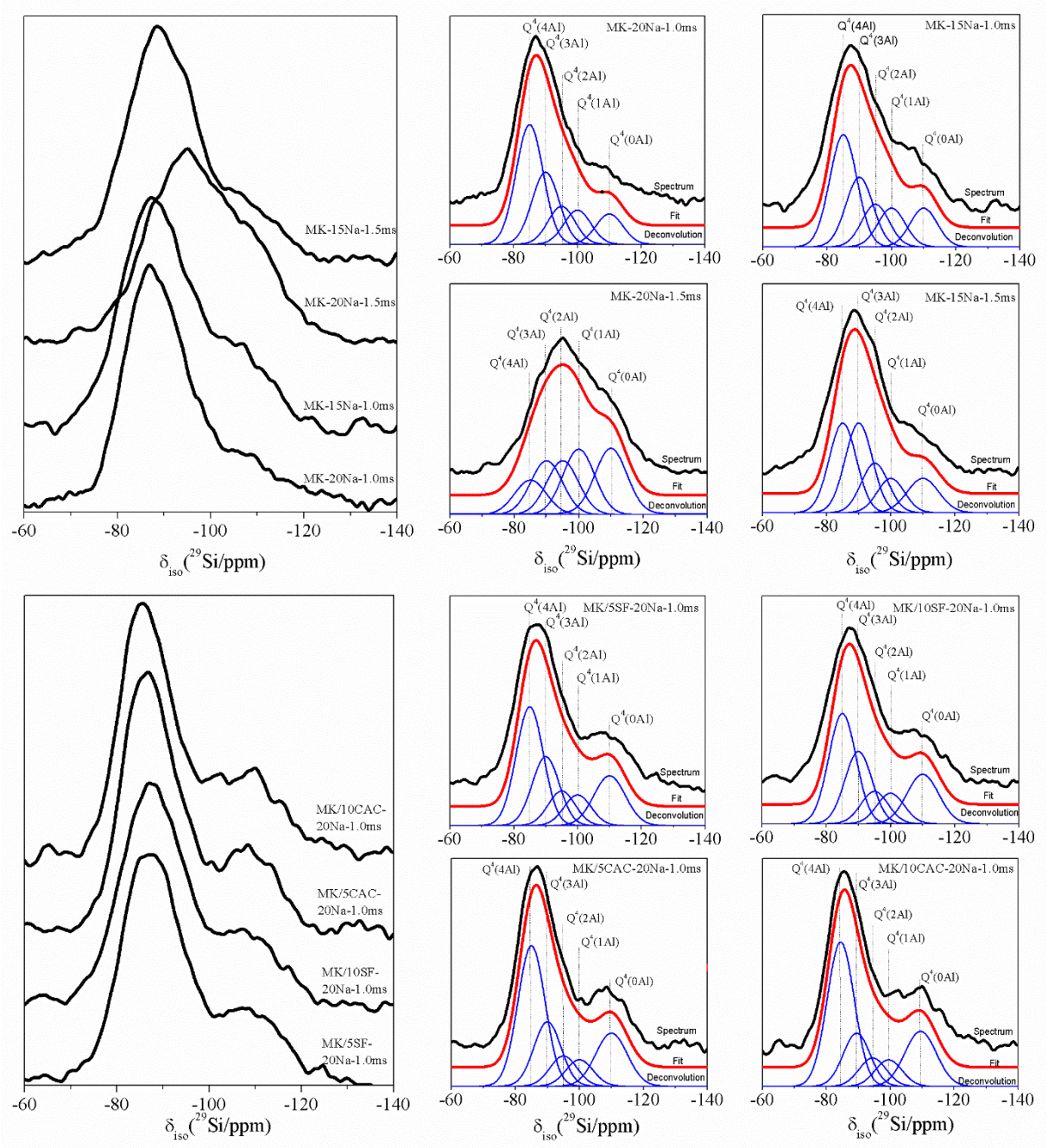

Figura 74 - ^{29}Si MAS NMR of geopolymer systems

7.3.6 Scanning electron microscopy

A set of selected geopolymers were assessed by SEM with the aim to identify the morphology differences associated to the different strategies used to reduce the efflorescence formation. The imagens obtained are shown in Figure 75. The pieces of geopolymers were collected from the internal part of sample without exposure to carbonation and a direct efflorescence formation after one year of curing. The samples were collected at this point in order to evaluate how these microstructural features can influence the reduction of efflorescence. Figure 70A shows the MK-20Na-1.5ms with a dense and compact matrix, which is the system does not show any

efflorescence formation (Figure 64B). Unreacted metakaolin particles are also identified, however, leachable alkalis show that lower amount is available. The addition of small amount of silica fume (Figure 70B), also contributes to the paste densification. It is not identified the presence of unreacted particles, increasing the amount of silica in the gel, which contributed to increase the compressive strength and reduced expressively the amount of leachable alkalis. This factor leads the formation of a geopolymer without severe efflorescence formation. Unreacted particles of CAC were not identified in the MK/CAC-based geopolymers (Figure 75 C). This material, rich in alumina and calcium oxide induced the formation of a different product morphology in some specific points, and these products also increased the compressive strength and reduced the amount of leachable alkalis, providing one more option to produce geopolymers without efflorescence formation. As explained previously, one strategy to reduce the efflorescence formation was the reduction of activator, associated to addition of other sources of aluminosilicates. The geopolymers MK-15Na-1.5ms, were produced with less amount of activator (lower alkalinity concentration, 15%Na_2O), but higher amount of sodium silicate (through higher MS ratio) (Figure 75D). This strategy is efficient, the matrix looks dense and compact, the results of compressive strength and leachable alkalis are similar than those system with higher amount of activator and any efflorescence formation was observed. However, the addition of other aluminosilicate precursors, as well as alternative sources of silica or calcium seems to be not effective. The use of 25% of fly ash in the precursor (MK/25FA-25Na-1.0ms) (Figure 75E), presents a high amount of unreacted fly ash particles. This behaviour was also observed by the MK/GBFS-based geopolymers (Figure 75F). In these two conditions, part of the precursors are not contributing to improve the properties, it means that, part of the aluminosilicate minerals are not dissolved and the activator designed to be consumed with these particles remains in the mix, increasing the soluble alkalis available. These two strategies reduce the compressive strength, increase the amount of leachable alkalis and generated more efflorescence formations than MK-based geopolymers.

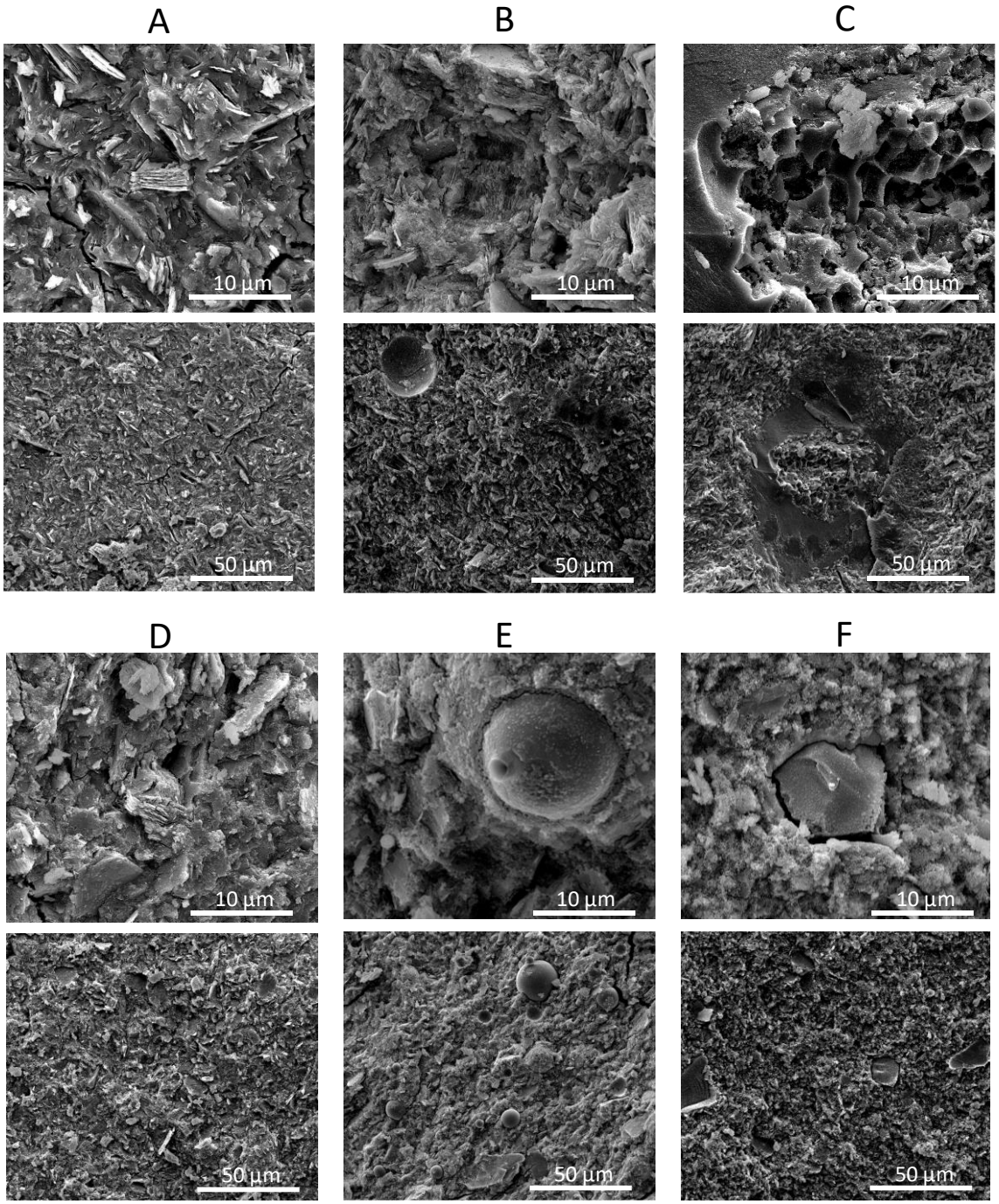

Figura 75 - SEM imagens of geopolymers A. MK-20Na-1.5ms, B. MK/5SF-20Na-1.0ms, C. MK/5CAC-20Na-1.0ms, D. MK-15Na-1.5ms, E. MK/25FA-15Na-1.0ms, F. MK/5GBFS-15Na-1.0ms

7.4. CONCLUSIONS

In this work, different strategies related to synthesis parameter and raw materials selection were assessed for the reduction in the efflorescence formation. A set of 21 geopolymers mixtures based on type and concentration of the activator, use of SCM's and inclusion of additives were studied. The visual efflorescence formation was correlated with compressive strength, water absorption, leaching and some microstructural properties.

The optimization of synthesis parameters were adjusted by increasing the amount of sodium silicate at different alkali activation. The results showed that there exists a correct amount of sodium silicate can control the efflorescence formation. The value identifies in this study was a MS ratio of 1.5, which is represented by the SiO_2/Na_2O molar ration within the alkali cativator solution. This amount of sodium silicate provides a higher compressive strength, lower water absorption and lower alkali leaching when compared to the reference systems (geopolyer produced with lower MS). The reduction of alkali concentration in the activation from 20% to 15% of Na_2O is also positive to efflorescence control when the MS ratio is also increased up to 1.5.

The replacement of metakaolin by fly ash and blast furnace slag are not reasonable under the evaluated criteria due to the extensive efflorescence formation. The compressive strength and water absorption are similar to the MK-based geopolymers, however the content of leachable alkalis is higher especially by the addition of GBFS. This behaviour is attributed to the insufficient reactivity of precursors, either due to intrinsic properties or inappropriate synthesis parameters. On the other way, the addition in small amounts of silica fume (as an alternative source of SiO_2) or calcium aluminate cement (source of calcium and aluminium) is effective in the control of efflorescence formation. By the addition of SF, the leaching is reduced, attributed to the higher imprisonment of alkalis. The effectiveness in mitigate the efflorescence formation by the SF is similar when compared to those geopolymer systems produced with traditional sodium silicate. The addition of CAC induces higher water absorption and higher amount of leachable materials, however, no efflorescence formation is observed, indicating high solubility of the carbonate phase formed. The use of dispersive/hydrophobic additive and silicone oil are effective to reduce the efflorescence formation. The improvement is due to the reduction of water absorption and reduction of leached alkali.

In general, even with different adjustment in synthesis parameters, all geopolymers exhibited a certain amount of free or leachable alkali from the reacted products. The stability of these alkalis in the framework structure is related to the degree of reaction and gel formed, which also allows the formation of a denser and less permeable material. The reduction of porosity difficult the movement of fluids and delays the leaching process. These properties associated can contribute to the efflorescence control in metakaolin-based geopolymers.

REFERENCES:

BERNAL, A. et al. Materiales de Construcción, Vol 65, No 318 (2015). v. 65, n. 318, p. 1–9, 2020.

BERNAL, Susan A. et al. Gel nanostructure in alkali-activated binders based on slag and fl y ash , and effects of accelerated carbonation. **Cement and Concrete Research**, v. 53, p. 127–144, 2013.

BERNAL, Susan A. Microstructural Changes Induced by CO2 Exposure in Alkali-Activated Slag/Metakaolin Pastes. **Frontiers in Materials**, v. 3, n. September, p. 1–10, 2016.

BOUZÓN, N. et al. Refluxed rice husk ash/NaOH suspension for preparing alkali activated binders. **Materials Letters**, v. 115, p. 72–74, 2014.

BRUS, J. et al. **Advances in ^{27}Al MAS NMR Studies of Geopolymers**. v. 88

BURCIAGA-DÍAZ, Oswaldo et al. Statistical analysis of strength development as a function of various parameters on activated metakaolin/slag cements. **Journal of the American Ceramic Society**, v. 93, n. 2, p. 541–547, 2010.

CAO, Yi Fang et al. Effect of calcium aluminate cement on geopolymer concrete cured at ambient temperature. **Construction and Building Materials**, v. 191, p. 242–252, 2018.

CRIADO, M. et al. Effect of the SiO2/Na2O ratio on the alkali activation of fly ash. Part II: 29Si MAS-NMR Survey. **Microporous and Mesoporous Materials**, v. 109, n. 1–3, p. 525–534, 2008.

DAHLAN, Irvan et al. Evaluation of various additives on the preparation of rice husk ash (RHA)/CaO-based sorbent for flue gas desulfurization (FGD) at low temperature. **Journal of Hazardous Materials**, v. 161, n. 1, p. 570–574, 2009.

DUXSON, P. et al. Geopolymer technology: the current state of the art. **Journal of Materials Science**, v. 42, n. 9, p. 2917–2933, 2006.

DUXSON, Peter et al. Si NMR Study of Structural Ordering in Aluminosilicate Geopolymer Gels. p. 3028–3036, 2005.

FERNÁNDEZ-JIMÉNEZ, A. et al. The role played by the reactive alumina content in the alkaline activation of fly ashes. **Microporous and Mesoporous Materials**, v. 91, n. 1–3, p. 111–119, 2006.

HE, Pingping et al. A ternary optimization of alkali-activated cement mortars incorporating glass powder, slag and calcium aluminate cement. **Construction and Building Materials**, v. 240, p. 117983, 2020.

LLOYD, Redmond R.; PROVIS, John L.; VAN DEVENTER, Jannie S. J. Pore solution composition and alkali diffusion in inorganic polymer cement. **Cement and Concrete Research**, v. 40, n. 9, p. 1386–1392, 2010.

LONGHI, Márlon A. et al. New selective dissolution process to quantify reaction extent and product stability in metakaolin-based geopolymers. **Composites Part B: Engineering**, v. 176, p. 107172, 2019.

LONGHI, Márlon A. et al. Metakaolin-based geopolymers: Relation between formulation, physicochemical properties and efflorescence formation. **Composites Part B: Engineering**, v. 182, n. October 2019, 2020.

MASSIOT, Dominique et al. Modelling one- and two-dimensional solid-state NMR spectra. **Magnetic Resonance in Chemistry**, v. 40, n. 1, p. 70–76, 2002.

MEJÍA, J. M.; MEJÍA DE GUTIÉRREZ, R.; PUERTAS, F. Ceniza de cascarilla de arroz como fuente de sílice en sistemas cementicios de ceniza volante y escoria activados alcalinamente. **Materiales de Construccion**, v. 63, n. 311, p. 361–375, 2013.

NAJAFI, Ebrahim; ALLAHVERDI, Ali; PROVIS, John L. Efflorescence control in geopolymer binders based on natural pozzolan.pdf. [s. l.], v. 34, p. 25–33, 2012.

PALOMO, Angel et al. Alkaline Activation of Fly Ashes : NMR Study of the Reaction Products Alkaline Activation of Fly Ashes : NMR Study of the Reaction Products. **Journal of the …**, v. 1145, n. November 2015, p. 1141–1145, 2008.

PALOMO, Angel; ALONSO, Santiago; FERNANDEZ-JIMÉNEZ, Ana. Alkaline Activation of Fly Ashes : NMR Study of the Reaction Products. **Journal of the American Ceramic Society**, v. 87, n. 6, p. 1141–1145, 2004.

PENA, P. et al. Solid-state 27Al and 29Si NMR characterization of hydrates formed in calcium aluminate–silica fume mixtures. **Journal of Solid State Chemistry**, v. 181, n. 8, p. 1744–1752, 2008.

PROVIS, John L. et al. Modeling speciation in highly concentrated alkaline silicate solutions. **Industrial and Engineering Chemistry Research**, v. 44, n. 23, p. 8899–8908, 2005. a.

PROVIS, John L. et al. Statistical Thermodynamic Model for Si/Al Ordering in Amorphous Aluminosilicates. **Chemistry of Materials**, v. 17, n. 11, p. 2976–2986, 2005. b.

PROVIS, John L.; BERNAL, Susan a. Geopolymers and Related Alkali-Activated Materials. **Annual Review of Materials Research**, v. 44, n. 1, p. 140205180727009, 2014.

PROVIS, John L.; LUKEY, Grant C.; VAN DEVENTER, Jannie S. J. Do geopolymers actually contain nanocrystalline zeolites? A reexamination of exixting results. **Chemical mater**, v. 17, p. 3075–3085, 2005.

PUERTAS, F.; TORRES-CARRASCO, M. Use of glass waste as an activator in the preparation of alkali-activated slag. Mechanical strength and paste characterisation. **Cement and Concrete Research**, v. 57, p. 95–104, 2014.

RODRÍGUEZ, Erich D. et al. Structure of Portland Cement Pastes Blended with Sonicated Silica Fume. v. 24, n. OCTOBER, p. 1295–1304, 2012.

ROWLES, M. R. HANNA, J. V. PIKE, K. J, SMITH, M. E, O'connor B. H. Si, Al, 1 H and 23 Na MAS NMR Study of the Bonding Character in Aluminosilicate Inorganic Polymers 27. **Applied Magentic Resonance**, v. 32, p. 663–689, 2007.

ŠKVÁRA, František et al. Aluminosilicate polymers - Influence of elevated temperatures, efflorescence. **Ceramics - Silikaty**, v. 53, n. 4, p. 276–282, 2009.

ŠKVÁRA, František et al. A weak alkali bond in (N, K)-A-S-H gels: Evidence from leaching and modeling. **Ceramics - Silikaty**, v. 56, n. 4, p. 374–382, 2012.

WALKLEY, B.; PROVIS, J. L. **Solid-state nuclear magnetic resonance spectroscopy of cementsMaterials Today Advances**, 2019.

WALKLEY, Brant et al. Phase evolution of Na2O–Al2O3–SiO2–H2O gels in synthetic aluminosilicate binders. **Dalton Transactions**, v. 45, n. 13, p. 5521–5535, 2016. a.

WALKLEY, Brant et al. Phase evolution of $Na_2O–Al_2O_3–SiO_2–H_2O$ gels in synthetic aluminosilicate binders. **Dalton Transactions**, v. 45, n. 13, p. 5521–5535, 2016. b.

YAO, Xiao; YANG, Tao; ZHANG, Zuhua. Compressive strength development and shrinkage of alkali-activated fly ash–slag blends associated with efflorescence. **Materials and Structures/Materiaux et Constructions**, v. 49, n. 7, p. 2907–2918, 2016.

YIP, C. K.; LUKEY, G. C.; VAN DEVENTER, J. S. J. The coexistence of geopolymeric gel and calcium silicate hydrate at the early stage of alkaline activation. **Cement and Concrete Research**, v. 35, n. 9, p. 1688–1697, 2005.

ZHANG, Zuhua et al. Quantitative kinetic and structural analysis of geopolymers. Part 2. Thermodynamics of sodium silicate activation of metakaolin. **Thermochimica Acta**, v. 565, p. 163–171, 2013.

ZHANG, Zuhua et al. Cement and Concrete Research Fly ash-based geopolymers : The relationship between composition , pore structure and ef fl orescence. v. 64, p. 30–41, 2014. a.

ZHANG, Zuhua et al. Fly ash-based geopolymers: The relationship between composition, pore structure and efflorescence. **Cement and Concrete Research**, v. 64, p. 30–41, 2014. b.

ZHANG, Zuhua et al. Efflorescence and subflorescence induced microstructural and mechanical evolution in fly ash-based geopolymers. **Cement and Concrete Composites**, v. 92, n. March, p. 165–177, 2018.

ZHENG, Lei et al. Immobilization of MSWI fly ash through geopolymerization: Effects of water-wash. **Waste Management**, v. 31, n. 2, p. 311–317, 2011.

8 CONSIDERAÇÕES FINAIS

Como idealizado na estruturação desta tese, o documento foi dividido em capítulos específicos, os quais foram escritos na forma de artigos, onde em cada um são apresentados o estado da arte sobre o tema, os materiais e o método experimental utilizado, bem como os resultados, discussões e principais conclusões de cada etapa. Desta forma, se faz um fechamento destas etapas individuais e as principais conclusões do trabalho são aqui apontadas.

A partir do processo de dissolução seletiva proposto foi possível identificar e quantificar as parcelas de material não reativo, gel formado e materiais solúveis. Maiores teores de ativadores, bem como a adição de silicato de sódio, proporcionam uma maior dissolução de partículas do precursor, assim como uma maior formação de gel. O efeito da maior quantidade de gel formado é visível a partir da análise da resistência à compressão das misturas, principalmente nos sistemas com elevado teor de silicato de sódio. Essa melhora na resistência mecânica se deve ao maior teor de Si presente nas ligações tetraédricas do tipo $Q^4(m\text{Al})$, observada a partir das análises de ressonância nuclear magnética, o que torna a matriz mais reticulada e consequentemente mais densa e resistente. No entanto, estes sistemas, mesmo com maior resistência à compressão apresentaram um elevado teor de álcalis solúveis em um ambiente de pH neutro, o que indica o elevado potencial de lixiviação dos álcalis nessas estruturas geopoliméricas. Além disso, o processo de lixiviação causa efeitos microestruturais associados principalmente à estrutura do alumínio, referente à redução dos sítios tetraédricas ricos em alumínio $Q^4(4\text{Al})$, o que indica a remoção e a instabilidade de algumas fases. Esse efeito de redução é menor para sistemas com maior teor de silicato solúvel, onde se observa a formação de uma estrutura de gel com maior estabilidade.

A lixiviação dos álcalis livres na estrutura ou fracamente ligados ao gel dá início ao processo de formação de eflorescência. Apesar do potencial de lixiviação observado a partir do processo de dissolução seletiva, e quantificado a partir do uso de análises químicas, em situações de aplicação do geopolímero, essa lixiviação também é dependente da estrutura porosa da capilaridade da matriz. Essa quantidade de álcali lixiviado pode ser considerada como potencial de eflorescência, visto que, em contato com o CO_2 do ambiente, há a formação de diferentes fases carbonáticas. Essa quantidade de álcalis solúveis é altamente dependente de propriedades como densidade e porosidade, as quais, por sua vez, são condicionados aos parâmetros de dosagem dos materiais. Observou-se que a adição de elevados teores de silicato de sódio na

mistura auxiliou na redução da formação de eflorescência. Essa melhora está associada ao refinamento da porosidade e ao maior aprisionamento dos álcalis na estrutura do gel rico em silício. Ainda, o incremento de temperatura para cura térmica é outro fator que influencia nas propriedades, inclusive na formação de eflorescência. Além disso, o tipo de álcali utilizado também é um fator importante na formação de eflorescência visual. No entanto, o tipo de carbonato formado é determinante para a extensão de eflorescência visível sendo que a formação do cristal é dependente da solubilidade do mesmo. A formação de eflorescência visual não pode ser diretamente relacionada com a resistência à compressão, no entanto, tem uma relação evidente com a quantidade de sódio lixiviado e a estrutura porosa do material. Do mesmo modo, uma maior quantidade de gel formado (determinado pelo o processo de dissolução seletiva) não apresenta uma relação diretamente proporcional, visto que a estabilidade do álcali também é dependente do tipo de estrutura molecular formada.

A partir das observações feitas durante a pesquisa, a formação da eflorescência foi sistematizada como sendo um fenômeno constituído por 3 mecanismos principais, sendo eles: a lixiviação de álcalis; a carbonatação interna e cristalização em forma de eflorescência. Por isso, relativo aos efeitos ocasionados durante o processo de formação de eflorescência, observa-se que cada um desses mecanismos gera um efeito diferentes nas propriedades mecânicas e microestruturais dos geopolímeros. A resistência à compressão é afetada negativamente perante exposição aos mecanismos de carbonatação interna e eflorescência externa. Essa redução se dá devido a carbonatação e excessiva formação de cristais na superfície e nas primeiras camadas do material, que compreende a face externa até 5mm internos, o que gera uma tensão interna proveniente da formação e crescimento do cristal de carbonato. A partir do momento que essa tensão interna é superior a resistência à tração, há a degradação do material. A degradação e formação de cristais superficiais pode ser observada visualmente, já internamente é possível identificar a carbonatação com o uso de TGA, DRX e MEV. Por outro lado, as resistências à tração e flexão são mais susceptíveis quando expostas à condição de lixiviação, onde observa-se uma redução de resistência expressiva. Essa redução está associada ao processo de remoção dos álcalis, que causa uma mudança microestrutural associada às ligações molecular do alumínio, com isso, foi observada uma mudança de morfologia da estrutura, atribuída inicialmente à remoção das parcelas menos estáveis do gel. Os efeitos mecânicos da formação de eflorescência são mais nocivos para sistemas com reduzido teor de silicato solúvel na mistura, o que indica uma maior estabilidade das fases ricas em silício.

A mitigação da formação de eflorescência se torna necessária visto o efeito negativo da ocorrência de seus fenômenos associados ao comportamento mecânico. Foi verificado a partir do programa experimental proposto que algumas alternativas se mostraram promissoras na mitigação da eflorescência. O refinamento da porosidade associado com a maior aprisionamento dos álcalis na estrutura apresenta uma redução de formação da eflorescência bastante expressiva. O elevado teor de silicatos no ativador proporciona um maior teor de sílica na estrutura tetraédrica do tipo Q^4(xAl), o que gera uma estrutura mais reticulada e densa, auxiliando no aprisionamento do álcali e reduzindo a porosidade do sistema. Essa melhora pode ser obtida a partir de um correto teor de silicato de sódio no proporcionamento dos materiais, com o uso de óleo silicoso ou adicionando baixos teores de sílica ativa na mistura. Do mesmo modo, com a adição de uma fonte extra de alumínio, aumenta-se a quantidade de alumínio em uma coordenação tetraédrica Al(IV) o que indica uma maior quantidade de álcali atomicamente ligados ao alumínio para estabelecer o equilíbrio iônico da ligação. Desta forma, o uso de um cimento aluminoso (base aluminato de cálcio) apresentou efeito positivo. Ainda, além do ajuste dos parâmetros de dosagem para otimizar a mistura, ainda foi possível reduzir a movimentação de fluídos no corpo de prova a partir do uso de aditivos hidrofóbicos na composição da mistura, um mecanismo de bloqueio que dificulta a formação de eflorescência.